

**VICTORIA
UNIVERSITY**

**Thermal Stability of Concrete and
Concrete-Filled Steel Tubular
Arches**

by

Yanni Bouras

Thesis submitted in fulfilment of the requirement for the degree of

Doctor of Philosophy

College of Engineering and Science, Victoria University, Australia

Abstract

The stability of arches is a classical mechanics and pragmatic engineering problem that has been extensively studied by many researchers over the years. Despite the comprehensive construction and research of arches throughout history, their complex behaviour still presents a challenge to engineers and ensures they are the subject of continual investigation. The problem of arch stability is of contemporary relevance due to the surging popularity of concrete-filled steel tubular (CFST) arch bridges. Hence, due to the inherent complex structural function of arches when coupled with the increasing construction of CFST arches, research into the response and stability of CFST arches under all possible environmental conditions is necessitated. However, investigations into the effects of extreme temperatures on concrete and CFST arches have not been conducted.

This thesis presents a comprehensive analytical and numerical investigation into the stability of circular concrete and CFST arches subjected to combined mechanical and thermal loading. Original models are derived for the non-linear prebuckling and buckling analysis including closed-form solutions for the in-plane elastic buckling loads of concrete and CFST arches, and non-discretisation mechanically-based numerical models for their elastic and inelastic analysis prebuckling analysis. Additionally, a numerical methodology to determine the elastic flexural-torsional buckling loads of CFST arches is proposed. Furthermore, a novel fractional viscoelastic creep law is developed for concrete at elevated temperatures in order to analyse the significance of basic creep strain on thermal response and stability boundaries. The fractional-derivative creep law proves to be a robust and compact method of modelling basic creep strain under stress and temperature varying conditions. Finite difference schemes are employed to numerically approximate the fractional derivative and incorporate basic creep into the

prebuckling and stability analyses. Finite Element (FE) models are developed to verify the derived models and to also investigate the inelastic buckling strength and fire performance of concrete and CFST arches.

The findings of this study provide a detailed understanding of the fundamental thermo-mechanical behaviour and failure modes of concrete and CFST arches. Consequently, engineers may utilise the results detailed herein to assess and improve the fire resistance of concrete and CFST arch structures. Additionally, the developed creep law has widespread application in the analysis of concrete structures under elevated temperatures. The proposed inelastic numerical models also provide efficient tools for the analysis of other structures such as steel arches and beams.

Declaration

"I, Yanni Bouras, declare that the PhD thesis by publication entitled 'Thermal Stability of Concrete and Concrete-filled Steel Tubular Arches' is no more than 100,000 words in length including quotes and exclusive of tables, figures, appendices, bibliography, references and footnotes. This thesis contains no material that has been submitted previously, in whole or in part, for the award of any other academic degree or diploma. Except where otherwise indicated, this thesis is my own work".

Signature:



Date: 20/02/2020

Acknowledgements

Firstly, I would like to acknowledge Victoria University, the College of Engineering and Science and the Institute for Sustainable Industries and Liveable Cities (ISILC), for financially supporting my studies through the Vice Chancellor's Graduate Research Scholarship award.

To my co-supervisors Professor Atanacković and Professor Dusan Zorica, thank you for hosting my stay in Serbia and for your time and patience when working together. You are both an inspiration and I hold very fond memories of my time in Novi Sad.

To my principle supervisor Associate Professor Zora Vrcelj, words cannot express my gratitude for all you have done throughout my studies. You have believed in me when I have not believed in myself, you fully supported me throughout all my successes and failures alike, and have provided me with many amazing opportunities. Thank you Zora.

To my parents and brothers, thank you for putting up with a moody PhD student for many years. Though I may have lived in my head for all this time, you were all always there to make me laugh. And to my old man Costa, who always told me to go to school and learn my *γράμματα*.

And finally to my wife Julie, you are my biggest fan and my rock. Thank you for your constant love and support. I dedicate this thesis to you and the next chapter of our lives together.

List of Publications

Based on the research reported in this thesis, the candidate has produced the following papers, which have been published or are under review for publication in various international journals and peer-reviewed conferences.

Journal Articles

1. Y. Bouras, D. Zorica, T.M. Atanacković and Z. Vrcelj. 2018. A non-linear thermo-viscoelastic rheological model based on fractional derivatives for high temperature creep in concrete. *Applied Mathematical Modelling*, 55, pp.551-568.
2. Y. Bouras, and Z. Vrcelj. 2017. Non-linear in-plane buckling of shallow concrete arches subjected to combined mechanical and thermal loading. *Engineering Structures*, 152, pp.413-423.
3. Y. Bouras, and Z. Vrcelj. 2019. In-plane stability of shallow concrete arches under fire. *Journal of Structural Fire Engineering*, DOI: 10.1108/JSFE-11-2018-0039.
4. Y. Bouras, and Z. Vrcelj. 2020. Thermal in-plane stability of concrete-filled steel tubular arches. *International Journal of Mechanical Sciences*, 163, p.105130.
5. Y. Bouras, and Z. Vrcelj. 2020. Out-of-plane stability of concrete-filled steel tubular arches at elevated temperatures. Submitted to *International Journal of Mechanical Sciences*, Under Review.

Conference Papers

1. Y. Bouras and Z. Vrcelj. 2016. Effect of transient thermal strain on the stability of shallow concrete arches. In *Mechanics of Structures and Materials XXIV: proceedings of the 24th Australian Conference on the Mechanics of Structures and Materials* (ACMSM24, Perth, Australia, 6-9 December 2016 (pp. 963-970). CRC Press.
2. Y. Bouras, E. Torres-Don and Z. Vrcelj. 2017. Thermal in-plane buckling of concrete-filled steel tubular arches. In *Tubular Structures XVI: Proceedings of the 16th International Symposium for Tubular Structures* (ISTS 2017, 4-6 December 2017, Melbourne, Australia) (p. 101). CRC Press.

PART A:
DETAILS OF INCLUDED PAPERS: THESIS BY PUBLICATION

Please list details of each Paper included in the thesis submission. Copies of published Papers and submitted and/or final draft Paper manuscripts should also be included in the thesis submission

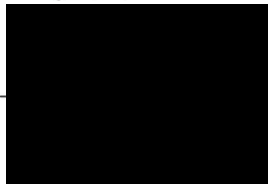
Item/ Chapter No.	Paper Title	Publication Status (e.g. published, accepted for publication, to be revised and resubmitted, currently under review, unsubmitted but proposed to be submitted)	Publication Title and Details (e.g. date published, impact factor etc.)
3	A non-linear thermo-viscoelastic rheological model based on fractional derivatives for high temperature creep in concrete	Published	Applied Mathematical Modelling, 2018, 55, pp.551-568. Q1 Ranked journal Impact Factor: 2.841
4	Effect of transient thermal strain on the stability of shallow concrete arches	Published	Mechanics of Structures and Materials XXIV: Proceedings of the 24th Australian Conference on the Mechanics of Structures and Materials (ACMSM24, Perth, Australia, 6-9 December 2016 (pp. 963-970). CRC Press.
4	Non-linear in-plane buckling of shallow concrete arches subjected to combined mechanical and thermal loading	Published	Engineering Structures, 2017, 152, pp.413-423. Q1 Ranked journal Impact Factor: 3.084
5	In-plane stability of shallow concrete arches under fire	Published	Journal of Structural Fire Engineering, 2020, DOI: 10.1108/JSFE-11-2018-0039 Q2 Ranked journal Impact Factor: 0.62
6	Thermal in-plane buckling of concrete-filled steel tubular arches. In Tubular Structures	Published	Tubular Structures XVI: Proceedings of the 16th International Symposium for Tubular Structures (ISTS 2017, 4-6 December 2017, Melbourne, Australia) (p. 101). CRC Press.
6	Thermal in-plane stability of concrete-filled steel tubular arches	Published	International Journal of Mechanical Sciences, 2019, 163, p.105130. Q1 Ranked journal Impact Factor: 4.134
7	Out-of-plane stability of concrete-filled steel tubular arches at elevated temperatures	Submitted for publication (Under Review)	International Journal of Mechanical Sciences Q1 Ranked journal Impact Factor: 4.134

Declaration by [candidate name]:

Signature:

Date:

YANNI BOURAS



11/02/2020

Contents

Abstract	i
Declaration	iii
Acknowledgements	iv
List of Publications	vi
Details of Included Papers: Thesis by Publication	viii
1 Introduction	1
1.1 Structural Arches	1
1.2 Fractional Calculus and Viscoelasticity	4
1.3 Research Significance	6
1.4 Research Aims	8
1.5 Thesis Layout	10
2 Literature Review	13
2.1 Introduction	13
2.2 Theory of Stability	14
2.2.1 Elastic stability	14
2.2.2 Inelastic stability	16
2.3 Elastic buckling of arches	17
2.3.1 In-plane stability	17
2.3.2 Out-of-plane stability	25
2.4 Inelastic buckling of arches	31
2.4.1 In-plane stability	32
2.4.2 Out-of-plane stability	33
2.5 Thermal buckling of arches	36
2.5.1 In-plane stability	36

2.5.2	Out-of plane stability	42
2.5.3	Discussion	43
2.6	Creep buckling of arches	44
2.6.1	In-plane stability	44
2.6.2	Out-of-plane stability	47
2.6.3	Temperature-time coupling	48
2.6.4	Discussion	49
2.7	Future research	50
2.8	Conclusion	51
3	Basic creep in concrete at elevated temperatures	53
3.1	Introduction	53
3.2	Declarations	56
3.3	A non-linear thermo-viscoelastic rheological model based on fractional derivatives for high temperature creep in concrete	58
3.4	Concluding Remarks	76
4	In-plane thermo-elastic buckling of shallow concrete arches	77
4.1	Introduction	77
4.2	Declarations	79
4.3	Effect of transient thermal strain on the stability of shallow concrete arches	83
4.4	Non-linear in-plane buckling of shallow concrete arches subjected to combined mechanical and thermal loading	89
4.5	Concluding Remarks	100
5	Inelastic buckling of shallow concrete arches under fire loading	102
5.1	Introduction	102
5.2	Declarations	104
5.3	In-plane stability of shallow concrete arches under fire	106
5.4	Concluding Remarks	128

6	Thermal in-plane stability of concrete-filled steel tubular arches	129
6.1	Introduction	129
6.2	Declarations	131
6.3	Thermal in-plane buckling of concrete-filled steel tubular arches	135
6.4	Thermal in-plane stability of concrete-filled steel tubular arches	143
6.5	Concluding Remarks	158
7	Thermal out-of-plane stability of concrete filled steel tubular arches	160
7.1	Introduction	160
7.2	Declarations	162
7.3	Out-of-plane stability of concrete-filled steel tubular arches at elevated temperatures	164
7.4	Concluding Remarks	192
8	Conclusions	194
8.1	Summary	194
8.2	Novel Contributions	197
8.3	Further Research	199
	References	200

Chapter 1

Introduction

1.1 Structural Arches

Arches are a historic construction form which originated in second century B.C and flourished during the rule of the Roman Empire. A structural arch is a member curved in elevation, loaded in its plane and features a radius that is large relative to the cross-section depth [1]. Differentiation between arches and curved beams may be made based on the degree of freedom at the arch ends; supports that are free to move apart can be classed as curved beams due to the greater significance of bending actions and reduced in-plane stiffness and strength [2]. The popularity of arches arose as a structural member due to their ability to resist loads primarily in compression consequently resulting in

a high in-plane strength and stiffness, which made them ideal for masonry materials. Despite their use since antiquity, arches are still commonly utilised in modern society for the construction of tunnels, bridges and building structures for this very same reason. The safe design and maintenance of arch structures is thus of vital importance for public safety, in addition to the associated historical and economical significance.

Despite featuring a high in-plane strength, arches are subject to instability. An arch sufficiently restrained in the lateral direction exhibits the possibility of stability loss in its plane of loading. Two in-plane buckling modes exist which include the anti-symmetric bifurcation buckling mode and the symmetric snap-through type, both depicted in Figure 1.1. Classical or bifurcation buckling is categorised as a transition from a pre-buckled equilibrium configuration to an adjacent, or infinitesimally close, buckled equilibrium configuration as the load passes through the critical level [3]. Symmetric snap-through buckling or limit instability is defined as a sudden jump to another non-adjacent equilibrium configuration which features noticeably greater deformations than the initial position. Additionally, an arch featuring a large free standing portion may buckle out-of-plane in a flexural-torsional type mode. Flexural-torsional bifurcation buckling of arches involves the rapid out-of-plane deformation from an initial pre-buckled state caused by in-plane loading. The associated deformations include lateral displacements and twist rotations.

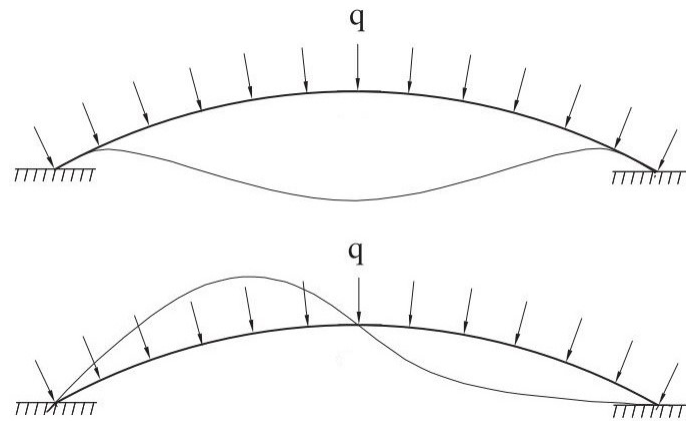


Figure 1.1: Symmetric instability (top) and anti-symmetric bifurcation buckling (bottom) [4]

This problem of arch stability is becoming of increasing relevance and importance in modern engineering. Circular concrete-filled steel tubular (CFST) arch bridges have recently surged in popularity with over 400 constructed worldwide [5], 300 built in China alone in the last 20 years [6]. The increased construction of CFST arches can be attributed to the superior performance of CFST members when compared to their reinforced concrete and steel counterparts. In addition to many other benefits, CFST members feature enhanced compressive strength often resulting in the use of slender members. As arches experience primarily compression, the use of slender elements significantly increases the possibility of stability loss. Even if deemed stable, CFST arches may also buckle in time due to creep of the concrete core. The viscoelastic behaviour of the concrete core further convolutes the non-linear behaviour of arches and significantly reduces the their load carrying capacity. It is thus of paramount importance that design engineers understand the complex behaviour of arches and adopt accurate methodologies for analysis of their stability.

1.2 Fractional Calculus and Viscoelasticity

Fractional calculus is the study of performing integration or differentiation to a degree of non-integer (real) value. For example, consider a function $f(x) = x^3$ with the derivative of the function being denoted as $\frac{d^n}{dx^n} f(x)$. The first order derivative ($n = 1$) is simply $\frac{d}{dx} f(x) = 3x^2$ and the second order derivative $\frac{d^2}{dx^2} f(x) = 6x$. However if $0 < n < 1$, the solution is no longer as simple and commonly recognized as if it were an integer. The physical meaning and practical application of such an operation is also questioned. Fractional calculus owes its origin to a question raised by L'Hopital in 1695 and presented to Leibniz. L'Hopital asked what would be the result of $\frac{d^n}{dx^n} f(x) = x$ if $n = 1/2$. Leibniz's response was "an apparent paradox, from which one day useful consequences will be drawn" [7]. Many famous mathematicians including Euler, Laplace, Riemann and Liouville have since contributed to its development and formed multiple varying definitions. The Riemann-Liouville and Caputo definitions of the derivative are the most commonly adopted and will be defined herein.

Let the fractional integration of a function $f(x)$ be denoted as ${}_c D_x^{-v} f(x)$ where v is a positive real number and the subscripts c and x are the limits of integration. The Riemann-Liouville fractional integral of order v is defined as;

$${}_c D_x^{-v} f(x) = \frac{1}{\Gamma(v)} \int_c^x (x-t)^{v-1} f(t) dt, \quad (1.2.1)$$

where $x \in R^+$ and $\Gamma(x)$ is the Gamma function (generalisation of the factorial for all real numbers) known as;

$$\Gamma(x) = \int_0^\infty e^{-t} t^{x-1} dt. \quad (1.2.2)$$

The fractional derivative of a function $f(x)$ of order u is defined as;

$$D_x^u f(x) = D^n [D^{-v} f(x)], \quad (1.2.3)$$

where ${}_c D_x^u f(x)$ represents the fractional derivative of real order $u > 0$, $v = n - u$ satisfying $0 < v < 1$ and n is the smallest integer greater than u . The Caputo definition of the fractional derivative is known as;

$$D_x^u f(x) = \frac{1}{\Gamma(1-u)} \int_0^x \frac{D_t^1 f(t)}{(x-t)^u} dt. \quad (1.2.4)$$

Despite being considered an *old* problem, it is only in the last 100 years that the most significant applications of fractional calculus in engineering and scientific applications have been found [8]. Some of these include inverse mechanical problems, motion in viscous fluids, biophysics, medicine and astrophysics. Another major application of fractional calculus is in the theory of Viscoelasticity. Viscoelastic materials can be defined as exhibiting both viscous and elastic properties during deformation. Traditional viscoelastic models, including the Kelvin-Voigt, Maxwell and Zener, consist of an arrangement of elastic springs and viscous dampers in series and/or parallel, see Figure 1.2. Despite their common adoption, these models cannot accurately describe the dynamic behaviour of real materials [9]. The cause for the inaccuracy lies in the linear differential stress-strain equation being of integer order. High levels of accuracy can be obtained when viscoelastic chains are employed to describe material behaviour. However, the required multitude of viscoelastic elements results in a great number of material parameters to be characterised which can convolute analytical and numerical modelling [10]. In fractional rheology, the spring-dashpot models of viscoelasticity are generalised by adopting fractional order derivatives in place of the integer ones in the constitutive stress-strain equations. For example, the stress-strain relation for the

Maxwell model which consists of a spring and dashpot in series is;

$$D_t^1 \epsilon(t) = \frac{1}{E} D_t^1 \sigma(t) + \frac{\sigma(t)}{\eta}. \quad (1.2.5)$$

where E is the elastic modulus of the spring and η is the dynamic viscosity of the dashpot. By replacing the first order derivative in Eq.(1.2.5) with real order $0 < u < 1$, the fractional maxwell model is obtained as;

$$D_t^u \epsilon(t) = \frac{1}{E} D_t^u \sigma(t) + \frac{\sigma(t)}{\eta}. \quad (1.2.6)$$

where the fractional derivative operator $D_t^u()$ can be defined using the Riemann-Liouville or Caputo definition. Fractional viscoelastic models have proven to robust descriptors of material behaviour [11] whilst featuring a small number of parameters to be characterized.

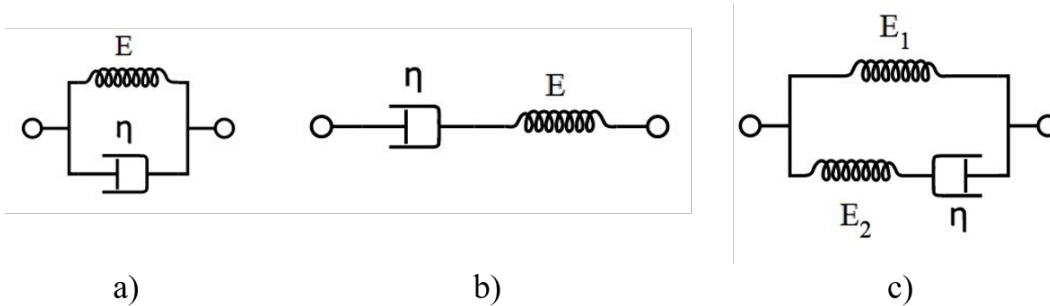


Figure 1.2: Kelvin-Voigt (a), Maxwell (b) and Zener (c) viscoelastic models.

1.3 Research Significance

The common construction of arches in building, tunnel and bridge applications makes their performance during elevated temperatures, as caused by fire exposure, of high importance. Commonly occurring building fires represent a danger to steel arches

used in roofing applications. Vehicle accidents and gasoline burning [12], gas pipe explosions [13] and terrorist attacks are existing possibilities which may expose tunnel or bridge arches to high levels of heat. In the paper published by the New York Department of Transportation [14], it was reported that 50 bridges have collapsed in the past 50 years in the U.S.A due to fire exposure. This averages to one bridge failure per year, a result greater than that of seismic related collapses. In Australia, 78 vehicle fires were reported in major road tunnels between 1992 and 2016 [15]. The safety of tunnels in fires is of increasing importance as the average distance Australians are travelling through road tunnels is climbing annually.

The stability of steel arches subject to elevated temperatures have been thoroughly investigated, however research on concrete and CFST arches under such conditions has not been conducted. Due to the accelerating construction of circular CFST arch bridges, it is paramount that their behaviour under both typical and extreme loading and environments be thoroughly investigated. Studies of concrete arches subject to such loading scenarios are also required due to their frequent use for tunnels and bridge applications. This is convoluted by the geometric non-linearity of arches which require non-linear methodologies for their analysis. Additional complexities arise when considering the material non-linearities of steel, concrete and composite CFST structures which consist of yielding, plasticity, confinement and contact.

In addition to thermal expansion and instantaneous mechanical strain, deformations also experienced by steel at high temperatures, concrete experiences elevated basic creep and transient thermal strain (TTS), often referred to as transitional thermal creep. TTS is irrecoverable and only occurs during virgin heating. Furthermore, TTS only manifests in concrete members mechanically loaded prior to heating. It is thus a consequence of the coupling effect of thermo-mechanical loading. Despite causing significant deformations in concrete members, the effects of elevated creep and TTS on

arch stability are yet to be reported. This research seeks to address this knowledge gap through investigation of the behaviour and stability boundaries of concrete and CFST arches subject to combined mechanical and thermal while considering creep and TTS.

Hence, the stability and integrity of concrete and CFST arches when exposed to elevated temperatures caused by fires represents an important engineering problem. Design engineers require feasible models and methodologies for the analysis of behaviour and stability of concrete and circular CFST arches subjected to thermal loading in order to ensure safety requirements are satisfied.

1.4 Research Aims

The aim of this research is to investigate the non-linear elastic and inelastic responses and stability boundaries of concrete and CFST arches subjected to combined mechanical and thermal loading. Extreme elevated temperatures will be the primary focus of this work, that is temperatures exceeding 100°C . This will be achieved through the derivation of novel analytical and numerical models, and Finite Element (FE) analysis. Additionally, a fractional viscoelastic model will be proposed to incorporate basic creep into the analyses and assess its influence on behaviour and buckling loads. Closed-form solutions and non-discretisation based numerical techniques will be derived to solve pre-buckling equilibrium configurations and buckling loads for the simplified cases of elastic material behaviour and/or uniform thermal loading. FE models will be developed to analyse the more convoluted scenarios of inelastic buckling and non-uniform thermal loading.

The aims of the research can be stated as follows:

1. To develop a novel creep law based on the theory of fractional viscoelasticity for concrete under extreme elevated temperatures;
2. To investigate the non-linear elastic pre-buckling behaviour and in-plane buckling loads of shallow concrete arches subjected to combined mechanical and uniform thermal loading whilst considering basic creep and TTS;
3. To study the non-linear inelastic response and in-plane failure modes of mechanically pre-loaded shallow concrete arches under fire loading;
4. To analyse the non-linear elastic and inelastic pre-buckling behaviour and in-plane stability boundaries of CFST arches under mechanical loading and elevated temperature fields; and
5. To examine the effects of thermal loading on the elastic and inelastic flexural-torsional buckling loads of CFST arches.
6. To provide design recommendations for concrete and CFST arches susceptible to high temperature environments or fire exposure by determining key parameters influencing buckling strength and fire resistance time.

This research will provide an in-depth understanding of the effects of high temperature conditions on the behaviour and failure modes of mechanically loaded concrete and CFST arches. These developed models will aid the practising structural engineer to safely design arch structures against fire loading and to simulate the performance of existing arches when exposed to elevated temperature fields. Moreover, the developed models may be utilised for the assessment fire-damaged arches. The development of novel fractional-derivative based viscoelastic models for high temperature creep deformations of concrete is not limited to fire related studies and has widespread application. These models may be applied to analyse long-term behaviour of concrete under high temperature working conditions, such as in nuclear reactor vessels. Generalisations

such as incorporation of humidity variations can be made in future research projects. Furthermore, the proposed inelastic numerical models provide efficient tools for the analysis of other structures such as steel arches and beams.

1.5 Thesis Layout

This thesis consists of eight chapters. This first chapter has provided an introduction to arch stability and the theory of fractional viscoelasticity, in addition to stating the research aims and highlighting the practical significance of the project. Chapter 2 presents an extensive review of pertinent literature surrounding the stability of arch structures. The literature review is segmented into four primary categories consisting of elastic buckling, inelastic strength, thermal stability and creep buckling of arches. These four groups are further divided into studies analysing in-plane stability and out-of-plane stability. Limitations in the current state of the art are subsequently discussed and areas requiring research focus are highlighted.

In Chapter 3, a novel rheological creep law is developed for concrete at extreme elevated temperatures based on the theory of fractional viscoelasticity. Model parameters, including the dynamic viscosities and the fractional exponents, are calibrated based on temperature level in order to map the creep compliance functions of the springpots with existing experimental data. As the fractional exponent is a function of temperature, under time-varying temperature conditions, a variable-order fractional differential equation is formulated. Numerical approximations of the fractional differential creep laws are made using a finite difference scheme. The result is a compact method for analytically and numerically modelling creep strain for cases of time-varying stress and/or temperature level. This is demonstrated by applying the developed model to determine

axial deformations in columns and transverse deflections in beams.

Chapter 4 presents analytical investigations into the elastic prebuckling behaviour and in-plane stability of circular shallow concrete arches subjected to uniformly distributed radial loading and time-varying uniform temperature fields with pinned or fixed end supports. Creep strain is modelled using the fractional viscoelastic rheological model developed in Chapter 3. The principle of virtual work is employed to derive the non-linear equations of equilibrium and the first correspondence principle is invoked. The first correspondence principle, or elastic-viscoelastic analogy, allows the problem to be treated statically, with the viscoelastic solution being obtained by replacing the elastic modulus in the corresponding elastic solution with the creep operator. An in-plane buckling analysis is then performed and closed form solutions for the anti-symmetric bifurcation and symmetric snap-through buckling loads are presented.

In Chapter 5, the inelastic response and in-plane failure modes of mechanically preloaded shallow concrete arches subjected to fire loading are numerically studied. A three-dimensional FE model is first constructed which considers geometric and material nonlinearities. To verify the FE model, a non-discretisation mechanical-based numerical method is derived for the non-linear inelastic analysis of shallow concrete arches subjected to uniformly distributed radial loading and uniform temperature fields. Further verification of the FE model is made by comparison to the inelastic buckling loads of concrete arches predicted using the tangent modulus theory. Subsequently, an extensive parametric study is conducted which illustrates the governing failure mode of concrete arches under mechanical and fire loading, and the effect of various parameters including arch included angle, concrete compressive strength, cross-section size, mechanical load level and fire type on fire resistance time.

Chapter 6 provides elastic and inelastic prebuckling and in-plane buckling analyses

of circular shallow and deep CFST arches under uniformly distributed radial loading and elevated temperature fields. The effect of thermal loads on the response of CFST arches with pinned, fixed and crown-pinned support cases are analysed. Closed-form solutions are presented for the elastic anti-symmetric bifurcation loads of CFST arches and the effect of temperature level on both anti-symmetric buckling and symmetric snap-through buckling loads demonstrated. Inelastic in-plane buckling strength is investigated through the development of a FE model which is verified by comparison to models derived herein and existing in the literature. Additionally, detailed parametric studies and sensitivity analyses illustrate the influence of various parameters on critical buckling loads and fire resistance time of CFST arches.

Elastic and inelastic flexural-torsional buckling of CFST arches subjected to combined mechanical and thermal loading is investigated in Chapter 7. A numerical model to determine the elastic out-of-plane buckling loads of CFST arches at elevated temperatures is derived using energy methods and is shown applicable to the mechanical loading cases of uniformly distributed and central concentrated loads, and for pinned or fixed end supports. The impact of thermal loading on elastic flexural-torsional buckling loads is examined in addition to assessing the significance of basic creep strain on the thermo-elastic pre-buckling response. Additionally, FE analysis is employed to study the inelastic lateral buckling strength of CFST arches under uniform temperature field or fire loading. The FE model is validated by comparison to the elastic out-of-plane buckling loads predicted by the numerical methodology derived herein. Parametric and sensitivity analyses are then presented to highlight the significance of numerous parameters on lateral buckling strength.

The eighth chapter concludes the thesis by presenting the current study's major findings, novel contributions and the associated practical implications. Furthermore, recommendations for future research works on the thermal stability of arches are provided.

Chapter 2

Literature Review

2.1 Introduction

The aim of this chapter is to present the state-of-the-art on the stability of arches under static loading. First, a brief discussion on the theory of stability for elastic and inelastic bodies is presented. Subsequently, literature on arch stability is considered and is segmented into four categories; elastic buckling, inelastic buckling, thermal buckling and creep buckling. Further classifications are made into in-plane and out-of-plane buckling. Analytical, numerical and experimental studies are all considered. Detailed descriptions of the mathematical components of various studies will not be provided, with a focus instead on the discussion of arch behaviour and methodology of analysis.

A summary is provided highlighting identified gaps in the literature to promote areas in need of research focus.

2.2 Theory of Stability

2.2.1 Elastic stability

Failures of structural elements is caused by either material failure or structural instability. The former is governed by material strength and is generally independent of the geometry of the structure. However, loss of stability is less dependant on material strength is primarily influenced by the material stiffness and structural geometry, mostly slenderness [10]. Stability can be defined, in basic terms, as the ability of the properties of a mechanical system to remain unchanged, or to change in a small quantity, when subject to perturbations [16]. Alternatively, stability loss can be said to have occurred when a structure changes from one deformation pattern to an adjacent one [3].

Analysing infinitesimally close equilibrium configurations is the oldest method of stability analysis and has many names including the classical, equilibrium, Euler and bifurcation method. This static analysis is based on the fact that under given loading and boundary conditions, a structure could have more than one equilibrium configuration. In this case, a state of equilibrium is defined as stable if under given boundary and loading conditions, there are no adjacent equilibrium positions. This is illustrated using the common example of a straight column in pure compression which suddenly changes (bifurcates) to a deformed equilibrium configuration of combined bending and compression as the applied load reaches the critical value. At the critical load level, the

structure contains multiple configurations where equilibrium can be maintained.

Analysis of static stability can also be conducted using the potential energy method. This method is based on the energy stability criteria for conservative mechanical systems with finite number of degrees of freedom. This can be expressed in the form of the Lagrange-Dirichlet theorem which states that a basic equilibrium configuration of a conservative system is stable if it has a minimum in terms of potential energy when compared to adjacent configurations. Adjacent positions differ from the basic configuration in finite virtual displacements. Thus, a structure subjected to conservative loads can be defined as stable if the total potential energy of the equilibrium configuration assumes a local minimum in the class of virtual displacements that satisfy geometric constraints.

The dynamic or kinematic definition of stability will now be discussed. This method involves the assessment of the equations governing free vibrations of a structure caused by external conditions. The equilibrium configuration is said to be stable if small disturbances to the initial conditions causes movements which are close to the original position for all of time. An unstable configuration is defined as when any disturbances to initial conditions or velocities cause a finite deviation from the initial position and increasing amplitudes of vibration with time.

As stated before, a structure is said to be unstable when the applied load reaches a critical value where multiple adjacent equilibrium positions exist simultaneously. A structure *buckles* if it moves from the initial equilibrium position to an adjacent one. This type of buckling is defined as *bifurcation buckling*. Two other primary types of buckling exist and include *snap-through buckling* and *finite-disturbance buckling*. Snap-through buckling involves a structure noticeably jumping from an initial equilibrium state to a non-adjacent equilibrium position where the displacements are significantly

larger [3]. Finite-disturbance buckling occurs when there is a great loss of stiffness due to buckling, and in order to maintain equilibrium in the buckled state, the load level significantly reduces. Of relevance to stability of arches is bifurcation and snap-through buckling.

2.2.2 Inelastic stability

In the preceding discussion, structural failure was stated to be caused by either material failure or instability failure. However, in reality a combination of the two failure modes is likely to occur in most structures. The high load levels required to induce buckling in non-slender structures may exceed the elastic range. Furthermore, inelastic deformations may destabilise a structure. The energy method of stability analysis requires the existence of the potential energy function. This is inapplicable to inelastic bodies which are non-conservative. Therefore, other methods of stability analysis must be employed when considering plasticity. Two methods of time-independent inelastic stability analysis of structures will be discussed; the reduced modulus method and the tangent modulus method.

At the commencement of column buckling, one side of the column is subjected to additional compressive loading and axial shortening. Whilst the other side experiences unloading assuming a constant axial force during buckling [10]. For an inelastic stress-hardening material, the shortening side of the column will be governed by the tangent modulus E_t and the extending side will behave according to the unloading modulus E_u . The original elastic modulus $E > E_t$ and $E_u > E_t$. This difference in moduli in the cross-section causes a bi-linear stress distribution in the column. Upon obtaining the bending moment in the cross-section based, one may derive the critical buckling load

which is dependant on the reduced modulus E_r which is a function of E_t and E_u . For smooth non-linear stress-strain curves, E_r is a function of normal stress and is therefore solved iteratively.

The reduced modulus theory tends to over predict the real buckling load of plastic columns [10]. This is due to the possibility of columns deflecting prior to the critical reduced modulus load. Therefore, the buckling load is not constant, and unloading caused by buckling deflections is compensated for by further increases in axial load level. Thus, at the onset of buckling, the strain distribution across the cross-section is constant and governed by E_t for both non-linear and bi-linear elasto-plastic behaviour. The tangent modulus buckling load is obtained by replacing E in the elastic solution with E_t . This also obtained iteratively due to the dependence of E_t on the stress level.

2.3 Elastic buckling of arches

2.3.1 In-plane stability

The elastic in-plane stability of arches is a classical mechanics and pragmatic engineering problem that has been extensively studied by many researchers over the years and continues to be an area of great research focus. Early analytical studies on the in-plane elastic stability of arches include the works of Timoshenko and Gere [17], Vlasov [18], Gjelsvik and Bodner [19], Austin [20], Simitzes and Hutchinson [21], Schreyer and Masur [22] and Dickie and Broughton [23]. The results of early research on arch stability have been summarised in the Guide to Stability Design of Metal Structures [1,24,25], the Handbook of Structural Stability [26] and by DaPeppo and Schmidt [27]. Fukumoto [28]

presented a state of the art of the elastic and inelastic stability of arches in 1996. This review will hence focus on more recent research.

In these early investigations on the elastic stability of arches [17–23], classical buckling theory was adopted. However, it was later shown experimentally [19, 23] and numerically [29] that the classical theory was inaccurate, caused by simplifying assumptions made regarding the pre-buckling behaviour [29, 30]. Classical buckling theory ignores the effects of pre-buckling deformations on displacements and geometrical stiffness, and linearises stress resultants. These assumptions result in a linearised buckling solution which prevents a post-buckling analysis [29, 30]. Classical theory only provides accurate solutions for deep arches, as the rise of the arch is much greater than the magnitude of pre-buckling deformations [29]. Conversely in shallow arches, the pre-buckling deformations are significant and highly non-linear. As a result, the linear resultants for axial compressive force $N \approx qR$ and bending moment $M \approx 0$ prior to buckling, where q and R are the uniformly distributed radial load and arch radius respectively, do not hold true for shallow arches. The use of classical theory for the analysis of shallow arches leads to an overestimation of the buckling strength, thus the elastic buckling load of a shallow arch must be obtained using non-linear methods.

The use of numerical and FE schemes to investigate arch stability then became popular among researchers [31–37]. However, these early numerical models generated for the non-linear analysis of elastic arches did not fully account for strain non-linearity, as bending strains were assumed linear and the influence of axial deformations on curvature were not considered. Additionally, pre-buckling deformations were ignored in the study by Kang and Yoo [37]. Pi and Trahair [38] incorporated higher-order curvature terms caused by bending actions, in addition to the effects of pre-buckling deformations, into a FE model developed for the non-linear analysis of arches. This model was extended to analyse in-plane buckling and post-buckling behaviour by the authors in [29]. The

higher order bending strains were found to have a profound effect on the stability of deep arches.

Research analytically investigating the in-plane elastic stability of arches, while considering the effects of pre-buckling deformations, will now be discussed. The in-plane elastic stability of a circular elastic arch under uniform radial load and with an arbitrary cross section was investigated by Pi et al. [30] and Pi and Bradford [39]. Geometric non-linearity was considered by adopting the following non-linear longitudinal normal strain formulation;

$$\epsilon = w' - v + \frac{1}{2}(v')^2 - y\frac{v''}{R}, \quad (2.3.1)$$

where ϵ is the total strain at an arbitrary point in the cross section, $w = \hat{w}/R$, $v = \hat{v}/R$, \hat{w} and \hat{v} are the axial and radial displacements respectively, y is the vertical coordinate of the point, R is the arch radius, $(\)' = d(\)/d\theta$, $(\)'' = d^2(\)/d\theta^2$ and θ is the angular coordinate. The third term of Equation (2.3.1) accounts for geometric non-linearity. Energy methods were employed to derive the non-linear equilibrium and buckling equilibrium equations, for both pinned-ended and fixed boundary conditions. For the case of a uniform radial load, the principle of virtual work requires that;

$$\delta\Pi = \int_V \sigma\delta\epsilon dV - \int_{-\Theta}^{\Theta} qR^2\delta v d\theta = 0, \quad \forall \delta v, \delta v', \delta v'', \delta w, \delta w' \quad (2.3.2)$$

where V is the volume of the arch, Θ is half the included angle and $\delta v, \delta v', \delta v'', \delta w$ and $\delta w'$ are kinematically admissible variations of displacements. By integrating Equation (2.3.2) by parts, the non-linear equations of equilibrium for a shallow arch are derived;

$$N' = 0, \quad (2.3.3)$$

$$-M'' + NRv'' + NR - qR^2 = 0, \quad (2.3.4)$$

where N is the axial force and M the bending moment. Buckling equilibrium equations

were subsequently derived by performing the second variation of the potential energy function. The critical axial loads for anti-symmetric buckling was obtained as;

$$N_p = \frac{\pi^2 EI}{(S/2)^2} \text{ for pinned ends, } N_p = \frac{(1.4303\pi)^2 EI}{(S/2)^2} \text{ for fixed ends.} \quad (2.3.5)$$

The resulting closed-form and approximate solutions for the elastic buckling loads were verified via FE analysis. Additionally, criteria for classifying buckling behaviour was provided based on arch slenderness and arch rise-to-span ratio. These two studies analytically proved that classical buckling solutions are valid only for deep arches. Building on this, Bradford et al. [40] investigated the generalised case of a central concentrated load Q . For this case, the potential energy function becomes;

$$\int_V \sigma \delta \epsilon \, dV - \frac{Q}{2} \delta v_0 = 0, \quad \forall \delta v, \delta v', \delta v'', \delta w, \delta w'. \quad (2.3.6)$$

which upon integration over half the larch length gives the following non-linear equilibrium equations;

$$N' = 0, \quad (2.3.7)$$

$$-M'' + NR(1 + v'') = 0. \quad (2.3.8)$$

Analytical solutions were then obtained using energy methods for the anti-symmetric bifurcation and symmetric snap-through buckling modes for pin-ended and fixed shallow arches. Approximations for the symmetric buckling loads of fixed non-shallow arches and for the anti-symmetric buckling loads of pinned arches were also presented and verified via FE analysis. It was found that symmetric buckling dominates fixed arches, and the existence of bifurcation buckling is not a sufficient condition for its occurrence [29, 40]. Rubin [41] applied the theory of a Cosserat Point to the elastic buckling problem of a circular fixed arch subject to a central concentrated load. It was shown that the deformations and critical loads can be accurately predicted for elastic arches using the aforementioned theory, as existing test results covering a range of geometries

were found to be in excellent agreement. Furthermore, it was shown that buckling loads are highly influenced by variations in arch thickness.

Hodges [42] analysed the in-plane deformation and buckling behaviour of deep circular arches subjected to a distributed load acting normal to the reference line of the deformed axis, a close representation of hydrostatic loading. A geometrically exact theory was adopted for the description of non-linear strains. The in-plane stability of circular arches under hydrostatic loading and uniformly distributed loading directed towards the arch center was studied by Simitse and Hodges [3]. Gengshu et al. [43] investigated buckling of deep circular arches under constant-directed uniformly distributed radial load. Non-linear equilibrium equations were derived based on the principle of virtual work while considering the non-linear effects of longitudinal, shear and transverse stresses in addition to pre-buckling deformations. Buckling equations were obtained through linearisation and new solution for the anti-symmetric buckling load of a simply-supported arch was developed. The shear forces, bending moments and pre-buckling deformations were found not to have a significant impact on the buckling loads of deep arches. These results were compared to those obtained by other researchers [17,18,21,30,37,42,44,45]. Variations among solutions were attributed to contrasting stress and strain formulations and the use of different analysis methodologies. Furthermore, the commonly adopted axial in-extensibility assumption was examined and found to violate axial equilibrium, with valid applicability only in the case of hydrostatic loading. Although shear effects were incorporated into the model developed in [43], displacements associated with shear were not. Attard et al. [46] developed a finite strain formulation for the in-plane buckling analysis of elastic deep circular arches that included the effects of shear deformations. Timoshenko beam theory was adopted for the incorporation of shear deformations and a hyper-elastic constitutive equation was employed for the stress-strain description. Closed-form buckling solutions were developed and verified with existing results in the literature and by FE analysis. The authors extended this study to nu-

merically investigate the effect of shear deformations on the buckling and post-buckling behaviour of circular arches with varied loading and boundary conditions [47]. In addition to the slenderness ratio and included angle, the axial-to-shear rigidity ratio was found to influence the buckling behaviour. The critical loads decreased with an increase of axial-to-shear rigidity ratio. Furthermore, shear deformations were found to significantly effect the buckling loads and modes. Zhu et al. [48] conducted a similar study for funicular arches.

The in-plane elastic stability of shallow pin-ended parabolic arches under vertically distributed loads were analysed by Moon et al. [49]. A generic non-linear equilibrium equation was adopted in order to derive the load-displacement relationship, which was used to determine the thresholds of different buckling modes in terms of the dimensionless rise parameter. The critical load for symmetric buckling was determined using the equilibrium equation and an assumed shape of the buckling form. The results were verified using FE analysis and found to be in good agreement. However, inaccuracies occurred at interaction buckling, that is at threshold boundaries. The in-plane elastic stability of a fixed parabolic arch was investigated by Cai et al. [50]. Analytical solutions for the symmetric limit point and anti-symmetric bifurcations buckling loads were obtained using the principle of virtual work. A cable system was suggested to increase the buckling loads which increased in effectiveness with slenderness ratio. Recently, Bradford et al. [51] examined the accuracy of the common simplifying assumption, adopted by many researchers [49,50,52–55] when analysing stability of parabolic arches, that the derivative of the vertical coordinate with respect to the horizontal $(dy/dz)^2 \ll 1$. The analytical solutions for the elastic in-plane buckling of pin-ended and fixed parabolic arches produced via this assumption were compared with FE results. The aforementioned assumption was found applicable only in the case of extremely shallow parabolic arches, specifically when the rise-to-span ratio $f/l < 0.08$. The critical buckling loads are overestimated for greater rise-to-span ratios and the errors increase with rise-to-

span ratio. The authors concluded that the effect of the simplifying assumption on the in-plane buckling analyses of high arch arches and on flexural-torsional buckling behaviour requires further investigation.

Arch structures can be realistically modelled by horizontal springs at the supports which replicate the behaviour of typical engineering foundations such as rock [52] or adjacent structures [56]. Shallow arches experience high levels of compressive force which results in large horizontal reactions (thrust) at the supports causing relative movement in the embedded foundation. The in-plane elastic stability of shallow parabolic arches subject to uniform vertical loading and supported by elastic springs was studied in [52]. Accounting for pre-buckling deformations, a non-linear buckling analysis was performed which provided accurate closed-form solutions for critical loads causing snap-through and bifurcation buckling. The elastic springs significantly influenced both the buckling load and the parameters determining buckling mode. A decrease in spring stiffness reduces the critical load and increases the modified slenderness for buckling mode characterisation. Critical load for a tied-arch was also determined and the tie stiffness that delineates buckling and stability was provided. The companion paper [57] experimentally validated the analytical solutions. Two shallow reinforced concrete arches were loaded until failure in a short time frame to avoid the viscoelastic effects of creep and shrinkage. Pi et al. [56] analytically investigated non-linear behaviour and in-plane buckling of elastically supported circular arches subjected to uniformly distributed radial loads. As with the study by Bradford et al. [52] for parabolic arches, it was found that critical loads decreased with increasing flexibility of the elastic restraints, and that the criteria delineating between buckling modes was influenced by stiffness of the elastic end supports.

Supporting action provided by foundations or adjacent structures may also be modelled as elastic rotational end restraints. Pi et al. [58] studied the in-plane stability boundaries

for a pin-ended circular arch under a central concentrated load with elastic rotational end restraints. It was found that the stiffness of the rotational restraints influence the buckling loads and the buckling and post-buckling behaviour. The critical loads increase with the stiffness of rotational restraints, and become that for a pin-ended arch when rotational stiffness is zero, and that for a fixed-ended arch for an infinitely stiff restraint. Furthermore, the slenderness parameter delineating between buckling modes increases with the stiffness of the rotational restraint. The buckling of these arches under uniform radial loading was analysed by Pi and Bradford [59] who derived buckling loads, limit points and the post-buckling equilibrium paths. Kiss [60] furthered these studies by presenting an analysis of rotationally restrained shallow circular arches under concentrated loads and arbitrary distributed loads, while accounting for cross-section heterogeneity. Pi et al. [61, 62] studied the in-plane buckling of circular arches subjected to central concentrated loads with unequal rotational end restraints. The equilibrium equations were derived using the theory of stationary potential energy. The non-linear behaviours were observed to be of greater complexity when compared to the cases with equal rotational end restraints. Moreover, it was found that arches with unequal rotational restraints cannot buckle in a bifurcation mode, as is typical in arches with symmetrical supports, and that failure only occurs in a limit point stability mode.

The in-plane stability of arches with supports that stiffen under compression have been investigated [54, 63, 64]. Plaut [63] studied the in-plane stability of sinusoidal arches under uniformly distributed load. The arch ends were immovable and rotationally restrained with elastic springs. The stiffness of the springs increased with the distributed load. Additionally, the case of unequal spring stiffness was explored. However, pre-buckling deformations were not incorporated in the analysis. This was done by Cai and Feng [54] in their buckling analysis of shallow parabolic arches subject vertically distributed loading. As is to be expected, buckling loads were sensitive to spring stiffness

and were found to increase with initial stiffness and stiffening rate. This effect being more significant in relation to anti-symmetric buckling. The authors extended this study to investigate the centrally loaded parabolic arch in [64].

2.3.2 Out-of-plane stability

In addition to the possibility of in-plane stability loss, an arch may suddenly displace laterally and twist out of plane when subject to in-plane bending and/or compression in a flexural-torsional type buckling mode [65], see Figure 2.1. Classic studies investigating elastic flexural-torsional buckling of arches include the work of Timoshenko and Gere [17], who developed closed form solutions for simply supported arches of rectangular cross section under uniform compression and bending, and Vlasov [18] who extended Timoshenko and Gere's study to mono-symmetric cross sections. Since these works, many researchers have investigated elastic flexural-torsional buckling of arches [2, 37, 44, 45, 66–68]. As with in-plane stability analysis, out-of-plane buckling problems have been investigated using two methods which include the static equilibrium and energy methods, adopted in [17, 18] and [2, 17, 37, 44, 45, 66–68] respectively. Critical reviews of these studies were conducted by Papangelis and Trahair [44] and Kang and Yoo [37]. Therefore the proceeding discussion will focus on research conducted after this time.

Pi et al. [65] investigated elastic flexural-torsional buckling of circular arches when subjected to uniform bending and uniform compression, caused by hydrostatic loads or distributed radial loads directed to the arch center, using both energy and static equilibrium methods. Particular emphasis was provided to the discrepancies found in existing solutions [2, 17, 18, 37, 44, 45, 66, 67] for the buckling moment in arches under uniform bending. The contrasting solutions available in the literature were attributed

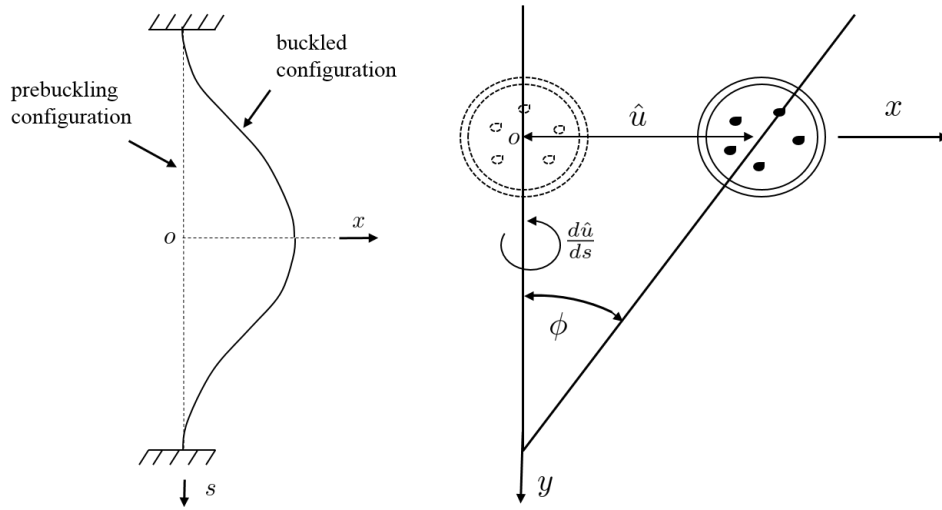


Figure 2.1: Flexural-torsional buckling of CFST arch

to the use of the analogy of curved members to straight members, which neglects certain coupling terms, and due to the varying derivations of longitudinal and uniform torsional shear strains. The lateral components of hydrostatic loads were found to increase the buckling loads of arches in uniform compression. These results were initially questioned on the basis that hydrostatic, or follower forces, are non-conservative. This concern was addressed in [69] and will not be discussed further. For further studies conducted on the elastic flexural-torsional buckling of arches subjected to hydrostatic pressure, see [70]. Furthermore, it was concluded in [65] that only first-order buckling deformations are required in the use of static equilibrium approaches, whilst energy methods require the use of correct non-linear second-order strains.

The aforementioned studies focused primarily on the stability of simply-supported arches. The lack of research on the lateral buckling of fixed arches motivated Pi and Bradford [71] and Bradford and Pi [72] to their development. Using energy methods, the authors developed closed-form solutions for the flexural-torsional buckling of circular arches under uniform bending and compression. The potential energy of an elastic

arch under uniform bending in a flexural-torsional buckled state was expressed as;

$$\Pi = \int_V \frac{1}{2} (E\epsilon_{ss}^2 + G\gamma_x^2 + G\gamma_y^2) dV - \sum_{i=1}^2 M_i\theta_i. \quad (2.3.9)$$

where ϵ_{ss} is the longitudinal normal strain, γ_x and γ_y are the shear strains, G is the shear modulus, M_1 and M_2 are the end moments and θ_1 and θ_2 are the rotation conjugates of the end moments. The buckling moment can then be derived by setting the second variation of the potential energy function to zero for all possible perturbations of displacements. It was found that increasing the included angle of a fixed arch under uniform positive bending results in an increase of the first mode critical moment, which contrasts the reduction in second mode buckling moment observed in pinned arches. This effect increases with slenderness. When subjected to negative moment, laterally fixed and pinned arches show an increase buckling moment with included angle. A complexity arising in the analysis of the flexural-torsional buckling of fixed arches is the accurate prediction of the buckling shape [73]. Dou et al. [73] studied the elastic flexural-torsional buckling mode shapes of fixed arches under uniform compression and bending using FE analysis in conjunction with an eigenvalue analysis. The authors derived analytical solutions for the flexural-torsional buckling loads of fixed arches and proposed simplified approximate solutions. It was found that by increasing the rise-to-span ratio, the buckling shapes of fixed arches become more convoluted than beams and shallow arches thus requiring more terms in the Fourier trigonometric series describing the buckling shape. Moreover, the effective length approach, commonly adopted for the buckling analysis of columns, was determined to be inaccurate for arches.

All of the studies mentioned so far have focused on arches featuring constant curvature, typically circular. Very limited research has been conducted on the flexural-torsional buckling of arches with a varying curvature, such as parabolic arches. Research in this area includes the work of Tokarz and Sandhu [74], Tufekci and Dogruer [75] and Moon

et al. [76]. Tokarz and Sandhu [74] derived buckling equations for pin-ended and fixed parabolic arches subject to uniformly distributed loading. Tufekci and Dogruer [75] studied the out-of-plane buckling of arches with varying curvature and cross section. Moon et al. [76] derived buckling equations for arches with varying curvatures subject to uniform compression and bending, and used these to determine the buckling loads for parabolic arches. The buckling loads for circular and parabolic arches are similar for low rise-to-span ratios, however diverge at higher rise-to-span ratios.

Arches are commonly connected with other structural members which provide restraining actions, consequently influencing lateral buckling resistance [77, 78]. When the restraining members are not closely spaced, they may be considered as discrete restraints, resisting deformations at the connection points between the arch and the member. Bradford and Pi [77] studied the effects of discrete elastic restraints located at the arch crown on the buckling loads of arches in uniform compression and bending. The effectiveness of the lateral translational restraints were found to be greater in arches than in columns when under uniform compression. Similarly, the effect of rotational restraints during uniform bending are more significant in arches than in beams. Discrete restraints may completely prevent buckling deformations at the point at which they act, if completely rigid. Rigid restraints fragment the arch into individual segments joined at the points of restraint. These arch sections may laterally buckle if the length between elastic restraints is large [79]. The adjoining segments however provide a form of elastic restraint at the ends of the unsupported segment, resulting in an increased buckling moment.

Guo et al. [79] studied the out-of-plane elastic buckling of circular arch segments of doubly symmetric cross-section supported with elastic end restraints. Approximate out-of-plane elastic buckling loads were derived for arch segments featuring elastic rotational and/or warping restraints of equal and unequal magnitudes. The threshold stiffness for

discrete lateral braces, that is the stiffness required to prevent lateral buckling, was investigated by Guo et al. [80], where analytical solutions were derived for circular steel arches under uniform compression. The minimum number of restraints required and maximum arch segment spans were determined. Connecting members may also provide continuous buckling restraint to an arch. The behaviour and elastic out-of-plane stability of arches continuously restrained were studied by Pi and Bradford [78]. Continuous elastic restraints were found to significantly influence the flexural-torsional buckling behaviour. The authors obtained closed-form solutions using energy methods for the flexural-torsional buckling moments and buckling loads for arches subjected to uniform bending and compression respectively. Torsional buckling moments were obtained for both bending and compressive arches. The buckling modes were found to be highly sensitive to the properties and types of restraint. For a greater level of discussion on buckling modes dependence on restraints, see [78].

In the previously discussed studies on the out-of-plane stability of arches, classical buckling method was used to obtain the critical load, thus the effects of in-plane pre-buckling deformations were ignored. In-plane pre-buckling deformations alter the curvature of an arch, which significantly influences the out-of-plane buckling resistance [81]. The effect of pre-buckling deformations on the elastic lateral-torsional buckling of simply supported arches subjected to uniform bending were studied in [66,67,81]. To consider prebuckling deformations, the potential energy function is generalised as (assuming uniform bending);

$$\Pi = \int_V \frac{1}{2} (E\epsilon_{ss}^2 + G\gamma_x^2 + G\gamma_y^2) + \sigma_0\epsilon_{ss,0} dV - \sum_{i=1}^2 M_i\theta_i. \quad (2.3.10)$$

where σ_0 and $\epsilon_{ss,0}$ denote the constant prebuckling longitudinal stress and strain. In these works, the in-plane pre-buckling deformations were found to increase the moments causing lateral instability. Furthermore, Pi et al. [81] discovered that incorporating pre-

buckling deformations in stability analyses allows torsional buckling to occur, in the case when lateral displacements are fully restrained. As the lateral buckling behaviour of fixed arches differs from that of simply-supported arches, the pre-buckling effects on buckling of fixed arches cannot be assumed the same as for pinned arches [82]. Under uniform positive bending, the pre-buckling deformations reduce the moments causing lateral instability in fixed arches, contrasting the increase observed in pinned arches [82]. These effects are magnified with an increasing included angle and out-of-plane slenderness ratio. When an arch is subjected to negative bending, the pre-buckling deformations cause a reduction in critical moment when the included arch angle is small. However, an increase in buckling moment occurs when the included angle exceeds a specific value and continues to rise with an increasing included angle. For a greater level of discussion regarding the effects of pre-buckling deformations on the flexural-torsional buckling of fixed arches, see [82]. The effects of in-plane pre-buckling deformations on the elastic lateral stability of arches are significant and thus cannot be ignored. Although researchers and designers may adopt a conservative approach and ignore them due to the resulting increase in buckling moment in pinned arches, particular care should be taken as torsional buckling is still possible, and a decrease in buckling moment can occur in fixed arches.

The influence of pre-buckling deformations on the flexural-torsional buckling behaviour of arches under uniformly distributed radial loads has been researched [83–85]. Pi and Bradford [83] generated a three-dimensional curved beam FE model for the numerical determination of flexural-torsional buckling loads and post-buckling analysis of circular thin-walled simply-supported shallow arches. Analytical solutions for arches subjected to the same conditions were produced by Pi et al. [84]. In these studies, it was found that the flexural-torsional buckling loads may be underestimated if in-plane pre-buckling behaviour is ignored [83, 84]. Generalisations to in-plane fixed supports and variable load height was made by Bradford and Pi [85]. The use of in-plane fixed connections

greatly increase the lateral buckling load of the arch. The height of load application also significantly influences stability boundaries.

Arches under a central concentrated load experience combined axial compression and bending moment, which are dependent on arch slenderness and included angle and vary throughout the length of the arch [86]. The buckling analysis of such arches is complicated and highly dependent on pre-buckling stresses. Pi et al. [86] developed the first analytical solutions to the elastic lateral-torsional buckling problem of a circular arch subjected to a central concentrated load by using the principle of virtual work and the Rayleigh-Ritz method. The in-plane fixed and out-of-plane pinned cases were analysed, in addition to investigating the effects of load position. As with the uniformly distributed case, both in-plane boundary conditions and load application position greatly influenced critical loads. Building on this study, Pi and Bradford [87] investigated the generalised case of rotational end restraints, where the sensitive relationship between buckling load and rotational restraint stiffness was analytically derived. The results for both studies [86,87] were verified by FE analysis and a curved beam element code developed by the authors in [88].

2.4 Inelastic buckling of arches

The in-plane failure modes of arches consist of buckling of slender arches, and the plastic collapse of stocky arches. Generally, in-plane failure will involve an interaction between stability loss and material yielding, which is governed by the arch's loading and geometrical configuration, residual stresses and geometric imperfections [89]. Although research on the inelastic buckling and strength of arches is less comprehensive than elastic buckling, the subject has been explored in several studies.

2.4.1 In-plane stability

Mirmiran and Amde [90] studied inelastic buckling and post-buckling of pre-stressed homogeneous and sandwich using a non-linear FE model. Non-linear inelastic analysis of in-plane buckling and strength of circular steel I-section arches subjected to various loading cases was numerically investigated by Pi and Trahair [91]. The influence of initial crookedness, rise-to-span ratio, residual stresses, and ratio of dead load to total load on the behaviour, stability and strength of steel arches were analysed. Moon et al. [92] conducted an inelastic buckling analysis of parabolic arches for various loading cases and proposed new design methodologies.

Pi and Trahair [93] developed a non-linear FE model to investigate the inelastic in-plane buckling of pin-ended circular shallow and deep arches in uniform compression. It was found that classical buckling theory overestimates anti-symmetric bifurcation and symmetric snap-through buckling loads of shallow arches. As a result, the use of straight beam-column interaction equations for arch design are restricted to deep arches. Furthermore, straight beam-column interaction equations assume uniform compression or bending, which may lead to conservative arch design as moment and axial force vary throughout the arch length when under transverse loads. Novel interaction equations were proposed which consider distribution of bending moment and axial compression throughout the arch length and moment redistribution for shallow and deep arches subjected to uniform compression and combined compression and bending. The authors generalised this work to fixed circular steel arches in [94]. Design equations were proposed for fixed arches under uniform compression and combined compression and bending, which consider the effects of residual stresses, initial in-plane geometric imperfections and non-uniform distributions of bending moments and axial compressive forces.

2.4.2 Out-of-plane stability

Pi and Trahair [95] investigated the out-of-plane inelastic buckling strength of circular I-section steel arches in uniform compression and bending through the development of a non-linear three dimensional FE model. In-plane curvature, included angle, initial geometric imperfections, large deformations residual stresses and material inelasticity were all considered. The effects of in-plane curvature and included angle were found to substantially influence the buckling strength of the arches. An increase in arch angle and curvature results in a decreased flexural-torsional buckling strength. Initial geometric imperfections, including crookedness and twist, also greatly influenced the strengths of arches in both uniform compression and bending. The effects of residual stresses were found prominent in compression arches and less so in bending arches. This model was extended to account for general loading scenarios including concentrated loads and uniformly distributed transverse loads by the authors in [96]. It was found that the buckling moments under central concentrated loads were generally less than for arches under a quarter point concentrated load. Similarly, buckling loads of arches subjected to uniformly distributed loading over their entire length were less than when loaded with a uniformly distributed load over half the arch. Pi and Bradford [97] conducted a similar study for fixed I-section arches subject to uniform compression, uniform bending and combined compression and bending. Design equations for pin-ended arches were deemed insufficient for use on fixed arches and hence novel design equations were proposed for fixed arches. The out-of-plane strength of high strength steel arches was analysed in [98] where design recommendation were proposed for the cases of uniform compression, uniform bending and combined compression and bending.

The inelastic flexural-torsional buckling and strength of circular steel arches with central elastic-torsional restrains was studied in [99]. Central torsional restraint were found

to increase the strength of steel arches. However, this improvement in strength reduces with decreasing arch slenderness. The stiffness of the central rotational restraint was determined to reach a threshold value at which further increases in stiffness did not strengthen the arch. Slenderness and included angle were found to be the key factors influencing the threshold stiffness. Furthermore, the threshold stiffness is less for arches that fail inelastically, then that for arches buckling elastically. Wu et al. [100] investigated the elastic and elastic-plastic buckling of fixed parabolic CFST arches and developed a novel method for predicting the in-plane strength, and Pi et al. [101] proposed design equations considering non-linear bending actions.

Pi and Bradford [102] proposed a three-dimensional curved beam element model for the non-linear elastic-plastic flexural-torsional buckling and post-buckling analysis of circular steel arches under a central concentrated which accounts for large twist rotations. The included angle, arch slenderness, torsional parameter and material yielding were found to greatly influence buckling behaviour. Stocky arches featuring low included angles fail in an elastic-plastic mode. For the case when stocky arches feature large included angles, the elastic-plastic and elastic buckling loads for pin-ended arches are identical, whilst for fixed arches, the elastic-plastic critical load is smaller than the elastic buckling load. The elastic-plastic and elastic buckling loads for slender arches are equal as the arch lose stability prematurely. The load carrying capacity decreases as the arch deforms during elastic-plastic post-buckling, while it increases during elastic post-buckling. Compressive forces relax during elastic post-buckling buckling, and when the arch is fixed at its ends, moment redistribution occurs.

A state of the art of experimental work on the flexural-torsional buckling of arches was recently provided by La Poutre et al. [103] and will thus not be recounted here. The work by La Poutre et al. [103] and experiments conducted since [104, 105] will only be discussed. In the experiments by La Poutre et al. [103], 15 roller-bent circular I-section

steel arches were loaded at the crown till flexural-torsional elastic-plastic buckling occurred. Geometric imperfections were measured prior to testing and showed large variability. All arches featured subtended angle between 90° and 180° . At approximately 60% of the ultimate load, the arches began exhibiting non-linear behaviour. When approaching the ultimate load, sections of the arch showed significant deformations, twists and yielding. Dou et al. [104] experimentally investigated the flexural-torsional buckling resistance of in-plane pinned and out-of-plane semi-restrained circular steel arches. Three arches were tested; the first arch consisted of a rise-to span ratio of 0.15 and a radius of 5.45 meters, while the second and third arches featured rise-to span ratios of 0.3 and radii of 3.4 meters. The first and second arches were loaded symmetrically with three point loads. Two point loads were applied to the third arch in an asymmetric fashion. All arches failed in and out-of-plane mode in an asymmetric S-shape. The geometric imperfections, out-of-plane boundary conditions and loading conditions were found to greatly influence the buckling modes and loads. Further experimental work was conducted by Guo et al. [105] to assess the effects of initial geometric imperfections and non-symmetric loading on the lateral inelastic buckling strength of fully fixed steel arches. Four circular I-section arches were tested, each featuring a span of 6 meters and a rise-to-span ratio of 0.3. Two of the arches were loaded with three point loads in a symmetric fashion, whilst the remaining two were subjected to two point loads asymmetrically. Each arch featured varying initial out-of-plane imperfections. The loads were applied monotonically and removed once the arches reached their out-of-plane inelastic strength. Initial geometric imperfections were found to reduce buckling strength and influence inelastic buckling modes. Furthermore, asymmetrically loaded arches featured lower out-of-plane strengths when compared to their symmetrically loaded counterparts.

2.5 Thermal buckling of arches

Thermal loads may induce stability loss of important load bearing elements subsequently causing structural collapse. Research conducted on thermal buckling of steel and FGM arches will now be discussed.

2.5.1 In-plane stability

The in-plane thermoelastic behaviour of a circular steel arch subjected to a uniform temperature field supported by longitudinal elastic springs attached to end rollers was studied by Bradford [106]. Consideration of a uniform thermal strain ϵ_{th} results in the following definition of non-linear longitudinal strain;

$$\epsilon = \frac{\sigma}{E} + \epsilon_{th} = w' - v + \frac{1}{2}(v')^2 - y\frac{v''}{R}, \quad (2.5.1)$$

The thermal strain is assumed constant and therefore vanishes in the potential energy function. Therefore, the same non-linear pre-buckling and buckling equilibrium equations are derived as when elevated temperatures are not considered. The changes are seen in the constitutive material relations for axial force, which is defined as;

$$N = - \int_A \sigma dA = EA \left(\epsilon_{th} - w' + v - \frac{1}{2}(v')^2 \right). \quad (2.5.2)$$

The authors found that steel arches deflect upwards with increasing temperature, see Figure 2.2, and that the end-restrained axial expansion caused by thermal straining resulted in equal and opposite support reactions. Compressive forces and bending moments are produced due to this restrained thermal expansion and the arch experiences

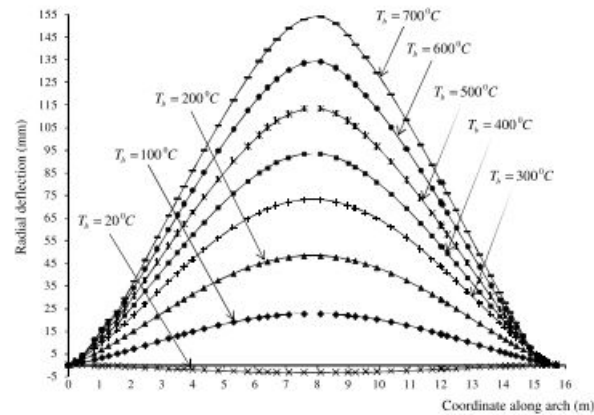


Figure 2.2: Effect of temperature on the radial deflections of a steel arch [109]

a state of compressive stress. However, as the arch displaces upwards, its length subsequently increases resulting in the formation of tensile strains [107], which may reduce axial compressive stress. Furthermore, thermoelastic buckling of arches was determined to be possible only under the following two scenarios; when the arch was completely flat and thus behaves as a column, or when the arch was pinned at its ends, obtained when the stiffness of elastic springs approach infinity. This study was extended to the tubular steel arch with rotational end restraints by Pi and Bradford [108]. In this paper, an approximate thermoelastic analysis of a tubular steel arch under uniform thermal loading was conducted assuming a constant axial compressive force throughout the arch length. This simplifying assumption was found to yield accurate results when compared with an exact analysis. A linear analysis of pin-ended and fixed circular steel arches under uniform thermal loading was presented by Pi and Bradford [107]. Thermal stresses and strains in shallow arches were observed to be substantially greater than those in deep arches. Additionally, the authors conducted a classical buckling analysis for shallow arches and found that violation of serviceability criteria or material yielding is likely to precede buckling due to the high temperatures required to induce stability loss.

Symmetric or anti-symmetric buckling may be triggered in arches when subjected to combined mechanical and thermal loading [4,55,110]. Thermal loads increase the axial

force produced by the mechanical load and the magnitude of displacements and bending moments, which are typically reverse in direction. Cai et al. [55] performed a thermo-elastic stability analysis of steel parabolic arches subject to central concentrated loads and elevated temperatures. Critical loads for symmetric and anti-symmetric buckling and criteria delineating buckling modes were analytically derived. The buckling loads were significantly effected by thermal loading, displaying an increase with temperature in an approximately linear fashion. Additionally, the influence of temperature on the critical load increases with greater arch span-rise ratio, i.e temperature effects are more pronounced in shallow arches. This result was also obtained in the study by Pi and Bradford [4] where an elastic circular arch was subjected to a uniformly distributed radial load and uniform temperature field. The derived critical axial forces for anti-symmetric buckling were the same as Equations (2.3.5). This is due to the uniform thermal strain not influencing the equilibrium and buckling equilibrium equations as discussed earlier. However, the anti-symmetric buckling loads are impacted by temperature level due to the constitute material equation, see Equation (2.5.2). The non-linear behaviour and stability boundaries of crown-pinned arches are similarly effected by the coupling of thermal and mechanical loading [111]. For this case, the utilisation of linear analysis results in the temperature field causing no additional stresses and strains in the arch. The importance of non-linear methods in the analysis of crown-pinned arches is thus emphasized. Furthermore, crown-pinned arches may only buckle in a symmetric fashion.

In reality, arch structures would experience a temperature distribution or gradient through the cross section in a elevated temperature environment. This typically occurs in building and tunnel fires as the concave side of the arch heats is exposed and therefore heats more rapidly than the convex side. Temperature gradients result in both axial expansion and curvature changes in the arch. Assuming a linear temperature gradient through the cross-section, the constitutive material relations for an elastic

material become;

$$N = - \int_A \sigma \, dA = EA \left(\epsilon_{th,ave} - w' + v - \frac{1}{2}(v')^2 \right). \quad (2.5.3)$$

$$M = \int_A \sigma y \, dA = -EI_x \left(\frac{v''}{R} + \frac{\alpha \Delta T}{h} \right). \quad (2.5.4)$$

where $\epsilon_{th,ave}$ is the average thermal strain in the cross-section, α is the coefficient of thermal expansion and ΔT is the temperature difference between the extremes of the cross-section. A study on the non-linear thermoelastic stability of shallow steel circular arches with pinned ends subjected to thermal gradients was conducted by Pi and Bradford [112]. The authors discovered that arches may experience snap-through or bifurcation buckling when subjected to a thermal gradient, due to the increasing bending and axial compression caused by curvature changes and axial expansion respectively. The bending actions produced by the temperature gradients are complex [112], due to the resulting opposing deformations. The bending actions created by end reactions cause the arch to deflect in the convex direction, whilst bending produced by temperature differential result in concave deflections. Furthermore, it was determined that anti-symmetric buckling was the dominant failure mode and symmetric buckling could only occur for slender shallow arches. The non-linear thermoelastic stability of shallow steel parabolic arches subject to combined mechanical and thermal loading, in the form of thermal gradients and uniformly distributed loading, was investigated by Cai et al. [113]. Pin-ended and rotationally restrained arches via elastic springs were considered. As with previously mentioned studies, the effects of temperature variations significantly effected the critical loads for symmetric and anti-symmetric buckling and the post-buckled behaviour. It was found the critical loads increased with an increasing uniform temperature field. Conversely, the critical loads decreased with an increasing temperature gradient. The effects of uniform temperature fields increased with the rotational spring stiffness. However this increase in spring stiffness caused a reduction in the effects of temperature gradients. Bradford [53] conducted a non-linear thermoe-

lastic analysis of a long-span shallow steel arch subjected to fire loading. The arch featured elastically restrained pinned ends and was supported by a cable tie. The analysis permitted any type of temperature distribution through the cross-section depth, however was assumed constant along the length of the arch. The effect of spring and cable tie stiffness were found to greatly influence the response of the arch to thermal loading. It was also found that symmetric buckling was the dominant buckling mode, and anti-symmetric bifurcation buckling was highly unlikely.

Heidarpour et al. [114] proposed a generic mechanical based model for the non-linear thermoelastic analysis of steel circular arches with translational and rotational elastic restraints acted on by uniformly distributed loads and non-uniform elevated temperatures. The model considered geometrical non-linearities, and was verified using FE analysis. The authors extended the model in [109] to incorporate inelastic behaviour. Heidarpour et al. [115] developed an analytical model to analyse the non-linear thermoelastic behaviour of a composite steel-concrete arch subject to the same loading and boundary conditions as the aforementioned studies. Partial interaction and variation of axial force were considered, however, the effects of concrete creep and shrinkage were not. These three models were not developed for analysis of stability.

A non-linear thermoelastic and buckling analysis was conducted for functionally graded material (FGM) shallow arches by Asgari et al. [116]. Using the method of virtual work and accounting for non-linear pre-buckling deformations, the authors presented analytical solutions for pin-ended FGM arches subjected to a uniform temperature field. The effect of various parameters on the critical buckling were numerically studied which included the power-law index of the constituent volume fraction, included arch angle and length-thickness ratio. The critical temperature was found to be sensitive to the power-law index and featured a non-uniform relationship. Critical buckling temperatures generally increased with included angle and decreased with an increasing

length-thickness ratio. The critical temperatures for arches featuring a smaller length-thickness ratio were found to be extremely high, thus it was concluded that material failure will likely precede stability loss. Linear thermal gradients were applied to shallow circular FGM arches in the work of Asgari and Eslami [117]. Closed form solutions for the critical buckling temperatures were derived using the adjacent equilibrium method. The effect of thermal gradients and mechanical loading on the stability of FGM arches have also been the subject of recent research [118]. Bateni and Eslami [118] studied the stability of pin-ended shallow FGM arches subjected to uniformly distributed loads, concentrated loads and a linear temperature gradient. The bifurcation buckling loads increases with thermal gradient.

Song and Li [119] analysed the in-plane stability of FGM shallow arches with fixed ends subjected to uniformly distributed follower force and elevated temperature. Anti-symmetric bifurcation buckling was observed to precede symmetric snap-through buckling and hence defined as the governing failure mode. A non-linear analysis of FGM shallow arches with pinned ends supported on a non-linear elastic Pasternak foundation and subjected to uniformly distributed lateral pressure and elevated temperatures was conducted by Babaei et al. [120]. The third-order deformation of von Karman type was employed to derive the non-linear equilibrium equations. Analytical solutions were formulated by employing a two-step perturbation technique for the maximum deflection. The authors generalised the study to fixed-ends in [121]. Li et al. [122] conducted an elastic anti-symmetric buckling analysis on FGM shallow arches when under combined in-plane pressures and uniform thermal loads. The obtained analytical solutions for the buckling loads were validated using FE analysis. It was found that thermal loads induced upward displacements consequently increasing the elastic buckling strength, whilst simultaneously decreasing the critical load due to a deteriorating elastic modulus. This response aligns with that of homogeneous arches such as steel. Reversing the material distribution in FGM arches gives inverted or optimised FGM arches, which

show a significant increase in buckling strength for the same volume portion of the material constituents [123].

The stability of a FGM shallow arch rigidly confined and subjected to a external pressure was analytically and numerically studied by Li et al [124]. Confinement effects were found to substantially increase buckling pressures. Conversely, a reduction in buckling strength was obtained when increasing the volume fraction exponent. Yang et al. [125] analysed in-plane stability of shallow functionally graded graphene reinforced composite arches with fixed ends and subjected to mechanical and thermal loading. The arches were composed of multiple graphene platelet reinforced composite (GPLRC) layers. The principle of virtual work was adopted to obtain the non-linear equilibrium equations and the Halpin-Tsai micromechanics model was adopted for materials properties of the GPLRC layer. Analytical solutions were formulated for the limit point and bifurcations buckling loads, and it was demonstrated that great increases in buckling resistance can be achieved by increasing graphene platelets filler content.

2.5.2 Out-of plane stability

Upon reaching a critical temperature, an arch may buckle laterally in a flexural-torsional mode due to the increased axial compression and bending moments. However, this phenomenon has received far less research attention when compared to in-plane thermo-elastic buckling. The work by Heidarpour et al. [126] appears to be the only work on this subject. Adopting the non-discretisation mechanical based method developed in [114] to model the non-linear pre-buckling behaviour, the critical temperatures causing elastic flexural-torsional buckling in circular steel arches with doubly symmetric I-shape cross-sections were determined using classical buckling theory. A parametric study was

then performed to investigate the effect of multiple parameters on critical buckling temperatures which included the included angle, slenderness ratio and imposed load for pinned, fixed and spring supported arches. Similarly to in-plane stability, an increase in included angle and stockiness of the member resulted in a higher magnitude of buckling temperature. In addition, the influence of the ratio of the temperature in the top fibre of the cross section to the temperature in the bottom fibre on the critical temperatures was analysed and deemed significant. Conversely, the size of external load was found to have a smaller impact on critical temperatures. Post-yield behaviour of the steel was not considered, with the yielding point determined via the von Mises' yield criterion.

2.5.3 Discussion

The effects of elevated temperatures on the behaviour and stability of steel and FGM arches have been extensively studied through analytical and numerical means. Various support conditions including pin-ended, fixed and crown-pinned arches and loading scenarios including uniform temperature fields and temperature gradients have been analysed. Although the developed analytical models have commonly been verified by FE analysis, it appears that no experimental testing has been performed. Although the large expenses associated with such experiments is recognised [126], the literature would greatly benefit from experimental data. Various assumptions made by researchers including thermoelastic behaviour could be further verified. Complex heating scenarios such as localised fires, which are difficult to model analytically, could also be performed. In addition, it is evident that studies on the thermal stability of damaged steel arches have yet to be conducted. Yang and Bradford [127] analysed the thermoelastic buckling and post-buckling of damaged steel columns. Buckling temperature was found to be substantially influenced by weakening of the column. The significance of damage on the thermal stability of steel arches is yet to be investigated.

2.6 Creep buckling of arches

The viscoelastic effects of creep and shrinkage in concrete structures have been extensively researched over the years. The phenomenon of creep buckling has however not received the same attention [128]. Time-dependent deformations can significantly reduce the long-term load carrying capacity of compression members including columns and arches, and hence must be carefully considered in engineering practice, especially when designing slender elements. Creep buckling problems can be classified into two main categories [10]: loss of stability induced by increasing deflections under sustained load, typically expressed as critical buckling time, and instability caused by instantaneous overload. The proceeding discussion reviews studies on time-dependant stability of concrete and CFST arches. Additionally, relevant research relating to creep modelling in arches is examined, with focus on the temperature dependence of creep and the subsequent effect on arch behaviour.

2.6.1 In-plane stability

Wang et al. [128] analytically and experimentally studied the long-term in-plane stability of elastically restrained shallow parabolic concrete arches subjected to sustained uniformly distributed vertical loading. The creep was modelled using the commonly adopted age-adjusted effective modulus method [129], and the time-dependant equilibrium and buckling equilibrium equations were formulated using the principle of virtual work. Therefore, the governing equations of equilibrium and constitutive material relations remain the same as those presented in Equations (2.3.3), (2.3.4) and (2.3.5), with the exception that the elastic modulus is time dependant and governed by the age-

adjusted effective modulus. Results show that concrete arches experience an increasing axial compressive force, bending moment and axial and radial displacements in time, due to creep and shrinkage strains. The changing equilibrium configuration of the arch may reach an unstable position at which symmetric or anti-symmetric buckling is possible. Furthermore, critical snap-through and bifurcation buckling loads were found to decrease with time. Experimental tests were conducted to validate the proposed analytical models. Three concrete arches were tested, with each arch featuring a 4.25 m span and rectangular cross section. All arches failed within several months due to time effects, with each arch buckling in an anti-symmetric fashion. The critical buckling times predicted by the analytical models agreed well with the experimental behaviour. Despite representing a significant structural engineering problem, the work by Wang et al. [128] appears to be the only research on stability loss due to viscoelasticity in concrete arches.

The time-dependent behaviour and stability of CFST arches have however received greater research focus in recent times [5, 130–134], with all studies belonging to the first kind of creep buckling problem - sustained loading. Bradford et al. [5] analytically studied long term in-plane behaviour of circular CFST arches, and creep buckling of deep circular CFST arches, subjected to sustained uniformly distributed loading. The creep was modelled using the age-adjusted effective modulus method. It was shown that as the concrete core deforms in time, stress redistribution occurs between the steel tube and concrete. The time-dependent deformations cause the compressive forces in the steel tube to increase, whilst the confinement provided by the steel tube decreases compression in the concrete, due to the application of tensile forces [130], see Figure 2.3. Additionally, the bending moment and radial and axial displacements significantly increase with time. The limit point and bifurcation buckling loads are also time-dependant, and may in time become equal to the sustained load. At this point in the time domain, limit point and bifurcation buckling is possible for a CFST arch.

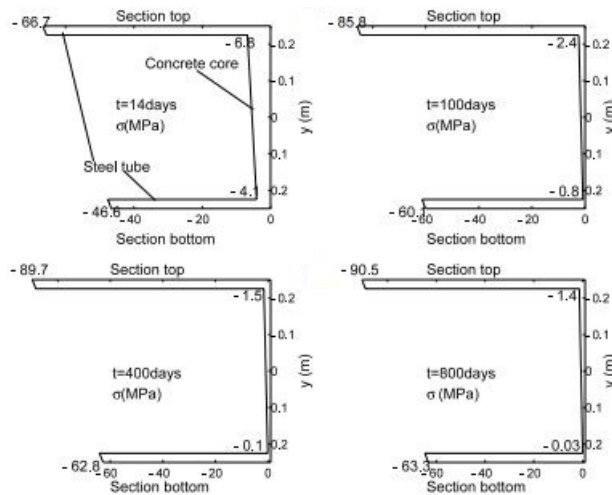


Figure 2.3: Redistribution of stress between concrete core and steel tube through time [5]

Creep buckling of shallow circular CFST arches was then the subject of analysis in the works by Pi et al. [130] and Luo et al. [131, 132] for the loading cases of uniformly distributed loads and central concentrated point loads respectively. These studies analytically investigated the significance of geometric non-linearity on the long-term response and time-dependant stability boundaries. It was found that non-linear analysis predicted greater time dependant deformations and stresses than when compared to those predicted by linear analysis. Thus, non-linear methods for the long-term analysis of shallow CFST arches are required.

The long-term behaviour and in-plane stability of crown-pinned CFST arches subject to sustained concentrated point loading were investigated by Bradford and Pi [133, 134]. In both these studies, the creep was modelled using the age-adjusted effective modulus and the long-term equilibrium equations were derived using the principle of virtual work. It was found that crown-pinned CFST arches may only buckle in time in a symmetric snap-through mode, and that geometric non-linearity substantially increases the long-term deformations, internal compressive forces and bending moments in both deep and shallow crown-pinned arches.

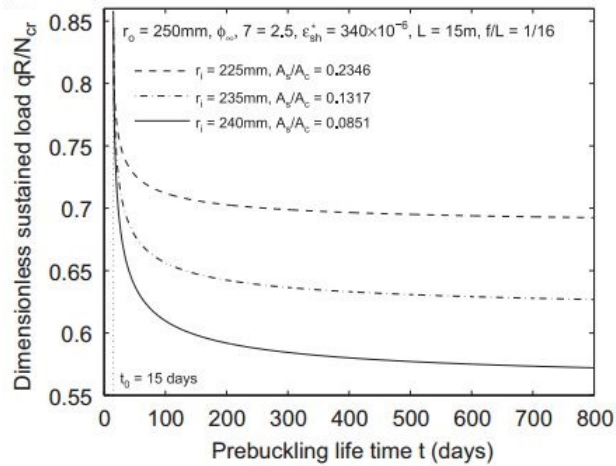


Figure 2.4: Pre-buckled life for a pin-ended CFST arch [130]

The influence of steel ratio and initial loading age on the long-term in-plane stability of CFST arches are significant [6, 130]. As is to be expected, an increase in the long-term buckling load is achieved through the increase of steel in the cross section, see Figure 2.4. Moreover, the critical load is found to decrease in a log-linear fashion when increasing the initial loading age. This result satisfies intuitive expectations as majority of deformations caused by creep and shrinkage occur within the first month for CFST elements [135], and are further influenced by the presence of loading [136]. However from the perspective of construction, the delay of load application may not be pragmatic.

2.6.2 Out-of-plane stability

In contrast to in-plane creep buckling, studies on the out-of-plane stability loss caused by viscoelastic effects in CFST arches are rare in the open literature. Jiang and Lu [137] studied the reliability and sensitivity of the out-of-plane buckling loads of CFST arches while considering creep effects using a time-integrated approach and the FE

reliability method. More recently, Geng et al. [138] developed a three-dimensional FE model to numerically investigate the effects of pre-buckling deformations induced by creep and shrinkage on the out-of-plane stability of fixed-ended parabolic CFST arches subjected to instantaneous overload. The FE model was validated by comparison to the experimental results reported by [139] for out-of-plane buckling loads of CFST arches. Through an extensive parametric study, it was found that up to a 18% reduction in out-of-plane buckling loads can be caused by creep and shrinkage. Additionally, time effects were more pronounced in arches with higher strength concretes, lower steel yield strengths and higher sustained load levels.

2.6.3 Temperature-time coupling

Temperature substantially influences the creep behaviour of concrete elements [136]. Therefore, in order to realistically model the long-term behaviour of concrete and CFST arches, temperature changes caused by typical daily and seasonal variations must be considered. No studies so far have analysed the long-term stability of concrete or CFST arches subject to altering temperature or humidity. The long-term behaviour of a crown-pinned circular CFST arch subjected to a constant temperature change was analysed by Luo et al. [140] to investigate the significance of the coupling effects between time and temperature. The temperature change was found to greatly increase the long-term deformations and internal forces in the arch. Wang et al. [141] studied the effect of non-constant temperatures on the creep behaviour of a CFST arch bridge. This was achieved through the incorporation of the micro-prestress solidification theory [142], the age-adjusted effective modulus and an average temperature history into a FE program. The Yajisha bridge in China was replicated in the program and results were verified from measurements taken of the bridge one year after construction. The results indicated that the increase in creep caused by temperature variations are not negligible. The dif-

ferences in creep deformations and stresses at midspan when considering temperature variations were found to be 9% and 7-18% respectively. These findings indicate that the long-term behaviour and stability of arches must incorporate temperature changes in order for accurate and safe results to be obtained. Significant complications however manifest when attempting to incorporate the effect of temperature into the long-term analysis of CFST arches. Temperature fields throughout the cross section due to ambient temperature and solar radiation must be accurately modelled. Fluctuating ambient temperatures and position of the sun thus require consideration.

2.6.4 Discussion

As creep significantly impacts the long-term behaviour and stability of concrete and CFST arches, accurate modelling of creep is of paramount importance. A review on creep in CFST arches was conducted by Shrestha et al. [135]. The authors indicated that although multiple creep prediction models currently exist in the literature, a robust method for modelling the time dependent behaviour of CFST arches is still in urgent requirement. For example, Jiang and Lu [6] compared the pre-buckling life of circular CFST arches when adopting two different creep laws; the simplified Arutyunyan-Maslov method and Age-adjusted effective modulus method. Differences were found between the results produced by both models. Creeping mechanics of arches are further convoluted by temperature changes, which have proven to significantly influence long-term behaviour. Thus, further research is required in creep modelling in concrete and CFST arches in order to allow accurate and safe analysis of long-term behaviour and stability. Additionally, the study by Geng et al. [138] appears to be the only research available on creep buckling of CFST arches due to instantaneous overload, for both in-plane and out-of-plane stability.

2.7 Future research

The ubiquitous use of arches in civil and structural engineering applications, in addition to their inherent complex behaviour, results in a heightened importance of accurate analysis and design practices. It is thus paramount that research on the behaviour and stability of arches continues in an attempt to develop accurate and efficient analysis methodologies which address all possible mechanical and environmental conditions, including typical and extreme events. In order to achieve such an objective, the following areas require research attention:

- The accuracy of the assumption that the derivative of the vertical coordinate with respect to the horizontal $(dy/dz)^2 \ll 1$ when analysing in-plane stability of deep parabolic arches and lateral buckling of parabolic arches requires investigation.
- Experiments on the thermal buckling of steel arches do not appear to have been conducted. Although many analytical and numerical models currently exist, the literature would greatly benefit from experimental data.
- Investigations into the thermal buckling of damaged steel arches are needed. Such damage may occur as a result of corrosion, impact or fatigue.
- Studies on the behaviour and stability of concrete and CFST arches when exposed to extreme temperatures are required. Although the behaviour of steel arches under such conditions have been thoroughly investigated, the behaviour of concrete greatly differs from that of steel during fire. The effects of elevated creep and TTS, occurring in concrete under high temperatures, on the behaviour and stability of concrete arches are not currently known.
- Research on the long-term stability of concrete and CFST arches when consid-

ering typical temperature conditions is limited. As creep is greatly influenced by temperature and temperature variations, the stable life of an arch may be overestimated if ignored.

- Out-of-plane stability loss induced by viscoelastic effects in CFST arches has not been extensively studied. More research is required on varied cross-section shapes, arch profiles and loading conditions.
- Further investigations into creep buckling of CFST arches due to instantaneous overloading are required for both in-plane and out-of-plane stability in order for the formulation of comprehensive design methodologies.

2.8 Conclusion

A state of the art report has been presented on the static in-plane and out-of-plane stability of arches which includes reviews on research investigating buckling induced by time and temperature effects. It can be concluded that despite the extensive research over many years on arch stability, they are not completely understood and still present a challenge to researchers and engineers. A high level of caution is advised when determining the in-plane and out-of-plane critical loads for arches, as they are sensitive to loading conditions, boundary supports and geometrical configuration. Non-linear methods which include the effects of in-plane pre-buckling deformations must be adopted for both the in-plane and out-of-plane stability analysis of shallow arches. Classical buckling methods may however be utilised for studies of deep arches. Assumptions regarding axial-extensibility, shear deformations and geometrical non-linearities should also be made with care.

An arch may be subjected to thermal loads during fire exposure. Elevated temperatures increase the axial compression and bending moments in a steel arch, and upon reaching a critical value, can cause symmetric snap-through or bifurcation type buckling. Thermal behaviour must therefore be considered for arches constructed in areas where fire exposure is a possibility. The performance of concrete and CFST arches during fire are however yet to be investigated.

The long-term stability of concrete and CFST arches, especially when slender, must be considered by structural designers due to the viscoelastic effects of creep and shrinkage. This problem of creep buckling is becoming more relevant due to the increasing popularity of CFST arch bridges. Despite the sensitivity of creep to temperature, the coupling effects of time and temperature on long-term stability of concrete and CFST arches have not yet been investigated and thus require research attention.

Chapter 3

Basic creep in concrete at elevated temperatures

3.1 Introduction

In this chapter, a novel fractional viscoelastic law is developed to model basic creep in concrete at extreme elevated temperatures. The rheological model consists of two springpots placed in series; one which models linear creep strain and the other for non-linear creep which is triggered in high stress and/or temperature loading conditions. Springpots contain fractional-order of derivatives in the governing stress-strain equations in place of the first-order derivative of classical Newtonian fluids (dashpots). Hence, the theories of fractional calculus and fractional viscoelasticity are central to the analysis and model development presented in this chapter. Two model parame-

ters for each springpot require characterization. These include the dynamic viscosity and the fractional exponent (order of derivative). This is achieved by calibrating the creep compliance function to existing experimental data of basic creep. The experimental results reported by Gillen [143] were utilised where the basic creep strain in pre-heated concrete cylinders was measured under constant stress and temperature conditions over a range of 22 °C to 649 °C for expanded shale lightweight, calcareous and siliceous aggregates. An accurate representation of creep strain is achieved which is further highlighted upon comparison to the experimental data recorded by Cruz [144]. For the case of time-varying temperature, concrete creep is governed by a variable-order fractional differential equation due to the temperature dependency of the order of differentiation. A finite difference scheme is then derived to numerically approximate the creep strain for cases of varying stress and temperature, and for when adopting two different definitions of the fractional derivative; one which considers the history of the order of differentiation and one which does not.

The power law form of the creep compliance allowed an accurate representation of creep strain to be obtained with few model parameters. Additionally, the fractional derivative-based creep law proves to be an efficient method of modelling creep strain in concrete structures for time-varying stress and/or temperature conditions. Hence, the developed model will be employed in Chapter 4 to incorporate basic creep strain in the prebuckling and in-plane stability analyses of concrete arches when subjected to mechanical and thermal loading, and in Chapter 7 to assess the significance of viscoelastic effects on the thermal response of CFST arches.

The following paper is included in this chapter;

1. Y. Bouras, D. Zorica, T.M. Atanacković and Z. Vrcelj. 2018. A non-linear thermo-

viscoelastic rheological model based on fractional derivatives for high temperature creep in concrete. *Applied Mathematical Modelling*, 55, pp.551-568.



THE NEW WAY TO DO UNI

OFFICE FOR RESEARCH TRAINING, QUALITY AND INTEGRITY

DECLARATION OF CO-AUTHORSHIP AND CO-CONTRIBUTION: PAPERS INCORPORATED IN THESIS

This declaration is to be completed for each conjointly authored publication and placed at the beginning of the thesis chapter in which the publication appears.

1. PUBLICATION DETAILS (to be completed by the candidate)

Title of Paper/Journal/Book:	A non-linear thermo-viscoelastic rheological model based on fractional derivatives for high temperature creep in concrete		
Surname:	Bouras	First name:	Yanni
Institute:	Institute for Sustainable Industries and Liveat	Candidate's Contribution (%):	55
Status:		Date:	
Accepted and in press:	<input type="checkbox"/>	Date:	
Published:	<input checked="" type="checkbox"/>	Date:	02/12/2017

2. CANDIDATE DECLARATION

I declare that the publication above meets the requirements to be included in the thesis as outlined in the HDR Policy and related Procedures – policy.vu.edu.au.

Yanni Bouras	Digitally signed by Yanni Bouras Date: 2020.02.10 15:07:34 +11'00'	10/02/2020
Signature		Date

3. CO-AUTHOR(S) DECLARATION

In the case of the above publication, the following authors contributed to the work as follows:

The undersigned certify that:

1. They meet criteria for authorship in that they have participated in the conception, execution or interpretation of at least that part of the publication in their field of expertise;
2. They take public responsibility for their part of the publication, except for the responsible author who accepts overall responsibility for the publication;

PO Box 14428, Melbourne,
Vic 8001, Australia
+61 3 9919 6100

Victoria University ABN 83776954731
CRICOS Provider No. 00124K (Melbourne),
02475D (Sydney), RTO 3113



THE NEW WAY TO DO UNI

3. There are no other authors of the publication according to these criteria;
4. Potential conflicts of interest have been disclosed to a) granting bodies, b) the editor or publisher of journals or other publications, and c) the head of the responsible academic unit; and
5. The original data will be held for at least five years from the date indicated below and is stored at the following location(s):

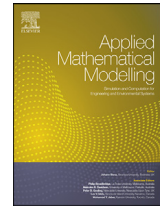
Victoria University, Footscray Park, Ballarat Road, Melbourne, VIC 3011, Australia

Name(s) of Co-Author(s)	Contribution (%)	Nature of Contribution	Signature	Date
Yanni Bouras	55	Conceived concept. Literature review. Model calibration and analysis. Writing manuscript		10/02/2020
Dusan Zorica	20	Discretization and numerical modelling		17/2/2020
Teodor Alanackovic	20	Assessing use of different fractional differential equations definitions		14/2/2020
Zora Vrceļ	5	Critical review of manuscript. Final approval of manuscript.		11/02/2020

Updated: September 2019

PO Box 14428, Melbourne,
Vic 8001, Australia
+61 3 9919 6100

Victoria University ABN 83776954731
CRICOS Provider No. 00126x (Melbourne),
02475D (Sydney), RTO 3113



A non-linear thermo-viscoelastic rheological model based on fractional derivatives for high temperature creep in concrete

Yanni Bouras^a, Dušan Zorica^{b,c}, Teodor M. Atanacković^d, Zora Vrcelj^{a,*}

^a College of Engineering and Science, Centre for Environmental Safety and Risk Engineering (CESARE), Victoria University, Melbourne, VIC, Australia

^b Mathematical Institute, Serbian Academy of Arts and Sciences, Kneza Mihaila 36, Beograd 11000, Serbia

^c Department of Physics, Faculty of Sciences, University of Novi Sad, Trg D. Obradovića 3, Novi Sad 21000, Serbia

^d Department of Mechanics, Faculty of Technical Sciences, University of Novi Sad, Trg D. Obradovića 6, Novi Sad 21000, Serbia

ARTICLE INFO

Article history:

Received 8 May 2017

Revised 20 September 2017

Accepted 15 November 2017

Available online 2 December 2017

Keywords:

Creep

Fractional derivatives

Thermo-viscoelasticity

ABSTRACT

In this paper, a novel non-linear thermo-viscoelastic rheological model based on fractional derivatives for high temperature creep in concrete is proposed. The rheological model consists of a linear springpot unit placed in series with a second springpot used for non-linear creep which activates under high stress and temperature. The model parameters which include the dynamic viscosities of the springpots and the fractional exponent are calibrated using existing experimental data of basic creep strain in concrete under constant stress and temperatures for various aggregate types. The power law form of the naturally resulting creep compliance allows an accurate representation of experimental data with the use of only a few model parameters. Furthermore, the variable-order fractional differential stress-strain equation provides a compact method for analytical and numerical modelling of basic creep under conditions of time-varying stress and temperature. In addition, applications of the proposed model to determine axial deformations in columns and transverse deflections in beams under constant and varying temperatures are demonstrated.

© 2017 Elsevier Inc. All rights reserved.

1. Introduction

The macroscopic deformations experienced in loaded concrete when subjected to a transient temperature increase include an instantaneous mechanical strain, shrinkage and drying shrinkage, thermal dilatation and transient thermal strain. In addition, a time-dependant creep strain is exhibited under constant stress, moisture and temperature conditions. The literature divides studies on basic creep at elevated temperatures into two categories; moderate elevated temperatures less than 100 °C and extreme temperatures greater than 100 °C.

At moderate elevated temperatures (< 100 °C), two processes are responsible for influencing creep in concrete. One of which is the acceleration of bond breakage which increases creep rate. Conversely, the second process decreases creep rate as the heightened temperature ages the concrete due to faster cement hydration [1]. Bažant et al. [2] extended the microprestress-solidification theory, developed in [3,4], to capture the effect of moderate temperatures on concrete creep. In addition to transient thermal strain and the drying creep effect, this model considers the duality of the

* Corresponding author.

E-mail address: zora.vrcelj@vu.edu.au (Z. Vrcelj).

temperature effect on basic creep and thus remains the most complete concrete creep model at moderate temperatures albeit numerically intensive.

Basic creep is greatly accelerated at extreme temperatures ($> 100^\circ\text{C}$) which may result in significant short term deformations [5]. In addition to bond ruptures, creep strain rate is further accelerated in this temperature range due to moisture movement and possible dehydration [1,6]; opposite to the hydration effect observed at temperatures less than 100°C . Though dehydration is typically insignificant below 400°C [1]. The basic creep of concrete at extreme temperatures has been experimentally investigated with few results existing in the literature [7–14]. Stress level, temperature, humidity content and concrete mix are the key factors governing the magnitude and nature of creep strain. Variables including age at loading, specimen size and initial compressive strength have proven to be less influential. Discrepancies however exist within available experimental data which can be attributed to non-uniform testing standards [15,16]. Consequently, the development of a constitutive creep model which accurately reflects a wide range of experimental data is convoluted. In the case of sustained mechanical loading and short-term temperature increases, transient thermal and mechanical strains dominate behaviour and greatly exceed the magnitude of basic creep, leading many authors to consider it implicitly [17] or neglect it completely [18]. However, explicit basic creep models are necessitated by conditions of coupled non-linear structural behaviour and high stresses and temperatures, despite the transient nature of the thermal load.

Multiple high temperature creep models have been proposed which can be categorized as: purely phenomenological models derived from observation of experimental data and the rate-type viscoelastic models [19]. The disadvantages associated with the former are their restriction to the experimental data utilised for model construction. Furthermore, generalizations to variable stress and temperature lead to stress-strain relations in integral form. Time-step integral creep laws require the values of stress and strain to be stored and applied in following time steps, thus storage requirements and computation times for large structures become problematic [20]. This issue of history dependence is avoided when adopting rate-type creep laws. Bazant [1,21] proposed rate-type Kelvin and Maxwell viscoelastic chains for high temperature creep in concrete. In order to achieve high levels of accuracy, a large number of elements in the chain are typically required. Complexities arise due to the multitude of material parameters to be characterised [22], ultimately requiring intensive numerical simulations and comprehensive experimental data sets. As a result, the practicality of employing viscoelastic chains in both analytical and numerical investigations is diminished.

The aforementioned disadvantages associated with viscoelastic chain models may be averted through the use of fractional calculus based viscoelastic laws. Fractional viscoelastic models are generalisations of existing viscoelastic models where the integer based order of derivative in the constitutive stress-strain equation is replaced by a fractional, or real, order. Fractional viscoelastic models, such as the fractional Kelvin-Voigt (FKV), fractional Maxwell and fractional Zener, have proven to be robust descriptors of material behaviour [23], as experimental data can be accurately reflected with a minimal number of material parameters. Papoulia et al. [24] proved that the models of fractional viscoelasticity are obtained when the number of units in a generalised viscoelastic chain approach infinity. Successful applications of fractional viscoelastic models to time-dependant behaviour of real materials in the structural and civil engineering fields include creep in rocks [25–27], foundation settlement [28] and the dynamic behaviour of bituminous binders [29] and viscous dampers [30–32]. Despite the evident power of fractional viscoelasticity, its application to time-dependent studies of concrete is limited to a few recent studies [33–36]. Barpi and Valente [33] combined a micro-mechanical model and fractional viscoelastic element to investigate crack propagation in concrete and Katicha and Flintsch [35] employed fractional viscoelastic models to characterize the time-dependent properties of asphalt concrete.

In this paper, a novel creep law is proposed based on the fractional derivative models of viscoelasticity for modelling basic creep strain in concrete at elevated temperatures. The model parameters are calibrated using existing experimental data of short-term creep in concrete of various aggregate types under constant temperature and stress levels. Two applications of the model are presented in order to demonstrate its practicality for use in analytical and numerical studies. Studies of concrete in fire and under high temperature working conditions, such as nuclear reactor vessels, represent possible applications of the model.

2. Introduction to fractional viscoelasticity

2.1. Fractional calculus definitions

Multiple definitions of the fractional derivative exist [37]. The left-sided Riemann–Liouville fractional integral of a function f of order $\alpha > 0$ is defined as

$$D_t^{-\alpha} f(t) = \frac{1}{\Gamma(\alpha)} \int_0^t (t - \tau)^{\alpha-1} f(\tau) d\tau. \quad (1)$$

The left-sided Riemann–Liouville fractional derivative of a function f of order $0 \leq \alpha \leq 1$, is given as

$$D_t^\alpha f(t) = \frac{1}{\Gamma(1 - \alpha)} D_t^1 \int_0^t \frac{f(\tau)}{(t - \tau)^\alpha} d\tau, \quad (2)$$

where Γ denotes the Gamma function defined as

$$\Gamma(\alpha) = \int_0^\infty e^{-t} t^{\alpha-1} dt, \quad (3)$$

and $D_t^1 f(t) = df(t)/dt$. The left-sided Caputo definition of the fractional derivative is defined as

$$D_t^\alpha f(t) = \frac{1}{\Gamma(1-\alpha)} \int_0^t \frac{D_t^1 f(\tau)}{(t-\tau)^\alpha} d\tau. \tag{4}$$

2.2. Fractional viscoelasticity

It is well known that ideal fluid behaves according to Newtons law $\sigma(t) = \eta d\epsilon(t)/dt = \eta D_t^1 \epsilon(t)$ and the ideal solid is governed by Hook’s law $\sigma(t) = E\epsilon(t) = E D_t^0 \epsilon(t)$. Replacing the order of derivative in the stress-strain equation for the Newtonian fluid with a fractional order α leads to

$$\sigma(t) = \eta D_t^\alpha \epsilon(t) \tag{5}$$

where $0 \leq \alpha \leq 1$ and the unit of the dynamic viscosity η is $\text{Pa} \cdot \text{s}^\alpha$. The literature refers to an element governed by a stress-strain relation of the type shown in Eq. (5) fractional dashpot, springpot, Abel dashpot, fractional soft-matter element and Scotts-Blair element [38]. Both the Reimann–Liouville and Caputo fractional derivatives in the limiting cases of α become the classical definitions. Hence, if $\alpha = 0$, Eq. (5) reverts to that of the ideal solid, and if $\alpha = 1$, Newtons law is obtained. Thus material exhibiting both viscous and elastic properties can be described by Eq. (5).

The creep equation ϵ_{cr} for a springpot is obtained as

$$\epsilon_{cr}(t) = \frac{\sigma_0}{\eta} \frac{t^\alpha}{\Gamma(\alpha + 1)}, \tag{6}$$

by solving the fractional differential Eq. (5) under constant stress

$$\sigma(t) = \sigma_0 H(t), \tag{7}$$

where H is the Heaviside function. Similarly, the stress-relaxation function

$$\sigma_{sr}(t) = \eta \epsilon_0 \frac{t^{-\alpha}}{\Gamma(1-\alpha)}, \tag{8}$$

is obtained under constant strain

$$\epsilon(t) = \epsilon_0 H(t). \tag{9}$$

The power law form of Eqs. (5) and (8) accurately reflect the behaviour of real materials including the increasing creep strain as time $t \rightarrow \infty$. This is not captured by traditional viscoelastic models due to the presence of exponential operators resulting in the creep strain taking an asymptotic value. Moreover, only two parameters are required to fully characterize the time-dependent behaviour of springpots; the dynamic viscosity η and the order of derivative in the stress-strain equation α .

The Maxwell and Kelvin-Voigt models of viscoelasticity may be generalised by replacing the Newtonian dashpots in the mechanical analogues with springpots [39,40]. Thus, the stress–strain equation for the fractional Maxwell model, consisting of a spring and springpot in series, is obtained as

$$D^\alpha \epsilon(t) = \frac{1}{E} D_t^\alpha \sigma(t) + \frac{\sigma(t)}{\eta}. \tag{10}$$

Solving Eq. (10) with stress defined by Eq. (7), yields the creep function

$$\epsilon_{cr}(t) = \frac{\sigma_0}{E} + \frac{\sigma_0}{\eta} \frac{t^\alpha}{\Gamma(1+\alpha)}. \tag{11}$$

By placing an elastic spring and springpot in parallel, the fractional Kelvin-Voigt (FKV) model is obtained with the constitutive stress-strain equation defined by

$$\sigma(t) = E\epsilon(t) + \eta D_t^\alpha \epsilon(t), \tag{12}$$

and the resulting creep function given as

$$\epsilon_{cr}(t) = \frac{\sigma_0}{E} \left(1 - E_\alpha \left[-\left(\frac{Et}{\eta} \right)^\alpha \right] \right). \tag{13}$$

In Eq. (13), E_α is the Mittag–Leffler function defined as

$$E_\alpha(x) = \sum_{n=0}^{\infty} \frac{x^n}{\Gamma(\alpha n + 1)}. \tag{14}$$

It is noted that the solutions to Eqs. (10) and (12) are independent of the definition of fractional derivative. The viscoelastic models discussed thus far have been restricted to constant orders of differentiation in time. A viscoelastic material exhibiting time-varying properties, such as solidification, may be described by a variable-order fractional viscoelastic stress-strain equation:

$$\sigma(t) = \eta D_t^{\alpha(t)} \epsilon(t), \tag{15}$$

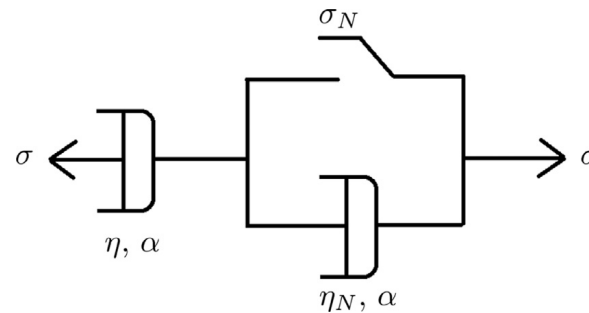


Fig. 1. Rheological model.

where α is a known function [41,42]. Variable order fractional differential equations and their numerical approximation are discussed in Section 5.2.

3. Experimental data

The experimental data obtained by Gillen [11] is utilised for the model development, where five hour creep tests were conducted on pre-heated concrete cylinders subjected to three different stresses; $0.3f'_c$, $0.45f'_c$ and $0.6f'_c$ over a temperature range of 22°C to 649°C , with f'_c denoting cold compressive strength of concrete. The temperature was maintained constant and the static load was applied after the cylinder reached the desired temperature. In addition, three aggregate types were tested which included expanded shale lightweight, calcareous and siliceous aggregates, which featured cold compressive strengths of 24.0 MPa, 23.2 MPa and 22.2 MPa respectively. The concrete cylinders measured 51×102 mm.

The creep data at 93°C is ignored due to the extremely high magnitudes of creep strains observed, higher than the those at 204°C . This increase is caused by moisture migration occurring near the boiling temperature of water [11]. Effects of moisture content and moisture migration are not incorporated into the model proposed in this paper.

Tests were also conducted on larger, older and stronger specimens in order to evaluate the influence of size, age and compressive strength on creep respectively. The effects of size and age were generally deemed insignificant and hence are not considered in this paper. Similarly, creep of higher strength concrete at elevated temperatures was found comparable to standard strength concrete for both the siliceous ($f'_c = 41.7$ MPa) and calcareous ($f'_c = 42.4$ MPa) aggregate types. Thus, for application to higher strength concretes, the viscosity parameter η must be scaled by the ratio of the concrete compressive strength used for parameter calibration and the actual compressive strength.

4. Model development

4.1. Rheological model

The thermo-viscoelastic rheological model proposed herein consists of a linear fractional dashpot placed in series with a non-linear dashpot, see Fig. 1. The second element is utilised to model non-linear creep occurring at high stresses and/or temperatures. Prior to the onset of non-linear behaviour, a single springpot will describe the creep strain. During this linear range, only two model parameters require calibration at each temperature level; the dynamic viscosity η and the fractional exponent α . Thus, the parameters are dependant on temperature and it can be stated that $\eta = \eta(T)$ and $\alpha = \alpha(T)$. When considering non-linear behaviour, the creep strain for the rheological model depicted in Fig. 1 is given as

$$\begin{aligned} \epsilon_{cr}(t) &= \frac{\sigma}{\eta} \frac{t^\alpha}{\Gamma(\alpha + 1)}, & \sigma < \sigma_N, \\ \epsilon_{cr}(t) &= \frac{\sigma}{\eta} \frac{t^\alpha}{\Gamma(\alpha + 1)} + [\sigma - \sigma_N] \frac{1}{\eta_N} \frac{t^\alpha}{\Gamma(\alpha + 1)}, & \sigma > \sigma_N, \end{aligned} \quad (16)$$

where σ_N is the stress at which non-linear strain manifests and η_N denotes the dynamic viscosity of the non-linear springpot. Both element feature the same fractional exponent and thus only a single additional parameter requires calibration when in the non-linear range. Knowledge of the activation stress σ_N is however required, traditionally taken as a percentage of the temperature reduced compressive strength f'_{cr} .

4.2. Parameter calibration

The method of least squares was employed to fit the creep compliance functions to the experimental data and to determine model parameters. This fitting procedure was completed for the three aggregate types at each temperature level. As stated previously, the model parameters are assumed to be dependant only on temperature regardless of the applied

Table 1
Model parameters.

Temperature (°C)	Calcareous			Expanded shale			Siliceous		
	α	η	η_N	α	η	η_N	α	η	η_N
22	0.450	80.0		0.290	36.0		0.250	40.0	
204	0.385	24.5		0.345	15.0		0.377	15.5	
316	0.410	15.5		0.330	10.5				
427	0.460	10.5		0.400	6.5		0.345	4.9	5.5
538	0.420	7.8	1.2	0.368	6.5	0.46	0.260	1.9	1.8
649	0.373	2.8	4.2	0.432	4.0	3.2			

η and $\eta_N = \times 10^4 \text{ MPa} \cdot \text{min}^\alpha$

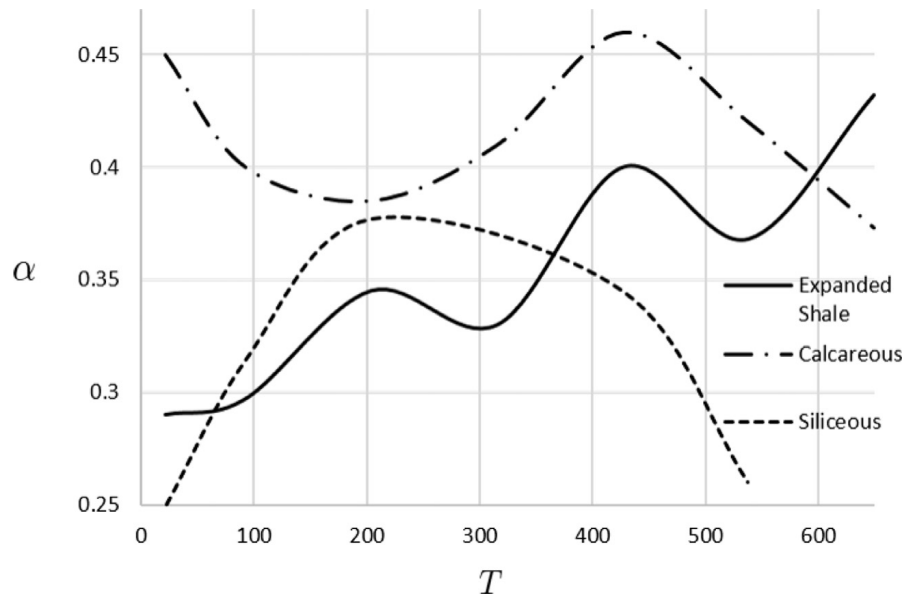


Fig. 2. Relationship between fractional exponent α and temperature T (°C).

stress. However, due to inherent variable nature of experimental data, and possible stress dependency, the model parameters were adjusted so as to provide the best average result across the three stress levels. Stress dependant parameters would significantly convolute the model, which is not warranted due to the small variations observed.

During the model parameter calibration, it was found that the majority of the experimental data could be accurately described using the linear springpot. However, deviations from linearity manifested at combinations of high stress and high temperatures. For the calcareous and lightweight aggregates, non-linear behaviour was observed at temperatures exceeding 538 °C, when the applied stress was $\sigma = 0.6f'_c$. The activation stress for the calcareous and lightweight aggregates was thus estimated as $\sigma_N = 0.75f'_{cT}$. Non-linear creep strain occurred in the siliceous concrete specimens when the applied stress was $\sigma = 0.6f'_c$ at a temperature of 427 °C, and for stress $\sigma = 0.45f'_c$ at a temperature level of 538 °C. Based on this observation, it was approximated that $\sigma_N = 0.6f'_{cT}$ for the siliceous aggregate concrete. The relationships proposed by Knaak [43] were adopted to determine the temperature reduced compressive strength f'_{cT} .

The results of the parameter calibration are shown in Table 1 and Fig. 2, with the experimental data and model predictions graphically shown in Figs. 3–10. It can be seen that the dynamic viscosities η generally decreased with increasing temperatures in a decaying type fashion which can be attributed to reduction in material stiffness. The only exception is the viscosities of the expanded shale aggregate remaining constant between 427 °C and 538 °C. Conversely, an increase in the viscosity η_N with temperature was obtained for the non-linear springpot of the calcareous and lightweight aggregates. Non-monotonic relationships between the order of derivative α and temperature are observed, see Fig. 2. Additionally, this relationship is unique for each of the three aggregate types.

The proposed model accurately reflects the experimental data at elevated temperatures. However the model does not agree well with the creep data at 22 °C. The creep strains at room temperature are highly variable due to parameters not considered, such as moisture content and age at loading, therefore inaccuracies at this temperature are expected and deemed insignificant due to their small magnitudes. Additionally, anomalies appear in the result set. The creep curve of the calcareous aggregate concrete cylinder at 427 °C under a stress of $\sigma = 0.45f'_c$ shows atypical behaviour, as the initial creep rate is comparable to that of the stress level $\sigma = 0.6f'_c$. In addition, the creep data for the siliceous aggregate concrete subjected to a stress of $\sigma = 0.6f'_c$ and temperature of 204 °C is significantly smaller than is expected according to the assumption of linearity, consequently the model overestimates the creep strain.

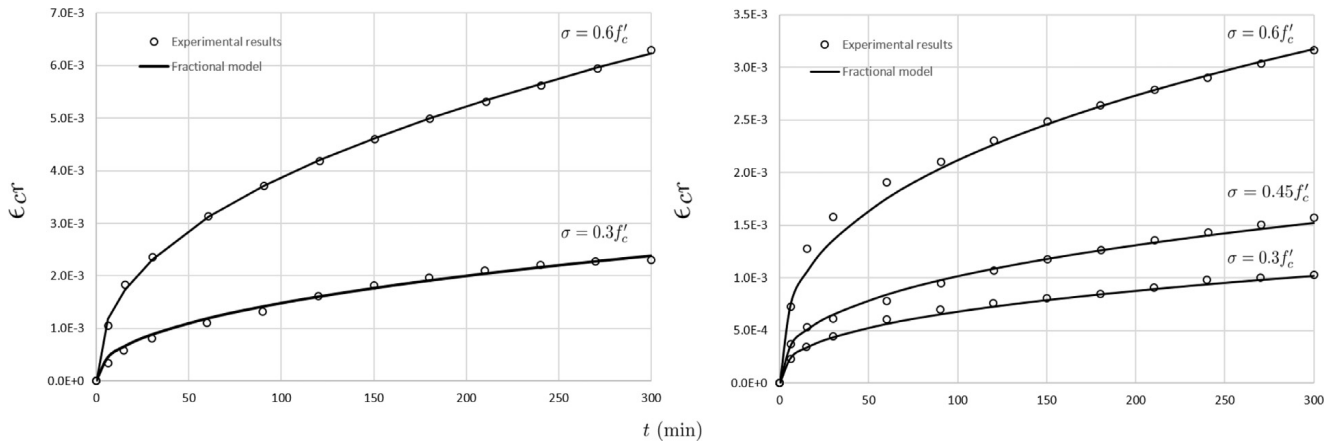


Fig. 3. Creep strains for lightweight aggregate concrete. $T = 649\text{ }^{\circ}\text{C}$ (left) and $T = 538\text{ }^{\circ}\text{C}$ (right).

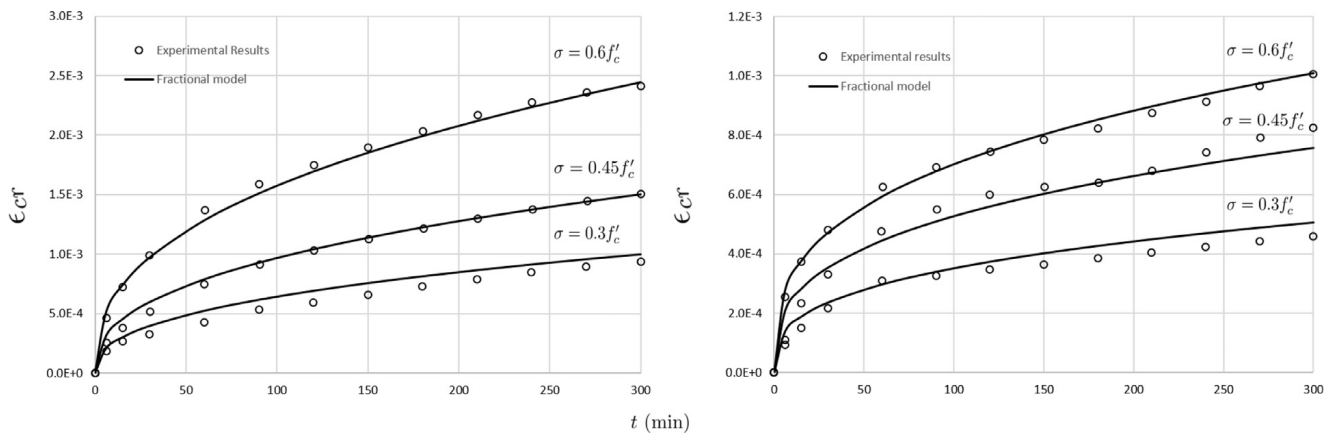


Fig. 4. Creep strains for lightweight aggregate concrete. $T = 427\text{ }^{\circ}\text{C}$ (left) and $T = 316\text{ }^{\circ}\text{C}$ (right).

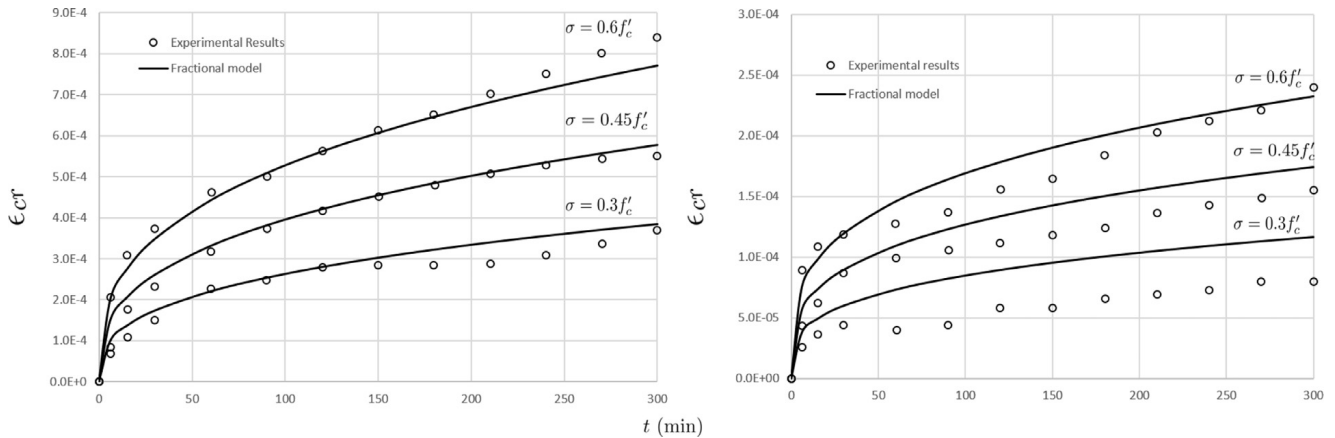


Fig. 5. Creep strains for lightweight aggregate concrete. $T = 204\text{ }^{\circ}\text{C}$ (left) and $T = 22\text{ }^{\circ}\text{C}$ (right).

4.3. Comparison to additional experimental data

Cruz [7] conducted 5 hour creep tests at constant stress and temperature levels for a carbonate aggregate concrete with compressive strength $f'_c = 28\text{ MPa}$. The temperatures ranged from $24\text{ }^{\circ}\text{C}$ to $650\text{ }^{\circ}\text{C}$ and the applied stress was $\sigma = 0.439f'_c$. Three tests were performed at the lower temperature levels (24 , 149 and $316\text{ }^{\circ}\text{C}$) and five at the higher temperatures (482 and $649\text{ }^{\circ}\text{C}$). The results for each temperature level were averaged, and then compared with the predictions of the fractional dashpot model, see Fig. 11. The model provides a good estimation of the experimental data.

Discrepancies exist with the remaining experimental data available in the literature. The rapid increase in creep, or onset of non-linear behaviour, was recorded by [9,10,13] as approximately $400\text{ }^{\circ}\text{C}$. Khoury et al. [12] recorded this temperature as

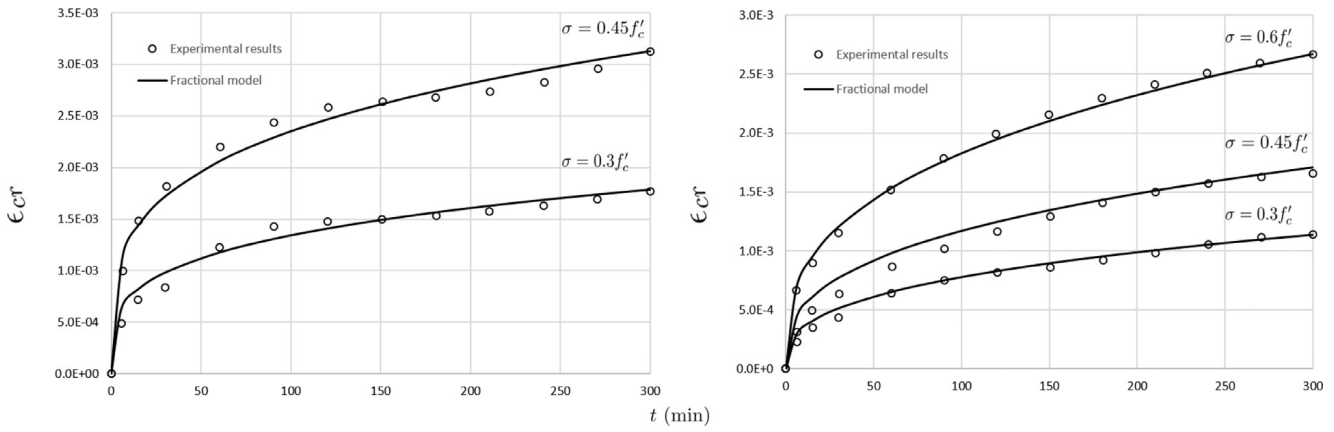


Fig. 6. Creep strains for siliceous aggregate concrete. $T = 538\text{ }^{\circ}\text{C}$ (left) and $T = 427\text{ }^{\circ}\text{C}$ (right).

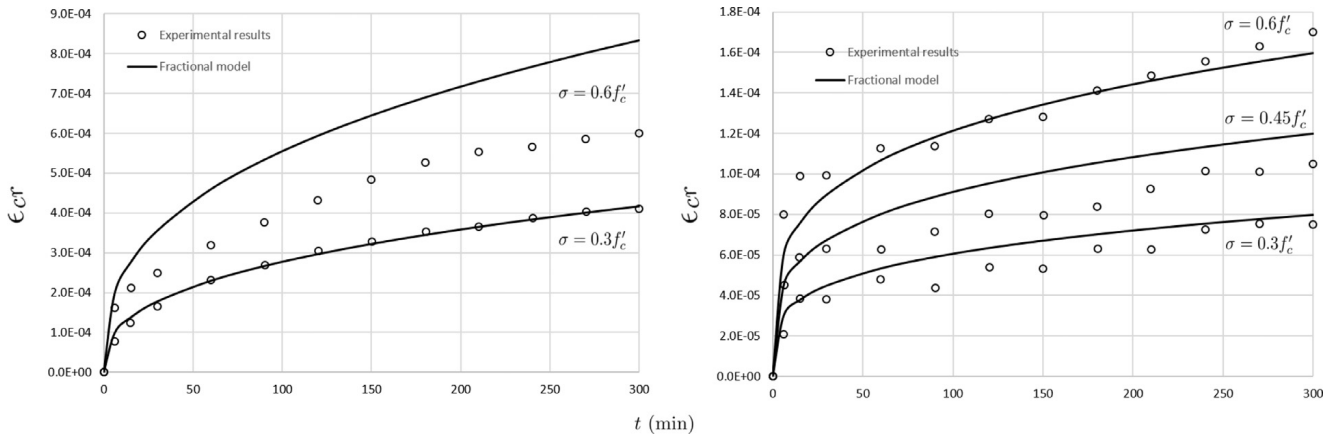


Fig. 7. Creep strains for siliceous aggregate concrete. $T = 204\text{ }^{\circ}\text{C}$ (left) and $T = 22\text{ }^{\circ}\text{C}$ (right).

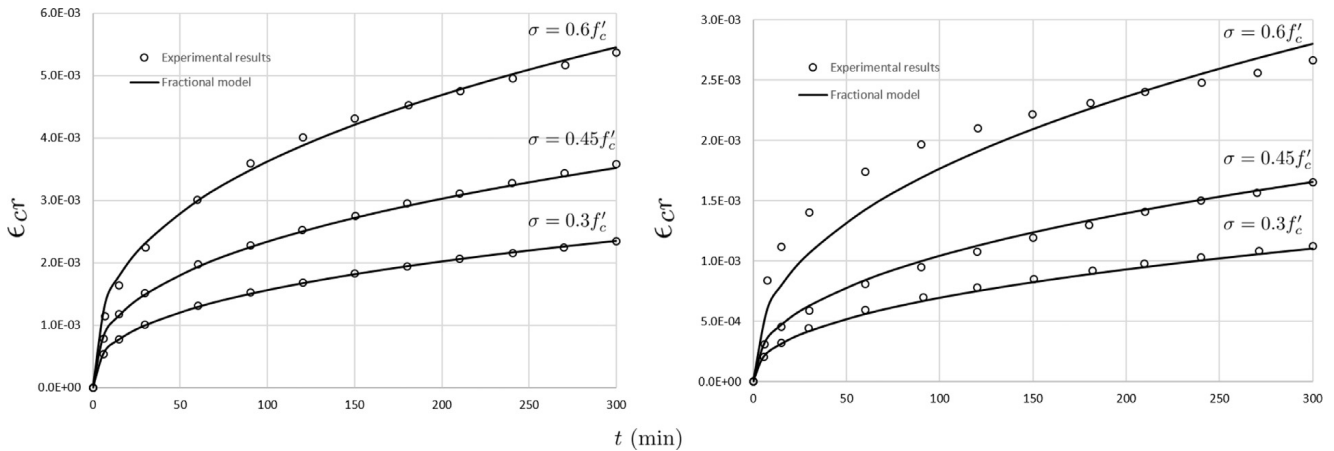


Fig. 8. Creep strains for calcareous aggregate concrete. $T = 649\text{ }^{\circ}\text{C}$ (left) and $T = 538\text{ }^{\circ}\text{C}$ (right).

350 °C and 600 °C for gravel and lightweight concrete respectively. Additionally, the creep strains at temperatures less than 400 °C are greater in the results of Cruz [7] and Gillen [11] than those reported by [9,10,12,13]. An experimental anomaly also appears exclusive to the data reported by Gillen [11]. The creep curves at temperatures of 427 °C and 538 °C and stress levels of $0.3f'_c$ and $0.45f'_c$ for the calcareous and lightweight aggregates are practically identical; no increase in creep with temperature is observed. This stabilization of creep has not been reported by any other researchers, and thus it may be justifiable to ignore the characterized model parameters at 427 °C.

Variations in experimental data can be attributed to the different concrete mixes and aggregate types tested. It is therefore recommended that the springpot model parameters be calibrated for application to contrastive concretes.

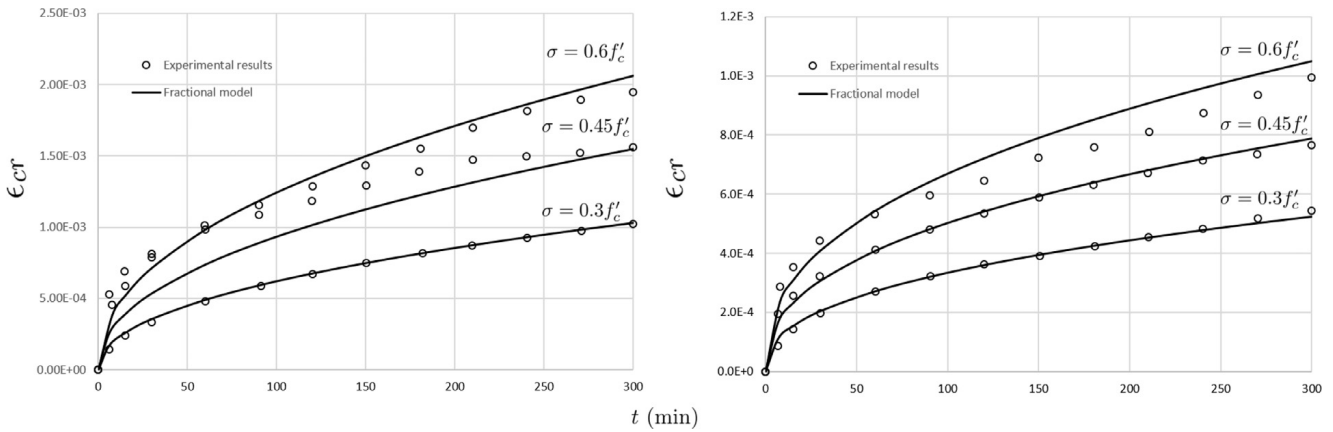


Fig. 9. Creep strains for calcareous aggregate concrete. $T = 427\text{ }^{\circ}\text{C}$ (left) and $T = 316\text{ }^{\circ}\text{C}$ (right).

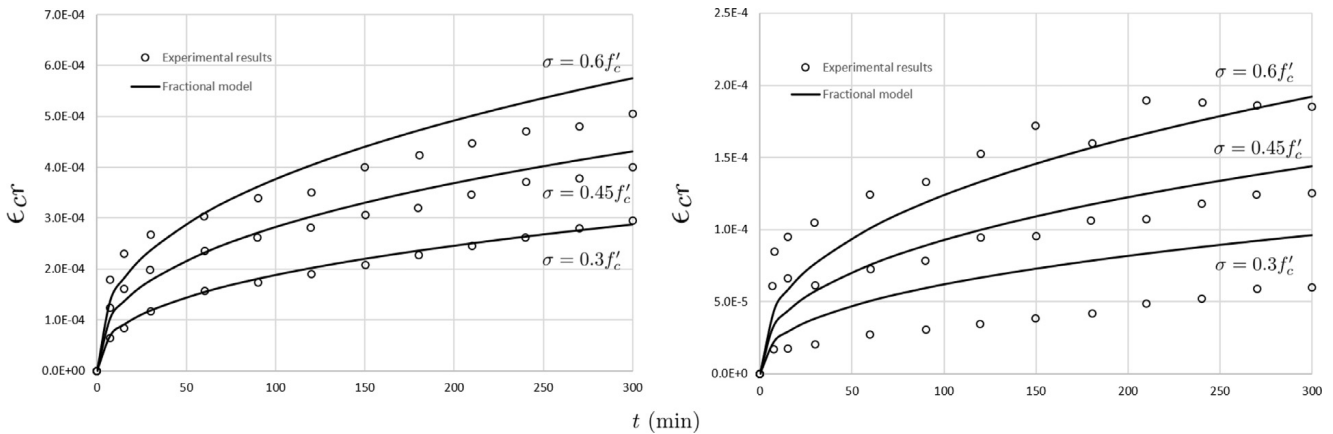


Fig. 10. Creep strains for calcareous aggregate concrete. $T = 204\text{ }^{\circ}\text{C}$ (left) and $T = 22\text{ }^{\circ}\text{C}$ (right).

4.4. Long-term creep

It is well known that the creep rate of concrete significantly decays with time, which also holds true at elevated temperatures [8,9,12]. Application of the springpot for long durations does not mirror this behaviour, resulting in a significant overestimation of creep. The FKV model of viscoelasticity yields a greater representation of behaviour for longer time periods whilst still able to mirror short-term creep. However, an additional elastic spring requires characterization. The creep deformations predicted by the springpot and FKV models for a period of 10 days are depicted in Fig. 12. It can be seen that the results produced by the two models are initially similar, but diverge at approximately two days of loading, as the decay of creep rate is greater in the FKV model. In this example the model parameters for the springpot are $\alpha = 0.345$ and $\eta = 45000\text{ MPa} \cdot \text{min}^{\alpha}$, and for the FKV model $\alpha = 0.4$, $\eta = 56294\text{ MPa} \cdot \text{min}^{\alpha}$ and $E = 1000\text{ MPa}$. These parameters are calibrated using the experimental results of Gillen [11] for siliceous aggregate concrete.

The long term creep predictions of the FKV are significantly influenced by the modulus of the elastic spring, despite having a small effect in the short term. Consequently, multiple combinations of model parameters may reflect a given creep curve for short durations. Therefore, long term creep data is required for model parameter characterization. Thus, it is recommended that the springpot model be employed for short term creep modelling and the FKV for longer durations.

5. Variable stress and temperature

5.1. Time-varying stress

The stress in a concrete member subject to elevated temperatures is not likely to remain constant in time as a consequence of the creep, transient and expansion or shrinkage strains. This is especially true in cases of time-varying temperature; a more accurate representation of real conditions. Non-constant stresses and temperatures significantly influence basic creep strain. The fractional differential form of the proposed viscoelastic model provides a compact method of determining basic creep under conditions of time-varying stress and temperature.

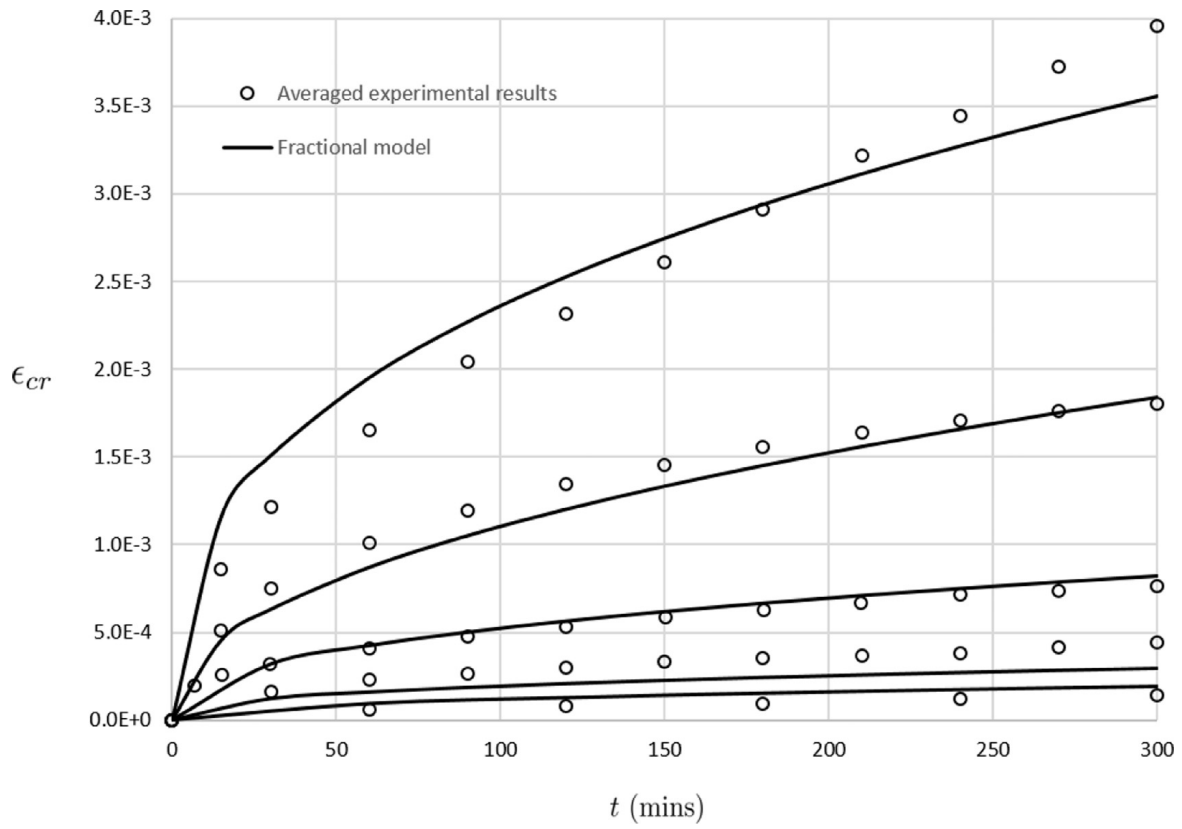


Fig. 11. Averaged creep results of Cruz [7] and springpot model.

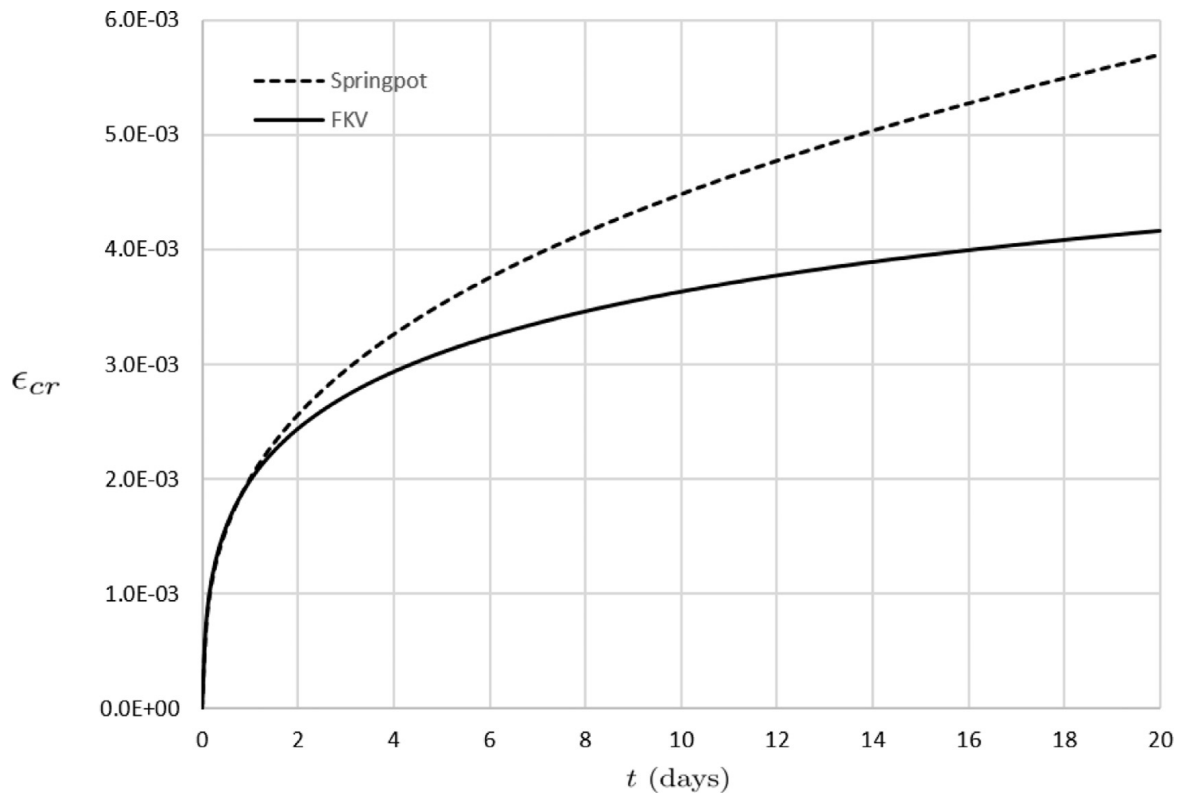


Fig. 12. Comparison of springpot and FKV models for longer term creep. $\sigma = 0.3f'_c$ and $T = 427^\circ\text{C}$.

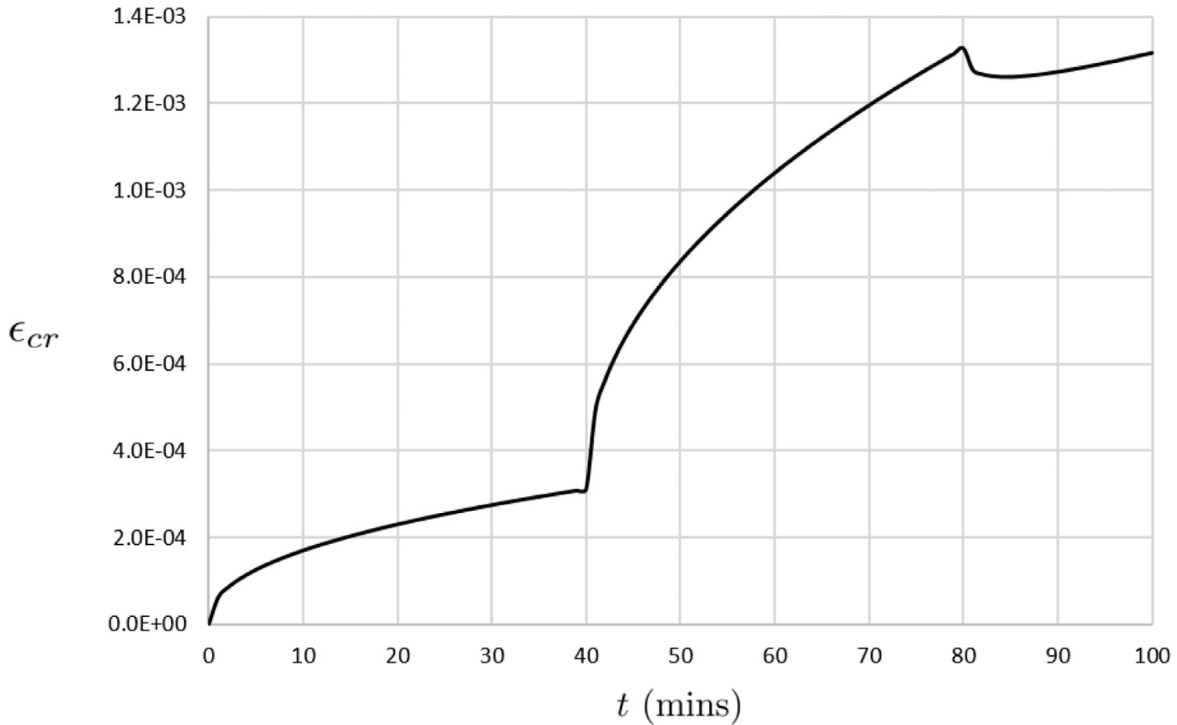


Fig. 13. Creep strains of calcareous aggregate subject to varying stress levels. $\alpha = 0.4379$ and $\eta = 87602 \text{ MPa} \cdot \text{min}^\alpha$.

For the case of a known stress history $\sigma = \sigma(t)$ and constant temperature, the creep strain can be expressed in fractional differential form as

$$D_t^\alpha \epsilon(t) = \frac{\sigma(t)}{\eta}, \tag{17}$$

or in integral

$$\epsilon(t) = \int_0^t \epsilon_{cr}(t - \tau) D_t^1 \sigma(\tau) d\tau, \tag{18}$$

where ϵ_{cr} is the creep compliance of the viscoelastic model.

Consider a stress history of $\sigma(t) = 0.2f'_c$ for $t = 0 - 40$ min, followed by a stress of $\sigma(t) = 0.6f'_c$ when $40 < t < 80$ mins and a stress of $\sigma = 0.4f'_c$ at $t > 80$. For this loading profile, the creep strain is derived using Eqs. (18) and (6) as

$$\epsilon(t) = \frac{1}{\eta \Gamma(\alpha + 1)} [0.2f'_c t^\alpha + 0.4f'_c(t - 40)^\alpha H(t - 40) - 0.2f'_c(t - 80)^\alpha H(t - 80)]. \tag{19}$$

The model predictions are depicted in Fig. 13 for a compressive strength of $f'_c = 24 \text{ MPa}$ and temperature of 500°C .

Very few experimental results have been reported in the literature on the basic creep strain in concrete subject to non-constant stress at temperatures greater than 100°C . The spring-pot model agrees with the experimental results reported in [13] during the increasing stress period, when $t < 80$ min. Contrasting behaviour however exists when the stress is reduced ($t > 80$). Greater recovery is predicted by the fractional dashpot model than in the experimental results, which show no decrease of creep.

The nature and magnitude of creep recovery at elevated temperatures is not well represented in the literature and various assumptions were made when modelling its effect on creep. Anderberg and Thelandersson [10] accepted decreasing creep due to stress and temperature reductions over small time periods, whereas Guo and Shi [16] proposed that the creep-time curve should remain horizontal. For small stress and temperature reductions, either method may be adopted, however the validity of these assumptions in cases of large decreases in stress and temperatures requires further experimental investigation.

5.2. Time-varying temperature

If the temperature varies with time, it can be stated that $T = T(t)$, consequently the dynamic viscosity $\eta = \eta(T(t))$ and fractional exponent $\alpha = \alpha(T(t))$. Thus, the fractional derivative stress-strain equation becomes of variable order, and can

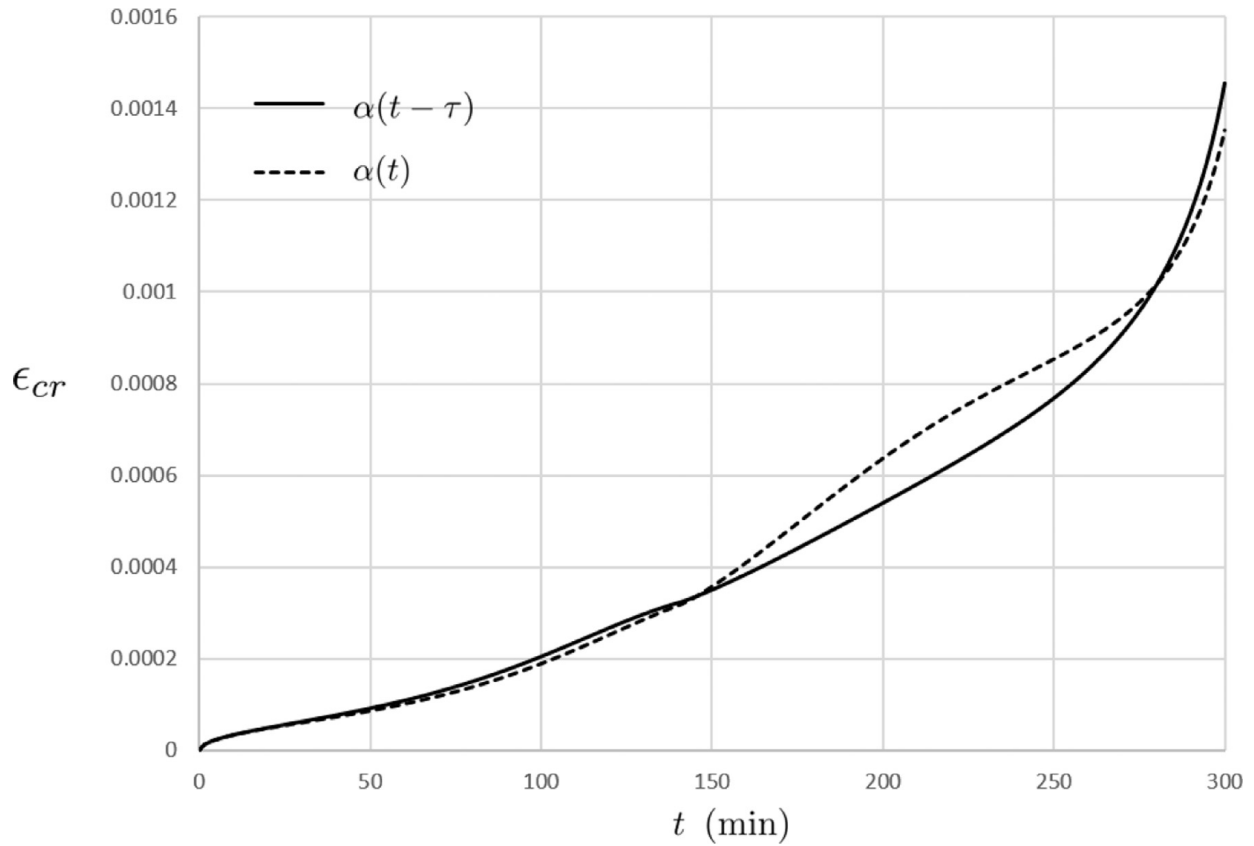


Fig. 14. Creep strains of calcareous aggregate subject to increasing temperature.

be expressed as

$$D_t^{\alpha(T(t))} \epsilon(t) = \frac{\sigma(t)}{\eta(T(t))}. \tag{20}$$

Various definitions of the variable order fractional derivative exist [42,44]. Adopting the Caputo type of fractional derivative, the variable order derivative of a function f is defined as

$$D_t^{\alpha(t)} f(t) = \frac{1}{\Gamma(1 - \alpha(t))} \int_0^t \frac{D^1 f(\tau)}{(t - \tau)^{\alpha(t)}} d\tau. \tag{21}$$

In this definition, the memory effect changes in time and is determined at the current time instant [45]. Alternatively, the variable order fractional derivative of Caputo type may be expressed as

$$D_t^{\alpha(t)} f(t) = \int_0^t \frac{D_t^1 f(\tau)}{\Gamma[1 - \alpha(t - \tau)](t - \tau)^{\alpha(t - \tau)}} d\tau. \tag{22}$$

Eq. (22) possesses a memory of the order of differentiation, as the order α is dependent on the kernel τ , which is not contained in Eq. (21). The difference in results when adopting Eq. (21) or Eq. (22) on the predicted creep strain is shown in Figs. 14 and 15.

The relationships between the order of derivative and temperature can be derived using the calibrated material parameters found in Table 1 for a given aggregate type. Assuming calcareous, the following equation is obtained (T in Fahrenheit $^{\circ}F$)

$$\begin{aligned} \alpha(T) &= -5.36 \times 10^{-10}(T - 759.6741)^3 - 7.849 \times 10^{-11}T^2 \\ &\quad + 0.000253T + 0.257, \quad T < 600^{\circ}F, \\ \alpha(T) &= 1.73 \times 10^{-9}(T + 931.86)^3 - 1.01 \times 10^{-5}T^2 \\ &\quad + 0.00057883T - 2.5093, \quad T > 600^{\circ}F. \end{aligned} \tag{23}$$

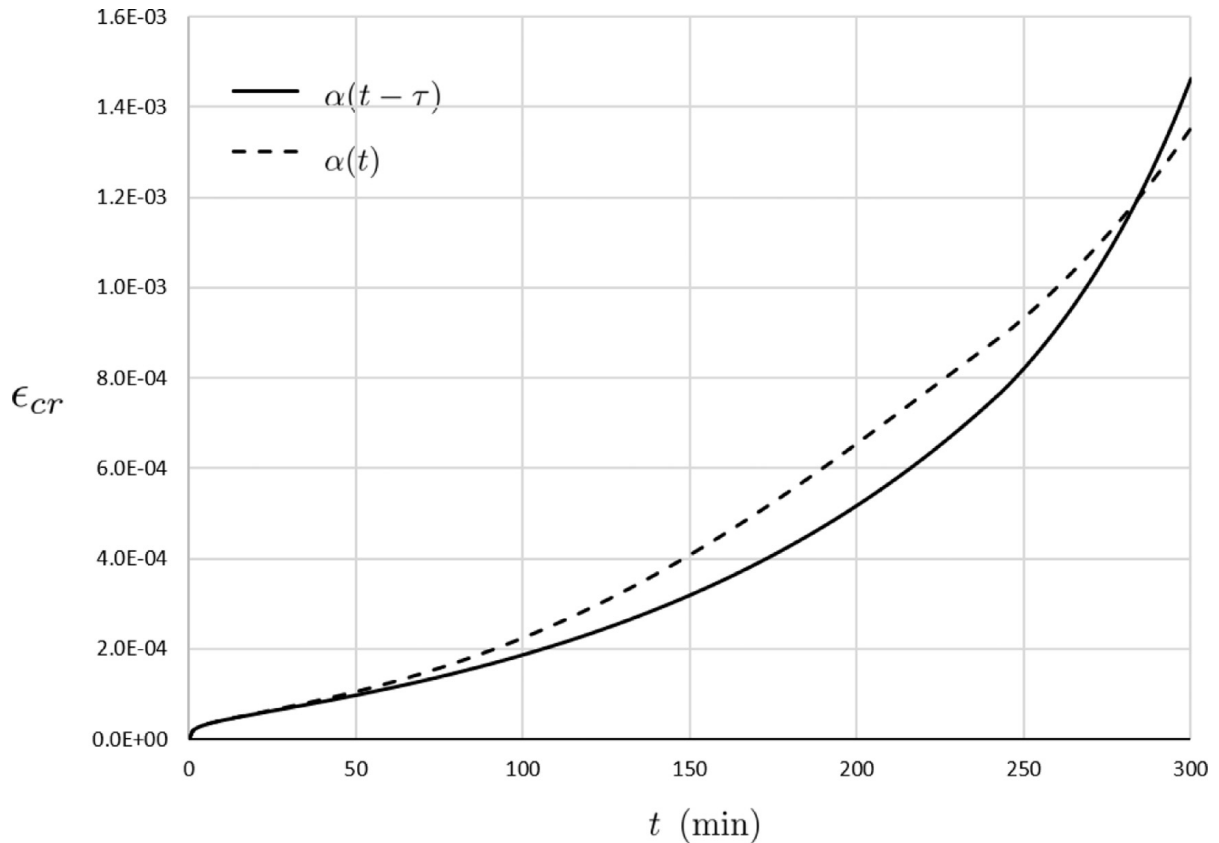


Fig. 15. Creep strains of siliceous aggregate subject to increasing temperature.

Similarly, the dynamic viscosity is determined as

$$\begin{aligned} \eta(T) &= 2.3382(T - 596.2261)^2 + 1.55 \times 10^5, & T < 600^\circ F, \\ \eta(T) &= 9.3568 \times 10^{-4}(T - 900)^3 - 127.43333T + 206400, & T > 600^\circ F. \end{aligned} \tag{24}$$

The temperature dependence of the fractional exponent and viscosity for siliceous concrete are obtained as

$$\begin{aligned} \alpha(T) &= 5.7323 \times 10^{-11}(T - 677.8124)^3 - 5.9015 \times 10^{-7}T^2 \\ &\quad + 6.3136 \times 10^{-4}T + 0.2201 \end{aligned} \tag{25}$$

and

$$\begin{aligned} \eta(T) &= 495020e^{-0.0029T}, & T < 800^\circ F, \\ \eta(T) &= 0.1985(T - 1270)^2 + 5000, & T > 800^\circ F, \end{aligned} \tag{26}$$

respectively. For a given temperature history, the variable order fractional differential Eq. (20) with known model parameters can be numerically solved. In this example, a solution is obtained by discretization of (21) and (22), see Appendix for details. A similar approach has been adopted in studies by [45,46].

The effect of increasing temperature on the basic creep strain of a calcareous concrete subject to constant stress of $0.3f'_c$ is depicted in Fig. 14. Initial temperature is 22 °C and increases at a rate of 1.95 °C/min over a period of 5 h. Both definitions of the variable order fractional derivative yield similar results. When Eq. (22) is adopted, the creep rate increases throughout the loading period. A short decrease in creep rate is however observed in the temperature range $427(^\circ\text{C}) \leq T \leq 536(^\circ\text{C})$, when the fractional derivative is defined using Eq. (21). This can be attributed to the comparable experimental creep curves at the temperatures extremes (Figs. 8 and 9). The case of siliceous aggregate concrete under a constant stress of $\sigma = 0.3f'_c$ and heating rate of 1.67 °C/min, with an initial temperature of 22 °C, is shown in Fig. 15. Both definitions of the fractional derivative yield increasing creep rates with temperature. Throughout majority of the heating period, a greater creep strain is obtained when history of α is not considered. However, this is not the case in the higher temperature range. This behaviour is also seen in the calcareous case.

Experimental verification of the effect of time-varying temperatures on basic creep is convoluted due to the manifestation of transient thermal strain which inhibits the isolation of basic creep. The results predicted by the variable order spring-

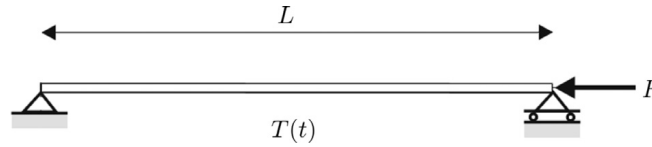


Fig. 16. Column loading and geometrical configuration.

pot model do however satisfy intuitive expectations. As both definitions of the variable order fractional derivative produce comparable results, for practical applications either may be adopted.

6. Applications

6.1. Axial strain in columns

The fractional derivative creep law will now be applied to model the axial deformations in a concrete column. Consider a simply-supported concrete column of length L subjected to an axial concentrated load of intensity F , which induces a compressive stress $-\sigma$, and to a time-varying uniform temperature field $T = T(t)$, see Fig. 16. As one of the supports permits horizontal displacements, additional axial stress will not be generated due to restrained thermal expansion. The total strain ϵ in a concrete member subject to a compressive load and temperature increase is

$$\epsilon(\sigma, t, T) = e_{el}(t, T) + \epsilon_{cr}(\sigma, t, T) + e_{th}(T) + e_{tr}(\sigma, T), \tag{27}$$

where e_{el} is the instantaneous elastic strain, e_{th} is the thermal strain and e_{tr} is the transient thermal strain. The elastic strain is known as

$$e_{el} = \frac{\sigma}{E(T)}, \tag{28}$$

where E is the temperature dependent elastic modulus, which will be modelled using the following relationship proposed by Nielsen [47]

$$E(T) = E_0 \left(1 - \frac{\Delta T}{1000} \right)^2, \quad 0 \leq \Delta T \leq 1000, \tag{29}$$

where E_0 denotes the initial elastic modulus of the concrete and $\Delta T = T - 20^\circ\text{C}$. The thermal strain is defined as

$$e_{th} = a\Delta T, \tag{30}$$

where a is the coefficient of thermal expansion. The Nielsen model of transient thermal strain will be employed, given as

$$e_{tr} = \frac{\sigma}{f'c} (A\theta^2 + B\theta), \quad \theta < \theta_{tr},$$

$$e_{tr} = \frac{\sigma}{f'c} [C(\theta - \theta_{tr})^2 + A\theta_{tr}(2\theta - \theta_{tr}) + B(\theta - \theta_{tr})], \quad \theta > \theta_{tr}, \tag{31}$$

where A , B and C are free model parameters assumed as 0.5×10^{-3} , 0.7×10^{-3} and 20×10^{-3} respectively and θ_{tr} is the transition temperature (defined at 470°C) using the following reduced temperature scale

$$\theta = \frac{\Delta T}{100} = \frac{T - 20^\circ\text{C}}{100}. \tag{32}$$

The constitutive stress-strain equation for the basic creep strain is defined by Eq. (20).

The aforementioned numerical routine is adopted to determine basic creep strain, which is then added to the remaining strain components in order to determine the total axial strain. Eqs. (23) and (24) are adopted for the model parameters. The total axial strains for a concrete column subject to various stress levels and an increasing temperature are depicted in Fig. 17. The initial temperature is 22°C and increases at a rate of $2.09^\circ\text{C}/\text{min}$.

6.2. Beam deflections

The transverse creeping deflections of a simply-supported concrete beam of length L subjected to a constant uniformly distributed load w and time-varying temperature T , depicted in Fig. 18, will now be modelled. As with the example in Section 6.1, axial forces will not be generated by restrained thermal expansion due to the simply-supported boundary conditions. Paola et al. [48] proved that the two correspondence principles hold for fractional viscoelastic beams. Of relevance is the first principle, which states that the stresses in a viscoelastic beam subjected to constant loading applied at initial time are the same as those in the elastic case. Whilst the strains and displacements are time dependant and are obtained

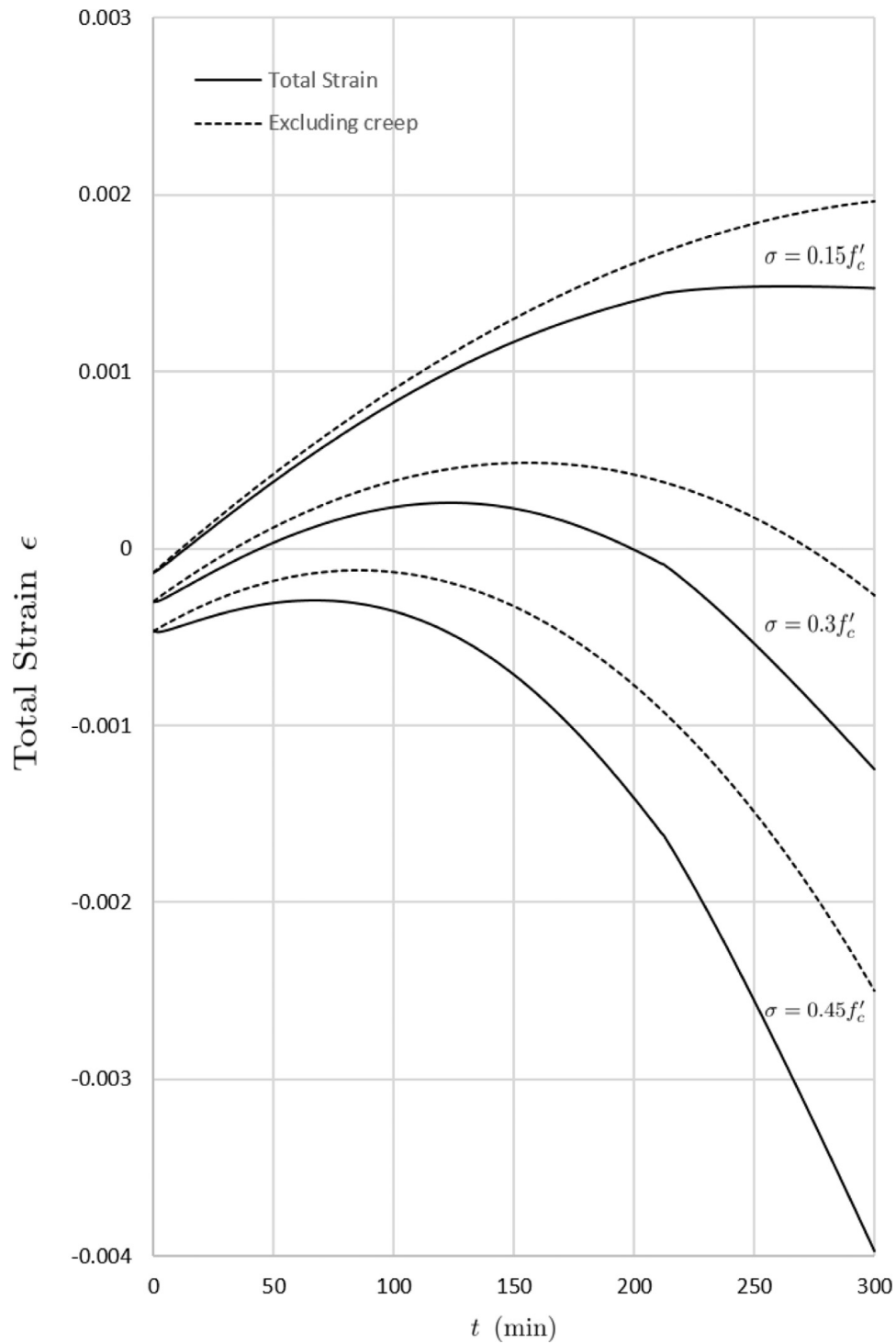


Fig. 17. Total axial strain in concrete column subject to constant load and increasing temperature. $f'_c = 32$ MPa, $E_0 = 30, 100$ MPa and $\alpha = 10 \times 10^{-6} \text{ } ^\circ\text{C}^{-1}$.

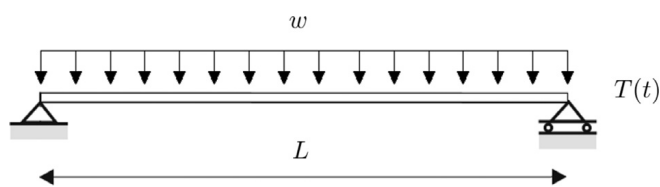


Fig. 18. Beam loading and geometrical configuration.

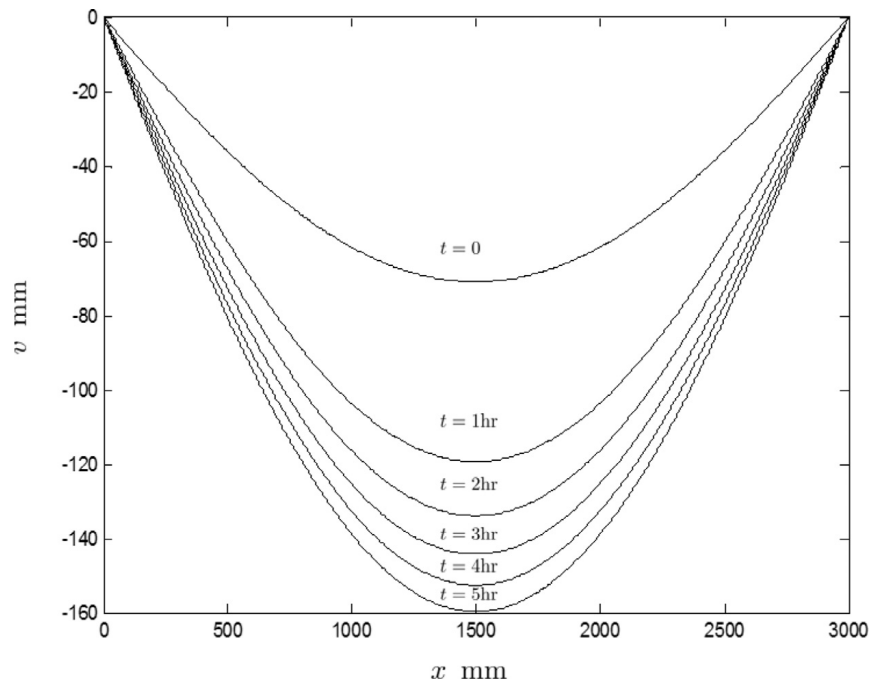


Fig. 19. Deflections of concrete beam subject to uniformly distributed load $w = 15 \text{ kPa}$ and uniform temperature field of 649°C . $E_0 = 30, 100 \text{ MPa}$, $I = 6 \times 10^7 \text{ mm}^4$ and $L = 3000 \text{ mm}$.

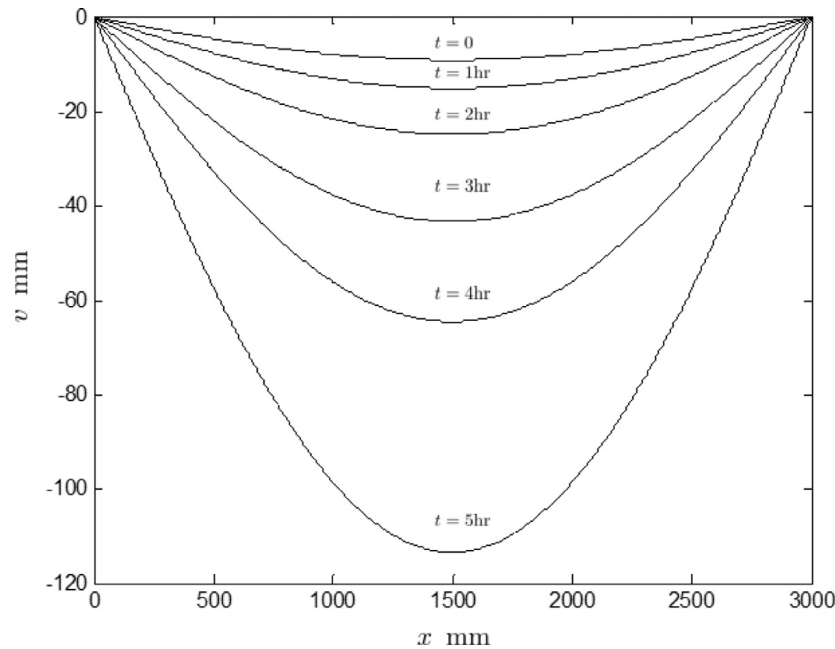


Fig. 20. Deflections of concrete beam subject to uniformly distributed load $w = 10 \text{ kPa}$ and increasing temperature field. $E_0 = 30, 100 \text{ MPa}$, $I = 6 \times 10^7 \text{ mm}^4$ and $L = 3000 \text{ mm}$.

by replacing the elastic modulus with the inverse of the creep function in the elastic solution. Thus, for the described beam the bending moment is independent of time and temperature.

The elastic solution \mathcal{V} for transverse deflection is simply

$$\mathcal{V}(x) = -\frac{w x}{24 E I} (x^3 - 2 L x^2 + L^3), \tag{33}$$

where x is the coordinate along the beam axis and I is the second moment of area of the beams cross-section. Ignoring transient thermal strain, the total bending strains e_B in the concrete beam consist of the sum of the instantaneous elastic strain e_{el} and the creep strain e_{cr} , thus the mechanical analogue is the fractional Maxwell model. The creep compliance for the fractional Maxwell model is given by Eq. (11). In accordance with the correspondence principle, the transverse deflection

equation for the beam under constant stress and temperature becomes

$$\nu(x, t) = -\frac{wX}{24I} (x^3 - 2Lx^2 + L^3) \left[\frac{1}{E} + \frac{1}{\eta} \frac{t^\alpha}{\Gamma(1+\alpha)} \right] \quad (34)$$

The deflections for a concrete beam subject to a uniform temperature field of 649 °C for a duration of 5 h are depicted in Fig. 19. For the case of variable temperature, the deflection equation is derived as

$$\nu(x, t) = -\frac{wX}{24I} (x^3 - 2Lx^2 + L^3) \left[\frac{1}{E(T)} + \epsilon_{cr} \right], \quad (35)$$

where ϵ_{cr} is the creep compliance determined by numerically solving Eq. (20).

A numerical solution is obtained using the aforementioned method. The results for an initial temperature of 22 °C which increases at a rate of 2.09 °C/min for a five hour period are shown in Fig. 20.

7. Conclusion

A novel non-linear creep law based on the fractional derivative models of viscoelasticity for application to concrete subject to short-term high temperature conditions is developed in this paper. The rheological model consists of two springpots placed in series; the second modelling non-linear creep which manifests at high stresses and temperatures. The temperature dependent model parameters were calibrated using benchmark experimental data of creep in concrete cylinders subject to constant stress and temperatures for various aggregate types. The developed model provides good agreement with experimental results at elevated temperatures, however is less accurate at ambient conditions. The advantages of the developed model include the use of few model parameters and simple employability to problems involving variable stress and temperatures, thus averting complexities caused by existing models. Two example applications are presented which include modelling the axial deformations in columns and transverse deflections in beams.

It was shown that the model parameters show significant variation for the three aggregate types investigated. Therefore, parameter calibration is advised for application of the fractional model to different concrete mixes. Further generalisations include incorporating the effects of moisture migration and analysis of model performance over longer periods. Moreover, further research on the application of fractional viscoelastic models to concrete creep at ambient and lower temperatures is required.

Acknowledgements

The first author acknowledges Victoria University for the financial support provided through the Vice Chancellor's Graduate Research Scholarship award. This research is supported by the project 174005 of the Serbian Ministry of Science and Education, as well as by the project 114 – 451 – 2098 of the Provincial Secretariat for Higher Education and Scientific Research.

Appendix A

A1. Discretisation of Eq. (21)

The variable-order fractional derivative, for the case when the memory of the order of derivative is not considered, is discretised as follows

$$\begin{aligned} D_t^{\alpha(t)} y(t) &= \frac{1}{\Gamma(1-\alpha(t))} \int_0^t \frac{y'(\tau)}{(t-\tau)^{\alpha(t)}} d\tau \\ &\approx \frac{1}{\Gamma(1-\alpha_n)} \sum_{j=0}^{n-1} \int_{j\Delta t}^{(j+1)\Delta t} \frac{y'(\tau)}{(t-\tau)^{\alpha_n}} d\tau \\ &= \frac{1}{\Gamma(1-\alpha_n)} \sum_{j=0}^{n-1} \int_{j\Delta t}^{(j+1)\Delta t} \frac{\frac{y_{j+1}-y_j}{\Delta t}}{(t-\tau)^{\alpha_n}} d\tau \\ &= \frac{1}{\Gamma(1-\alpha_n)} \sum_{j=0}^{n-1} \frac{y_{j+1}-y_j}{\Delta t} \int_{j\Delta t}^{(j+1)\Delta t} \frac{d\tau}{(t-\tau)^{\alpha_n}} \\ &= \frac{1}{\Gamma(2-\alpha_n)(\Delta t)^{\alpha_n}} \sum_{j=0}^{n-1} (y_{j+1}-y_j) [(n-j)^{1-\alpha_n} - (n-j-1)^{1-\alpha_n}] \\ &= \frac{1}{\Gamma(2-\alpha_n)(\Delta t)^{\alpha_n}} \sum_{j=0}^{n-2} (y_{j+1}-y_j) [(n-j)^{1-\alpha_n} - (n-j-1)^{1-\alpha_n}] \\ &\quad + \frac{y_n - y_{n-1}}{\Gamma(2-\alpha_n)(\Delta t)^{\alpha_n}} \end{aligned}$$

where Δt is the time step, $t = n\Delta t$, $n = 2 \dots t_f/\Delta t$, t_f is the final time, $\tau = j\Delta t$ and $(\cdot)'_n = (\cdot)'(n\Delta t)$. The creep strain ϵ for the fractional dashpot model of viscoelasticity is hence determined as

$$\epsilon_n = \epsilon_{n-1} - \sum_{j=0}^{n-2} (\epsilon_{j+1} - \epsilon_j) [(n-j)^{1-\alpha_n} - (n-j-1)^{1-\alpha_n}] + \frac{\sigma_n}{\eta_n} \Gamma(2 - \alpha_n) (\Delta t)^{\alpha_n}$$

with the creep strain at $n = 1$ derived as

$$\epsilon_1 = \frac{\sigma_1}{\eta_1} \Gamma(2 - \alpha_1) (\Delta t)^{\alpha_1} + \epsilon_0 \tag{36}$$

and $\epsilon_0 = 0$.

A2. Discretisation of Eq. (22)

Adopting the same notation and approach as in Section A.1, the variable order differential equation with memory of order is discretised as

$$\begin{aligned} D_t^{\alpha(t)} y(t) &= \int_0^t \frac{y'(\tau)}{\Gamma[1 - \alpha(t - \tau)](t - \tau)^{\alpha(t-\tau)}} d\tau \\ &\approx \sum_{j=0}^{n-1} \frac{y_{j+1} - y_j}{\Gamma(1 - \alpha_{n-j}) \Delta t} \int_{j\Delta t}^{(j+1)\Delta t} \frac{d\tau}{(t - \tau)^{\alpha_{n-j}}} \\ &= \sum_{j=0}^{n-1} \frac{y_{j+1} - y_j}{\Gamma(1 - \alpha_{n-j})} (\Delta t)^{\alpha_{n-j}} [(n-j)^{1-\alpha_{n-j}} - (n-j-1)^{1-\alpha_{n-j}}] \\ &= \sum_{j=0}^{n-2} \frac{y_{j+1} - y_j}{\Gamma(1 - \alpha_{n-j})} (\Delta t)^{\alpha_{n-j}} [(n-j)^{1-\alpha_{n-j}} - (n-j-1)^{1-\alpha_{n-j}}] \\ &\quad + \frac{y_n - y_{n-1}}{\Gamma(2 - \alpha_1) (\Delta t)^{\alpha_1}} \end{aligned} \tag{37}$$

where $\alpha_{n-j} = \alpha(n\Delta t - j\Delta t)$. Upon application to the springpot model, the creep strain is obtained as

$$\begin{aligned} \epsilon_n &= \epsilon_{n-1} - \Gamma(2 - \alpha_1) (\Delta t)^{\alpha_1} \sum_{j=0}^{n-2} \frac{\epsilon_{j+1} - \epsilon_j}{\Gamma(2 - \alpha_{n-j})} \\ &\quad \times [(n-j)^{1-\alpha_{n-j}} - (n-j-1)^{1-\alpha_{n-j}}] + \frac{\sigma_n}{\eta_n} \Gamma(2 - \alpha_1) (\Delta t)^{\alpha_1} \end{aligned} \tag{38}$$

with the creep strain at $n = 1$ obtained as

$$\epsilon_1 = \frac{\sigma_1}{\eta_1} \Gamma(2 - \alpha_0) (\Delta t)^{\alpha_0} + \epsilon_0 \tag{39}$$

and $\epsilon_0 = 0$.

References

- [1] Z.P. Bažant, Mathematical model for creep and thermal shrinkage of concrete at high temperature, Nuclear Eng. Des. 76 (2) (1983) 183–191.
- [2] Z.P. Bažant, G. Cusatis, L. Cedolin, Temperature effect on concrete creep modeled by microprestress-solidification theory, J. Eng. Mech. 130 (6) (2004) 691–699.
- [3] Z.P. Bažant, A.B. Huggaard, S. Baweja, F.-J. Ulm, Microprestress-solidification theory for concrete creep. I: aging and drying effects, J. Eng. Mech. 123 (11) (1997) 1188–1194.
- [4] Z.P. Bažant, A.B. Huggaard, S. Baweja, Microprestress-solidification theory for concrete creep. II: algorithm and verification, J. Eng. Mech.-Proc. ASCE 123 (11) (1997) 1195–1201.
- [5] K. Willam, Y. Xi, D.J. Naus, Concrete under High Temperature, John Wiley & Sons, Ltd, 2014, pp. 439–457.
- [6] V. Kodur, Properties of concrete at elevated temperatures, ISRN Civil Eng., 2014.
- [7] C.R. Cruz, Apparatus for measuring creep of concrete at high temperatures, J. Pca. Res. & Dev. Laboratories (1968).
- [8] J. Marechal, Creep of concrete as a function of temperature, ACI Special Publication 34 (1972) 547–564.
- [9] H. Gross, High-temperature creep of concrete, Nuclear Eng. Des. 32 (1) (1975) 129–147.
- [10] Y. Anderberg, S. Thelandersson, Stress and Deformation Characteristics of Concrete at High Temperatures: Experimental Investigation and Material Behavior Model, Division of Structural Mechanics and Concrete Construction, 1976.
- [11] M. Gillen, Short-term creep of concrete at elevated temperatures, Fire Mater. 5 (4) (1981) 142–148.
- [12] G. Khoury, W.P. Dias, P. Sullivan, Deformation of concrete and cement paste loaded at constant temperatures from 140 to 724°C, Mater. Struct. 19 (2) (1986) 97–104.
- [13] J. Nan, Experimental investigation of mechanical behaviour of concrete considering temperature-stress coupling, (Master’s thesis), Tsinghua University, Beijing, 1994.

- [14] J.C. Mindeguia, P. Pimienta, I. Hager, C. La Borderie, H. Carré, Experimental study of transient thermal strain and creep of an ordinary concrete at high temperatures, *Proceedings of the Fourth International Workshop on Structures in Fire (SIF 2006)*, 2006, pp. 697–708.
- [15] D. Naus, A Compilation of Elevated Temperature Concrete Material Property Data and Information for Use in Assessments of Nuclear Power Plant Reinforced Concrete Structures: Prepared by DJ Naus, US Nuclear Regulatory Commission, Office of Nuclear Regulatory Research, 2010.
- [16] Z. Guo, X. Shi, *Experiment and Calculation of Reinforced Concrete at Elevated Temperatures*, Elsevier, 2011.
- [17] G.A. Khoury, B.N. Grainger, P.J. Sullivan, Strain of concrete during first heating to 600 c under load, *Mag. Concr. Res.* 37 (133) (1985) 195–215.
- [18] S. Thelandersson, Modeling of combined thermal and mechanical action in concrete, *J. Eng. Mech.* 113 (6) (1987) 893–906.
- [19] K. Willam, Y. Xi, K. Lee, B. Kim, *Thermal Response of Reinforced Concrete Structures in Nuclear Power Plants*, University of Colorado, 2009.
- [20] Z.P. Bažant, S.T. Wu, Thermo-viscoelasticity of aging concrete, *J. Eng. Mech. Div.* 100 (3) (1974) 575–597.
- [21] Z.P. Bažant, J.-C. Chern, Stress-induced thermal and shrinkage strains in concrete, *J. Eng. Mech.* 113 (10) (1987) 1493–1511.
- [22] Z. Bažant, L. Cedolin, *Stability of Structures: Elastic, Inelastic, Fracture and Damage Theories*, World Scientific, 2010.
- [23] R. Bagley, P. Torvik, On the fractional calculus model of viscoelastic behavior, *J. Rheol.* 30 (1) (1986) 133–155.
- [24] K.D. Papoulia, V.P. Panoskaltis, N.V. Kurup, I. Korovajchuk, Rheological representation of fractional order viscoelastic material models, *Rheol. Acta* 49 (4) (2010) 381–400.
- [25] H.W. Zhou, C.P. Wang, B.B. Han, Z.Q. Duan, A creep constitutive model for salt rock based on fractional derivatives, *Int. J. Rock Mech. Min. Sci.* 48 (1) (2011) 116–121.
- [26] H. Chen, W. Xu, W. Wang, R. Wang, C. Shi, A nonlinear viscoelastic-plastic rheological model for rocks based on fractional derivative theory, *Int. J. Mod. Phys. B* 27 (25) (2013) 1350149.
- [27] Y. Kawada, T. Yajima, H. Nagahama, Fractional-order derivative and time-dependent viscoelastic behaviour of rocks and minerals, *Acta Geophys.* 61 (6) (2013) 1690–1702.
- [28] H.-H. Zhu, L.-C. Liu, H.-F. Pei, B. Shi, Settlement analysis of viscoelastic foundation under vertical line load using a fractional Kelvin-Voigt model, *Geomech. Eng.* 4 (1) (2012) 67–78.
- [29] A. Saporita, P. Cornetti, A. Carpinteri, O. Baglieri, E. Santagata, The use of fractional calculus to model the experimental creep-recovery behavior of modified bituminous binders, *Mater. Struct.* 49 (1–2) (2016) 45–55.
- [30] N. Makris, M. Constantinou, Fractional-derivative Maxwell model for viscous dampers, *J. Struct. Eng.* 117 (9) (1991) 2708–2724.
- [31] S. Park, Analytical modeling of viscoelastic dampers for structural and vibration control, *Int. J. Solids Struct.* 38 (44) (2001) 8065–8092.
- [32] F. Rüdinger, Tuned mass damper with fractional derivative damping, *Eng. Struct.* 28 (13) (2006) 1774–1779.
- [33] F. Barpi, S. Valente, Creep and fracture in concrete: a fractional order rate approach, *Eng. Fract. Mech.* 70 (5) (2002) 611–623.
- [34] S. Katicha, G. Flintsch, Use of fractional order viscoelastic models to characterize asphalt concrete, in: *Proceedings of the Transportation and Development Institute Congress*, pp. 677–687.
- [35] S. Katicha, G.W. Flintsch, Fractional viscoelastic models: master curve construction, interconversion, and numerical approximation, *Rheol. Acta* 51 (8) (2012) 675–689.
- [36] S. Katicha, A. Apeageyi, G. Flintsch, A. Loulizi, Universal linear viscoelastic approximation property of fractional viscoelastic models with application to asphalt concrete, *Mech. Time-Depend. Mater.* 18 (3) (2014) 555–571.
- [37] A. Kilbas, H. Srivastava, J. Trujillo, *Theory And Applications of Fractional Differential Equations*, North-Holland Mathematics Studies, Elsevier Science & Tech, 2006.
- [38] F. Mainardi, G. Spada, Creep, relaxation and viscosity properties for basic fractional models in rheology, *Eur. Phys. J. Spec. Top.* 193 (1) (2011) 133–160.
- [39] T. Pritz, Analysis of four-parameter fractional derivative model of real solid materials, *J. Sound Vib.* 195 (1) (1996) 103–115.
- [40] F. Mainardi, *Fractional Calculus and Waves in Linear Viscoelasticity: An Introduction to Mathematical Models*, World Scientific, 2010.
- [41] T. Atanacković, M. Janev, S. Pilipović, D. Zorica, An expansion formula for fractional derivatives of variable order, *Open Phys.* 11 (10) (2013) 1350–1360.
- [42] D. Tavares, R. Almeida, D.F. Torres, Caputo derivatives of fractional variable order: numerical approximations, *Commun. Nonlinear Sci. Nume. Simul.* 35 (2016) 69–87.
- [43] A.M. Knaack, *Stress-strain properties of concrete at elevated temperatures*, University of Notre Dame, 2009 Ph.D. thesis.
- [44] T.M. Atanacković, S. Pilipović, B. Stanković, D. Zorica, *Fractional Calculus with Applications in Mechanics: Vibrations and Diffusion Processes*, Wiley-ISTE, 2014.
- [45] H. Sun, W. Chen, H. Wei, Y. Chen, A comparative study of constant-order and variable-order fractional models in characterizing memory property of systems, *Eur. Phys. J. Spec. Top.* 193 (1) (2011) 185–192.
- [46] K. Diethelm, N.J. Ford, A.D. Freed, A predictor-corrector approach for the numerical solution of fractional differential equations, *Nonlinear Dyn.* 29 (1–4) (2002) 3–22.
- [47] C.V. Nielsen, Experimental investigation of combined thermal and mechanical behaviour of Danish and Swedish concrete subject to high temperatures, *Nordic Concr. Res. Publ.* 30 (2003) 1–20.
- [48] M.D. Paola, R. Heuer, A. Pirrotta, Fractional visco-elastic Euler-Bernoulli beam, *Int. J. Solids. Struct.* 50 (22) (2013) 3505–3510.

3.4 Concluding Remarks

This chapter presented the derivation of a novel viscoelastic rheological model for elevated temperature creep in concrete based on fractional derivatives. The model parameters consisting of the dynamic viscosity of the dashpot and fractional exponent were calibrated using existing experimental data. In summary, the following contributions are made in this chapter;

1. A novel non-linear fractional viscoelastic creep law is developed for short-term high temperature creep in concrete;
2. An accurate representation of benchmark experimental data is achieved with only few model parameters;
3. Dynamic viscosity and fractional exponent of the springpots are found to vary with temperature level and concrete aggregate type; and
4. Efficient numerical solutions for creep strain are presented by employing a finite difference scheme to approximate the variable-order fractional differential equation for cases of time-varying stress and temperature.

Chapter 4

In-plane thermo-elastic buckling of shallow concrete arches

4.1 Introduction

In this chapter, the thermo-elastic prebuckling behaviour and in-plane stability of circular shallow concrete arches subjected to uniformly distributed radial loading and uniform temperature fields are analytically investigated. Total longitudinal strain is considered as the sum of the instantaneous elastic strain, thermal expansive strain, basic creep strain and TTS. The virtual work principle is invoked to derive the non-linear equations of equilibrium, and an in-plane buckling analysis is performed resulting in

closed form solutions for the elastic anti-symmetric and symmetric buckling loads for pin-ended and fixed ended arches. The concrete arches are assumed to be mechanically pre-loaded so that TTS can be incorporated in the analysis. Subsequently, basic creep strain is considered. To analyse the thermal response and effect of temperature on buckling loads when considering creep, the elastic-viscoelastic analogy was employed which allows the elastic modulus in the elastic solution to be replaced by a creep operator. Creep is modelled using the fractional derivative-based creep law developed in Chapter 3. Additionally, the factors governing in-plane buckling mode are analytically defined.

The following papers are included in this chapter;

1. Y. Bouras and Z. Vrcelj. 2016. Effect of transient thermal strain on the stability of shallow concrete arches. In *Mechanics of Structures and Materials XXIV: proceedings of the 24th Australian Conference on the Mechanics of Structures and Materials* (ACMSM24, Perth, Australia, 6-9 December 2016 (pp. 963-970). CRC Press.
2. Y. Bouras, and Z. Vrcelj. 2017. Non-linear in-plane buckling of shallow concrete arches subjected to combined mechanical and thermal loading. *Engineering Structures*, 152, pp.413-423.



THE NEW WAY TO DO UNI

OFFICE FOR RESEARCH TRAINING, QUALITY AND INTEGRITY

DECLARATION OF CO-AUTHORSHIP AND CO-CONTRIBUTION: PAPERS INCORPORATED IN THESIS

This declaration is to be completed for each conjointly authored publication and placed at the beginning of the thesis chapter in which the publication appears.

1. PUBLICATION DETAILS (to be completed by the candidate)

Title of Paper/Journal/Book:	Effect of transient thermal strain on the stability of shallow concrete arches		
Surname:	Bouras	First name:	Yanni
Institute:	Institute for Sustainable Industries and Liveat	Candidate's Contribution (%):	95
Status:			
Accepted and in press:	<input type="checkbox"/>	Date:	
Published:	<input checked="" type="checkbox"/>	Date:	06/12/2016

2. CANDIDATE DECLARATION

I declare that the publication above meets the requirements to be included in the thesis as outlined in the HDR Policy and related Procedures – policy.vu.edu.au.

Yanni Bouras	Digitally signed by Yanni Bouras Date: 2020.02.10 15:46:00 +11'00'	10/02/2020
Signature		Date

3. CO-AUTHOR(S) DECLARATION

In the case of the above publication, the following authors contributed to the work as follows:

The undersigned certify that:

1. They meet criteria for authorship in that they have participated in the conception, execution or interpretation of at least that part of the publication in their field of expertise;
2. They take public responsibility for their part of the publication, except for the responsible author who accepts overall responsibility for the publication;

PO Box 14428, Melbourne,
Vic 8001, Australia
+61 3 9919 6100

Victoria University ABN 83776954731
CRICOS Provider No. 00124K (Melbourne),
02475D (Sydney), RTO 3113



THE NEW WAY TO DO UNI

3. There are no other authors of the publication according to these criteria;
4. Potential conflicts of interest have been disclosed to a) granting bodies, b) the editor or publisher of journals or other publications, and c) the head of the responsible academic unit; and
5. The original data will be held for at least five years from the date indicated below and is stored at the following location(s):

Victoria University, Footscray Park, Ballarat Road, Melbourne, VIC 3011, Australia

Name(s) of Co-Author(s)	Contribution (%)	Nature of Contribution	Signature	Date
Yanni Bouras	95	Conceived concept. Literature review. Analytical/numerical modelling. Writing manuscript	[REDACTED SIGNATURE]	11/02/2020
Zora Vrcelj	5	Critical review of manuscript. Final approval of manuscript.		11/02/2020

Updated: September 2019

PO Box 14428, Melbourne,
Vic 8001, Australia
+61 3 9919 6100

Victoria University ABN 83776954731
CRICOS Provider No. 00124K (Melbourne),
02475D (Sydney), RTO 3113



THE NEW WAY TO DO UNI

OFFICE FOR RESEARCH TRAINING, QUALITY AND INTEGRITY

DECLARATION OF CO-AUTHORSHIP AND CO-CONTRIBUTION: PAPERS INCORPORATED IN THESIS

This declaration is to be completed for each jointly authored publication and placed at the beginning of the thesis chapter in which the publication appears.

1. PUBLICATION DETAILS (to be completed by the candidate)

Title of Paper/Journal/Book:	Non-linear in-plane buckling of shallow concrete arches subjected to combined mechanical and thermal loading		
Surname:	Bouras	First name:	Yanni
Institute:	Institute for Sustainable Industries and Liveat	Candidate's Contribution (%):	95
Status:			
Accepted and in press:	<input type="checkbox"/>	Date:	
Published:	<input checked="" type="checkbox"/>	Date:	29/09/2017

2. CANDIDATE DECLARATION

I declare that the publication above meets the requirements to be included in the thesis as outlined in the HDR Policy and related Procedures – policy.vu.edu.au.

Yanni Bouras	Digitally signed by Yanni Bouras Date: 2020.02.10 15:13:37 +11'00'	10/02/2020
Signature		Date

3. CO-AUTHOR(S) DECLARATION

In the case of the above publication, the following authors contributed to the work as follows:

The undersigned certify that:

1. They meet criteria for authorship in that they have participated in the conception, execution or interpretation of at least that part of the publication in their field of expertise;
2. They take public responsibility for their part of the publication, except for the responsible author who accepts overall responsibility for the publication;

PO Box 14428, Melbourne,
Vic 8001, Australia
+61 3 9919 6100

Victoria University ABN 83776954731
CRICOS Provider No. 00124K (Melbourne),
02475D (Sydney), RTO 3113



**VICTORIA
UNIVERSITY**

THE NEW WAY TO DO UNI

3. There are no other authors of the publication according to these criteria;
4. Potential conflicts of interest have been disclosed to a) granting bodies, b) the editor or publisher of journals or other publications, and c) the head of the responsible academic unit; and
5. The original data will be held for at least five years from the date indicated below and is stored at the following location(s):

Victoria University, Footscray Park, Ballarat Road, Melbourne, VIC 3011, Australia

Name(s) of Co-Author(s)	Contribution (%)	Nature of Contribution	Signature	Date
Yanni Bouras	95	Conceived concept. Literature review. Analytical/numerical modelling. Writing manuscript		11/02/2020
Zora Vrcelj	5	Critical review of manuscript. Final approval of manuscript.		11/02/2020

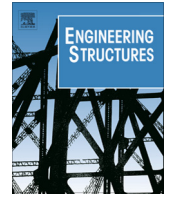
Updated: September 2019

PO Box 14428, Melbourne,
Vic 8001, Australia
+61 3 9919 6100

Victoria University ABN 83776954731
CRICOS Provider No. 00124K (Melbourne),
02475D (Sydney), RTO 3113

Y. Bouras and Z. Vrcelj. 2016. Effect of transient thermal strain on the stability of shallow concrete arches. In *Mechanics of Structures and Materials XXIV: proceedings of the 24th Australian Conference on the Mechanics of Structures and Materials (ACMSM24, Perth, Australia, 6-9 December 2016* (pp. 963-970). CRC Press.
<https://doi.org/10.1201/9781315226460>

The full-text of this article is subject to copyright restrictions, and cannot be included in the online version of the thesis.



Non-linear in-plane buckling of shallow concrete arches subjected to combined mechanical and thermal loading



Yanni Bouras, Zora Vrcelj*

College of Engineering and Science, Centre for Environmental Safety and Risk Engineering (CESARE), Victoria University, Melbourne, VIC, Australia

ARTICLE INFO

Article history:

Received 8 May 2017

Revised 8 September 2017

Accepted 12 September 2017

Keywords:

Buckling

Creep

Fractional derivatives

Limit instability

Shallow arches

Transient thermal strain

ABSTRACT

In this paper, non-linear elastic pre-buckling and in-plane buckling analysis for a circular shallow concrete arch subjected to a uniformly distributed load and time-varying uniform temperature field is performed. Transient thermal strain and basic creep strain are considered, the latter modelled using a fractional derivative creep law, to investigate the coupling effects of time, temperature and geometric non-linearity on mechanical behaviour and stability boundaries. The first correspondence principle is invoked allowing the problem to be treated elastically and statically, with the non-linear equilibrium equations derived using the principle of virtual work. Numerical solutions to the variable order fractional derivatives are obtained through a finite-difference based discretisation scheme. Results show that the coupling effect between transient thermal strain and geometric non-linearity is significant as it influences pre-buckling behaviour and reduces buckling strength. Basic creep strain is less influential, causing a slight enhancement of the effects of transient thermal strain.

© 2017 Elsevier Ltd. All rights reserved.

1. Introduction

As linear analyses of shallow arches lead to an over-estimation of anti-symmetric bifurcation and symmetric snap-through buckling loads, caused by geometric non-linearity, non-linear methods are required for their analysis. Due to the common application of shallow arches in civil engineering, coupling effects of this inherent geometric non-linearity and additional complexities, including temperature changes and viscoelasticity, require research attention.

The effects of uniform thermal loading on the behaviour and in-plane elastic stability of shallow steel arches were investigated [1–3]. Elevated temperatures induce compressive stresses in arches due to end restrained thermal expansion and cause upward deflections. These thermal induced stresses and displacements are enhanced in shallow arches due to geometric non-linearity. Additionally, uniform temperature loading may cause anti-symmetric bifurcation buckling or symmetric limit instability failure. When shallow steel arches are subjected to combined mechanical and uniform temperature loading, additional axial compressive forces are generated and the radial deflections are reduced [4–8]. Furthermore, the critical in-plane buckling loads increase with temperature. Pi and Bradford [9] studied the thermoelastic stability of

shallow steel circular arches subjected to thermal gradients. The authors discovered that arches may experience snap-through or bifurcation buckling when subjected to a thermal gradient due to increasing bending and axial compression caused by curvature changes and axial expansion respectively. Furthermore, it was found that anti-symmetric buckling is the dominant case and symmetric buckling can only occur for slender shallow arches. Cai et al. [10] investigated the stability of shallow steel parabolic arches subjected to temperature gradients and mechanical loading. Results showed that critical buckling loads increased with an increasing uniform temperature field. Conversely, the critical loads decreased with an increasing temperature gradient. However, less work has been completed on the behaviour and stability of concrete arches at elevated temperatures. Bouras and Vrcelj [11] conducted a pre-buckling and stability analysis of shallow circular concrete arches subjected to combined mechanical and thermal loading in order to analyse the effect of transient thermal strain (TTS). It was found that when considering TTS, axial compressive force increased with temperature and the arch deflected downwards. Moreover, TTS significantly magnified the reduction in buckling strength of concrete arches at elevated temperatures. Basic creep strain was not considered.

Concrete and concrete-filled steel tubular (CFST) arches deform in time due the viscoelastic effects of creep and shrinkage. These quasi-static changes in the non-linear equilibrium configuration may induce loss of stability under the sustained load, despite

* Corresponding author.

E-mail address: zora.vrcelj@vu.edu.au (Z. Vrcelj).

initially being deemed as stable. The phenomenon of creep buckling has received research attention for both concrete [12] and CFST [13–16] arches. Axial force, bending moment and displacements increase with time due to creep and shrinkage. Subsequently, the creep strain is magnified due to the increased stress levels, causing the deformations and stresses to continually grow and reach an unstable equilibrium configuration at which buckling is possible [12]. The significance of this behaviour is magnified in shallow arches due to geometric non-linearities. As the creep behaviour of concrete is sensitive to temperature variations [17], typical daily and seasonal fluctuations should be considered in long-term analyses of concrete and CFST structures. Luo et al. [18] investigated the time-dependent behaviour of a crown-pinned circular CFST arch under constant temperature change and found that the coupling between creep, shrinkage and temperature significantly influenced the long-term deformations and internal forces. Wang et al. [19] studied the effect of temperature fluctuations on the creep behaviour of a CFST arch bridge. Using the micro-prestress solidification theory [20] and the age-adjusted effective modulus method, they found that creep deformations and stresses at the arch mid-span increased by 9% and 7–18% respectively, when temperature changes were considered. These findings emphasize the importance of temperature-time coupling in arch structures. However, these two studies were restricted to low temperature variations (not exceeding 100 °C) and not extended to analyse stability.

Despite not accurately reflecting the behaviour of real materials [21], viscoelastic models have been widely adopted for the constitutive relation of materials exhibiting time-dependent properties. The inaccuracy is due to the linear differential stress-strain equation being of integer order. To overcome this, viscoelastic chains are constructed which consist of a multitude of viscoelastic units placed in series or parallel. However, as complexities arise due to the myriads of material parameters to be characterised [22], intensive numerical simulations and comprehensive experimental data sets are required. Hence, the practicality of employing viscoelastic chains in both analytical and numerical investigations is diminished. The inherent disadvantages associated with viscoelastic models are overcome using fractional calculus, which is a branch of mathematical analysis concerned with performing integration or differentiation to a degree of real value [23–25]. Despite the formulation of fractional calculus in the 17th century, the most significant developments in engineering and scientific applications have been found only in the last 100 years [23]. With fractional calculus, the spring-dashpot models of viscoelasticity may now be generalised by replacing the integer order of derivative in the constitutive stress-strain equation with a real order. Fractional viscoelastic models, such as the fractional Kelvin-Voigt, fractional Maxwell and fractional Zener, have proven to be robust descriptors of material behaviour [26], as experimental data can be accurately reflected with the use of a minimal number of material parameters. Papoulia et al. [27] proved that the models of fractional viscoelasticity are obtained when the number of units in a generalised viscoelastic chain approach infinity. Additional applications of fractional viscoelasticity to model the dynamic behaviour of concrete includes the work of Barpi and Valente [28], who combined a micro-mechanical model and fractional viscoelastic element to investigate crack propagation in concrete, and Katicha and Flintsch [29] who employed fractional viscoelastic models to characterize the time-dependent properties of asphalt concrete. More recently, Bouras et al. [30] developed a fractional calculus based viscoelastic model for high temperature creep in concrete.

In the present study, an elastic in-plane buckling analysis of a shallow plain concrete arch subjected to a uniformly distributed radial load and time-varying uniform temperature field, for both pinned and fixed ends, is undertaken. The arch is assumed to be

mechanically pre-loaded, so TTS will manifest when the concrete arch is heated. Basic creep strain is considered and modelled using the aforementioned variable order fractional derivative creep law. The influence of both transient thermal strain and basic creep strain on the behaviour and stability boundaries of shallow concrete arches under short-term temperature increases, are the focus of the investigation. Although creep strain is often neglected in studies of concrete under transient temperature increases such as those caused by fire, it warrants investigation in shallow arches due to their geometric non-linearities and increasing temperature-dependent stresses and deflections.

2. Material model

The total strain ϵ in pre-loaded concrete members subjected to an elevating temperature, a function of time t , stress $\sigma(t)$ and temperature $T(t)$, is defined as

$$\epsilon(\sigma, t, T(t)) = e(\sigma(t), T(t)) + e_{cr}(\sigma(t), T(t), t) + e_{th}(T(t)) + e_{tr}(\sigma(t), T(t)), \quad (1)$$

where e is the instantaneous mechanical strain, e_{cr} is the basic creep strain, e_{th} is the thermal strain and e_{tr} denotes TTS. Thermal strain is known as

$$e_{th} = a \Delta T, \quad (2)$$

with a representing the coefficient of thermal expansion, assumed constant at $8 \times 10^{-6}/^{\circ}\text{C}$, and $\Delta T = T - T_0$, where T_0 is the initial temperature. Considering only elastic behaviour, the instantaneous mechanical strain can be expressed as

$$e_{el} = \frac{\sigma}{E(T)}, \quad (3)$$

where $E(T)$ is the temperature dependent elastic modulus which will be modelled using the Eurocode 2 formulation [31]. The Anderberg model of TTS [32] is adopted and defined as

$$e_{tr} = \frac{\sigma}{f'_c} \beta a \Delta T. \quad (4)$$

where f'_c denotes the cold compressive strength and the constant $\beta = 2.35$. This model has been employed as the TTS is linear proportional to stress which simplifies the analytical analysis, and due to its common application in fire investigations. Adopting other TTS models does not qualitatively change behaviour however may cause quantitative differences in results, see [11].

A rheological model consisting of a fractional dashpot (spring-pot) unit will be employed to model the basic creep strain which is governed by the following variable order fractional derivative equation, see [30],

$$D_t^{\alpha(T)} e_{cr} = \frac{\sigma}{\eta(T)}. \quad (5)$$

In Eq. (5), $D_t^{\alpha(T)}$ is the operator of the fractional derivative of variable order $\alpha(T)$ with respect to time t , satisfying $0 < \alpha < 1$ and $t > 0$, and $\eta(T)$ is the temperature dependent dynamic viscosity. These parameters are available in Appendix A.1. Two definitions of the variable-order fractional derivative are adopted and subsequently examined; the Caputo fractional derivative of a function $f(t)$ known as

$$D_t^{\alpha(t)} f(t) = \frac{1}{\Gamma(1 - \alpha(t))} \int_0^t \frac{D^1 f(\tau)}{(t - \tau)^{\alpha(t)}} d\tau, \quad (6)$$

and the *memory of order* definition

$$D_t^{\alpha(t)} f(t) = \int_0^t \frac{D^1 f(\tau)}{\Gamma[1 - \alpha(t - \tau)](t - \tau)^{\alpha(t - \tau)}} d\tau, \quad (7)$$

where D^1 is the first order differential operator. In Eq. (7) the fractional exponent α is dependent on the kernel τ . The latter possesses a memory of the order of differentiation which is not considered in Eq. (6). The significance of the definition of the variable-order fractional derivative in non-linear pre-buckling and buckling behaviour will be a subject of analysis. For the case of time-invariant temperature, Eq. (5) reverts to constant order fractional derivative equation, allowing the basic creep strain to be expressed in integral form;

$$e_{cr} = \frac{1}{\eta} J_t^{-\alpha} \sigma = \frac{1}{\eta \Gamma(\alpha)} \int_0^t (t - \tau)^{\alpha-1} \sigma(\tau) d\tau. \quad (8)$$

The Reimann-Louville definition of the fractional integral is adopted in Eq. (8) and $J_t^{-\alpha}$ denotes the operator of the fractional integral of order α . The Gamma function $\Gamma(\alpha)$ is defined as

$$\Gamma(\alpha) = \int_0^\infty e^{-t} t^{\alpha-1} dt. \quad (9)$$

Upon substitution of (2)–(4) into (1), it is obtained that

$$\frac{\sigma}{\hat{E}} + e_{cr} = \epsilon - a \Delta T, \quad (10)$$

where the parameter \hat{E} is defined as

$$\hat{E} = E + \frac{f'_c}{\beta a \Delta T} \quad (11)$$

and e_{cr} is the solution to the variable-order fractional derivative Eq. (5). The elastic-viscoelastic analogy [22,33], often called the correspondence principle, is utilized for the analysis. It allows the solution of a linear creep problem to be obtained by replacement of the modulus E in the corresponding elastic problem by a creep operator \mathbf{E} defined as,

$$\mathbf{E}^{-1} \sigma = \frac{\sigma}{\hat{E}} + e_{cr}. \quad (12)$$

This method is applicable to cases of time-variant creep, such as due to non-constant temperature or ageing effects. Additionally, the creep operator can be manipulated according to the laws of algebra. Thus, Eq. (10) may be rewritten as

$$\mathbf{E}^{-1} \sigma = \epsilon - a \Delta T. \quad (13)$$

The definitions of axial compressive force N and bending moment M

$$N = - \int_A \sigma dA, \quad M = \int_A \sigma y dA, \quad (14)$$

used in conjunction with (13), yield the constitutive equations for axial force

$$\mathbf{E}^{-1} N = N / \hat{E} + e_{cr}(N) = A(\alpha \Delta T - \epsilon_m), \quad (15)$$

and moment curvature

$$\mathbf{E}^{-1} M = M / \hat{E} + e_{cr}(M) = - \frac{I v''}{R} \quad (16)$$

with I and R representing the second moment of area of the cross section and the arch radius respectively.

3. In-plane equilibrium

3.1. Non-linear equations of equilibrium

Consider a shallow circular arch, pinned or fixed at its ends, subjected to a uniformly distributed radial load q and a time-variant uniform temperature field $T(t)$ depicted in Fig. 1. The origin o is taken at the arch centroidal axis, with the axis oy always directed towards the center of the arch as its direction changes along the circumference and the axis os coinciding with the arches centroidal axis. In order to consider geometric non-linearity, the following non-linear formulation of longitudinal normal strain is adopted [34,35];

$$\epsilon = \epsilon_m + \epsilon_b \quad (17)$$

where ϵ_m and ϵ_b are the membrane and bending strains respectively, defined as

$$\epsilon_m = w' - v + \frac{1}{2} (v')^2, \quad \epsilon_b = -y \frac{v''}{R}, \quad (18)$$

and ϵ is the total strain at an arbitrary point \mathcal{P} in the arch cross section. In Eq. (18) $w = \hat{w}/R$, $v = \hat{v}/R$, \hat{w} and \hat{v} are the axial and radial displacements respectively, y is the coordinate of the point \mathcal{P} , $(\cdot)' = d(\cdot)/d\theta$, $(\cdot)'' = d^2(\cdot)/d\theta^2$ and θ is the angular coordinate.

Expression of the constitutive material model by using the elastic-viscoelastic analogy allows the pre-buckling analyses to be treated elastically and statically. The non-linear in-plane equilibrium equations are derived using the principle of virtual work, where it is required that

$$\delta \Pi = \int_V \sigma \delta \epsilon dV - \int_{-\Theta}^{\Theta} q R^2 \delta v d\theta = 0, \quad \forall \delta v, \delta v', \delta v'', \delta w, \delta w' \quad (19)$$

where V is the volume of the arch, Θ is half the included angle and $\delta v, \delta v', \delta v'', \delta w$ and $\delta w'$ are kinematically admissible variations of

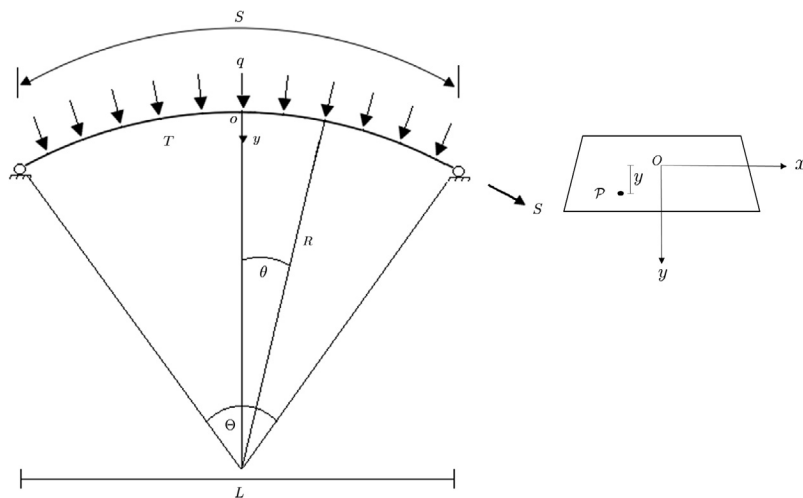


Fig. 1. Arch loading and geometrical configuration.

displacements. Substituting Eq. (18) into (19), and integrating by parts yields the non-linear equations of equilibrium,

$$N' = 0, \tag{20}$$

in the axial direction,

$$-M'' + NRv'' + NR - qR^2 = 0, \tag{21}$$

in the radial direction, and to the static boundary condition for a pin-ended arch

$$v''(\Theta) = v''(-\Theta) = 0. \tag{22}$$

The geometrical boundary conditions are known as

$$v(\Theta) = v(-\Theta) = w(\Theta) = w(-\Theta) = 0, \tag{23}$$

for a pin-ended arch, and

$$v(\Theta) = v(-\Theta) = v'(\Theta) = v'(-\Theta) = w(\Theta) = w(-\Theta) = 0, \tag{24}$$

for an arch fixed at its ends.

Upon substitution of Eq. (16) into (21), the differential equation of equilibrium in the radial direction is obtained as

$$\frac{v''''}{\mu^2} + v'' = P, \tag{25}$$

where the axial force parameter μ is defined as

$$\mu^2 = \mathbf{E}^{-1} N \frac{R^2}{I}, \tag{26}$$

and P denotes the dimensionless load parameter

$$P = \frac{qR - N}{N}. \tag{27}$$

Solving differential equation of equilibrium (25) by using the boundary conditions given in (22) and (23) for pinned arches and (24) for fixed arches, yields the dimensionless radial displacement

$$v = \frac{P}{\mu^2} \left[\frac{\Phi[\cos(\mu\theta) - \cos(\mu\Theta)]}{\cos(\mu\Theta)} + \frac{1}{2}(\mu^2\theta^2 - \mu^2\Theta^2) \right]. \tag{28}$$

where the parameter Φ is defined as

$$\begin{aligned} \Phi &= 1 && \text{for pin-ended arches,} \\ \Phi &= \mu\Theta / \tan(\mu\Theta) && \text{for fixed arches.} \end{aligned} \tag{29}$$

The non-linear equilibrium equation relating the axial compressive force parameter μ and the dimensionless load P is obtained by substituting Eqs. (18), (28) and (23) or (24) into (15), yielding

$$B_1 P^2 + B_2 P + B_3 = 0, \tag{30}$$

where

$$B_1 = \frac{\Phi^2}{4\mu^2\Theta^2} \left[1 - \frac{\tan(\mu\Theta)}{\mu\Theta} + \tan^2(\mu\Theta) \right] + \frac{\Phi}{\mu^2\Theta^2} \left[1 - \frac{\tan(\mu\Theta)}{\mu\Theta} \right] + \frac{1}{6}, \tag{31}$$

$$B_2 = \frac{\Phi}{\mu^2\Theta^2} \left[1 - \frac{\tan(\mu\Theta)}{\mu\Theta} \right] + \frac{1}{3}, \tag{32}$$

$$B_3 = \frac{\mu^2\Theta^2}{\lambda^2} - \frac{\alpha\Delta TS^2}{4\lambda^2 r_x^2}, \tag{33}$$

with the arch geometric parameter λ defined as

$$\lambda = R\Theta^2 / r_x = S\Theta / 2r_x. \tag{34}$$

Thus, for a given distributed load q and temperature history $T(t)$, the time-dependent axial force $N(t)$ can be obtained by solving Eq. (30), subsequently allowing the dimensionless displacement

$v(t)$ and bending Moment $M(t)$ to be obtained by solving (28) and (16) respectively.

3.2. Numerical methodology

The axial force parameter μ is dependent on the integer operator \mathbf{E}^{-1} which is governed by a constant-order fractional integral in the case of time-invariant temperature, and a variable-order fractional differential equation when the temperature field varies with time. A finite-difference based discretisation method is utilised for the numerical approximation of the fractional creep laws.

3.2.1. Time-invariant temperature

For the case of constant temperature in time, the creep strain can be expressed in the form of Eq. (8), hence μ can be written as

$$\mu^2 = \frac{NR^2}{\bar{E}I} + \frac{R^2}{\eta I} J_t^{-\alpha} N. \tag{35}$$

The fractional integral is approximated as

$$(J_t^{-\alpha} N)_n = \frac{(\Delta t)^\alpha}{\Gamma(\alpha + 1)} \sum_{j=0}^{n-1} N_j [(n-j)^\alpha - (n-j-1)^\alpha] \tag{36}$$

where Δt is the time step size, $t = n\Delta t, n = 1, 2, 3 \dots X, X = t_f / \Delta t, t_f$ is the loading duration and $\tau = j\Delta t$. The derivation of Eq. (36) is provided in Appendix A.2. The notation $(\cdot)_n$ and $(\cdot)_j$ denote $(\cdot)(n\Delta t)$ and $(\cdot)(j\Delta t)$ respectively. The axial force parameter μ thus becomes

$$\mu^2 = \frac{NR^2}{\bar{E}I} + \frac{R^2(\Delta t)^\alpha}{\eta I \Gamma(\alpha + 1)} \sum_{j=0}^{n-1} N_j [(n-j)^\alpha - (n-j-1)^\alpha]. \tag{37}$$

Using (36), Eq. (30) is solved at each time step beginning with $n = 1$. The algorithm however requires the initial axial force $N(t = 0)$ to be predetermined. This is achieved by simply solving the corresponding elastic problem, $\mu^2(0) = N(0)R^2/EI$.

3.2.2. Time-variant temperature

When time-varying temperature is considered, the axial force parameter is given as

$$\mu^2 = \frac{NR^2}{\bar{E}I} + \frac{R^2}{I} e_{cr}(N), \tag{38}$$

where the creep strain e_{cr} is governed by the fractional differential equation

$$D_t^{\alpha(T)} e_{cr} = \frac{N}{\eta(T)}. \tag{39}$$

When adopting Eq. (6) for the definition of the variable-order derivative, the creep strain is numerically approximated as

$$\begin{aligned} e_{cr,n} &= e_{cr,n-1} - \sum_{j=0}^{n-2} (e_{cr,j+1} - e_{cr,j}) [(n-j)^{1-\alpha_n} - (n-j-1)^{1-\alpha_n}] \\ &\quad + \frac{N_n}{\eta_n} \Gamma(2 - \alpha_n) \Delta t^{\alpha_n}. \end{aligned} \tag{40}$$

The numerical algorithm begins at time step $n = 2$, therefore the creep strain at $t = 1$ is required and is derived as

$$e_{cr}(1) = \frac{N_1}{\eta_1} \Gamma(2 - \alpha_1) (\Delta t)^{\alpha_1} + e_{cr}(0), \tag{41}$$

where the initial creep strain has the obvious value $e_{cr}(0) = 0$. The values of N are also required at the initial time steps of $n = 0$ and $n = 1$. These are obtained individually by solving Eq. (30) with $\mu^2(0) = N(0)R^2/\bar{E}I$ and $\mu^2(1) = N(1)R^2/\bar{E}(1)I + R^2 e_{cr}(1)/I$

respectively. The creep strain is also discretised when adopting Eq. (7) for the definition of the variable-order differential equation;

$$e_{cr,n} = e_{cr,n-1} - \Gamma(2 - \alpha_1) \Delta t^{\alpha_1} \sum_{j=0}^{n-2} \frac{e_{cr,j+1} - e_{cr,j}}{\Gamma(2 - \alpha_{n-j})} \times \left[(n-j)^{1-\alpha_{n-j}} - (n-j-1)^{1-\alpha_{n-j}} \right] + \frac{N_n}{\eta_n} \Gamma(2 - \alpha_1) \Delta t^{\alpha_1} \quad (42)$$

with the creep strain at $t = 1$ obtained as

$$e_{cr}(1) = \frac{N_1}{\eta_1} \Gamma(2 - \alpha_0) \Delta t^{\alpha_0} + e_{cr}(0) \quad (43)$$

and $e_{cr}(0) = 0$. A disadvantage of Eqs. (40) and (42) is the dependency on both stress and strain history at each time step. Consequently computation times are significantly higher when compared to Eq. (36) which requires only stress history. Therefore it would be beneficial if the order of derivative did not vary with temperature, allowing the creep strain to be expressed in fractional integral form with only a temperature-dependent viscosity. In this case, the axial force parameter becomes

$$\mu_n^2 = \frac{N_n R^2}{E_n I} + \frac{R^2 (\Delta t)^\alpha}{\Gamma(\alpha + 1)} \sum_{j=0}^{n-1} \frac{N_j}{\eta_j} [(n-j)^\alpha - (n-j-1)^\alpha]. \quad (44)$$

It would be shown in the following section, that the order of derivative may be assumed constant and still provide practically the same solution as if it were variable.

3.3. Pre-buckling behaviour

The time and temperature evolution of the axial force N can be obtained from Eq. (30) for a given distributed load q and temperature history $T(t)$. Figs. 2 and 3 depict the effect of linearly increasing temperature in time on the axial force for fixed and pinned ended arches respectively. The arches feature an included angle $\Theta = 34.3775^\circ$, slenderness ratio $S/r = 155.523$, geometric parameter $\lambda = 46.6568$, cold compressive strength $f_c = 32$ MPa, an initial elastic modulus $E_0 = 30,100$ MPa, are subject to a uniformly distributed radial load of $q = 25$ kN/m and are heated at a rate of $1.67^\circ\text{C}/\text{min}$ from an initial temperature of 22°C . The axial force increases with time and/or temperature and shows rapid jump as

the limit instability point is reached. As expected when neglecting creep strain, the rate of change in axial force is reduced and the arch reaches the limit instability point later in time. Anti-symmetric buckling is however the dominant buckling mode in shallow arches, therefore the limit instability point will not be reached except for very shallow arches [5].

The dimensionless radial deflections and bending moments at various time intervals are shown in Figs. 4 and 5 for pinned and fixed arches respectively. Definition (6) of the variable order fractional derivative is adopted. In both pinned and fixed ended arches, the radial deflection continues in the downward direction as time and temperature increase. As the critical time for limit instability is approached, a change in direction of displacement occurs in the outer regions of the arch. For the pin-ended case this occurs at approximately $t = 135$ mins and for the fixed arch at $t = 180$ mins, see Figs. 4 and 5. This shape change may be considered as a form of stability loss. It is however likely that anti-symmetric buckling will occur first as the deflected shape begins to change near the symmetric snap-through point. This manifestation of new modes is seen clearly in the moment evolution diagrams. For pinned arches (Fig. 4(b)), the bending moment reduces in time throughout the arch length. However, as the direction of displacement in the arch ends is reversed, the bending moment in the central region of the arch begins to increase and development of negative moment occurs in the outer segments. Similar behaviour is observed in fixed arches (Fig. 5(b)) albeit at a higher mode due to the existence of end moments which increase in time.

It has been found that practically no difference in results is obtained when adopting Eq. (6) or (7) for the definition of the variable order fractional derivative, as seen in Figs. 2 and 3. Thus the additional computation time and memory required by definition (7), due to the dependence of the history of $\alpha(T)$, is not warranted. A significant reduction in computation times may also be obtained when the order of derivative is assumed constant, in this case $\alpha = 0.4$. This value is determined by fitting the creep curve obtained for constant order to those obtained with a variable order and subjected to the same stress. Thus the constant value of the order of the fractional exponent is dependent on heating rate and is only applicable for uniform heating cases.

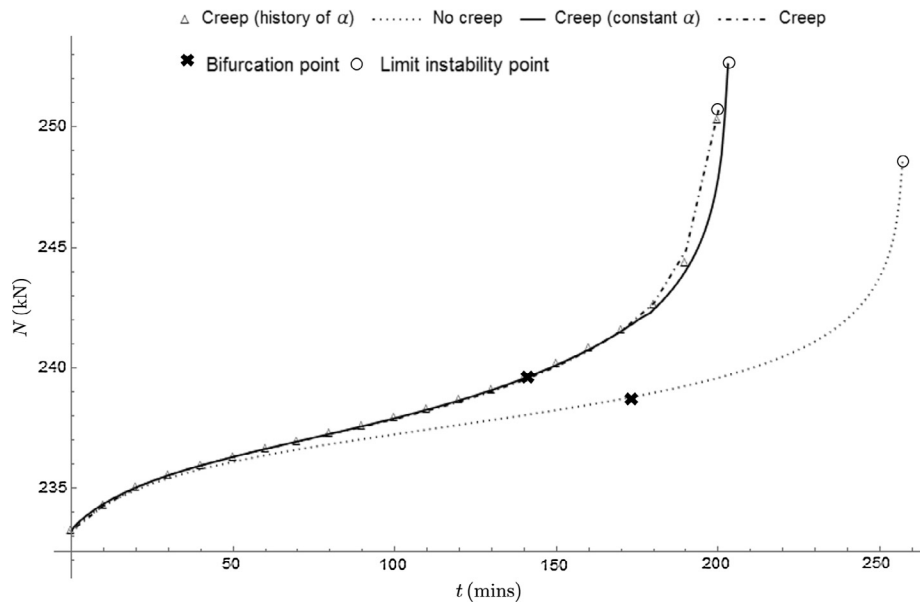


Fig. 2. Effect of increasing temperature on axial force (fixed ends).

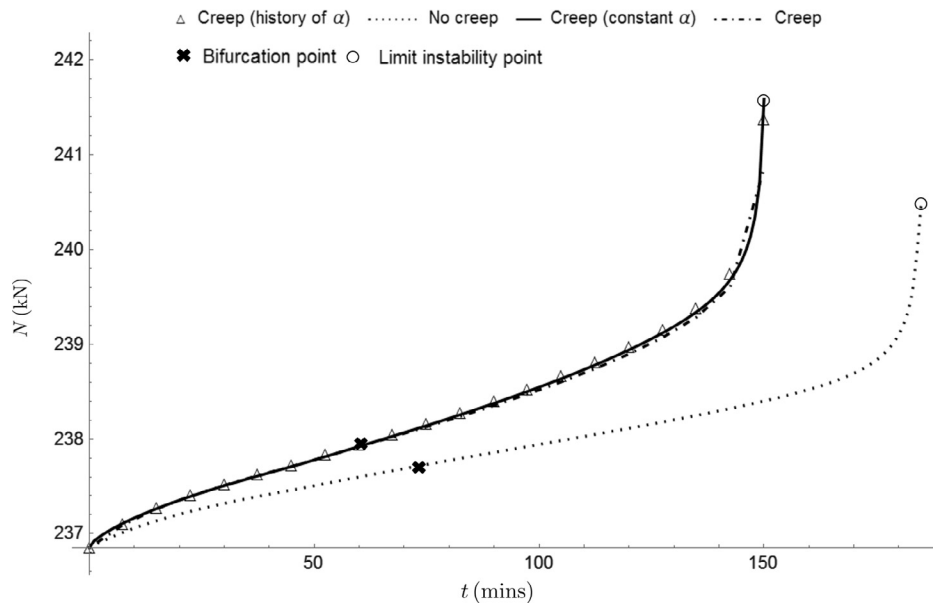


Fig. 3. Effect of linearly increasing temperature in time on axial force (pinned ends).

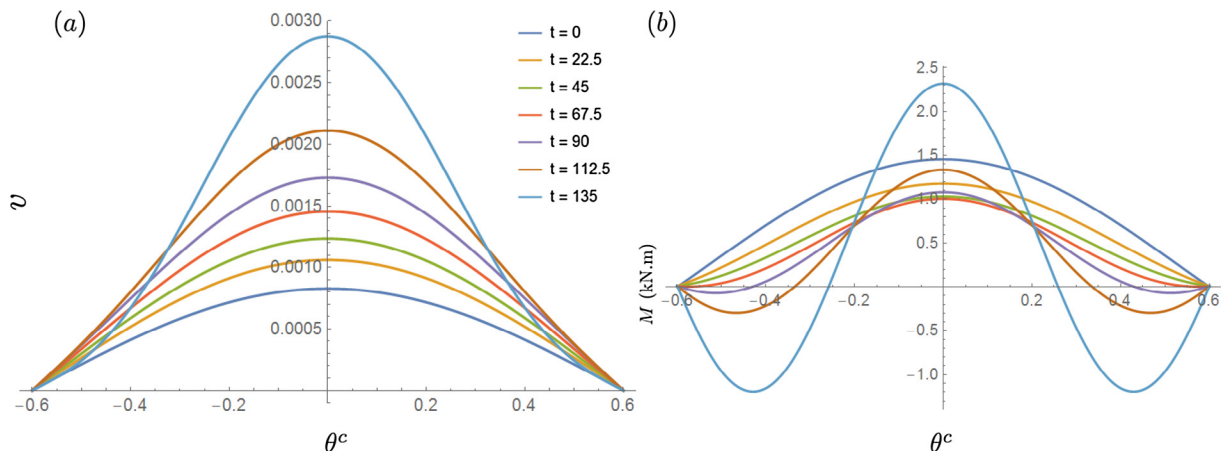


Fig. 4. Effect of linearly increasing temperature in time on deflection (a) and bending moment (b) for a pin-ended arch.

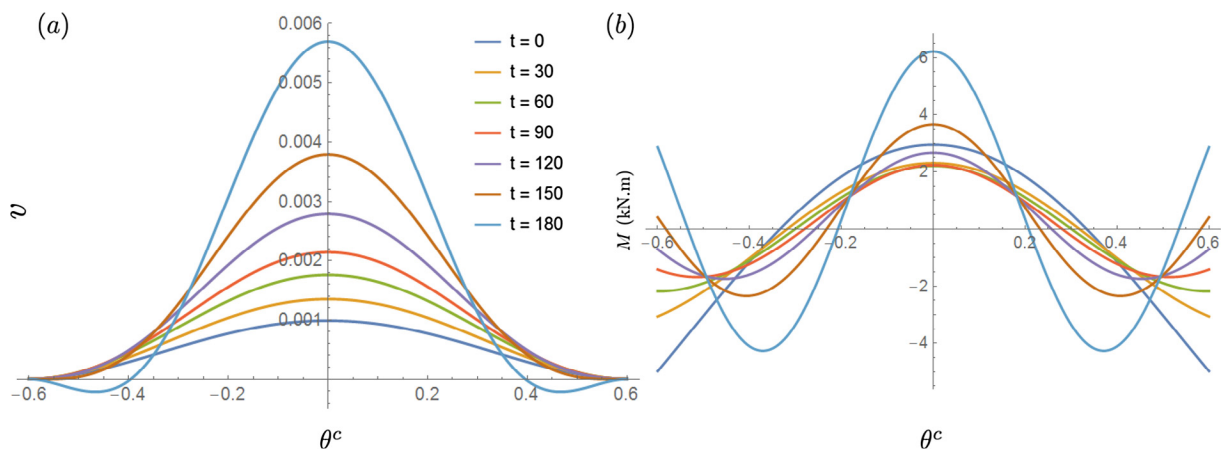


Fig. 5. Effect of linearly increasing temperature in time on deflection (a) and bending moment (b) for a fixed-ended arch.

4. Buckling analysis

4.1. Buckling equilibrium differential equations

Upon reaching a critical time or temperature, the arch may transition from a pre-buckled equilibrium configuration to an adjacent buckled equilibrium position characterised by $\bar{N} = N + N_b$, $\bar{M} = M + M_b$, $\bar{v} = v + v_b$, and $\bar{w} = w + w_b$, where N_b, M_b, v_b and w_b denote perturbations. Substituting the perturbed quantities into the pre-buckled equilibrium Eqs. (20) and (21), and neglecting higher order terms, yields the buckled equilibrium equations,

$$N'_b = 0, \tag{45}$$

and

$$RNv''_b + RN_b(1 + v'') - M''_b = 0, \tag{46}$$

and the buckled constitutive equations.

$$E^{-1}N_b = -A(w'_b - v_b + v'v'_b), \tag{47}$$

and

$$E^{-1}M_b = -\frac{Iv''_b}{R}. \tag{48}$$

when substituted into Eqs. (15) and (16). The static boundary conditions are similarly obtained as

$$w_b(\Theta) = w_b(-\Theta) = v_b(\Theta) = v_b(-\Theta) = v''_b(\Theta) = v''_b(-\Theta) = 0, \tag{49}$$

for pin-ended arches and

$$w_b(\Theta) = w_b(-\Theta) = v_b(\Theta) = v_b(-\Theta) = v'_b(\Theta) = v'_b(-\Theta) = 0, \tag{50}$$

for fixed arches.

4.2. Anti-symmetric bifurcation buckling

The anti-symmetric nature of bifurcation buckling results in the buckling displacement v_b being anti-symmetric. The derivative of the pre-buckling displacement v' is also anti-symmetric as v is symmetric prior to buckling. Thus when integrating Eq. (47) throughout the arch length, the terms v_b and v' vanish, producing

$$E^{-1}N_b = N/\hat{E} + e_{cr}(N_b) = 0, \tag{51}$$

which has the solution

$$N_b = 0. \tag{52}$$

Substituting Eqs. (48) and (52) into (46) gives the linear homogeneous differential equation for bifurcation buckling

$$\frac{v''''_b}{\mu^2} + v''_b = 0. \tag{53}$$

Solving Eq. (53) yields

$$v_b = C_1 \sin(\gamma\mu\theta) + C_2 \cos(\gamma\mu\theta) + C_3\theta + C_4, \tag{54}$$

where $C_1 \dots C_4$ are undetermined coefficients. For the existence of non-trivial coefficients, the first determinant of the coefficient matrix must vanish, leading to the following characteristic equations, as originally obtained by Pi et al. [35],

$$\begin{aligned} \sin(\gamma\mu\theta) \cos(\gamma\mu\theta) &= 0 && \text{for pinned arches} \\ [\mu\Theta \cos(\mu\Theta) - \sin(\mu\Theta)] \sin(\gamma\mu\theta) &= 0 && \text{for fixed arches.} \end{aligned} \tag{55}$$

The lowest solutions of characteristic Eqs. (55) when the first terms vanish are $\mu\theta = \pi$ for pin-ended arches, and $\mu\Theta = 1.4303\pi$ for fixed

arches. Substituting these solutions into Eq. (26) yields the critical axial force

$$E^{-1}N_p = \frac{\pi^2 I}{(S/2)^2} \quad \text{for pinned arches} \tag{56}$$

$$E^{-1}N_p = \frac{(1.4303\pi)^2 I}{(S/2)^2}. \quad \text{for fixed arches}$$

The numerical methods presented in Section 3.2 are then utilised for solving Eq. (56). Substituting (56) into (30) yields

$$D_1 P_b^2 + D_2 P_b + D_3 = 0 \tag{57}$$

where

$$D_1 = 15 + 2\pi^2, \quad D_2 = 12 + 4\pi^2, \quad D_3 = \frac{12\pi^4}{\lambda^2} - \frac{3\alpha\Delta T S^2 \pi^2}{\lambda^2 r^2}, \tag{58}$$

for pinned arches, and

$$D_1 = 5, \quad D_2 = 4, \quad dD_3 = \frac{12(1.4303\pi)^2}{\lambda^2} - \frac{3\alpha\Delta T S^2}{\lambda^2 r^2}, \tag{59}$$

for arches with fixed ends. The critical anti-symmetric buckling load is obtained at a given point in time by solving Eq. (58) for pin-ended arches or (59) for fixed arches, with the corresponding critical axial force being predetermined using Eq. (56).

The anti-symmetric bifurcation loads q_{cr} for pin-ended and fixed-ended arches are shown in Fig. 6. A heating rate of 1.67 °C/min is applied to the arches with initial temperature being ambient ($T(t=0) = 22$ °C). Both creep and TTS are analysed to determine their significance in relation to buckling strength. TTS drastically reduces the critical bifurcation loads of arches with pinned or fixed ends. When TTS is not considered, a small increase of buckling resistance is observed at low temperatures, in this case when $T < 100$ °C. A consequence of the Eurocode 2 model for instantaneous elastic modulus which assumes no reduction in the elastic modulus in this temperature range. Hence the arch displaces upwards due to thermal strain causing an increase in q_{cr} . However, as the elastic modulus degrades at higher temperatures, so does the buckling strength.

Further reduction in buckling strength occurs due to the basic creep strain albeit with less significance than when compared to TTS. Practically the same results are obtained for anti-symmetric buckling loads when adopting definition (6) or (7) for the fractional derivative, or when assuming the order of derivative as a constant of a pre-determined value ($\alpha = 0.4$ for results presented in Fig. 6). As the magnitude of basic creep strain is small when compared to TTS in the short-term, the obtained results satisfy intuitive expectations. Thus, as with other structural members such as beams and columns, the basic creep may also be neglected in the analysis of shallow concrete arches subject to transient temperature increases.

4.3. Symmetric buckling

In addition to anti-symmetric buckling, a shallow arch may fail in a symmetric snap-through mode. It was shown that for shallow arches, symmetric buckling is equivalent to limit instability [5]. For this case, the displacements v_b and v' do not vanish when integrated, resulting in the differential equation as shown

$$\frac{v''''_b}{\mu^2} + v''_b = -\frac{N_b}{N}(1 + v''). \tag{60}$$

Upon solving Eq. (60), substituting the solution v_b into (47) and integrating over the arch length, the equilibrium equation for limit instability is obtained as

$$C_1 P^2 + C_2 P + C_3 = 0, \tag{61}$$

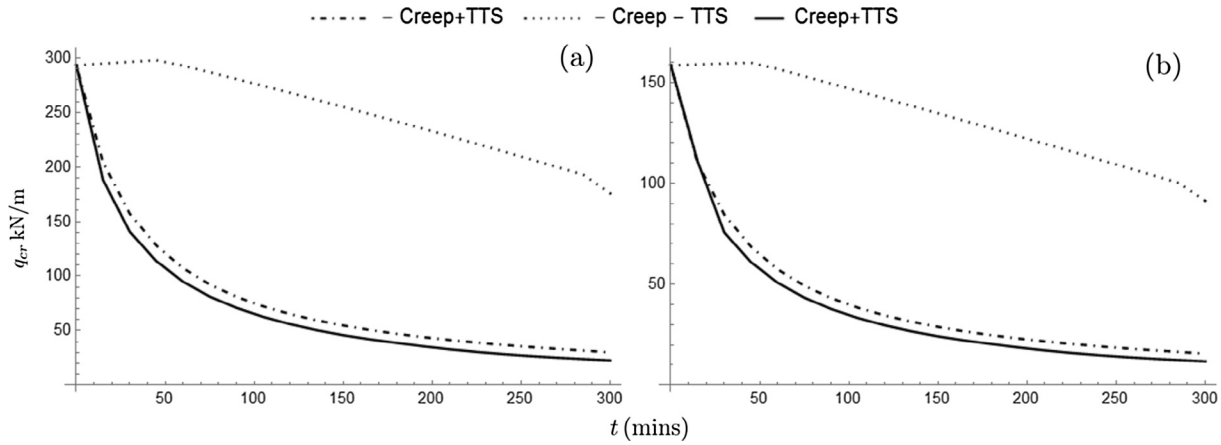


Fig. 6. Anti-symmetric buckling loads for fixed (a) and pinned (b) arches subjected to a heating rate of 1.67 °C/min.

where

$$C_1 = 2B_1 + C_4, \quad C_2 = 4B_1, \quad C_3 = B_2 - \frac{\mu^2 \Theta^2}{\lambda^2}, \quad (62)$$

and

$$C_4 = \frac{15}{8\mu^2 \Theta^2} - \frac{15 \tan(\mu\Theta)}{8\mu^3 \Theta^3} - \frac{\tan(\mu\Theta)}{4\mu\Theta \cos^2(\mu\Theta)} + \frac{7 \tan(\mu\Theta)^2}{8\mu^2 \Theta^2}$$

for pinned arches

$$C_4 = \frac{\mu\Theta}{4 \tan(\mu\Theta) \sin^2(\mu\Theta)} + \frac{3}{8 \sin^2(\mu\Theta)} + \frac{3}{8\mu\Theta \tan(\mu\Theta)} - \frac{1}{\mu^2 \Theta^2}$$

for fixed arches

(63)

Eq. (61) may also be obtained through implicit differentiation of Eq. (30), where the load q can be expressed as an implicit function of the axial force parameter μ , requiring that

$$-\frac{\partial F / \partial \mu}{\partial F / \partial q} = 0. \quad (64)$$

The symmetric snap-through loads are obtained when Eqs. (30) and (61) yield the same solutions at the same point in time.

It can be seen in Figs. 2 and 3 that basic creep strain significantly reduces the critical time to limit instability failure for both pinned and fixed arches. Creep is more influential in symmetric failure compared to bifurcation buckling as anti-symmetric stability loss occurs early, thus reducing the time required for creep development. Hence for arches failing in the symmetric snap-through mode, basic creep strain should be considered.

4.4. Lowest buckling loads

When $\cos(\gamma\mu\theta) = 0$ in characteristic Eq. (55), the lowest solution are $\gamma\mu\theta = \pi/2$ for pinned arches and $\gamma\mu\theta = \pi$ for fixed arches, which upon substitution in Eq. (26), yield

$$\mathbf{E}^{-1}N = \frac{\pi^2 I}{S^2} \quad \text{for pinned arches,} \quad (65)$$

$$\mathbf{E}^{-1}N = \frac{\pi^2 I}{(S/2)^2} \quad \text{for fixed arches.}$$

Pi and Bradford [35] found that the lowest critical buckling load is equal to the axial force, thus it can be stated that

$$qR = N = \mathbf{E} \frac{\pi^2 I}{S^2} \quad \text{for pinned arches,} \quad (66)$$

$$qR = N = \mathbf{E} \frac{\pi^2 I}{(S/2)^2} \quad \text{for fixed arches.}$$

4.5. Limiting arch geometric parameters

The existence of a real solution to the central radial displacement Eq. (28), when $\gamma\mu\theta = \pi/2$ and $\gamma\mu\theta = \pi$ for pinned and fixed arches respectively, leads to the limiting arch geometry parameter λ_s defining a switch between buckling and no buckling, originally obtained in [5], which is defined as

$$\lambda_s = \frac{\pi^3}{8} \sqrt{1 - \frac{\alpha\Delta T}{\pi^2} \left(\frac{S}{r}\right)^2} \quad \text{for pinned arches,} \quad (67)$$

$$\lambda_s = \pi^2 \sqrt{1 - \frac{\alpha\Delta T}{2\pi^2} \left(\frac{S}{r}\right)^2} \quad \text{for fixed arches.}$$

When the arch slenderness λ is less than λ_s , buckling is not possible. However, it is most likely that an arch experiencing increasing temperature, such as during a fire, will feature a slenderness $\lambda > \lambda_s$ as λ_s decreases with increasing temperature. Moreover, λ_s is independent of basic creep and TTS. It is also noted that lowest buckling load is a special case, only occurring when the slenderness of the arch satisfies Eq. (67).

Eqs. (57)–(59) lead to the arch geometric parameters λ_b which determine a switch between symmetric and anti-symmetric buckling, originally obtained in [5],

$$\lambda_b = \frac{\sqrt{2\pi^2 + 15}}{2\pi^2 + 6} \sqrt{12\pi^4 - 3\pi^2 \alpha\Delta T \left(\frac{S}{r}\right)^2} \quad \text{for pinned arches,}$$

$$\lambda_b = \sqrt{15(1.4303\pi)^2 - (15\alpha\Delta T/4) \left(\frac{S}{r}\right)^2} \quad \text{for fixed arches.} \quad (68)$$

If the arch slenderness satisfies $\lambda_s < \lambda < \lambda_b$, symmetric snap-through is the dominant buckling mode. When the arch slenderness $\lambda > \lambda_b$, the arch generally buckles in an anti-symmetric bifurcation mode. However, this bifurcation point may occur on the descending branch of the equilibrium path. For further discussion of this phenomenon, the reader is referred to [5]. TTS and creep strains have no effect on the geometric parameter λ_b , consequently the parameters governing the buckling mode for circular shallow steel arches under uniformly distributed radial loading and uniform temperature field are identical for concrete arches, see [5]. Thus, anti-symmetric bifurcation buckling is the dominant buckling mode for concrete arches subject to uniformly distributed radial loading and uniform thermal loading, and symmetric buckling is only possible in very shallow arches. Additionally, the dominant buckling mode may transition from symmetric to anti-symmetric for arches

under increasing temperature as λ_b decreases with increasing temperature.

5. Discussion

5.1. Validation of assumption of elasticity

The maximum normal stress to temperature reduced compressive strength ratio $f'_c/f'_{c,T}$ at initial loading and at the critical bifurcation times for two arch geometrical configurations when both pinned or fixed supported are depicted in Figs. 7 and 8. Arch 1 features a height of 1 m, a width of 8 m, a radius of 8.5 m and an included angle of 56.14°. The height, width, radius and included angle for arch 2 is 1 m, 6 m, 5 m and 73.74° respectively. Both arches feature a cross-section with and depth of 300 mm an 200 mm respectively, an initial elastic modulus $E_0 = 30,100$ MPa and were heated at a rate of 1.67 °C/min. It is shown that in three out of the four cases tested, the stress to temperature reduced compressive strength ratio remains under 0.5 when initially loaded to less than approximately 45% of the cold compressive strength. In the case of the fixed arch with the higher included angle, see Fig. 8b, the stress to strength ratio reached a maximum of 0.57, which exceeds the assumed elastic limit of 0.5. Buckling strength

increases with included angle, and as the Anderberg model does not consider the great increase in TTS at approximately 450 °C, the elastic range was exceeded as the compressive strength of the concrete substantially deteriorated at the high temperature required to induce stability loss. It is expected that adopting another TTS model the would result in anti-symmetric buckling failure prior to plastic straining.

Cracking would occur if the arch was initially loaded to a state of tensile stress, or if during the heating period the stress transitioned from compressive to tensile. However, this is only probable in very shallow arches which behave more beam like and withstand large bending moments relative to the axial compressive force. These arches would require reinforcement, and the assumption of elasticity rendered invalid. It is shown in Figs. 4 and 5 that a transition from a compressive to tensile stress state during heating is unlikely as the compressive force increases with temperature/-time, and the magnitude of the bending moments decrease throughout most of the heating period. Bifurcation buckling will occur prior to the large increase in bending moment which occurs as the arch approaches limit instability failure. Only very shallow arches are governed by symmetric buckling, which, as aforementioned, would likely require reinforcement and hence not behave elastically to begin with.

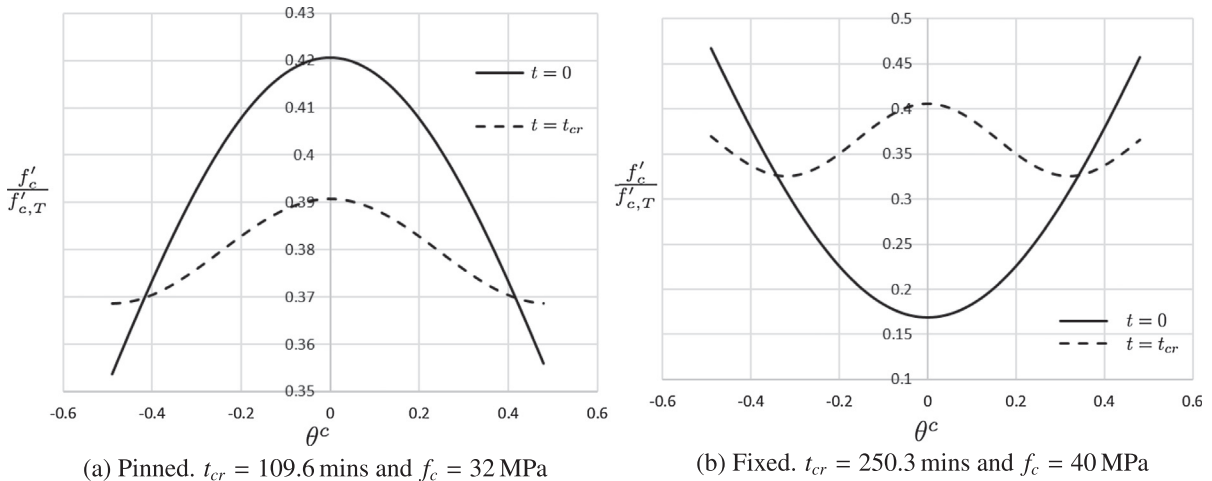


Fig. 7. Stress to compressive strength ratio at initial and critical bifurcation time in arch 1. $q = 80$ kN/m.

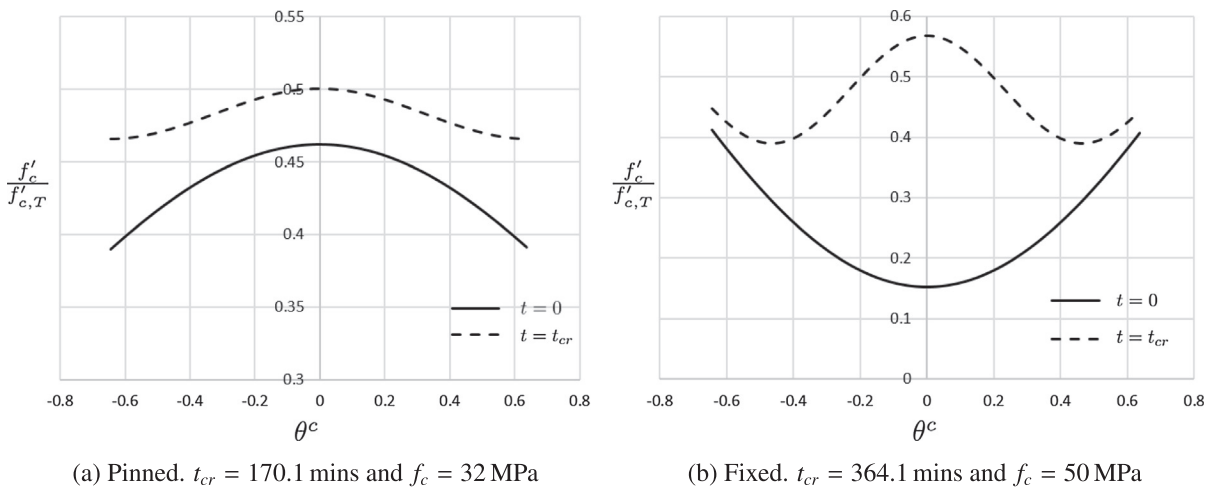


Fig. 8. Stress to compressive strength ratio at initial and critical bifurcation time in arch 2. $q = 150$ kN/m.

Thus, this study is restricted in its application to concrete arches loaded in the working range; total stresses less than approximately 45% of the compressive strength. Though caution is advised for very shallow arches which may feature an initial state of tensile stress, and stocky fixed arches with high included angles.

5.2. Effect of reinforcement

Concrete arches typically feature steel reinforcement despite the possible lack of tensile stress regions which has not been considered herein. Studies on the fire resistance of reinforced concrete columns have shown that incorporating and increasing the level of steel reinforcement does not noticeably influence the critical buckling temperature [36,37]. However, for concrete columns governed by material failure, the steel ratio plays a greater role in fire resistance time [38]. Assuming that steel reinforcement would similarly impact arch behaviour, it can be said that the inclusion of reinforcement would only slightly effect the pre-buckling behaviour and thermo-elastic buckling temperatures/times.

6. Conclusion

The non-linear pre-buckling behaviour and elastic stability boundaries of pinned and fixed shallow concrete arches subjected to uniformly distributed loading and time-varying temperatures were analytically and numerically investigated. Coupling effects of time and temperature with geometric non-linearity was the focus of the investigation. Basic creep strain was considered and modelled using a fractional derivative based law. The elastic-viscoelastic analogy was utilised in order to treat the problem elastically, and the principle of virtual work was employed for the derivation of the non-linear equilibrium equations. Numerical solutions were obtained by discretising the variable-order fractional derivatives using a finite-difference based approach. It was found that TTS interacts with geometric non-linearity and significantly influences pre-buckling behaviour and symmetric snap-through and anti-symmetric buckling loads, with basic creep strain magnifying its effects. Examination of the time and temperature evolution of radial deflections demonstrated symmetric shape changes manifesting at high times and temperatures prior to the symmetric snap-through point; causing substantial alterations in the bending moment. Additionally, TTS causes great reductions in the buckling resistance of both pinned and fixed concrete arches and hence must be considered in the analysis of pre-loaded shallow concrete arches subject to temperature increases. Basic creep further reduces the stability boundaries, however for most arches which fail in an anti-symmetric buckling mode, the effects of basic creep strain may be considered negligible for transient temperature increases.

Acknowledgements

The first author acknowledges Victoria University for the financial support provided through the Vice Chancellor's Graduate Research Scholarship award.

Appendix A

A.1. Spring-pot parameters

The parameters α and η are adopted from [30] for calcareous aggregate. The dependence of the order of derivative α on T is (T in Fahrenheit °F)

$$\alpha = -5.36 \times 10^{-10}(T - 759.6741)^3 - 7.849 \times 100^{-11}T^2 + 0.000253T + 0.257 \quad \text{for } T < 600 \text{ }^\circ\text{F}$$

$$\alpha = 1.73 \times 10^{-9}(T + 931.86)^3 - 1.01 \times 10^{-5}T^2 + 0.00057883T - 2.5093 \quad \text{for } T > 600 \text{ }^\circ\text{F}. \tag{69}$$

and the dynamic viscosity η (MPa.min $^\alpha$)

$$\eta = 2.3382(T - 596.2261)^2 + 1.55 \times 10^5 \quad \text{for } T < 600 \text{ }^\circ\text{F},$$

$$\eta = 9.3568 \times 10^{-4}(T - 900)^3 - 127.43333T + 206400 \quad \text{for } T > 600 \text{ }^\circ\text{F}. \tag{70}$$

A.2. Discretisation of fractional creep laws

A.2.1. Discretisation of fractional integral

$$J_t^{-\alpha} f(t) = \frac{1}{\Gamma(\alpha)} \int_0^t (t - \tau)^{\alpha-1} f(\tau) d\tau. \tag{71}$$

$$\approx \frac{1}{\Gamma(\alpha + 1)} \sum_{j=0}^{n-1} f_j \int_{j\Delta t}^{(j+1)\Delta t} (t - \tau)^{\alpha-1} d\tau. \tag{72}$$

$$= \frac{(\Delta t)^\alpha}{\Gamma(\alpha + 1)} \sum_{j=0}^{n-1} f_j [(n - j)^\alpha - (n - j - 1)^\alpha] \tag{73}$$

A.2.2. Discretisation of variable-order fractional derivative without memory of order

The variable-order fractional derivative, for the case when the memory of the order of derivative is not considered, is discretised as follows

$$D_t^{\alpha(t)} f(t) = \frac{1}{\Gamma(1 - \alpha(t))} \int_0^t \frac{f'(\tau)}{(t - \tau)^{\alpha(t)}} d\tau$$

$$\approx \frac{1}{\Gamma(1 - \alpha_n)} \sum_{j=0}^{n-1} \int_{j\Delta t}^{(j+1)\Delta t} \frac{y'(\tau)}{(t - \tau)^{\alpha_n}} d\tau$$

$$= \frac{1}{\Gamma(1 - \alpha_n)} \sum_{j=0}^{n-1} \int_{j\Delta t}^{(j+1)\Delta t} \frac{\frac{y_{j+1} - y_j}{\Delta t}(\tau)}{(t - \tau)^{\alpha_n}} d\tau$$

$$= \frac{1}{\Gamma(1 - \alpha_n)} \sum_{j=0}^{n-1} \frac{y_{j+1} - y_j}{\Delta t} \int_{j\Delta t}^{(j+1)\Delta t} \frac{d\tau}{(t - \tau)^{\alpha_n}}$$

$$= \frac{1}{\Gamma(2 - \alpha_n)\Delta t^{\alpha_n}} \sum_{j=0}^{n-1} (y_{j+1} - y_j)[(n - j)^{1 - \alpha_n} - (n - j - 1)^{1 - \alpha_n}]$$

$$= \frac{1}{\Gamma(2 - \alpha_n)\Delta t^{\alpha_n}} \sum_{j=0}^{n-2} (y_{j+1} - y_j)[(n - j)^{1 - \alpha_n} - (n - j - 1)^{1 - \alpha_n}]$$

$$+ \frac{y_n - y_{n-1}}{\Gamma(2 - \alpha_n)\Delta t^{\alpha_n}}$$

where Δt is the time step, $t = n\Delta t$, $n = 2 \dots t_f/\Delta t$, t_f is the final time, $\tau = j\Delta t$ and $(\cdot)'_n = (\cdot)'(n\Delta t)$. The creep strain ϵ for the fractional dash-pot model of viscoelasticity is hence determined as

$$\epsilon_n = \epsilon_{n-1} - \sum_{j=0}^{n-2} (\epsilon_{j+1} - \epsilon_j)[(n - j)^{1 - \alpha_n} - (n - j - 1)^{1 - \alpha_n}] + \frac{\sigma_n}{\eta_n} \Gamma(2 - \alpha_n)\Delta t^{\alpha_n}$$

with the creep strain at $t = 1$ derived as

$$\epsilon_1 = \frac{\sigma_1}{\eta_1} \Gamma(2 - \alpha_1) \Delta t^{\alpha_1} + \epsilon_0 \quad (74)$$

and $\epsilon_0 = 0$.

A.2.3. Discretisation of variable-order fractional derivative with memory of order

The variable order differential Eq. (7) is discretised as

$$D_t^{\alpha(t)} y(t) = \int_0^t \frac{y'(\tau)}{\Gamma[1 - \alpha(t - \tau)](t - \tau)^{\alpha(t - \tau)}} d\tau \quad (75)$$

$$\begin{aligned} &\approx \sum_{j=0}^{n-1} \frac{y_{j+1} - y_j}{\Gamma(1 - \alpha_{n-j}) \Delta t} \int_{j\Delta t}^{(j+1)\Delta t} \frac{d\tau}{(t - \tau)^{\alpha_{n-j}}} \\ &= \sum_{j=0}^{n-1} \frac{y_{j+1} - y_j}{\Gamma(1 - \alpha_{n-j})} \Delta t^{\alpha_{n-j}} \left[(n-j)^{1-\alpha_{n-j}} - (n-j-1)^{1-\alpha_{n-j}} \right] \\ &= \sum_{j=0}^{n-2} \frac{y_{j+1} - y_j}{\Gamma(1 - \alpha_{n-j})} \Delta t^{\alpha_{n-j}} \left[(n-j)^{1-\alpha_{n-j}} - (n-j-1)^{1-\alpha_{n-j}} \right] \\ &\quad + \frac{y_n - y_{n-1}}{\Gamma(2 - \alpha_1) \Delta t^{\alpha_1}} \end{aligned}$$

where $\alpha_{n-j} = \alpha(n\Delta t - j\Delta t)$. Upon application to the springpot model, the creep strain is obtained as

$$\begin{aligned} \epsilon_n = \epsilon_{n-1} - \Gamma(2 - \alpha_1) \Delta t^{\alpha_1} \sum_{j=0}^{n-2} \frac{\epsilon_{j+1} - \epsilon_j}{\Gamma(2 - \alpha_{n-j})} \\ \times \left[(n-j)^{1-\alpha_{n-j}} - (n-j-1)^{1-\alpha_{n-j}} \right] + \frac{\sigma_n}{\eta_n} \Gamma(2 - \alpha_1) \Delta t^{\alpha_1} \quad (76) \end{aligned}$$

with the creep strain at $t = 1$ obtained as

$$\epsilon_1 = \frac{\sigma_1}{\eta_1} \Gamma(2 - \alpha_0) \Delta t^{\alpha_0} + \epsilon_0 \quad (77)$$

and $\epsilon_0 = 0$.

References

- [1] Bradford MA. In-plane nonlinear behaviour of circular pinned arches with elastic restraints under thermal loading. *Int J Struct Stab Dyn* 2006;6(2):163–77.
- [2] Pi YL, Bradford MA. *Thermoelastic behaviour of elastically restrained tubular steel arches*. Taylor & Francis; 2008. pp. 659–67.
- [3] Pi Y-L, Bradford MA. In-plane thermoelastic behaviour and buckling of pin-ended and fixed circular arches. *Eng Struct* 2010;32(1):250–60.
- [4] Bradford MA. Long-span shallow steel arches subjected to fire loading. *Adv Struct Eng* 2010;13(3):501–11.
- [5] Pi Y-L, Bradford MA. Nonlinear in-plane elastic buckling of shallow circular arches under uniform radial and thermal loading. *Int J Mech Sci* 2010;52(1):75–88.
- [6] Cai J, Xu Y, Feng J, Zhang J. Effects of temperature variations on the in-plane stability of steel arch bridges. *J Bridge Eng* 2010;17(2):232–40.
- [7] Moghaddasie B, Stanciulescu I. Equilibria and stability boundaries of shallow arches under static loading in a thermal environment. *Int J Non-Linear Mech* 2013;51:132–44.
- [8] Pi Y-L, Bradford MA. Effects of nonlinearity and temperature field on in-plane behaviour and buckling of crown-pinned steel arches. *Eng Struct* 2014;74:1–12.
- [9] Pi Y-L, Bradford MA. Nonlinear thermoelastic buckling of pin-ended shallow arches under temperature gradient. *J Eng Mech* 2010;136(8):960–8.
- [10] Cai J, Xu Y, Feng J, Zhang J. In-plane elastic buckling of shallow parabolic arches under an external load and temperature changes. *J Struct Eng* 2012;138(11):1300–9.
- [11] Bouras Y, Vrcelj Z. Effect of transient thermal strain on the stability of shallow concrete arches. In: *Mechanics of structures and materials: advancements and challenges*. CRC Press; 2016. p. 963–70.
- [12] Wang T, Bradford MA, Ian Gilbert R. Creep buckling of shallow parabolic concrete arches. *J Struct Eng* 2006;132(10):1641–9.
- [13] Pi Y-L, Bradford MA, Qu W. Long-term non-linear behaviour and buckling of shallow concrete-filled steel tubular arches. *Int J Non-Linear Mech* 2011;46(9):1155–66.
- [14] Bradford MA, Pi Y-L, Qu W. Time-dependent in-plane behaviour and buckling of concrete-filled steel tubular arches. *Eng Struct* 2011;33(5):1781–95.
- [15] Luo K, Pi Y, Gao W, Bradford MA. Creep of concrete core and time-dependent non-linear behaviour and buckling of shallow concrete-filled steel tubular arches. *Comput Model Eng Sci* 2013;95(1):32–58.
- [16] Luo K, Pi Y-L, Gao W, Bradford MA, Hui D. Investigation into long-term behaviour and stability of concrete-filled steel tubular arches. *J Constr Steel Res* 2015;104(0):127–36.
- [17] Bažant ZP, Kaplan MF. *Concrete at high temperatures: material properties and mathematical models*. Longman Group Limited; 1996.
- [18] Luo K, Pi Y, Gao W, Bradford MA. Long-term analysis of crown-pinned concrete-filled steel tubular arches. In: *ICCM: proceedings of the 5th international conference on computational methods*, Cambridge, England, 28–30 July 2014; 2015.
- [19] Wang YF, Ma YS, Han B, Deng SY. Temperature effect on creep behavior of cfst arch bridges. *J Bridge Eng* 2013;18(12):1397–405.
- [20] Bažant ZP, Hauggaard AB, Baweja S, Ulm F-J. Microprestressing-solidification theory for concrete creep. i: Aging and drying effects. *J Eng Mech* 1997;123(11):1188–94.
- [21] Pritz T. Analysis of four-parameter fractional derivative model of real solid materials. *J Sound Vib* 1996;195(1):103–15.
- [22] Bažant Z, Cedolin L. *Stability of structures: elastic, inelastic, fracture and damage theories*. World Scientific; 2010.
- [23] Loverro A. *Fractional calculus: history, definitions and applications for the engineer*. Report. Notre Dame (IN 46556): Department of Aerospace and Mechanical Engineering.
- [24] Kimev J. *Fractional calculus: definitions and applications (Master's Thesis)*. Western Kentucky University; 2009.
- [25] Uchaikin VV. *Fractional derivatives for physicists and engineers*. Springer; 2013.
- [26] Bagley R, Torvik P. On the fractional calculus model of viscoelastic behavior. *J Rheol* 1986;30(1):133–55.
- [27] Papoulia KD, Panoskaltis VP, Kurup NV, Korovajchuk I. Rheological representation of fractional order viscoelastic material models. *Rheol Acta* 2010;49(4):381–400.
- [28] Barpi F, Valente S. Creep and fracture in concrete: a fractional order rate approach. *Eng Fract Mech* 2002;70(5):611–23.
- [29] Katicha S, Flintsch GW. Fractional viscoelastic models: master curve construction, interconversion, and numerical approximation. *Rheol Acta* 2012;51(8):675–89.
- [30] Bouras Y, Zorica D, Atanacković T, Vrcelj Z. A non-linear thermo-viscoelastic rheological model based on fractional derivatives for high temperature creep in concrete, unpublished.
- [31] EN 1992 1-2. Eurocode 2: design of concrete structures, Part 1-2, Structural fire design. European Committee for Standardization; 2004.
- [32] Anderberg Y, Thelandersson S. Stress and deformation characteristics of concrete at high temperatures: experimental investigation and material behavior model. *Divis Struct Mech Concr Construct* 1976.
- [33] Bažant Z. Linear creep problems solved by a succession of generalized thermoelasticity problems. *Acta Technica CSAV* 1967;12:581–94.
- [34] Pi Y-L, Trahair N. Non-linear buckling and postbuckling of elastic arches. *Eng Struct* 1998;20(7):571–9.
- [35] Pi Y-L, Bradford MA, Uy B. In-plane stability of arches. *Int J Solids Struct* 2002;39(1):105–25.
- [36] Huang S-S, Burgess I, Huang Z, Plank R. The buckling of slender concrete and concrete-filled columns in fire. In: *Fib workshop: fire design of concrete structures—from materials modelling to structural performance*, Coimbra, Portugal.
- [37] Bajc U, Saje M, Planinc I, Bratina S. Semi-analytical buckling analysis of reinforced concrete columns exposed to fire. *Fire Saf J* 2015;71:110–22.
- [38] Han L-H, Tan Q-H, Song T-Y. Fire performance of steel reinforced concrete columns. *J Struct Eng* 2014;141(4):04014128.

4.5 Concluding Remarks

This chapter presented the derivation of analytical models for the thermo-elastic response and in-plane stability boundaries of pinned or fixed shallow concrete arches under combined mechanical and thermal loading. The effect of temperature on the prebuckling response and buckling loads formed the focus of the investigation. This chapter provides an insight into the fundamental behaviour of shallow concrete arches in thermal environments, and outlines the overall significance of TTS and creep on behaviour. In summary, the following conclusions are drawn from this chapter;

1. Thermal loading increases the axial force and radial deflections in concrete arches, which rise exponentially as limit instability is approached;
2. Bending moment generally decreases in magnitude with temperature increase, though a great jump is observed as the arch begins to symmetrically change shape prior to instability failure;
3. Elevated temperature fields significantly reduce the in-plane elastic anti-symmetric and symmetric buckling loads of pinned and fixed concrete arches;
4. The effect of thermal loading is drastically enhanced when TTS is considered, and adopting different TTS models quantitatively influences results;
5. Basic creep strain increases the effects of thermal loading though to a much lesser extent than TTS. Hence, creep strain can be neglected for arches governed by anti-symmetric buckling when subjected to transient heating;
6. The definition of fractional derivative adopted for the creep strain equation has a negligible effect on arch behaviour;

7. Anti-symmetric bifurcation buckling is the governing failure mode for concrete arches under elevated temperature fields, with limit instability only possible in very shallow arches; and
8. The factors delineating between buckling modes are temperature dependant and thus governing failure mode may change during heating.

Chapter 5

Inelastic buckling of shallow concrete arches under fire loading

5.1 Introduction

In this chapter, the in-plane failure modes and fire resistance times of shallow concrete arches are numerically investigated using FE analysis. The arches are first mechanically loaded prior to heating where the fire load is assumed to act on the underside of the arch. Inelastic material models are adopted which consider TTS implicitly. In-plane anti-symmetric geometric imperfections are incorporated into the model by conducting an eigenvalue buckling analysis and subsequently reforming the arch geometry. This

is required for anti-symmetric bifurcation buckling to occur upon reaching a critical temperature distribution. Validation of the FE model is made by comparison to a novel non-discretisation numerical method derived for the non-linear inelastic analysis of shallow concrete arches subjected to uniformly distributed radial loading and uniform temperature fields. The non-linear equilibrium equations of shallow arches are coupled with an inelastic concrete material model to form a system of six first-order differential equations which can be numerically solved as a boundary-value problem (BVP) given the end restraints of pinned or fixed supports. Additionally, verification is made by examining the inelastic buckling loads predicted by the FE model and the tangent modulus theory; employed using the derived model and the analytical expressions for the elastic buckling load obtained in Chapter 4. The FE model is then utilised to conduct an extensive parametric study which highlights the effect of various parameters on fire resistance time and deduces the governing failure mode of shallow concrete arches under fire loading. By considering inelastic material behaviour and simulating fire loading, this chapter builds upon the results detailed previously which were limited to elastic response and uniform temperature fields. Thus, a more realistic understanding of the effect of thermal (fire) loading on the stability of concrete arches is obtained.

The following paper is included in this chapter;

1. Y. Bouras, and Z. Vrcelj. 2020. In-plane stability of shallow concrete arches under fire. *Journal of Structural Fire Engineering*, DOI: 10.1108/JSFE-11-2018-0039.



THE NEW WAY TO DO UNI

OFFICE FOR RESEARCH TRAINING, QUALITY AND INTEGRITY

DECLARATION OF CO-AUTHORSHIP AND CO-CONTRIBUTION: PAPERS INCORPORATED IN THESIS

This declaration is to be completed for each conjointly authored publication and placed at the beginning of the thesis chapter in which the publication appears.

1. PUBLICATION DETAILS (to be completed by the candidate)

Title of Paper/Journal/Book:	In-plane stability of shallow concrete arches under fire		
Surname:	Bouras	First name:	Yanni
Institute:	Institute for Sustainable Industries and Liveat	Candidate's Contribution (%):	95
Status:			
Accepted and in press:	<input type="checkbox"/>	Date:	
Published:	<input checked="" type="checkbox"/>	Date:	04/02/2020

2. CANDIDATE DECLARATION

I declare that the publication above meets the requirements to be included in the thesis as outlined in the HDR Policy and related Procedures – policy.vu.edu.au.

Yanni Bouras	<small>Digitally signed by Yanni Bouras Date: 2020.02.10 15:20:27 +11'00'</small>	10/02/2020
Signature		Date

3. CO-AUTHOR(S) DECLARATION

In the case of the above publication, the following authors contributed to the work as follows:

The undersigned certify that:

1. They meet criteria for authorship in that they have participated in the conception, execution or interpretation of at least that part of the publication in their field of expertise;
2. They take public responsibility for their part of the publication, except for the responsible author who accepts overall responsibility for the publication;

PO Box 14428, Melbourne,
Vic 8001, Australia
+61 3 9919 6100

Victoria University ABN 83776954731
CRICOS Provider No. 00124K (Melbourne),
02475D (Sydney), RTO 3113



**VICTORIA
UNIVERSITY**

THE NEW WAY TO DO UNI

3. There are no other authors of the publication according to these criteria;
4. Potential conflicts of interest have been disclosed to a) granting bodies, b) the editor or publisher of journals or other publications, and c) the head of the responsible academic unit; and
5. The original data will be held for at least five years from the date indicated below and is stored at the following location(s):

Victoria University, Footscray Park, Ballarat Road, Melbourne, VIC 3011, Australia

Name(s) of Co-Author(s)	Contribution (%)	Nature of Contribution	Signature	Date
Yanni Bouras	95	Conceived concept. Literature review. Numerical modelling. Writing manuscript	[Redacted Signature]	11/02/2020
Zora Vrceļj	5	Critical review of manuscript. Final approval of manuscript.		11/02/2020

Updated: September 2019

PO Box 14428, Melbourne,
Vic 8001, Australia
+61 3 9919 6100

Victoria University ABN 83776954731
CRICOS Provider No. 00124K (Melbourne),
02475D (Sydney), RTO 3113

In-plane stability of shallow concrete arches under fire

Yanni Bouras, Zora Vrcelj¹

College of Engineering and Science, Victoria University, Melbourne, VIC, Australia

Abstract

Concrete arch structures are commonly constructed for various civil engineering applications. Despite their frequent use, there is a lack of research on the response and performance of concrete arches when subjected to fire loading. Hence, this paper investigates the response and in-plane failure modes of shallow circular concrete arches subjected to mechanical and fire loading through the development of a three-dimensional finite element (FE) model. The FE model is verified by comparison to a non-discretisation numerical model derived herein and the tangent modulus buckling theory, both utilised for the non-linear inelastic analysis of shallow concrete arches subjected to uniformly distributed radial loading and uniform temperature field. Both anti-symmetric and symmetric buckling modes are examined, with analysis of the former requiring geometric imperfection obtained by an eigenvalue buckling analysis. The FE results show that anti-symmetric bifurcation buckling is the dominant failure mode in shallow concrete arches under mechanical and fire loading. Additionally, parametric studies are presented which illustrate the influence of arch included angle, concrete compressive strength, cross-section size, mechanical load level and fire type on the fire resistance time.

1. Introduction

Arches are a historic construction form still commonly utilised in modern civil engineering projects including the construction of bridges and buildings. The popularity of arches can be attributed to their ability to resist loads primarily in compression, making them more efficient structural members than straight beams. However, compressive action introduces the problem of stability. Three buckling modes exist for arches: the anti-symmetric bifurcation and symmetric snap through in-plane modes, and the out-of-plane flexural-torsional mode. The stability of arches is a classical problem that has been extensively studied over the years for both in-plane [1, 2, 3, 4, 5, 6, 7] and out-of-plane buckling [8, 9, 10, 11, 12, 13, 14]. In the early analytical studies on the stability of elastic arches classical buckling theory was adopted. This was later proven, experimentally [3, 7] and numerically [15], to be inaccurate due to simplifying assumptions made regarding the pre-buckling behaviour [15, 16]. Classical buckling theory ignores the effects of pre-buckling deformations on displacements and geometrical stiffness, and linearises stress resultants. Classical theory only provides accurate solutions for deep arches, as the rise of the arch is much greater than the magnitude of pre-buckling deformations [15]. Conversely in shallow arches, the pre-buckling deformations are significant and highly non-linear. The use of classical theory for the analysis of shallow arches leads to an overestimation of the

buckling strength, thus the elastic buckling load of a shallow arch must be obtained using non-linear methods. Arches are delineated between shallow and deep based on their included angle (2Θ); arches with $2\Theta > 90^\circ$ are classed as deep and are otherwise considered as shallow [16].

The ubiquitous use of arches makes their performance at elevated temperatures of high importance as thermal loading, such as caused by fire exposure, may induce stability loss. The effects of elevated temperature fields on the response and stability of shallow steel arches have been thoroughly investigated [17, 18, 19, 20, 21, 22, 23, 24, 25, 26, 27]. Uniform temperature fields and temperature differentials induce compressive stresses and bending moments in arches due to the end restrained thermal expansion and curvature changes respectively. Furthermore, in-plane anti-symmetric bifurcation buckling and limit instability loads increase with uniform temperature fields. Conversely, in-plane critical buckling loads decrease with an increase in temperature gradient. For the case of out-of-plane stability of steel arches, mechanical loads are less influential with stability being governed primarily by the critical buckling temperature [24]. Despite the extensive research conducted on thermal stability of steel arches, less work has been completed on the response of concrete and composite steel-concrete arches at elevated temperatures. Bouras and Vrceelj [28] conducted a pre-buckling and in-plane stability analysis of shallow circular concrete arches subjected to combined mechanical and thermal loading in order to analyse the influence of basic creep and Transient Thermal Strain (TTS); a strain thought to originate in the cement paste due to thermo-mechanical interaction which only manifests in mechanically pre-loaded concrete upon first time heating and is irreversible [29, 30, 31]. It was found that when considering TTS, axial compressive forces further increased with temperature and the concrete arch deflected downwards. Moreover, TTS significantly magnified the reduction in buckling strength of concrete arches at elevated temperatures. However, this study was limited to the simplifying assumptions made which include elastic material behaviour and uniform temperature loading. This appears to be the only study investigating the stability of concrete arches at extreme temperatures. Heidarpour et al. [32] analytically investigated the in-plane non-linear elastic behaviour of a composite steel-concrete arch under mechanical and non-uniform thermal loading. Luo et al. [33] studied the long-term behaviour of crown-pinned concrete-filled steel tubular (CFST) arches subjected to a uniform and constant temperature change in order to analyse the significance of time-temperature coupling. The non-linear elastic and inelastic in-plane buckling strength of CFST arches subjected to uniformly distributed radial loading and elevated temperature fields was investigated by the authors in [34]. It was found that thermal loading substantially influenced stability boundaries and that the inelastic buckling strength in stocky arches was governed by yielding of the steel tube.

Due the limited available research on the thermal stability of concrete arches, the significance of the problem can be highlighted by considering studies of reinforced concrete columns. Arches and columns share similar mechanical behaviour as both carry loads predominately as an axial compressive force, which if large enough, may cause bifurcation buckling. The critical axial force for a pinned or fixed-ended shallow arch in uniform compression is the same for an equivalent length column, which can be derived by stability analyses typically consisting of generalisations of those applied to straight members. As with arches, elevated temperature fields may cause instability in columns

[35, 36, 37, 38]. Although commonly governed by material strength, reinforced concrete columns are not exempt from the problem of instability when subjected to combined mechanical and thermal loading due to severe reductions in stiffness caused by high temperatures. A major contributor to stiffness degradation, and thus buckling load, is TTS. Few studies explicitly analyse the effect of fire loading on the stability of loaded concrete columns when considering TTS. Examples include the work by Franssen and Dotreppe [39], Bratina et al. [40], Huang et al. [35] and Bajc et al. [38]. Huang et al. [35] conducted an inelastic buckling analysis of reinforced concrete columns subjected to fire loading using Shanleys inelastic buckling theory and Finite Element (FE) analysis. It was found that global buckling is the dominant failure mode for slender reinforced concrete columns, and the reductions in buckling strength at elevated temperatures are significantly greater when considering TTS. Furthermore, the steel reinforcement ratio marginally increased critical buckling temperature. This result was also obtained by Bajc et al. [38] who proposed a semi-analytical model for the inelastic buckling analysis of concrete columns subjected to fire loading. Exposure time and slenderness were deduced as the critical factors behind fire resistance time.

Motivated by the adverse effect fire loading has on the critical buckling loads of reinforced concrete columns, and by the lack of research on concrete arches under the same conditions, the present study investigates the response and failure modes of shallow circular plain concrete arches subjected to fire loading through the development of a 3D Finite Element (FE) model using the commercially available software package ANSYS [41]. The large expenses associated with conducting full-scale experimental tests, in addition to the complexity of developing prescriptive methods, has led to performance-based numerical analysis, particularly FE, becoming the preferred fire engineering design tool for concrete structures [42, 43, 44]. Plain concrete arches are studied as stability is the primary concern. Concrete arches typically feature steel reinforcement uniformly distributed through the cross-section. However, as discussed earlier, studies on the fire resistance of reinforced concrete columns have shown that increasing the level of steel reinforcement does not noticeably influence the critical buckling temperature [35, 38]. However, for concrete columns governed by material failure, the steel ratio plays a greater role in fire resistance time [37]. Assuming that steel reinforcement would similarly impact arch behaviour, it can be said that the inclusion of reinforcement would only slightly influence their fire resistance. The FE model is validated by comparison to a non-discretisation based numerical model derived herein for the non-linear inelastic analysis of shallow concrete arches subjected to uniformly distributed radial loads and uniform temperature fields. In the FE model, a transient thermal analysis is first conducted where it is assumed that the temperature is constant through the length of the arch. Subsequently, two non-linear structural analyses are performed for each arch in order to investigate both anti-symmetric and symmetric buckling failure. Analysis of anti-symmetric buckling requires geometric imperfection in the FE model which is obtained via an eigenvalue buckling analysis. Geometrical and material non-linearities are both considered. Through the consideration of plasticity and adoption of non-uniform temperature distributions, this paper builds upon the work completed by the authors in [28]. Hence, a more realistic and pragmatic understanding of the effect of fire loading on the pre-buckling behaviour and in-plane stability of shallow concrete arches is obtained. The findings herein may be adopted in the fire design of shallow concrete arches.

2. Material properties and constitutive models

2.1. Compression Models

Three concrete material models are considered in this study: the Eurocode 2 (EC2) [45], the ASCE [46] model for normal-strength concrete (NSC) and the Kodur [47] model for high-strength concrete (HSC). The EC2 stress-strain relationship of concrete at a given elevated temperature T for the ascending portion is defined as

$$\frac{\sigma}{f'_{c,T}} = \frac{3\epsilon_{ch}}{\epsilon_{EC2}[2 + (\epsilon_{ch}/\epsilon_{EC2})^3]}, \quad (1)$$

where σ is the stress, $f'_{c,T} = f'_{c,T}(T)$ is the temperature reduced compressive strength, ϵ_{ch} is the mechanical strain and $\epsilon_{EC2} = \epsilon_{EC2}(T)$ is the peak stress strain (PSS). Eq.(1) is applicable to both NSC and HSC. Transient thermal strain is considered in this model, however due to the implicit nature of its incorporation [48] it is recoverable and independent on the order of heating and loading. These limitations are considered acceptable for the present analysis as all arches will be pre-loaded before being subjected to increases in temperature, and the temperature-time curves modelled do not feature cooling branches. The ASCE concrete model for NSC is defined as

$$\sigma = f'_{c,T} \left[1 - \left(\frac{\epsilon_{ch} - \epsilon_{max}}{\epsilon_{max}} \right)^2 \right], \quad (2)$$

where $\epsilon_{max} = \epsilon_{max}(T)$ is the temperature dependent PSS. The relationship between compressive strength and temperature for the ASCE model is

$$f'_{c,T} = \begin{cases} f'_c & \text{for } 22^\circ\text{C} \leq T \leq 450^\circ\text{C}, \\ f'_c [2.011 - 2.353(T - 20) \times 10^{-3}] & \text{for } 450^\circ\text{C} \leq T \leq 874^\circ\text{C}, \\ 0 & \text{for } 874^\circ\text{C} < T. \end{cases} \quad (3)$$

The Kodur concrete model for HSC is defined as

$$\sigma = f'_{c,T} \left[1 - \left(\frac{\epsilon_{max} - \epsilon_{ch}}{\epsilon_{max}} \right)^H \right], \quad (4)$$

where $H = 2.28 - 0.012f'_c$, and

$$f'_{c,T} = \begin{cases} f'_c [1.0 - 0.003125(T - 20)] & \text{for } T < 100^\circ\text{C}, \\ 0.75 f'_c & \text{for } 100^\circ\text{C} \leq T \leq 400^\circ\text{C}, \\ f'_c [1.33 - 0.00145 T] & \text{for } 400^\circ\text{C} < T. \end{cases} \quad (5)$$

2.2. Tensile Strength

Although arches are typically subjected to compression, regions of tensile stress may develop in the case of thermal loading due to great increases in bending moment. In order to account for this possibility, the EC2 relation between tensile strength and temperature is adopted, defined as:

$$f_{ck,t}(T) = \begin{cases} f_{ck,t} & \text{for } 20^\circ\text{C} \leq T \leq 100^\circ\text{C}, \\ f_{ck,t} [1.0 - (T - 100)/500] & \text{for } 100^\circ\text{C} \leq T \leq 600^\circ\text{C}, \end{cases} \quad (6)$$

where $f_{ck,t}$ is the cold tensile strength of concrete, available in the EC2.

3. Finite Element Model

This section details the FE model developed in ANSYS. Two separate analyses are conducted for each loading and geometrical configuration; one with anti-symmetric geometric imperfection, referred to as the anti-symmetric analysis, and the other without, now defined as the symmetric analysis. The formation of a new geometry with an anti-symmetric geometric imperfection can be conducted using the UPGEOM command following an eigenvalue buckling analysis. Geometric imperfections are required to trigger anti-symmetric bifurcation buckling upon reaching a critical temperature distribution. An imperfection size of arch length $S/1000$ is adopted. The symmetric analysis is conducted to obtain symmetric failure times. This is the first component of the anti-symmetric analysis. Subsequently, the transient thermal analysis is conducted, followed by the non-linear stress analysis.

3.1. Material Properties

The thermal and mechanical properties will be taken from the EC2 for siliceous concrete, which include thermal strain, thermal conductivity, density and specific heat. All parameters were tabulated in ANSYS for an ambient temperature of 22°C and for temperatures ranging from 100°C to 1100°C in increments of 100°C. ANSYS employs linear interpolation for material parameters at intermediate temperatures.

The available Drucker-Prager plasticity (DP) model was employed to incorporate the stress-strain characteristics of concrete. A yield stress of $0.4f'_{c,T}$ was selected with the elastic modulus calculated as the tangent at the yield stress. The DP model features two yield surfaces, one for compressive stress and one for tensile or tensile-compressive loading. Behaviour in tension is modelled as an elastic-perfectly plastic material with the yield stress defined by Eq.(6). A constant value of 0.18 is adopted for Poisson's ratio.

3.2. Geometrical configuration

Due to symmetry, only half the arch length is required in the symmetric analysis. To ensure continuity at the mid-span, the cross-section of the arch is restrained from axial displacements. The break of symmetry associated with anti-symmetric buckling disables the ability to analyse only half the arch, and thus the full length must be examined. Both models are depicted in Figure 1. All arches featured rectangular cross-sections and fixed-fixed supporting conditions. An element thickness of 50mm was decided to provide the best compromise between accuracy and computation time.

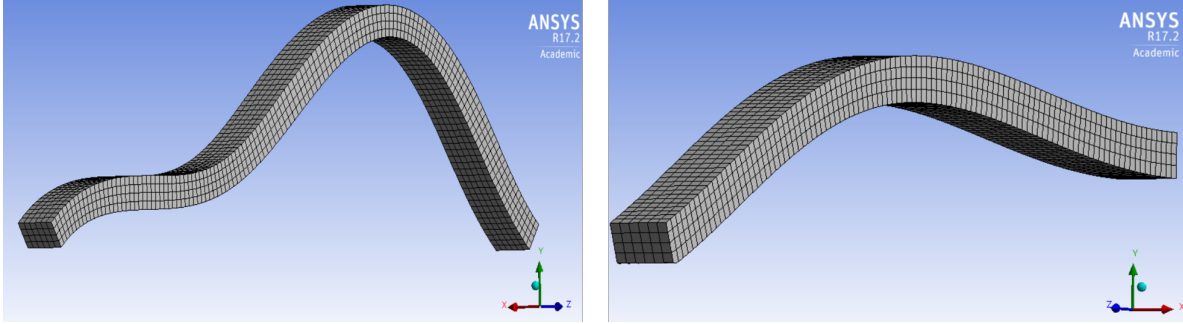


Figure 1: Discretisation of arch for anti-symmetric analysis (left) and symmetric analysis (right) with corresponding buckled shapes

3.3. Transient Thermal Analysis

Solid70 elements were employed to mesh the structure and conduct the transient thermal analysis. These elements were selected due to their equivalence with Solid186 elements, which are utilised in the following non-linear structural analysis. Solid70 elements feature 8 nodes per element, with each node possessing a single degree of freedom; temperature. The thermal loading is assumed to act on the underside of the arch and be uniform through the arch length and cross-section width. The underside is subjected to radiation, with the surface emissivity of concrete taken as 0.7, and convection, with the convection coefficient taken as 25 W/m² K and 50 W/m² K for standard ISO-834 and hydrocarbon (HC) fires respectively. The time-temperature curves for hydrocarbon and standard ISO-834 fires are

$$T_g = 20 + 1080 \left(1 - 0.325e^{-0.167t} - 0.675e^{-2.5t} \right), \quad (7)$$

and

$$T_g = 20 + 345 \log(8t + 1), \quad (8)$$

respectively, see Figure 2. An analysis period of 3 hrs is adopted, with the minimum and maximum time steps defined as 1s and 50s respectively. The initial time step was also taken as 1s. The surface temperature for a 200 mm deep cross-section is shown in Figure 2 with the temperature distribution at various time intervals depicted in Figure 3.

3.4. Temperature-stress Analysis

The final component of the analysis consists of the non-linear temperature-stress analysis. The arches are subjected to the mechanical loads and temperature history in two load steps, ensuring the arch is mechanically pre-loaded prior to heating. A non-linear static analysis is conducted at varying time intervals throughout the fire loading, with the initial, minimum and maximum time steps being identical to the transient thermal analysis. Geometric non-linearity is incorporated by activating the large deflection option and the existence of geometric imperfections allow anti-symmetric bifurcation buckling to occur upon reaching a critical state in time.

The structures were meshed using Solid186 elements which are a higher-order 3D element defined by 20 nodes with each node free to translate in three nodal directions; x , y and z . The element is capable of plastic, hyperelastic and creep straining. Additionally, the element supports stress stiffening, large deflections and strains.

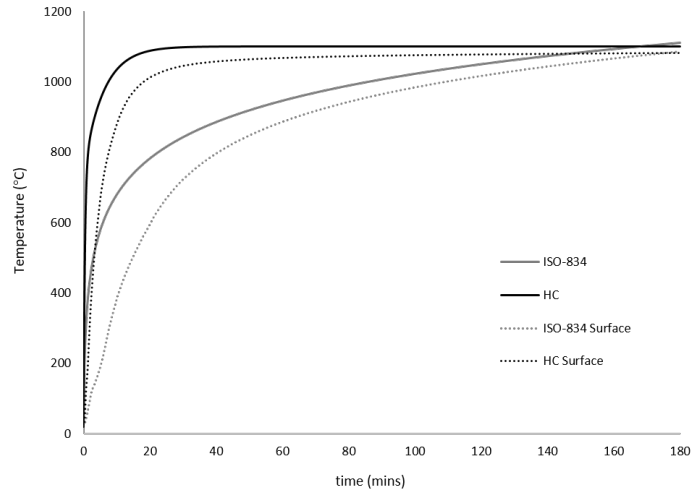


Figure 2: Gas and surface temperatures of a concrete section with a 200 mm depth for Hydrocarbon (HC) and standard ISO-834 fires

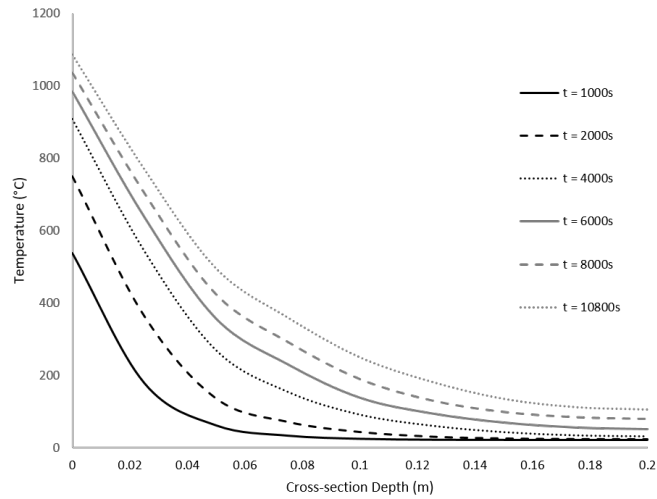


Figure 3: Temperature distribution through a 200 mm deep section exposed to ISO-834 fire

4. Inelastic pre-buckling and buckling analysis

In order to validate the FE model, a novel non-discretisation mechanical based method is derived for the non-linear inelastic analysis of a shallow CFST arch subjected to a uniformly distributed radial load and uniform temperature field. Due to the lack of experimental data, mechanically based analytical and numerical models have become the preferred methodology of analysis of arches at elevated temperatures. The present analysis generalises existing studies on the response of shallow circular arches under uniform temperature field and uniformly distributed loading [22, 28] by adopting an inelastic concrete material model. The analysis is based on the following assumptions:

- The arch is assumed to behave according to the Euler-Bernoulli hypothesis, i.e plane sections before deformation remain plane after deformation.
- The temperature field is uniform through the cross-section and through the arch length.
- Thermal expansions of the cross-section are small and thus negligible.
- Sufficient lateral restraints exist so as to prevent flexural-torsional buckling failure of the arch.

4.1. Pre-buckling Analysis

Consider a shallow circular concrete arch, pinned or fixed at its ends, subjected to a uniformly distributed radial load q and a non-uniform temperature field T , see Figure 4. The origin O is taken at the arch centroidal axis, with the axis oy always directed towards the centre of the arch as its direction changes along the circumference and the axis os coinciding with the arches centroidal axis. In order to consider geometric non-linearity, the following non-linear formulation of longitudinal normal strain is adopted [15, 16];

$$\epsilon = \epsilon_m + \epsilon_b = \epsilon_{ch} + \epsilon_{th}, \quad (9)$$

where ϵ_m and ϵ_b are the membrane and bending strains respectively, defined as

$$\epsilon_m = w' - v + \frac{1}{2}(v')^2, \quad \epsilon_b = -y \frac{v''}{R}, \quad (10)$$

ϵ is the total strain at an arbitrary point \mathcal{P} in the arch cross section, and ϵ_{th} is the thermal strain. In Eq. (10) $w = \hat{w}/R$, $v = \hat{v}/R$, \hat{w} and \hat{v} are the axial and radial displacements respectively, y is the coordinate of the point \mathcal{P} , R is the arch radius, $(\cdot)' = d(\cdot)/d\theta$, $(\cdot)'' = d^2(\cdot)/d\theta^2$ and θ is the angular coordinate. The total axial force N is defined as

$$N = - \int_A \sigma \, dA, \quad (11)$$

with the bending moment M given by

$$M = \int_A \sigma y \, dA, \quad (12)$$

where A is the cross-sectional area. Combining Eqs. (9)-(12) with constitutive Eq.(2) yields the equations for axial force N

$$N = \frac{f'_c}{\epsilon_{max}^2} \left(\frac{(v'')^2 I}{R^2} + \epsilon_{th}^2 A + 2A \epsilon_{th} \epsilon_{max} + A \epsilon_m^2 \right) - \epsilon_m \left[\frac{2A f'_c}{\epsilon_{max}} \left(1 + \frac{\epsilon_{th}}{\epsilon_{max}} \right) \right], \quad (13)$$

and bending moment

$$M = -\frac{2 I_c f'_c v''}{R \epsilon_{max}^2} (\epsilon_{max} - \epsilon_m + \epsilon_{th}). \quad (14)$$

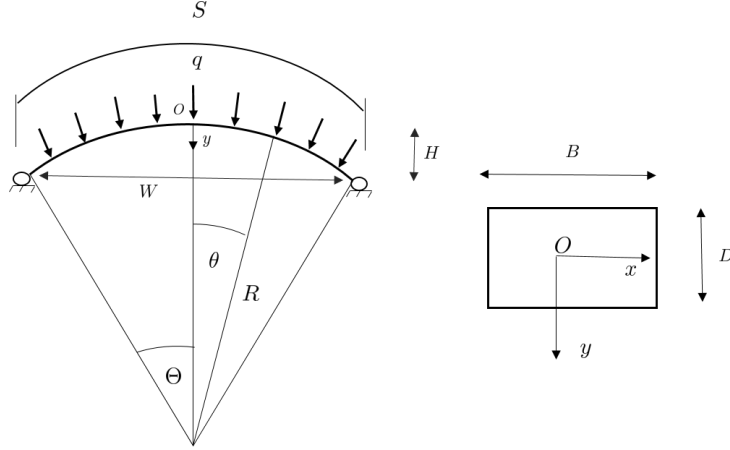


Figure 4: Arch loading and geometrical configuration

The non-linear in-plane equilibrium equations for a shallow arch are derived using the principle of virtual work [1], which requires that

$$\int_V \sigma \delta \epsilon dV - \int_{-\Theta}^{\Theta} q R^2 \delta v d\theta = 0, \quad \forall \delta v, \delta v', \delta v'', \delta w, \delta w' \quad (15)$$

where V is the volume of the arch, Θ is half the included angle and $\delta v, \delta v', \delta v'', \delta w$ and $\delta w'$ are kinematically admissible variations of displacements. Substituting Eqs. (10), (11) and (12) into (15), and integrating by parts yields the non-linear equations of equilibrium,

$$N' = 0, \quad (16)$$

in the axial direction, and

$$-M'' - qR^2 + NR(1 + v'') = 0, \quad (17)$$

in the radial direction.

Hence, a system of ordinary differential equations defined by equilibrium Eqs. (16) and (17) and constitutive Eqs. (13) and (14) is obtained. A set of dependent variables are introduced:

$$x_1 = v, \quad x_2 = v', \quad x_3 = M, \quad x_4 = M', \quad x_5 = N, \quad x_6 = w, \quad (18)$$

and upon differentiation yield,

$$x'_1 = x_2, \quad (19)$$

$$x'_2 = \frac{-x_3 \epsilon_{max}^2}{2 I_c f'_c (\epsilon_{max} - \epsilon_m + \epsilon_{th})}, \quad (20)$$

$$x'_3 = x_4, \quad (21)$$

$$x'_4 = -qR^2 + x_5 (1 + x'_2), \quad (22)$$

$$x'_5 = 0, \quad (23)$$

$$x'_6 = \epsilon_{max} + \epsilon_{th} + x_1 - 0.5 x_2^2 - \sqrt{\epsilon_{max}^2 \left(1 + \frac{x_5}{f'_c A}\right) + \frac{I_c (v'')^2}{A R^2}}. \quad (24)$$

Note that when solving quadratic Eq. (13) for the membrane strain x_6 , the lower solution was adopted which otherwise would lead to a membrane strain ϵ_m exceeding the maximum strain ϵ_{max} . Eqs.(19)-(24) form a system of first-order ordinary differential equations which can be numerically solved with prescribed boundary conditions. For a pin-ended arch, the boundary conditions are given as

$$x_1(\Theta) = x_1(-\Theta) = x_3(\Theta) = x_3(-\Theta) = x_6(\Theta) = x_6(-\Theta) = 0, \quad (25)$$

and for a fixed arch are known as

$$x_1(\Theta) = x_1(-\Theta) = x_2(\Theta) = x_2(-\Theta) = x_6(\Theta) = x_6(-\Theta) = 0. \quad (26)$$

As the boundary conditions are known at the arch ends, a boundary-value-problem (BVP) is formed. The software package MATLAB [49] is adopted to obtain numerical solutions to system (19)-(24) using the in-built BVP solver *bvp4c*. No convergence issues were experienced, and the model was found to be insensitive to initial guess values.

4.2. In-plane Buckling Analysis

The tangent modulus theory [12, 50] will be adopted to approximate the in-plane buckling loads of inelastic concrete arches. This theory states that the inelastic buckling load can be approximated by substituting the tangent modulus in place of the elastic modulus in the elastic buckling load solution. The tangent modulus corresponds to the average stress level, in this case obtained from solving system (19)-(24) for a given load and temperature.

The elastic anti-symmetric buckling load q_{cr} for a concrete arch under uniformly distributed radial loading and a uniform temperature field can be obtained by solving the following equation [28]:

$$D_1 \left(\frac{q_{cr}R - N_p}{N_p} \right)^2 + D_2 \left(\frac{q_{cr}R - N_p}{N_p} \right) + D_3 = 0 \quad (27)$$

where

$$D_1 = 15 + 2\pi^2, \quad D_2 = 12 + 4\pi^2, \quad D_3 = \frac{12\pi^4}{\lambda^2} - \frac{3\epsilon_{th}S^2\pi^2}{\lambda^2 r^2}, \quad (28)$$

for pinned arches, and

$$D_1 = 5, \quad D_2 = 4, \quad D_3 = \frac{12(1.4303\pi)^2}{\lambda^2} - \frac{3\epsilon_{th}S^2}{\lambda^2 r^2}, \quad (29)$$

for fixed arches. The critical axial force N_p is given as

$$\begin{aligned} N_p &= \frac{\pi^2 EI}{(S/2)^2} && \text{for pinned arches} \\ N_p &= \frac{(1.4303\pi)^2 EI}{(S/2)^2}. && \text{for fixed arches} \end{aligned} \quad (30)$$

with E denoting elastic modulus, r_x is the radius of gyration of the cross-section about the major axis and λ is the arch slenderness defined as

$$\lambda = \frac{R\Theta^2}{r_x} \quad (31)$$

As the anti-symmetric buckling load is dependent on the initial load, instability only occurs when they coincide.

4.3. Comparison with Finite Element Model

The developed FE model (symmetric) is now compared to the numerical method derived in the previous section. In the FE model, Eq. (2) was adopted for the concrete stress-strain, for consistency with system (19)-(24), and no lateral restraints were imposed. The radial deflections \hat{v} and axial force at the end fixed supports N determined by both models are depicted in Figure 5 at various temperature levels. It can be seen that an excellent agreement exists between the two models.

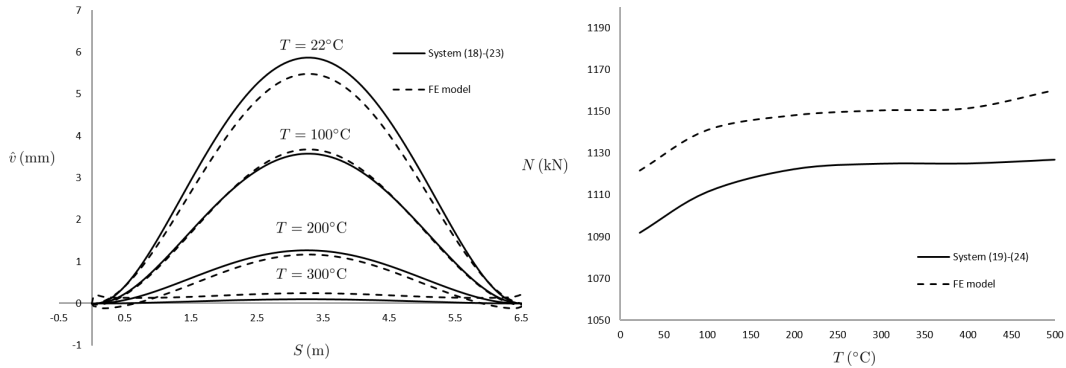


Figure 5: Comparison between system (19)-(24) and FE model for radial deflections (left) and axial force (right) at various temperature levels. $2\Theta = 73.74^\circ$, $R = 5$ m, $B = 300$ mm, $D = 200$ mm, $q = 200$ kN/m and $f'_c(T = 22^\circ\text{C}) = 32$ MPa

Comparisons between the anti-symmetric buckling loads as predicted by the anti-symmetric FE model and the tangent modulus theory are depicted in Figure 6. As with the pre-buckling analysis, the results produced by both methods are very similar and within a 10% variation.

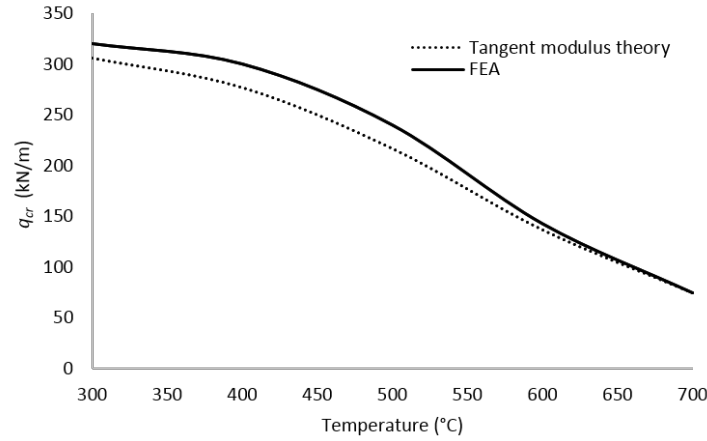


Figure 6: Comparison between tangent modulus theory and FE model for anti-symmetric buckling loads in Arch 3 at various temperature levels. $f'_c (T = 22^\circ\text{C}) = 32 \text{ MPa}$

5. Parametric Study

Seventeen geometrical configurations were subjected to various loading parameters and analysed in accordance with the aforementioned routine. Table 1 lists the geometry of each arch tested, including the arch height H , width W , radius R , arch length S , cross-section width B , cross-section depth D , subtended angle of the arch measured at the circular centre 2Θ and slenderness λ . All geometrical parameters are measured to the centre of the arch, see Figure 4. The uniformly distributed radial pressure q , concrete compressive strength, ratio of maximum stress prior to heating σ_{max} to compressive strength, anti-symmetric failure time t_A , symmetric failure time t_S and failure mode (FM) for each arch tested are displayed in Table 2 for ISO fires, and Table 3 for HC fires. B denotes buckling failure.

5.1. General Behaviour

The behaviour of a pre-loaded concrete arch subjected to thermal loading is dependant on the initial state of stress. When the mechanical load is low, upward displacements are observed throughout the heating period as the thermal expansive strain is greater than the mechanical and thermo-mechanical strains and thus governs behaviour. Conversely, at higher mechanical loads, concrete arches may begin to displace downwards throughout the heating period, or after an initial upward displacement, as the mechanical and transient thermal strains exceed the thermal strain due to a state of high compressive stress. The rate of change of deflection increases throughout the heating period for both upward and downward motion and rapidly increases as the arch approaches limit instability failure, see Figure 7. Opposite deflections may occur at the arch ends. This behaviour is qualitatively consistent with that as predicted by the analytical results for the simplified case of an elastic concrete arch under uniform temperature loading [28].

Table 1: Arch geometries

Arch I.D	H (m)	W (m)	R (m)	S (m)	2Θ (°)	λ	B	D (mm)
1	1.0	5	3.625	5.517	87.206	36.362	300	200
2	1.0	6	5.000	6.435	73.740	40.985	300	175
3	1.0	6	5.000	6.435	73.740	35.862	300	200
4	1.0	6	5.000	6.435	73.740	31.877	300	225
5	1.0	6	5.000	6.435	73.740	28.689	300	250
6	1.0	6	5.000	6.435	73.740	35.862	200	200
7	1.0	6	5.000	6.435	73.740	35.862	250	200
8	1.0	7	6.625	7.735	63.782	40.628	300	175
9	1.0	7	6.625	7.735	63.782	35.549	300	200
10	1.0	7	6.625	7.735	63.782	35.549	200	200
11	1.0	7	6.625	7.735	63.782	35.549	250	200
12	1.0	10	13.000	11.035	45.237	35.095	300	200
13	1.0	10	13.000	11.035	45.237	28.076	300	250
14	1.0	10	13.000	11.035	45.237	23.396	300	300
15	0.8	8	10.400	8.212	45.237	28.076	300	200
16	0.8	8	10.400	8.212	45.237	22.461	300	250
17	0.5	8	16.250	8.083	28.500	17.410	300	200

Compressive stresses increase and redistribute in concrete arches when subjected to fire loading. For upward-displacing arches, the axial compressive force increases due to the end restrained thermal expansion. This also holds for arches that deflect downwards, though it is caused by contraction. Additionally, bending moments are generated by the non-uniform temperature distribution through the cross-section. Prior to heating, the uniformly distributed radial load produces the greatest longitudinal normal stress in the extreme concave fibre at the arch ends due to the negative bending moment reactions at the fixed supports. As the underside of the arch is subjected to the thermal load directly, it heats rapidly. Consequently, the stresses degrade at the arch underside due to a decreasing ultimate strength, hence plastic straining increases drastically. Due to the significant decrease in concrete strength at the arch underside in addition to the increasing strains, stresses rapidly increase in the middle of the arch cross-section. These stresses will continue to grow through the cross-section until material failure or instability. Furthermore, the bending moment reactions at the fixed supports increase greatly during fire exposure and as a result typically transition from negative to positive bending. The central bending moment increases during heating, following an initial reduction in magnitude. The evolution of the central and end bending moments are depicted in Figure 8. Smaller variations to axial force are observed, which generally increase throughout fire loading and do so exponentially near the limit instability

point, see Figure 9.

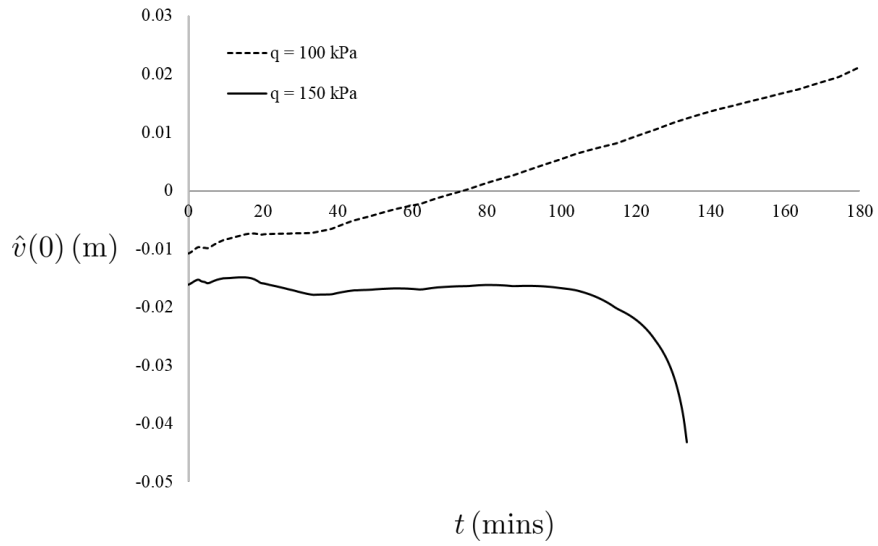


Figure 7: Central deflections in Arch 17 subjected to ISO-834 fire. $f'c(T = 22^\circ\text{C}) = 40$ MPa

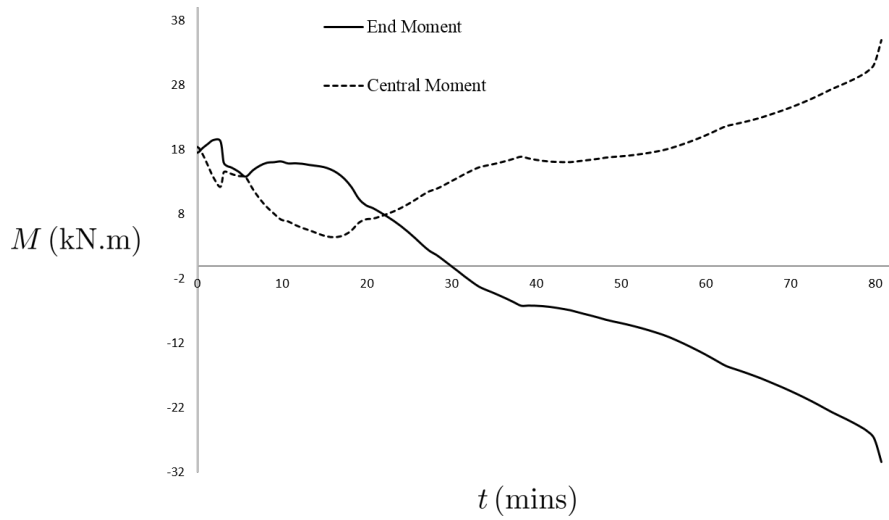


Figure 8: Bending moment in Arch 17 subjected to ISO-834 fire (symmetric analysis). $q = 200$ kPa and $f'c(T = 22^\circ\text{C}) = 40$ MPa

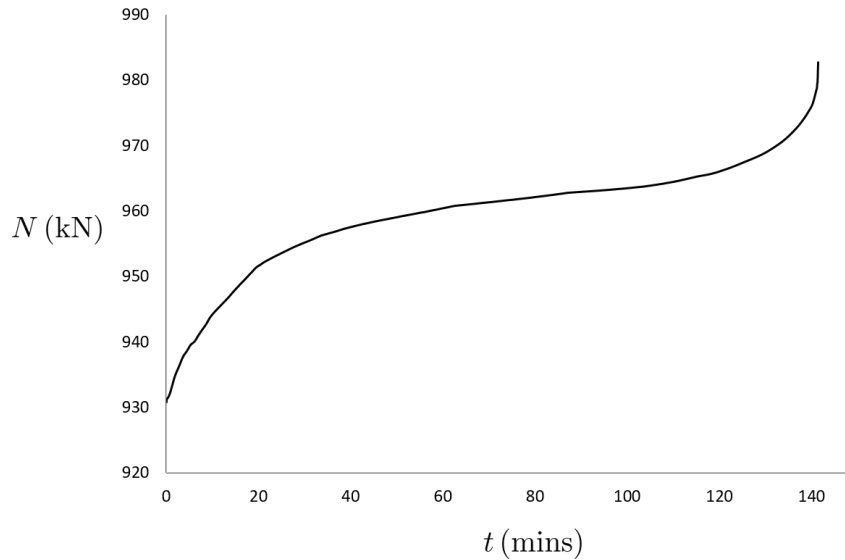


Figure 9: Central axial force in Arch 12 subjected to ISO-834 fire (symmetric analysis). $q = 200$ kPa and $f'c(T = 22^\circ\text{C}) = 40$ MPa

5.2. Buckling

Upon reaching a critical temperature distribution during the fire loading, shallow concrete arches may transition from a pre-buckled equilibrium configuration to an adjacent buckled configuration. If the anti-symmetric failure time occurred noticeably earlier than the symmetric one, the arch failed by anti-symmetric buckling. This was found to be the dominant failure mode as all tested configurations displayed this behaviour. The failure mode for the symmetric analysis was determined by examining the state of stress at the critical time. The normal stress at the critical time for an arch failing by symmetric instability is depicted in Figure 10. It can be seen the normal stress does not exceed the compressive strength. A small tensile stress zone occurs in the extreme convex fibres in the region of maximum (upward) displacement. Although symmetric snap-through buckling was observed in the symmetric analyses, it never preceded anti-symmetric buckling. Symmetric buckling is only possible in very shallow arches, and due to possible states of complete tensile stress caused by large bending moments, material failure in tension is likely.

Table 2: Failure times and modes for standard ISO-834 fires

I.D	Fire	f'_c (MPa)	q (kPa)	σ_{max}/f'_c	t_A (mins)	FM	t_S (mins)	FM
1	ISO	32	900	0.64	-		-	
1	ISO	32	1000	0.70	161.72	B	-	
1	ISO	32	1100	0.74	130.29	B	-	
1	ISO	40	1000	0.60	-		-	
1	ISO	40	1100	0.66	-		-	
1	ISO	40	1200	0.73	-		-	
2	ISO	32	750	0.34	33.6	B	74.09	B
3	ISO	32	500	0.53	-		-	
3	ISO	32	600	0.60	167.4	B	-	
3	ISO	32	750	0.71	101.09	B	-	
4	ISO	32	750	0.72	-		-	
6	ISO	32	750	0.75	110.97	B	-	
7	ISO	32	900	0.84	57.43	B	-	
8	ISO	32	500	0.69	40.71	B	96.08	B
9	ISO	32	400	0.55	156.92	B	-	
9	ISO	32	500	0.65	106.92	B	-	
9	ISO	32	750	0.87	16.94	B	31.94	
9	ISO	40	400	0.46	-		-	
9	ISO	40	500	0.56	157.31	B	-	
10	ISO	32	500	0.65	130.31	B	-	
10	ISO	32	750	0.87	17.77	B	31.94	B
11	ISO	32	500	0.65	106.92	B	-	
11	ISO	32	600	0.74	56.57	B	121.92	B
12	ISO	32	150	0.41	107.76	B	-	
12	ISO	32	200	0.52	74.42	B	151.09	B
12	ISO	32	250	0.61	40.26	B	101.92	B
12	ISO	40	150	0.36	115.43	B	-	
12	ISO	40	200	0.45	96.75	B	-	
12	ISO	40	250	0.54	73.59	B	151.09	B
12	ISO	50	250	0.43	96.73	B	-	
12	ISO	50	450	0.69	22.76	B	63.59	B
12	ISO	80	450	0.48	59.42	B	133.59	B
13	ISO	32	250	0.58	-		-	
13	ISO	32	300	0.66	132.76	B	-	
14	ISO	32	250	0.50	-		-	
15	ISO	32	150	0.48	-		-	
15	ISO	32	200	0.48	159.06	B	-	
15	ISO	32	250	0.56	132.40	B	-	
15	ISO	40	250	0.48	158.34	B	-	
15	ISO	40	300	0.56	137.40	B	-	
16	ISO	32	200	0.48	-		-	
17	ISO	32	100	0.31	47.16	B	161.09	B
17	ISO	40	100	0.31	30.85	B	-	
17	ISO	40	150	0.31	49.25	B	133.59	B
17	ISO	40	200	0.31	25.74	B	80.74	B

Table 3: Failure times and modes for HC fires

I.D	Fire	f'_c (MPa)	q (kPa)	σ_{max}/f'_c	t_A (mins)	FM	t_S (mins)	FM
1	HC	40	1000	0.60	-		-	
1	HC	40	1100	0.66	-		-	
1	HC	40	1200	0.73	-		-	
3	HC	32	500	0.53	-		-	
3	HC	32	600	0.60	141.28	B	-	
3	HC	32	750	0.71	86.02	B	-	
3	HC	40	600	0.51	-		-	
3	HC	40	750	0.61	142.62	B	-	
3	HC	40	900	0.69	85.12	B	-	
3	HC	50	750	0.51	-		-	
3	HC	50	900	0.59	158.44	B	-	
3	HC	50	1000	0.64	124.29	B	-	
3	HC	80	1000	0.44	-		-	
3	HC	80	1500	0.64	94.86	B	-	
3	HC	80	1700	0.71	64.03	B	-	
4	HC	40	900	0.66	-		-	
5	HC	40	900	0.58	-		-	
9	HC	40	400	0.46	178.90	B	-	
9	HC	40	500	0.56	132.77	B	-	
9	HC	50	500	0.46	177.97	B	-	
9	HC	50	600	0.53	139.37	B	-	
15	HC	40	300	0.48	60.63	B	-	

5.2.1. Load level

Generally, an increase in mechanical load level leads to a lower fire resistance time. This was observed in majority of the cases analysed. However, the expected inverse relationship between load and buckling time does not always hold true. The critical anti-symmetric fire resistance times for Arch 17 when subjected to ISO fire at $q = 100$ kPa is less than the resistance observed at the load level of $q = 150$ kPa. This surprising result can be attributed to the opposing directions of deflection, see Figure 7. At lower loads, the arches displace upwards which triggers an earlier anti-symmetric buckling failure. As the load increases, greater mechanical strains manifest which impose a greater resistance on the thermal strain reducing the deflection. However, above a certain load level, the mechanical strains dominate behaviour and further increase in load reduces the fire resistance time.

5.2.2. *Included angle*

The arch included angle proved to be one of the primary factors behind the fire resistance time. Fire resistance time significantly increases with included angle. This is clearly seen when comparing the failure times for Arches 1, 3, 11, 12 and 17, all which feature the same cross-section dimensions, when loaded to approximately the same ratio of maximum stress to compressive strength.

5.2.3. *Compressive strength*

To assess the influence of concrete compressive strength, simulations were conducted at strengths of 32, 40, 50 and 80 MPa. Numerical tests were also performed when the arches of different strengths were loaded at approximately the same ratio of maximum stress to compressive strength. The results show that when under the same mechanical load, a higher compressive strength typically increases the buckling resistance. A significant increase in fire resistance time is achieved in arches with higher included angles, see results for Arches 1,3, and 9. Though in Arch 17, an increase in compressive strength decreased the fire resistance time. This surprising result can be elucidated with the same discussion as the influence of mechanical load level. Furthermore, when loaded to the same ratio of maximum stress to compressive strength, the higher strength concrete fails by buckling much more rapidly than when compared to lower strength concrete.

5.2.4. *Cross-sectional area*

Increasing the cross-section depth proved to be the most effective method of increasing fire resistance time. As only the arch underside was heated, the cross-section depth plays a thermal, as well as a mechanical role. Great gains in fire resistance time can therefore be achieved by increasing the cross-section depth by small amounts. Increasing the cross-section width also positively impacted fire resistance time when under the same load, albeit to a lesser extent than the cross-section depth.

5.2.5. *Fire load*

As to be expected, the adopted time-temperature curve significantly influences the critical failure time. HC fires induce anti-symmetric failure earlier than ISO fires. In addition to the higher rates of heating, these results can be attributed to the larger curvatures produced by greater temperature differentials in the arch cross-section.

6. Sensitivity analysis

6.1. *Material Models*

The difference in fire resistance times when adopting the EC2 and ASCE or Kodur concrete models are compared in Table 4. The failure mode was the same across all models tested. For NSC, the ASCE model gives higher buckling failure times. This is due to the slower reduction in compressive strength with rise in temperature. Upon comparison of the fire resistance times for HSC, it can be seen that the EC2 and Kodur models lead to very similar fire resistance times. This is due to stability governing failure in high-strength slender structures.

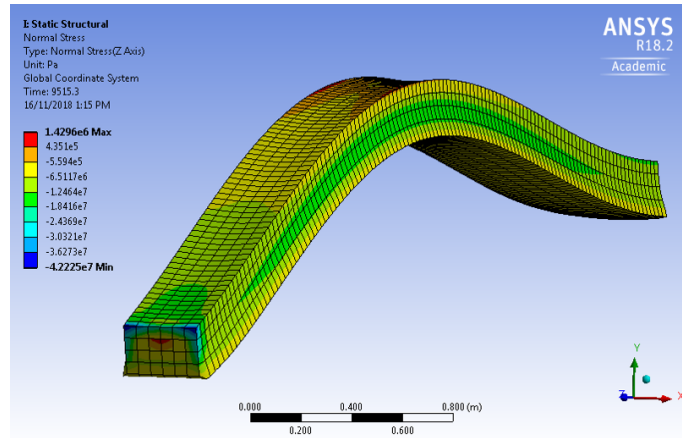


Figure 10: State of stress at critical times in Arch 17 displaying limit instability. $q = 100 \text{ kPa}$, $f'_c (T = 22^\circ\text{C}) = 32 \text{ MPa}$

6.2. Mesh Size

The influence of smaller mesh sizing on model performance has been analysed with the results shown in Table 5. Both the anti-symmetric and symmetric analyses were conducted for two arch geometries at various mesh sizes. It can be seen that adopting a smaller sized mesh has negligible effect on fire resistance.

7. Conclusion

The effects of fire loading on the behaviour and in-plane stability boundaries of shallow concrete arches were numerically investigated using FE analysis. The FE model was validated by comparison to a non-discretisation based numerical model derived herein for the non-linear inelastic analysis of shallow concrete arches under uniform thermal loading and the tangent-modulus buckling theory. Two simulations were conducted for each arch geometrical and loading configuration; one incorporating anti-symmetric geometric imperfection, obtained via an eigenvalue buckling analysis, and the second without initial deformation. The former allowing the transition from a pre-buckled equilibrium configuration to an adjacent anti-symmetric buckled equilibrium state upon reaching a critical time during thermal loading, with the results from the latter used to analyse general behaviour and to obtain symmetric buckling times. It has been observed that the direction of displacement is dependent on the level of mechanical loading; concrete arches with low levels of preheating stress deflect upwards, and concrete arches subjected to high loading displace downwards. The rate of change of deflection increases with time. Furthermore, the results show that fire loading may induce anti-symmetric buckling in shallow concrete arches, and that anti-symmetric buckling always preceded symmetric instability. Parametric investigations were conducted to assess the effects arch slenderness and included angle, fire type, mechanical loads and concrete compressive strength on failure times and mode. Fire resistance times noticeably increased with arch included angle and to a lesser extent with compressive strength. The impact of compressive strength was greater in arches with higher included angles. Increasing the mechanical load level did

not always reduce fire resistance times, as in some cases upward displacements induced earlier anti-symmetric buckling. Additionally, the difference in general behaviour and fire resistance time when adopting the EC2 and ASCE or Kodur concrete models was analysed, where it was observed that the ASCE model leads to higher fire resistance times when compared to the EC2 model for NSC, and that the HSC models give similar failure times.

Table 4: Effect of material models on anti-symmetric failure times

Arch I.D	Material model	Fire	f'_c (Mpa)	q kPa	t_A (mins)
3	EC2	ISO	32	600	167.40
3	EC2	ISO	32	750	101.09
3	ASCE	ISO	32	600	-
3	ASCE	ISO	32	750	123.64
3	EC2	HC	80	1000	-
3	EC2	HC	80	1500	94.86
3	EC2	HC	80	1700	64.03
3	Kodur	HC	80	1000	-
3	Kodur	HC	80	1500	98.80
3	Kodur	HC	80	1700	61.27
12	EC2	ISO	32	200	74.42
12	EC2	ISO	32	250	40.26
12	ASCE	ISO	32	200	91.09
12	ASCE	ISO	32	250	56.09
12	EC2	ISO	80	450	59.42
12	Kodur	ISO	80	450	48.76

Table 5: Effect of mesh size on fire resistance times

I.D	Fire	f'_c (MPa)	q (kPa)	Mesh Size (mm)	t_A (mins)	FM	t_S (mins)	FM
2	ISO	32	750	30	37.76	B	80.26	B
2	ISO	32	750	40	35.26	B	76.92	B
2	ISO	32	750	50	33.6	B	74.09	B
12	ISO	80	450	30	60.26	B	133.59	B
12	ISO	80	450	40	55.05	B	129.42	B
12	ISO	80	450	50		59.42 B	127.76	B

References

- [1] S. Timoshenko, Theory of elastic stability, Engineering societies monographs, McGraw-Hill, 1961.
- [2] V. Z. Vlasov, Thin-walled elastic beams, National Technical Information Service, 1984.
- [3] A. Gjelsvik, S. Bodner, The energy criterion and snap buckling of arches, Journal of the Engineering Mechanics 88 (1962) 87–134.
- [4] W. J. Austin, In-plane bending and buckling of arches, Journal of the Structural Division 97 (5) (1971) 1575–1592.
- [5] G. J. Simitses, J. Hutchinson, An introduction to the elastic stability of structures, Journal of Applied Mechanics 43 (1976) 383.
- [6] H. L. Schreyer, E. F. Masur, Buckling of shallow arches, Journal of the Engineering Mechanics Division 92 (4) (1966) 1–20.
- [7] J. F. Dickie, P. Broughton, Stability criteria for shallow arches, Journal of the Engineering Mechanics Division 97 (3) (1971) 951–965.
- [8] C. H. Yoo, P. A. Pfeiffer, Buckling of curved beams with in-plane deformation, Journal of Structural Engineering 110 (2) (1984) 291–300.
- [9] P. Vacharajittiphan, N. S. Trahair, Flexural-torsional buckling of curved members, Journal of the Structural Division 101 (6) (1975) 1223–1238.
- [10] J. P. Papangelis, N. S. Trahair, Flexural-torsional buckling of arches, Journal of Structural Engineering 113 (4) (1987) 889–906.
- [11] S. Rajasekaran, S. Padmanabhan, Equations of curved beams, Journal of engineering mechanics 115 (5) (1989) 1094–1111.
- [12] N. S. Trahair, Flexural-torsional buckling of structures, Vol. 6, CRC Press, 1993.
- [13] Y. J. Kang, C. H. Yoo, Thin-walled curved beams. ii: analytical solutions for buckling of arches, Journal of engineering mechanics 120 (10) (1994) 2102–2125.
- [14] N.-H. Lim, Y.-J. Kang, Out of plane stability of circular arches, International journal of mechanical sciences 46 (8) (2004) 1115–1137.
- [15] Y.-L. Pi, N. Trahair, Non-linear buckling and postbuckling of elastic arches, Engineering Structures 20 (7) (1998) 571–579.
- [16] Y.-L. Pi, M. A. Bradford, B. Uy, In-plane stability of arches, International Journal of Solids and Structures 39 (1) (2002) 105–125.
- [17] M. A. Bradford, In-plane nonlinear behaviour of circular pinned arches with elastic restraints under thermal loading, International Journal of Structural Stability Dynamics 6 (2) (2006) 163–177.
- [18] Y. L. Pi, M. A. Bradford, Thermoelastic behaviour of elastically restrained tubular steel arches, Taylor Francis, 2008, pp. 659–667.
- [19] Y.-L. Pi, M. A. Bradford, In-plane thermoelastic behaviour and buckling of pin-ended and fixed circular arches, Engineering Structures 32 (1) (2010) 250–260.
- [20] M. A. Bradford, Long-span shallow steel arches subjected to fire loading, Advances in Structural Engineering 13 (3) (2010) 501–511.
- [21] Y.-L. Pi, M. A. Bradford, Nonlinear in-plane elastic buckling of shallow circular arches under uniform radial and thermal loading, International Journal of Mechanical Sciences 52 (1) (2010) 75–88.
- [22] Y.-L. Pi, M. A. Bradford, Nonlinear thermoelastic buckling of pin-ended shallow arches under temperature gradient, Journal of engineering mechanics 136 (8) (2010) 960–968.
- [23] J. Cai, Y. Xu, J. Feng, J. Zhang, Effects of temperature variations on the in-plane stability of steel arch bridges, Journal of Bridge Engineering 17 (2) (2010) 232–240.
- [24] A. Heidarpour, M. A. Bradford, K. A. Othman, Thermoelastic flexural-torsional buckling of steel arches, Journal of Constructional Steel Research 67 (12) (2011) 1806–1820.
- [25] J. Cai, Y. Xu, J. Feng, J. Zhang, In-plane elastic buckling of shallow parabolic arches under an external load and temperature changes, Journal of Structural Engineering 138 (11) (2012) 1300–1309.
- [26] B. Moghaddasie, I. Stanciulescu, Equilibria and stability boundaries of shallow arches under static loading in a thermal environment, International Journal of Non-Linear Mechanics 51 (2013) 132–144.
- [27] Y.-L. Pi, M. A. Bradford, Effects of nonlinearity and temperature field on in-plane behaviour and buckling of crown-pinned steel arches, Engineering Structures 74 (2014) 1–12.
- [28] Y. Bouras, Z. Vrcelj, Non-linear in-plane buckling of shallow concrete arches subjected to combined mechanical and thermal loading, Engineering Structures 152 (2017) 413–423.
- [29] S. Thelandersson, Mechanical behaviour of concrete under torsional loading at transient, hightemperature conditions, Bulletin of Division of Structural Mechanics and Concrete Construction, Bulletin 46.

- [30] Y. Anderberg, S. Thelandersson, Stress and deformation characteristics of concrete at high temperatures: experimental investigation and material behavior model, Division of Structural Mechanics and Concrete Construction, 1976.
- [31] G. Torelli, P. Mandal, M. Gillie, V.-X. Tran, Concrete strains under transient thermal conditions: A state-of-the-art review, *Engineering Structures* 127 (2016) 172–188.
- [32] A. Heidarpour, T. H. Pham, M. A. Bradford, Nonlinear thermoelastic analysis of composite steelconcrete arches including partial interaction and elevated temperature loading, *Engineering Structures* 32 (10) (2010) 3248–3257.
- [33] K. Luo, Y. Pi, W. Gao, M. A. Bradford, Long-term analysis of crown-pinned concrete-filled steel tubular arches, in: ICCM: Proceedings of the 5th International Conference on Computational Methods, Cambridge, England, 28-30 July 2014, 2015.
- [34] Y. Bouras, Z. Vrcelj, Thermal in-plane stability of concrete-filled steel tubular arches, *International Journal of Mechanical Sciences* 163 (2019) 105130.
- [35] S.-S. Huang, I. Burgess, Z. Huang, R. Plank, The buckling of slender concrete and concrete-filled columns in fire', in: *Fib Workshop: Fire Design of Concrete Structures-from Materials Modelling to Structural Performance*, Coimbra, Portugal, 2007.
- [36] A. Sadaoui, A. Khennane, Effect of transient creep on the behaviour of reinforced concrete columns in fire, *Engineering Structures* 31 (9) (2009) 2203–2208.
- [37] L.-H. Han, Q.-H. Tan, T.-Y. Song, Fire performance of steel reinforced concrete columns, *Journal of Structural Engineering* 141 (4) (2014) 04014128.
- [38] U. Bajc, M. Saje, I. Planinc, S. Bratina, Semi-analytical buckling analysis of reinforced concrete columns exposed to fire, *Fire Safety Journal* 71 (2015) 110–122.
- [39] J.-M. Franssen, J.-C. Dotreppe, Fire tests and calculation methods for circular concrete columns, *Fire technology* 39 (1) (2003) 89–97.
- [40] S. Bratina, B. Čas, M. Saje, I. Planinc, Numerical modelling of behaviour of reinforced concrete columns in fire and comparison with eurocode 2, *International Journal of Solids and Structures* 42 (21) (2005) 5715–5733.
- [41] ANSYS Workbench, Release 17.2, Ansys Inc, Canonsburg, PA, 2016.
- [42] W. Gao, J.-G. Dai, J. Teng, G. Chen, Finite element modeling of reinforced concrete beams exposed to fire, *Engineering structures* 52 (2013) 488–501.
- [43] P. Bamonte, F. L. Monte, Reinforced concrete columns exposed to standard fire: Comparison among different constitutive models for concrete at high temperature, *Fire Safety Journal* 71 (2015) 310–323.
- [44] S. Albrifkani, Y. C. Wang, Explicit modelling of large deflection behaviour of restrained reinforced concrete beams in fire, *Engineering Structures* 121 (2016) 97–119.
- [45] EN 1992 1-2, Eurocode 2: Design of concrete structures, Part 1-2, Structural fire design, European Committee for Standardization, 2004.
- [46] Lie, T.T, Structural fire protection, American Society of Civil Engineers (ASCE), 1992.
- [47] V. Kodur, T. Wang, F. Cheng, Predicting the fire resistance behaviour of high strength concrete columns, *Cement and Concrete Composites* 26 (2) (2004) 141–153.
- [48] T. Gernay, J.-M. Franssen, A comparison between explicit and implicit modelling of transient creep strain in concrete uniaxial constitutive relationships, in: *Proceedings of the fire and materials 2011 conference*, Interscience Communications Ltd, 2011, pp. 405–416.
- [49] MATLAB Users Guide, Version 7, The MathWorks Inc.
- [50] Z. Bažant, L. Cedolin, Stability of Structures: Elastic, Inelastic, Fracture and Damage Theories, World Scientific, 2010.

5.4 Concluding Remarks

This chapter presented a numerical study into the inelastic in-plane failure modes of shallow concrete arches subjected to combined mechanical and fire loading. The results detailed herein outline the governing failure mode of shallow concrete arches under fire loading and highlight the key parameters governing fire resistance time. These findings can be used to improve the design of concrete arches that may be exposed to fire loading. Furthermore, a novel non-discretisation mechanical-based numerical method for the non-linear inelastic analysis of shallow concrete arches at elevated temperatures was derived. In summary, the following conclusions are drawn from this chapter;

1. Fire loading may trigger anti-symmetric bifurcation buckling in shallow concrete arches which is also the governing in-plane failure mode;
2. The mechanical load level influenced the direction of displacement. Low loads resulted in upward displacement throughout the heating period with higher loads causing downward deflections during fire exposure;
3. Increasing the mechanical load level did not always decrease fire resistance time as some upward displacing arches displayed anti-symmetric buckling earlier than when mechanically loaded to a higher level;
4. Increasing compressive strength at the same mechanical load level improved fire resistance time with this gain increasing with included angle. However, when loaded to the same ratio of maximum longitudinal stress to compressive strength, fire resistance times decreases at higher strengths; and
5. The arch included angle and cross-sections depth proved to significantly influence fire resistance time.

Chapter 6

Thermal in-plane stability of concrete-filled steel tubular arches

6.1 Introduction

In this chapter, the in-plane elastic and inelastic prebuckling and buckling behaviour of circular CFST arches under uniformly distributed radial loading and elevated temperature fields are analytically and numerically investigated. Closed-form solutions are derived using energy methods for the thermo-elastic prebuckling behaviour and in-plane anti-symmetric bifurcation buckling loads of shallow CFST arches with pinned or fixed ends. Additionally, a numerical technique is formulated in the form of a BVP which

can be employed to solve the elastic or inelastic prebuckling response of shallow and deep CFST arches under mechanical and thermal loading, which is applicable to fixed, pinned and crown-pinned boundary conditions. The inelastic in-plane buckling strength of CFST arches under uniform temperature fields and fire loading is then investigated through the development of a three-dimensional FE model. Verification of the FE model is achieved by comparison to analytical and numerical models derived for the elastic and inelastic analyses. Parametric studies and sensitivity analyses presented depict the influence of numerous parameters on critical buckling loads and fire resistance times.

The following papers are included in this chapter;

1. Y. Bouras, E. Torres-Don and Z. Vrcelj. 2017. Thermal in-plane buckling of concrete-filled steel tubular arches. In *Tubular Structures XVI: Proceedings of the 16th International Symposium for Tubular Structures (ISTS 2017, 4-6 December 2017, Melbourne, Australia)* (p. 101). CRC Press.
2. Y. Bouras, and Z. Vrcelj. 2019. Thermal in-plane stability of concrete-filled steel tubular arches. *International Journal of Mechanical Sciences*, 163, p.105130.



THE NEW WAY TO DO UNI

OFFICE FOR RESEARCH TRAINING, QUALITY AND INTEGRITY

DECLARATION OF CO-AUTHORSHIP AND CO-CONTRIBUTION: PAPERS INCORPORATED IN THESIS

This declaration is to be completed for each conjointly authored publication and placed at the beginning of the thesis chapter in which the publication appears.

1. PUBLICATION DETAILS (to be completed by the candidate)

Title of Paper/Journal/Book:	Thermal in-plane buckling of concrete-filled steel tubular arches		
Surname:	Bouras	First name:	Yanni
Institute:	Institute for Sustainable Industries and Liveat	Candidate's Contribution (%):	90
Status:			
Accepted and in press:	<input type="checkbox"/>	Date:	
Published:	<input checked="" type="checkbox"/>	Date:	04/12/2017

2. CANDIDATE DECLARATION

I declare that the publication above meets the requirements to be included in the thesis as outlined in the HDR Policy and related Procedures – policy.vu.edu.au.

Yanni Bouras	<small>Digitally signed by Yanni Bouras Date: 2020.02.10 15:47:25 +11'00'</small>	10/02/2020
Signature		Date

3. CO-AUTHOR(S) DECLARATION

In the case of the above publication, the following authors contributed to the work as follows:

The undersigned certify that:

1. They meet criteria for authorship in that they have participated in the conception, execution or interpretation of at least that part of the publication in their field of expertise;
2. They take public responsibility for their part of the publication, except for the responsible author who accepts overall responsibility for the publication;

PO Box 14428, Melbourne,
Vic 8001, Australia
+61 3 9919 6100

Victoria University ABN 83776954731
CRICOS Provider No. 00124K (Melbourne),
02475D (Sydney), RTO 3113



THE NEW WAY TO DO UNI

3. There are no other authors of the publication according to these criteria;
4. Potential conflicts of interest have been disclosed to a) granting bodies, b) the editor or publisher of journals or other publications, and c) the head of the responsible academic unit; and
5. The original data will be held for at least five years from the date indicated below and is stored at the following location(s):

Victoria University, Footscray Park, Ballarat Road, Melbourne, VIC 3011, Australia

Name(s) of Co-Author(s)	Contribution (%)	Nature of Contribution	Signature	Date
Yanni Bouras	90	Conceived concept. Literature review. Analytical/numerical modelling. Writing manuscript		11/02/2020
Zora Vrclj	5	Critical review of manuscript. Final approval of manuscript.		11/02/2020
Eduardo Torres-Don	5	Running finite element simulations for parametric study		12/02/2020

Updated: September 2019

PO Box 14428, Melbourne,
Vic 8001, Australia
+61 3 9919 6100

Victoria University ABN 83776954731
CRICOS Provider No. 00124K (Melbourne)
02475D (Sydney), RTO 3113



OFFICE FOR RESEARCH TRAINING, QUALITY AND INTEGRITY

DECLARATION OF CO-AUTHORSHIP AND CO-CONTRIBUTION: PAPERS INCORPORATED IN THESIS

This declaration is to be completed for each conjointly authored publication and placed at the beginning of the thesis chapter in which the publication appears.

1. PUBLICATION DETAILS (to be completed by the candidate)

Title of Paper/Journal/Book:	Thermal in-plane stability of concrete-filled steel tubular arches		
Surname:	Bouras	First name:	Yanni
Institute:	Institute for Sustainable Industries and Liveat	Candidate's Contribution (%):	95
Status:		Date:	
Accepted and in press:	<input type="checkbox"/>	Date:	
Published:	<input checked="" type="checkbox"/>	Date:	03/09/2019

2. CANDIDATE DECLARATION

I declare that the publication above meets the requirements to be included in the thesis as outlined in the HDR Policy and related Procedures – policy.vu.edu.au.

Yanni Bouras	Digitally signed by Yanni Bouras Date: 2020.02.10 15:24:40 +11'00'	10/02/2020
Signature		Date

3. CO-AUTHOR(S) DECLARATION

In the case of the above publication, the following authors contributed to the work as follows:

The undersigned certify that:

1. They meet criteria for authorship in that they have participated in the conception, execution or interpretation of at least that part of the publication in their field of expertise;
2. They take public responsibility for their part of the publication, except for the responsible author who accepts overall responsibility for the publication;



THE NEW WAY TO DO UNI

3. There are no other authors of the publication according to these criteria;
4. Potential conflicts of interest have been disclosed to a) granting bodies, b) the editor or publisher of journals or other publications, and c) the head of the responsible academic unit; and
5. The original data will be held for at least five years from the date indicated below and is stored at the following location(s):

Victoria University, Footscray Park, Ballarat Road, Melbourne, VIC 3011, Australia

Name(s) of Co-Author(s)	Contribution (%)	Nature of Contribution	Signature	Date
Yanni Bouras	95	Conceived concept. Literature review. Analytical/numerical modelling. Writing manuscript		11/02/2020
Zora Vrcelj	5	Critical review of manuscript. Final approval of manuscript.		11/02/2020

Updated: September 2019

PO Box 14428, Melbourne,
Vic 8001, Australia
+61 3 9919 6100

Victoria University ABN 83776954731
CRICOS Provider No. 00124K (Melbourne),
02475D (Sydney), RTO 3113

Y. Bouras, E. Torres-Don and Z. Vrcelj. 2017. Thermal in-plane buckling of concrete-filled steel tubular arches. In *Tubular Structures XVI: Proceedings of the 16th International Symposium for Tubular Structures (ISTS 2017, 4-6 December 2017, Melbourne, Australia)* (p. 101). CRC Press.
<https://www.taylorfrancis.com/books/e/9781351210843/chapters/10.1201/9781351210843-13>

The full-text of this article is subject to copyright restrictions, and cannot be included in the online version of the thesis.



Thermal in-plane stability of concrete-filled steel tubular arches

Yanni Bouras, Zora Vrcelj*

College of Engineering and Science, Victoria University, Melbourne, VIC, Australia

ARTICLE INFO

Keywords:

Buckling
CFST
Inelastic
Limit instability
Shallow arches
Thermal load

ABSTRACT

This paper analytically and numerically investigates the pre-buckling response and in-plane stability boundaries of circular concrete-filled steel tubular (CFST) arches subjected to combined thermal and mechanical loading. The governing non-linear equations of equilibrium are obtained using energy methods and both elastic and inelastic material behaviour is considered. A novel mechanically derived non-discretisation numerical method is proposed for the pre-buckling analysis. The stress-strain relation of the confining steel tube is described using a bi-linear plasticity model, and an inelastic material model is adopted for the concrete core which considers the effects of confinement and transient thermal strain. The result is a system of first-order differential equations which can be numerically solved with known boundary conditions including fixed ends, pinned ends or crowned-pinned cases. Closed-form solutions are presented for the elastic anti-symmetric bifurcation loads, whilst the inelastic anti-symmetric buckling strength was studied using finite element (FE) analysis. The FE model is verified by comparison to the derived analytical and numerical models which show a high level of agreement. Additionally, a sensitivity analysis is conducted which explores the influence of the constitutive material law for the concrete core and contact model for the steel-concrete interface on critical buckling loads.

1. Introduction

Concrete-filled steel tubular (CFST) arches are commonly constructed in civil engineering projects. Their popularity can be attributed to the structural benefits associated with the mechanical function of arches, and of composite steel-concrete sections. However, as arches are typically loaded to a state of compressive stress, the problem of stability must be carefully considered. Arches may buckle in their plane of loading in an anti-symmetric or symmetric fashion, and out of their plane of loading in a flexural-torsional buckling mode. Further complications arise in the analysis and design of arches due to geometrical nonlinearities which convolute the stability analysis and reduce buckling strength. Due to the inherent complex nature of arches, it is paramount that the behaviour of CFST arches under all possible mechanical and environmental environments be thoroughly investigated.

Elevated temperatures are a frequently occurring example of environmental loading which threatens existing structures. Thermal effects on the elastic behaviour and in-plane stability boundaries of steel arches have been extensively studied. Analytical solutions have been presented in [1–3] for the case of uniform thermal loading and in [4–8] for arches under mechanical and thermal loading. Elevated temperature fields may induce in-plane buckling in steel arches and leads to an increase in critical anti-symmetric and symmetric mechanical buckling loads. Pi and Bradford [9] derived closed-form solutions for the thermo-elastic in-

plane buckling loads of shallow circular arches subjected to thermal gradients, and Cai et al. [10] analytically investigated in-plane buckling of shallow parabolic arches subjected to uniformly distributed loading and to temperature gradients. It was shown that buckling loads reduce with an increasing temperature gradient. A non-discretisation mechanical-based model was proposed by Heidarpour et al. [11] for the non-linear thermo-elastic analysis of steel circular arches under uniformly distributed loads and non-uniform temperature fields. The authors extended the numerical model in [12] to incorporate inelastic behaviour. However, the models proposed in [11,12] were not developed for analysis of stability. In addition to in-plane buckling, elevated temperatures may trigger lateral buckling in arches. However, the phenomenon of thermal induced flexural-torsional buckling has received far less research attention when compared to in-plane buckling. The study by Heidarpour et al. [13] appears to be the only research on this subject, wherein the numerical method developed in [11] was employed to model the non-linear pre-buckling behaviour and the thermo-elastic flexural-torsional buckling loads in circular steel arches with doubly symmetric I-shape cross-sections. In contrast to in-plane buckling, it was found that lateral stability boundaries were governed primary by the critical buckling temperature and not greatly influenced by the mechanical load.

The thermal response of Functionally Graded (FG) arches have also received research interest. A non-linear thermoelastic and in-plane buckling analysis was conducted for functionally graded material (FGM)

* Corresponding author.

E-mail address: zora.vrcelj@vu.edu.au (Z. Vrcelj).

shallow arches subjected to a uniform temperature field by Asgari et al. [14]. The effect of linearly varying temperature profiles on the stability of shallow FGM arches was studied in the work of Asgari and Eslami [15]. In both these studies, energy methods were adopted to derive the non-linear equilibrium equations, and analytical solutions for the critical buckling temperatures were derived using the adjacent equilibrium method. It was found that the critical buckling temperature varied non-monotonically with power-law index, and that material failure was the likely failure mode due to the high temperatures required to induce stability loss. Bateni and Eslami [16] analysed the in-plane stability of pin-ended shallow FGM arches subjected to a linear thermal gradient and lateral applied uniformly distributed loads and central concentrated loads. An increase of the bifurcation buckling load with thermal gradient was observed. Song and Li [17] investigated the stability of fixed-fixed FGM shallow arches under thermal loading and a uniformly distributed follower force. As with steel arches, anti-symmetric bifurcation buckling was found to precede symmetric snap-through buckling. A large deflection analysis of pin-ended FGM shallow arches on non-linear Pasternak elastic foundation subjected to thermal loading and uniformly distributed lateral pressure was conducted by Babaei et al. [18]. The non-linear equilibrium equations were derived using third-order shear deformation theory of von Krmn type of strain-displacement relation. Closed-form solutions for the maximum deflection dependant on the applied load or temperature level was obtained by employing a two-step perturbation technique. The case of fixed ends was solved by the authors in [19]. Li et al. [20] conducted a thermo-elastic anti-symmetric buckling analysis on FGM shallow arches when subjected to combined in-plane external pressures and uniform temperature fields. The derived closed-form expressions for the critical buckling pressure were numerically validated via two-dimensional finite element analysis. Elevated temperatures were found to cause upward displacements consequently increasing the buckling pressure, and simultaneously reducing the Elastic modulus, which decreases the critical load. This is identical to the thermo-elastic response of homogeneous arches such as steel or concrete. Optimised or inverted FGM arches are obtained by reversing the material distribution in conventional FGM arches. These inverted FGM arches show a significant increase in buckling pressure when compared to conventional FGM arches with the same volume portion of the material constituents [21]. The problem of stability of a rigidly-confined FGM shallow arch under external pressure was analytically and numerically investigated by Li et al. [22]. Confinement effects were found to be beneficial and led to a great increase in stability boundaries of FGM arches, whilst increasing the volume fraction exponent reduced buckling strength. Yang et al. [23] investigated the non-linear in-plane buckling of fixed shallow functionally graded graphene reinforced composite arches subjected to mechanical and thermal loading. The arches consisted of multiple graphene platelet reinforced composite (GPLRC) layers. The principle of virtual work was employed to derive the equilibrium equations whilst describing the materials properties using the Halpin-Tsai micromechanics model for GPLRC layer, and closed-form solutions were derived for the limit point and bifurcations buckling loads. It was shown that great increases in buckling resistance can be achieved by increasing graphene platelets filler content.

CFST columns subjected to combined mechanical and thermal loading have been investigated analytically [24–26], numerically [27–30] and experimentally [31–33]. The fire response of CFST columns can be described as a four-stage sequence [27]. The first step involves the rapid rise in temperature in the steel tube when initially exposed to fire which causes it to expand and separate from the concrete core. Consequently, the axial load is primarily resisted by the steel tube as the concrete loses contact with the loading plate. The steel tube supports the load until a critical temperature is reached causing the steel to yield locally and contract. Yielding of the steel tube is defined as the second stage. As the column shortens, the stress is progressively transferred to the concrete which becomes the primary supporting element in the

column. The continual shortening of the column is known as the third stage. Eventually, the fourth and final step is reached which consists of the failure of the concrete core due to reduction of strength and stiffness caused by elevated temperatures. In addition to material failure, CFST columns may also experience loss of stability when subjected to heating [24,27,28,30]. A major contributor to stiffness degradation in the concrete core is transient thermal strain (TTS); a strain thought to originate in the cement paste due to thermo-mechanical interaction. Unique properties of TTS include its irreversibility, and its exclusive manifestation in mechanically pre-loaded concrete upon first time heating. The reductions in buckling strength of CFST in fire are significantly greater when considering TTS [28].

The aforementioned studies on thermal effects in arches were restricted to steel and FG arches. Fewer works are available in the open literature on concrete and composite steel-concrete arches. In addition to mechanical strain and thermal expansion, concrete experiences elevated creep and transient thermal strain (TTS) when subject to mechanical loading and temperature changes. Bouras and Vrcelj [34] performed an in-plane pre-buckling and buckling analysis of shallow concrete arches under mechanical loading and elevated temperatures whilst considering TTS and basic creep. TTS was found to magnify the reduction in buckling loads of concrete arches at high temperatures. This work was however limited to elastic material behaviour and uniform temperature fields. Heidarpour et al. [35] developed an analytical model to analyse the non-linear thermo-elastic behaviour of a composite steel-concrete arch with partial interaction subjected to mechanical and non-uniform thermal loading. The time-dependant response of crown-pinned CFST arches exposed to a constant temperature reduction was analytically analysed by Luo et al. [36] in order to study the coupling effects between time and temperature. The temperature change was found to greatly increase the time-varying deformations and forces. The influence of non-constant temperatures on the creeping mechanics of a CFST arch was investigated by Wang et al. [37] using a finite element model. This was achieved through the incorporation of the micro-prestress solidification theory [38], the age-adjusted effective modulus and an average temperature history into a finite element model. The Yajisha bridge in China was replicated in the program and results were verified from measurements taken of the bridge one year after construction. The results indicated that the increase in creep caused by temperature variations are not negligible. As the motivation behind the studies of Luo et al. [36] and Wang et al. [37] was the long-term response of CFST arches, the developed models were designed for temperature loads not exceeding 100°C. The response and failure modes of shallow fixed circular CFST arches subjected to mechanical and fire loading were numerically investigated by Bouras et al. [39] through the development of a finite element (FE) model in ANSYS. The simulations show that material failure is the dominant failure mode, with symmetric buckling governing failure in very shallow arches. It appears that this is the only study investigating the effects of extreme thermal loads (temperatures greater than 100°C) on CFST arches. However, the scope of this study was restricted to shallow arches with fixed ends and FE methods of analysis, with results presented as fire resistance times and not buckling loads. Consequently, more research, particularly analytical and numerical studies, on this subject is necessitated.

This study seeks to address the limited research on the effects of elevated temperature on the response and buckling loads of CFST arches by undertaking a non-linear pre-buckling and in-plane buckling analysis of circular CFST shallow and deep arches subjected to uniformly distributed radial loads and elevated temperature fields. Pinned, fixed and crown-pinned boundary conditions are considered. The delineating total included angle distinguishing between shallow and deep arches is defined herein as $2\theta < 90^\circ$, with very shallow arches categorised as total included angles of $2\theta < 20^\circ$. The analysis first considers the elastic case, which results in the derivation of a numerical model for pre-buckling response and analytical solutions for the anti-symmetric buckling loads. Subsequently, the numerical model is generalised to incorporate inelas-

tic material behaviour for both the steel tube and concrete core. These analyses are governed by the following assumptions:

- The arch is assumed to behave according to the Euler-Bernoulli hypothesis, i.e plain sections before deformation remain plane after deformation
- The temperature field is symmetrically distributed about both axes through the cross-section and is uniform through the arch length
- Thermal expansions of the cross-section are small and thus negligible.
- Sufficient lateral restraints exist so as to prevent flexural-torsional buckling failure of the arch
- A perfect bond exists between the concrete core and confining steel tube. Hence the longitudinal strains are equal at the interface for both materials.

Finally, the inelastic in-plane buckling loads are investigated through the development of a Finite Element (FE) model. Comparisons are made between the FE model and the derived analytical and numerical models. The validity of assuming a perfect bond between the steel tube and concrete core is explored by conducting a sensitivity analysis using the developed FE model.

2. Material models

2.1. Steel

The total strain in the outer steel tube of the CFST cross section is defined as;

$$\epsilon = \epsilon_{ch} + \epsilon_{s,th}, \quad (1)$$

where ϵ_{ch} represents the mechanical strain and $\epsilon_{s,th}$ is the steel thermal strain. The bi-linear stress-strain formulation proposed by Lie [40] is adopted in this paper to model the temperature dependent deformation properties of steel, defined as

$$\sigma_s = \begin{cases} E_{s,T} \epsilon_{ch} & \text{for } \epsilon_{ch} \leq \epsilon_p \\ (c_1 \epsilon_{ch} + c_2) \sigma_{y,T} - c_3 \sigma_{y,T}^2 / E_{s,T} & \text{for } \epsilon_{ch} > \epsilon_p, \end{cases} \quad (2)$$

where the yield strain is

$$\epsilon_p = \frac{c_2 \sigma_{y,T} - c_3 \sigma_{y,T}^2 / E_{s,T}}{E_{s,T} - c_1 \sigma_{y,T}}, \quad (3)$$

and the coefficients $c_1 = 12.5$, $c_2 = 0.975$ and $c_3 = 12.5$. When $\epsilon_{ch} \leq \epsilon_p$, the steel is in the linear elastic region, and if $\epsilon_{ch} > \epsilon_p$, inelastic behaviour occurs. The temperature dependent elastic modulus $E_{s,T}$, yield strength $\sigma_{y,T}$ and thermal strain $\epsilon_{s,th}$ are obtained from the Eurocode 3 (EC3) [41].

2.2. Concrete

Three models for the stress-strain relation of concrete are considered; one elastic and two inelastic. The linear elastic concrete material model defines the total strain as the sum of the elastic mechanical strain, the thermo-mechanical TTS and the thermal strain;

$$\epsilon = \frac{\sigma_c}{E_{c,T}} + \epsilon_{tr} + \epsilon_{c,th}, \quad (4)$$

where the TTS is modelled using the explicit Eurocode 2 (EC2) formulation [42]:

$$\epsilon_{tr} = \frac{\sigma_c}{f'_c} \phi(T) = \frac{2\sigma_c}{3f'_c} \left(\frac{\epsilon_{max} - \epsilon_{min}}{f'_{c,T} / f'_c} \right), \quad (5)$$

in which $E_{c,T}$ is the temperature reduced elastic modulus, $\epsilon_{c,th}$ is the thermal strain in the concrete, f'_c is the cold concrete compressive strength, $f'_{c,T}$ is the temperature reduced compressive strength, ϵ_{max} is the peak stress strain (PSS) accounting for TTS and ϵ_{min} denotes the minimum PSS obtained from steady state tests (thus not considering TTS). These

parameters are obtained from the EC2 [43] (siliceous concrete). Combining Eqs. (4) and (5) yields

$$\epsilon = \frac{\sigma_c}{E_{c,T}} + \epsilon_{c,th} = \sigma_c \left(\frac{1}{E_{c,T}} + \frac{\phi(T)}{f'_c} \right) + \epsilon_{c,th}. \quad (6)$$

The ASCE [25,40] concrete model is one of the inelastic models adopted defined as

$$\sigma = f'_c \left[1 - \left(\frac{\epsilon - \epsilon_{max}}{\epsilon_{max}} \right)^2 \right], \quad (7)$$

where ϵ_{max} is the temperature dependent PSS. The relationship between compressive strength and temperature for the ASCE model is

$$f'_{c,T} = \begin{cases} f'_c & \text{for } 22^\circ\text{C} \leq T \leq 450^\circ\text{C}, \\ f'_c [2.011 - 2.353(T - 20) \times 10^{-3}] & \text{for } 450^\circ\text{C} \leq T \leq 874^\circ\text{C}, \\ 0 & \text{for } 874^\circ\text{C} < T. \end{cases} \quad (8)$$

The ASCE model for concrete in CFST sections at elevated temperatures considers the effects of confinement and implicitly considers transient thermal strain. The EC2 stress-strain relationship of concrete is also considered and is defined as,

$$\frac{\sigma}{f'_{c,T}} = \frac{3\epsilon}{\epsilon_{max} [2 + (\epsilon/\epsilon_{max})^3]}, \quad (9)$$

Although arches are typically subjected to compression, regions of tensile stress may develop due to thermal loading. Hence, temperature dependent tensile strength is considered with the EC2 formulation adopted:

$$f_{ck,t}(T) = \begin{cases} f_{ck,t} & \text{for } 20^\circ\text{C} \leq T \leq 100^\circ\text{C}, \\ f_{ck,t} [1.0 - (T - 100)/500] & \text{for } 100^\circ\text{C} \leq T \leq 600^\circ\text{C}, \end{cases} \quad (10)$$

where $f_{ck,t}$ is the cold tensile strength of concrete, available in the EC2. Modelling of concrete in tension is relevant to the FE model developed and discussed in Section 6.

3. Non-linear elastic analysis

3.1. Non-linear equations of equilibrium

The geometrical and loading configuration adopted herein consists of a circular CFST arch loaded with a uniformly distributed radial mechanical load q and symmetrical thermal load $T(y)$. The origin o is positioned at the geometrical arch center. The axis oy alters direction along the arch circumference and always is directed to the arch center. The axis os aligns centroidal axis of the arch. Fig. 1 depicts the arch configuration. The non-linear longitudinal normal strain equation, proposed by Pi and Trahair [44] and Pi et al. [45], is adopted to incorporate geometric non-linearity into the analysis. This is defined as,

$$\epsilon = \epsilon_m + \epsilon_b \quad (11)$$

where ϵ_m is the membrane strain and ϵ_b denotes the bending strains, known as

$$\epsilon_m = w' - v + \frac{1}{2}(v' + w)^2, \quad \epsilon_b = -\frac{y}{R}(v'' + w'). \quad (12)$$

In Eq. (11), ϵ represents the total strain at a point \mathcal{P} in the CFST cross section. In Eq. (12), $w = \hat{w}/R$, $v = \hat{v}/R$, \hat{w} is the axial displacement, \hat{v} is the radial deflection, y is the vertical coordinate of \mathcal{P} , $(\cdot)' = d(\cdot)/d\theta$, $(\cdot)'' = d^2(\cdot)/d\theta^2$ and θ is the angular coordinate.

The non-linear equations of equilibrium are obtained by employing the virtual work principle which states that

$$\int_{V_s} \sigma_s \delta \epsilon \, dV_s + \int_{V_c} \sigma_c \delta \epsilon \, dV_c - \int_{-\theta}^{\theta} q R^2 \delta v \, d\theta = 0, \quad \forall \delta v, \delta v', \delta v'', \delta w, \delta w' \quad (13)$$

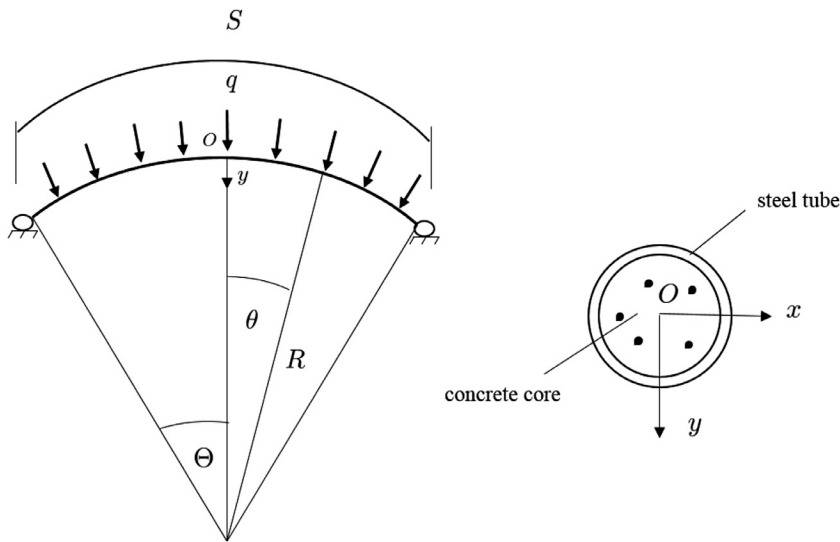


Fig. 1. CFST arch loading and geometrical configuration.

where V_s and V_c are the volumes of the steel tube and concrete core respectively, Θ is half the total included angle and δv , $\delta v'$, $\delta v''$, δw and $\delta w'$ are kinematically admissible displacement variations. The total axial force N is defined as

$$N = - \int_{A_c} \sigma_c dA_c - \int_{A_s} \sigma_s dA_s, \tag{14}$$

with the bending moment M given by

$$M = \int_{A_c} \sigma_c y dA_c + \int_{A_s} \sigma_s y dA_s, \tag{15}$$

where A_c and A_s are the cross-sectional areas of the concrete core and steel tube respectively. Integrating Eq. (13) by parts, considering strain formulation (11) and definitions (14) and (15), gives the equations of non-linear equilibrium,

$$N'R + M' - N(w + v') = 0, \tag{16}$$

$$-M'' + NR(1 + v'' + w') + N'R(v' + w) - qR^2 = 0, \tag{17}$$

in the axial and radial directions respectively. This also yields the static boundary condition for an arch with pinned-ends

$$v''(\Theta) = v''(-\Theta) = 0. \tag{18}$$

The known geometrical boundary conditions are

$$v(\Theta) = v(-\Theta) = w(\Theta) = w(-\Theta) = 0, \tag{19}$$

for a simply-supported arch, and

$$v(\Theta) = v(-\Theta) = v'(\Theta) = v'(-\Theta) = w(\Theta) = w(-\Theta) = 0, \tag{20}$$

for an arch with fixed supports. If considering a crown-pin, the virtual work principles is only applied to half the arch through its length. This gives the static boundary conditions for singly and three-pinned arches

$$M'(0) + N(0)Rv'(0) = 0, \text{ and } M(0) = 0, \tag{21}$$

and

$$M(\Theta) = 0, \tag{22}$$

for three-pinned arches. These adjoin the known kinematic boundary conditions for a three-pinned arch

$$v(\Theta) = w(\Theta) = w(0) = 0, \tag{23}$$

and for a singly-pinned arch

$$v(\Theta) = v'(\Theta) = w(\Theta) = w(0) = 0. \tag{24}$$

Combining Eqs. (2) and (6) with (14) yields the constitutive equation for axial force:

$$N = \widehat{EA}_s \widehat{\epsilon}_{s,th} + \widehat{EA}_c \widehat{\epsilon}_{c,th} - \epsilon_m (\widehat{EA}_s + \widehat{EA}_c), \tag{25}$$

where the thermal section properties for the steel tube are

$$\widehat{EA}_s \widehat{\epsilon}_{s,th} = \int_{A_s} E_{s,T} \epsilon_{s,th} dA_s, \text{ and } \widehat{EA}_s = \int_{A_s} E_{s,T} dA_s, \tag{26}$$

and are defined for the concrete core as

$$\widehat{EA}_c \widehat{\epsilon}_{c,th} = \int_{A_c} \widehat{E}_{c,T} \epsilon_{c,th} dA_c \text{ and } \widehat{EA}_c = \int_{A_c} \widehat{E}_{c,T} dA_c. \tag{27}$$

The constitutive moment-curvature relationship for the confining tube is obtained by substituting Eqs. (2), (6) and (12) into (15):

$$M = - \frac{(v'' + w')(\widehat{EI}_s + \widehat{EI}_c)}{R}, \tag{28}$$

where the thermal properties

$$\widehat{EI}_c = \int_{A_c} \widehat{E}_{c,T} y^2 dA_c, \text{ and } \widehat{EI}_s = \int_{A_{s,e}} E_{s,T} y^2 dA_{s,e}, \tag{29}$$

are the second moment of areas for the concrete core and steel area respectively. The integrals (26), (27) and (29) can be numerically solved simply using the Adaptive Quadrature technique.

The problem to be solved is a system of ordinary differential equations defined by equilibrium Eqs. (16) and (17) and constitutive Eqs. (25) and (28) subjected to boundary conditions (19), (20), (23) or (24). To solve this, a set of dependent variables are introduced:

$$x_1 = v, \quad x_2 = v', \quad x_3 = M, \quad x_4 = M', \quad x_5 = N, \quad x_6 = w, \tag{30}$$

and upon differentiation yield,

$$x'_1 = x_2, \tag{31}$$

$$x'_2 = \frac{-x_3 R}{\widehat{EI}_s + \widehat{EI}_c} - x'_6, \tag{32}$$

$$x'_3 = x_4, \tag{33}$$

$$x'_4 = x_5 R(1 + x'_2 + x'_6) + x'_5 R(x_2 + x_6) - qR^2, \tag{34}$$

$$x'_5 = x_5(x_6 + x_2) - \frac{x_3}{R}, \tag{35}$$

$$x'_6 = \frac{\widehat{EA}_s \widehat{\epsilon}_{s,th} + \widehat{EA}_c \widehat{\epsilon}_{c,th} - x_5}{\widehat{EA}_s + \widehat{EA}_c} + x_1 - 0.5(x_2 + x_6)^2. \tag{36}$$

System (31)–(36) contains first-order ordinary differential equations which can be numerically solved given the boundary conditions

$$x_1(\Theta) = x_1(-\Theta) = x_3(\Theta) = x_3(-\Theta) = x_6(\Theta) = x_6(-\Theta) = 0, \tag{37}$$

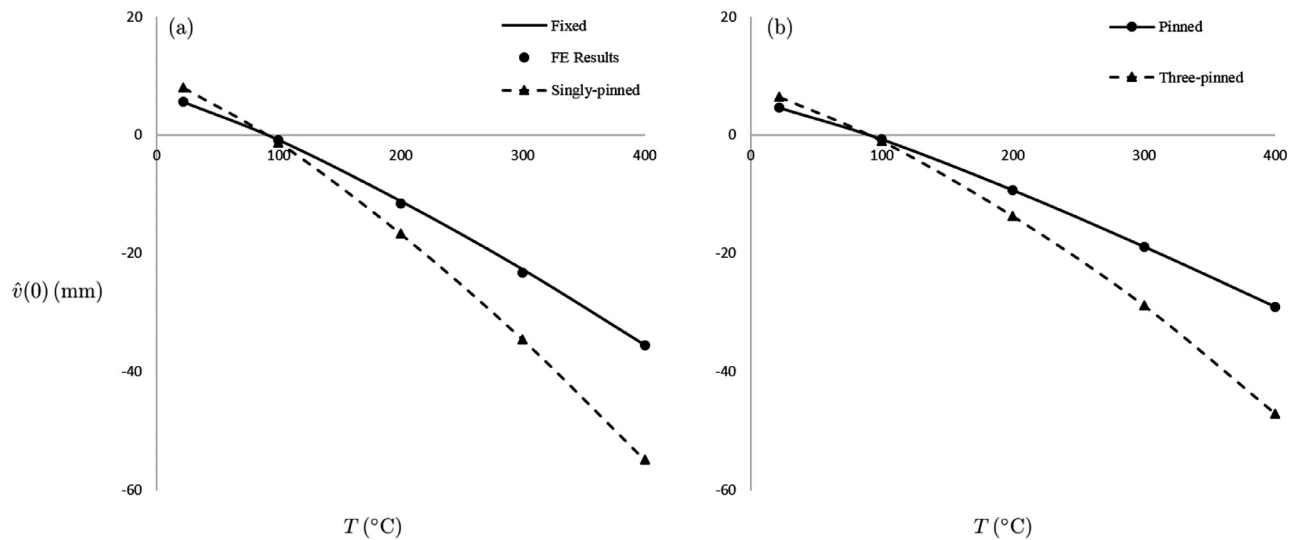


Fig. 2. Effect of temperature on central radial deflection for fixed-ended (a) and pin-ended (b) arches. $2\Theta = 120$, $q = 450$ kN/m, $R = 5000$ mm, $\sigma_y = 350$ MPa, $E_c = 32,800$ MPa, $D = 300$ mm and $t = 10$ mm.

for a pin-ended arch, and

$$x_1(\Theta) = x_1(-\Theta) = x_2(\Theta) = x_2(-\Theta) = x_6(\Theta) = x_6(-\Theta) = 0, \quad (38)$$

for an arch with fixed ends, and

$$x_1(\Theta) = x_3(\Theta) = x_3(0) = x_6(\Theta) = x_6(0) = x_4(0) + x_5(0)x_2(0)R = 0, \quad (39)$$

for three-pinned arch, and

$$x_1(\Theta) = x_2(\Theta) = x_3(0) = x_6(\Theta) = x_6(0) = x_4(0) + x_5(0)x_2(0)R = 0, \quad (40)$$

for a singly-pinned arch.

3.2. Pre-buckling elastic behaviour

System (31)–(36) is first solved for the case of a uniform temperature field in order to demonstrate the thermal response of CFST arches. The arch features a radius $R = 5$ m, steel yield strength $\sigma_y = 350$ MPa, an initial elastic modulus of concrete of $E_c = 32,800$ MPa, a diameter $D = 300$ mm and a steel tube thickness $t_s = 10$ mm. The central deflections, axial forces, bending moments and longitudinal stresses in the concrete core at various temperature levels are shown in Figs. 2–5 respectively for a shallow and deep arches with pin-ended, fixed ended, three-pinned and singly-pinned supports.

CFST arches deflect upwards with a rise in temperature in an approximately linear fashion. Evolution of axial force with temperature was found to be dependant on the arch included angle and boundary conditions. Small changes to axial force was observed for the deep arch, which slightly increased or decreased with temperature, see Fig. 3. For the case of the shallow arch, temperature level noticeably influenced axial force. This effect was substantially greater for arches with fixed ends. Thermal loading causes a reversal and subsequent increase in maximum bending moment. It can be seen that the change in maximum moments is significant for all cases analysed. However, as with axial force, the effect is greatest in shallow fixed arches. The stress levels in the concrete core generally decrease, and remain low, throughout the heating period as shown in Fig. 5. Regions of tensile stress may develop when due to the large increases in bending moment. This is likely in shallow arches with fixed ends, due to the large end moment reactions and great increase of moments with thermal load. Deep and pin-ended arches are typically exempt from this problem due to the smaller magnitude of bending moments.

The pre-buckling response of CFST arches to non-uniform thermal loading is also analysed. Three radially distributed temperature profiles

through the CFST cross section are considered, see Fig. 6. Labels A-D are given to each temperature profile, including no thermal load, for referencing in the proceeding results. The temperatures are highest at the confining steel tube and degrade curvilinearly toward the concrete centre. The effect of the combined non-uniform thermal loads and mechanical loading on the radial deflections and bending moments through the arch length are shown in Figs. 7 for fixed-ended arches. The response for the case of radially distributed temperature through the cross-section qualitatively follows behaviour as when under uniform thermal loading; the arch deflects upwards with temperature rise in the steel tube, bending moment distribution reverses and increases at higher temperature levels and changes to axial force are small in the case of deep arches. However, the stress distribution through the concrete core varies non-linearly with y due to temperature dependant elastic modulus and thermal strain. In cases of great temperature differentials across the cross-section, tensile stress may develop in the inner core due to the assumption of equal membrane strain across the steel and concrete and low thermal strain in the concrete. Hence in these cases, an elastic analysis may not be valid. The problem of rapid heating of the outer tube and possible tensile stress is considered in Section 6.

4. Elastic buckling analysis

4.1. Anti-symmetric buckling analysis

A CFST arch can move from a pre-buckled state of equilibrium to a buckled state when reaching a critical combination of mechanical load level and temperature profile. This adjacent buckled configuration is defined by $\bar{N} = N + N_b$, $\bar{M} = M + M_b$, $\bar{v} = v + v_b$, and $\bar{w} = w + w_b$, where N_b , M_b , v_b and w_b are perturbations. The perturbed quantities are substituted into the equilibrium equations derived for a shallow arch (see Appendices) giving the buckled equilibrium equations when ignoring higher order terms;

$$N'_b = 0, \quad (41)$$

and

$$RNv''_b + RN_b(1 + v'') - M''_b = 0. \quad (42)$$

The buckled variations of the constitutive equations are similarly obtained as:

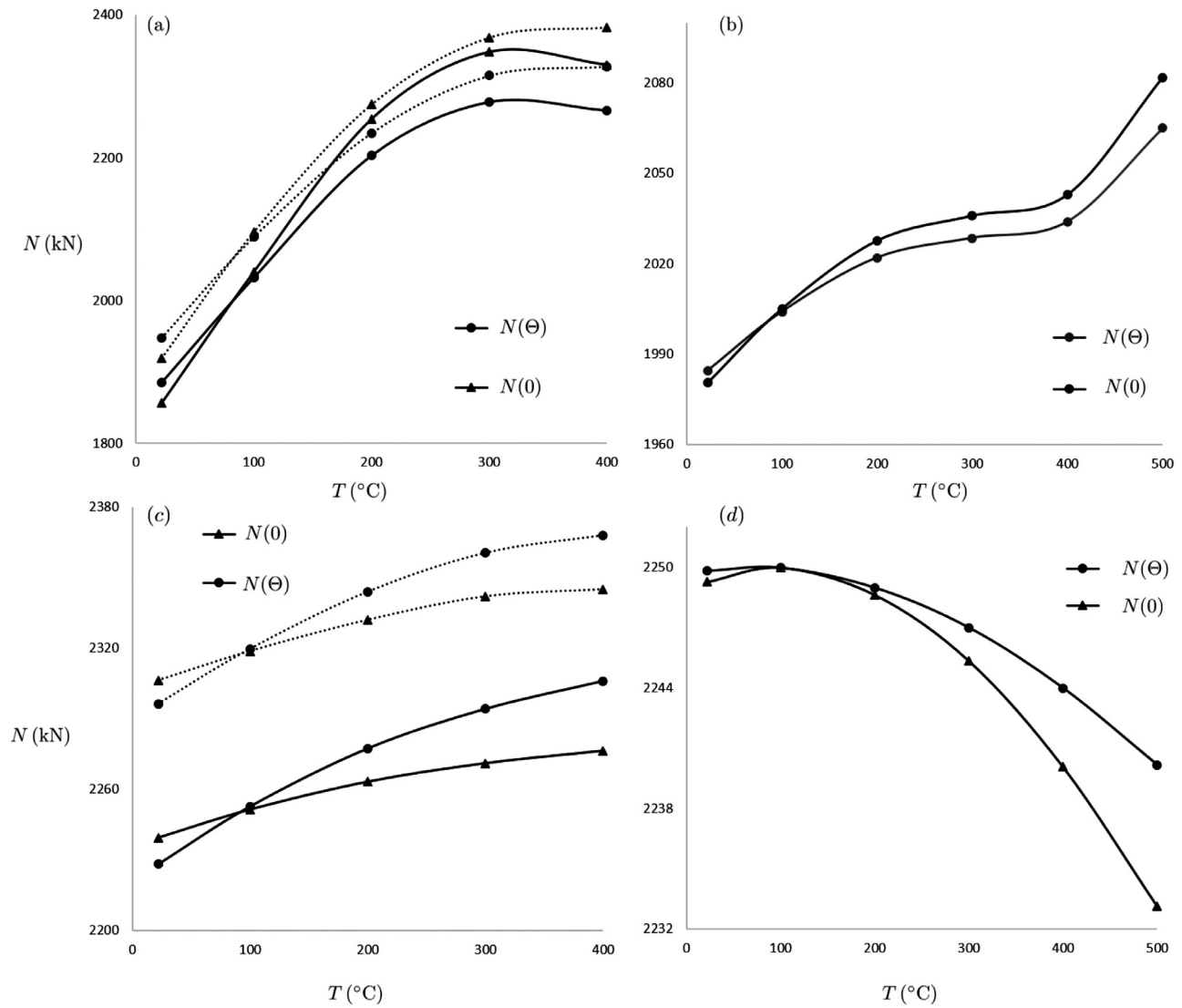


Fig. 3. Effect of temperature on axial force for fixed (a) and pinned (b) arches with $2\Theta = 73.74$ and fixed arches (c) and pinned arches (d) with $2\Theta = 120$. $q = 450$ kN/m, $R = 5000$ mm, $\sigma_y = 350$ MPa, $E_c = 32,800$ MPa, $D = 300$ m and $t_t = 10$ mm. Dashed line depicts FE results.

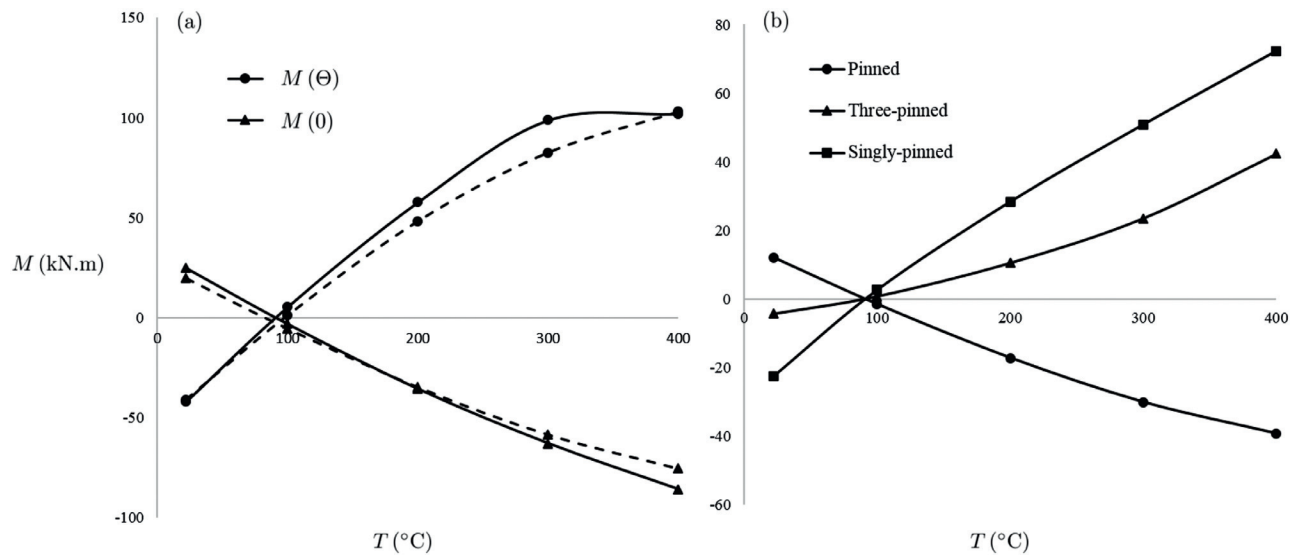


Fig. 4. Effect of temperature on maximum bending moment for fixed arches (a) and pinned and crown-pinned arches (b). $2\Theta = 120$, $q = 450$ kN/m, $R = 5000$ mm, $\sigma_y = 350$ MPa, $E_c = 32,800$ MPa, $D = 300$ m and $t_t = 10$ mm. Dashed line depicts FE results.

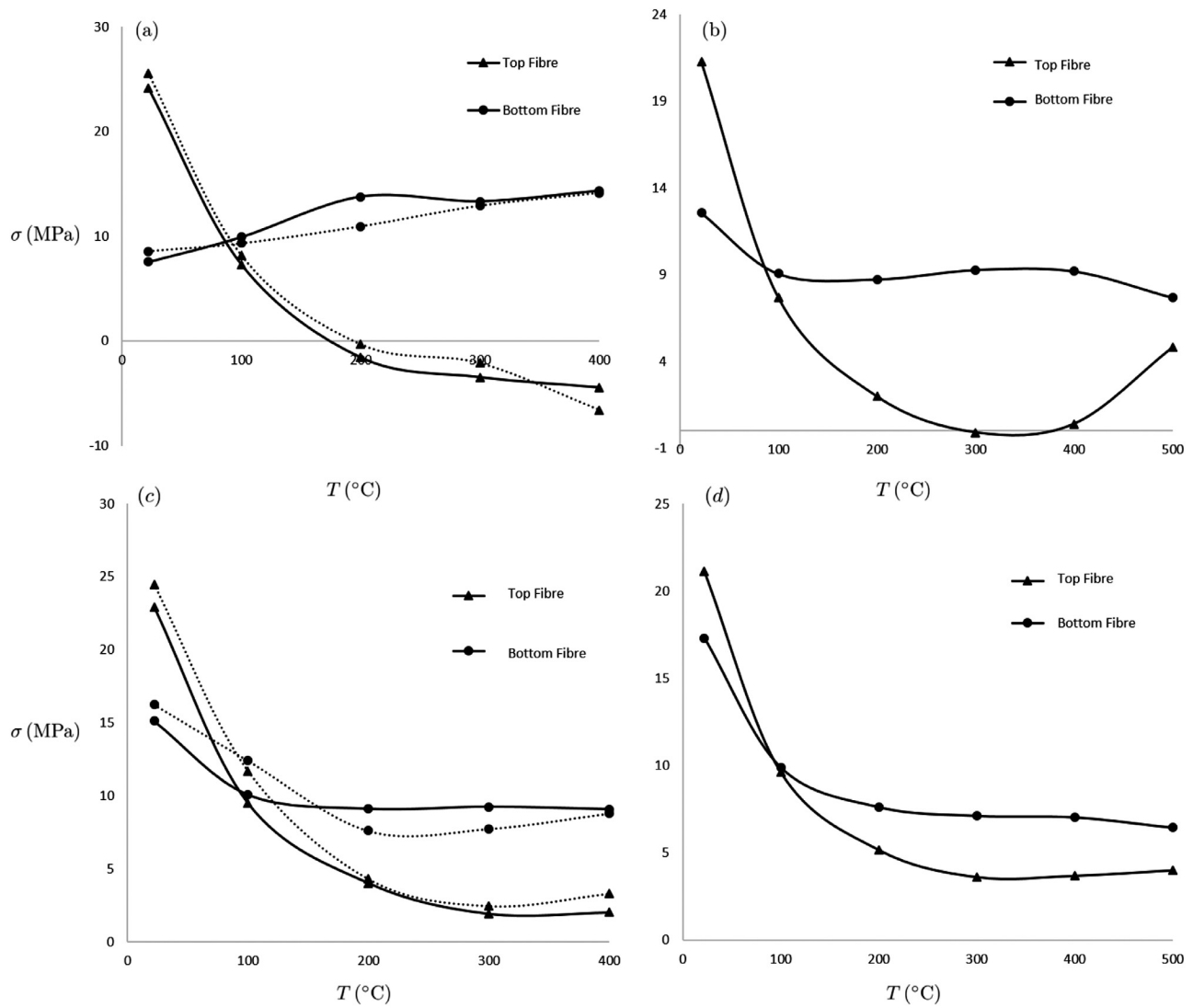


Fig. 5. Effect of temperature on longitudinal stress in extreme fibres of the concrete core at the mid-span for fixed (a) and pinned (b) arches with $2\Theta = 73.74$ and fixed (c) and pinned (d) arches with $2\Theta = 120$. $q = 450 \text{ kN/m}$, $R = 5000 \text{ mm}$, $\sigma_y = 350 \text{ MPa}$, $E_c = 32,800 \text{ MPa}$, $D = 300 \text{ m}$ and $t_f = 10 \text{ mm}$. Dashed line depicts FE results.

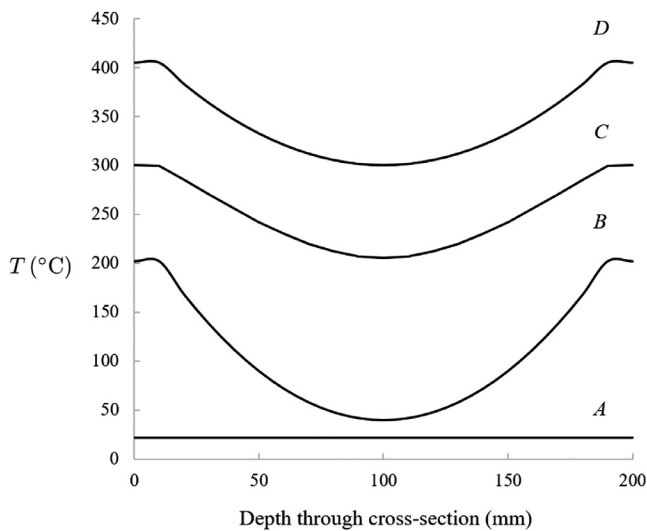


Fig. 6. Temperature profile through CFST cross-section.

$$N_b = -(w'_b - v_b + v'_b v'_b) (\widehat{EA}_s + \widehat{EA}_c), \tag{43}$$

and

$$M_b = -\frac{v''_b (\widehat{EI}_s + \widehat{EI}_c)}{R}. \tag{44}$$

The static buckled boundary conditions are

$$w_b(\Theta) = w_b(-\Theta) = v_b(\Theta) = v_b(-\Theta) = v'_b(\Theta) = v'_b(-\Theta) = 0, \tag{45}$$

for simply-supported arches, and

$$w_b(\Theta) = w_b(-\Theta) = v_b(\Theta) = v_b(-\Theta) = v'_b(\Theta) = v'_b(-\Theta) = 0, \tag{46}$$

for arches with fixed ends. Crown-pinned arches cannot buckle in an anti-symmetric mode [8].

In the case of anti-symmetric buckling, the displacement v_b and its second derivative v''_b are anti-symmetric through the arch length. Additionally, the pre-buckled slope v' is anti-symmetric as the radial deflection v in the pre-buckled state is symmetric. Hence, the terms v_b , v''_b and v' become zero when integrating Eq. (43) with respect to θ , giving

$$N_b = 0. \tag{47}$$

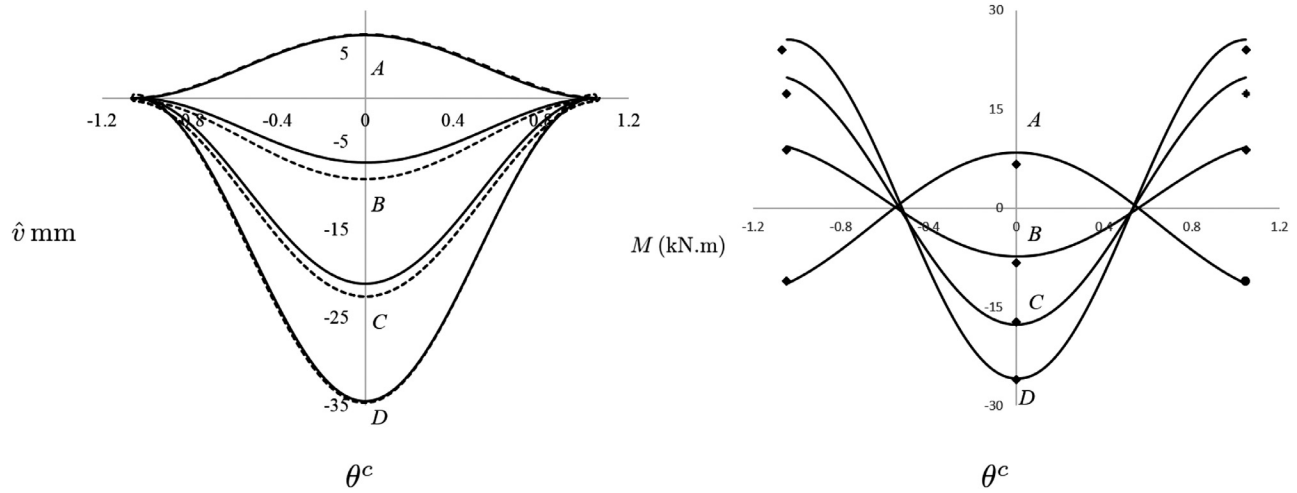


Fig. 7. Effect of non-uniform thermal loads A-D on radial deflections (left) and bending moment (right) for fixed-ended arches. Dashed line and markers depict FE results. $2\Theta = 120^\circ$, $q = 300$ kN/m, $R = 5000$ mm, $\sigma_y = 350$ MPa, $E_c = 32,800$ MPa, $D = 200$ mm and $t_r = 10$.

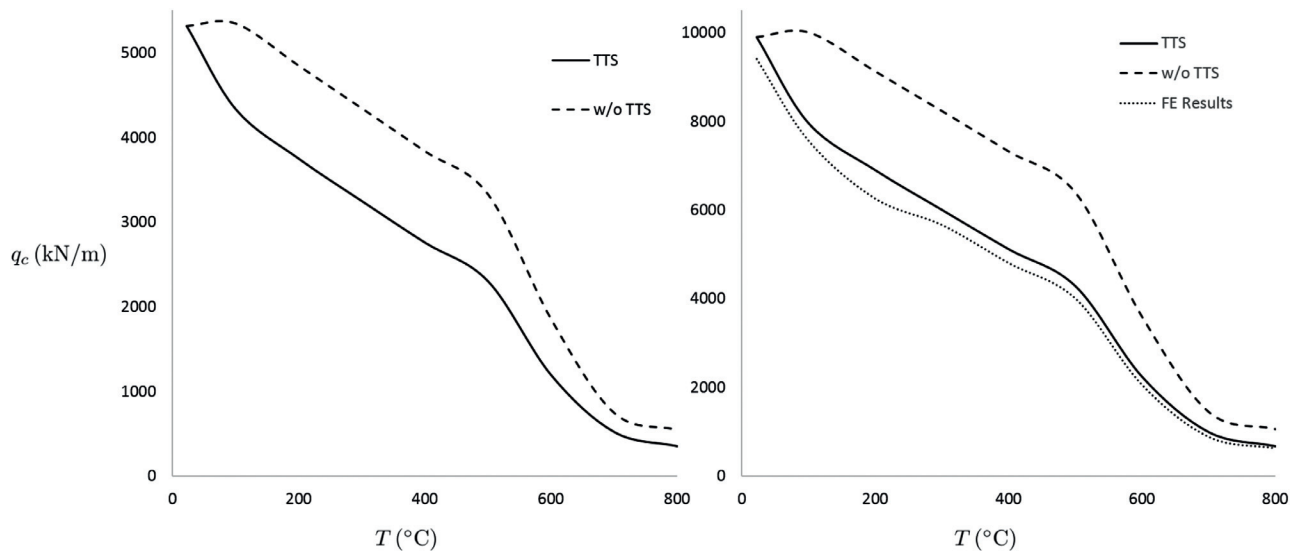


Fig. 8. Elastic anti-symmetric buckling loads for pinned (left) and fixed (right) CFST arches under uniform thermal load. $2\Theta = 73.34^\circ$, $R = 5000$ mm, $\sigma_y = 350$ MPa, $E_c = 32,800$ MPa, $D = 300$ mm and $t_r = 10$ mm.

The linear homogeneous differential equation for anti-symmetric bifurcation is obtained by substituting Eqs. (44) and (47) into (42), as

$$\frac{v_b''''}{\mu^2} + v_b'' = 0. \tag{48}$$

Solving Eq. (48) gives

$$v_b = C_1 \sin(\gamma\mu\theta) + C_2 \cos(\gamma\mu\theta) + C_3\theta + C_4, \tag{49}$$

where coefficients $C_1 \dots C_4$ are unknown. In order for non-trivial coefficients to exist, the coefficient matrix must have a first determinant equalling to zero. This leads to the equations obtained by Pi et al. [45],

$$\begin{aligned} \sin(\gamma\mu\theta) \cos(\gamma\mu\theta) &= 0 && \text{for pinned arches} \\ [\mu\Theta \cos(\mu\Theta) - \sin(\mu\Theta)] \sin(\gamma\mu\theta) &= 0 && \text{for fixed arches.} \end{aligned} \tag{50}$$

The lowest solution of Eq. (50), obtained when the first terms equal zero, are $\mu\theta = \pi$ for simply-supported arches, and $\mu\Theta = 1.4303\pi$ for fixed-ended arches. The critical axial force is obtained by substituting these solutions into Eq. (73),

$$N_p = \frac{\pi^2 (\widehat{EI}_c + \widehat{EI}_s)}{(S/2)^2} \tag{51}$$

for pinned arches, and

$$N_p = \frac{(1.4303\pi)^2 (\widehat{EI}_c + \widehat{EI}_s)}{(S/2)^2} \tag{52}$$

for fixed arches. Substituting (51) and (52) into (77) yields

$$D_1 P_b^2 + D_2 P_b + D_3 = 0 \tag{53}$$

where

$$\begin{aligned} D_1 &= 15 + 2\pi^2, \quad D_2 = 12 + 4\pi^2, \quad \text{and} \\ D_3 &= \frac{12\pi^4}{\lambda^2} - \frac{12\pi^2 (\widehat{EA}_c \epsilon_{c,th} + \widehat{EA}_s \epsilon_{s,th})}{\theta^2 (\widehat{EA}_c + \widehat{EA}_s)}, \end{aligned} \tag{54}$$

for pinned arches, and

$$D_1 = 5, \quad D_2 = 4, \quad \text{and} \quad D_3 = \frac{12(1.4303\pi)^2}{\lambda^2} - \frac{12 (\widehat{EA}_c \epsilon_{c,th} + \widehat{EA}_s \epsilon_{s,th})}{\theta^2 (\widehat{EA}_c + \widehat{EA}_s)}, \tag{55}$$

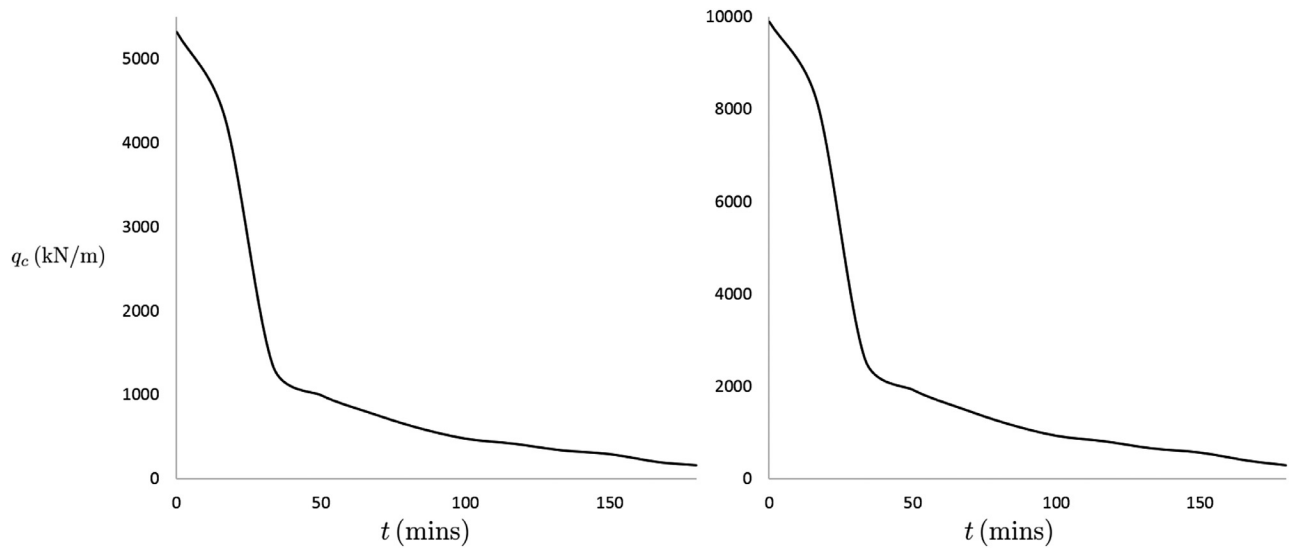


Fig. 9. Elastic anti-symmetric buckling loads for pinned (left) and fixed (right) CFST arches subjected to ISO fire load. $2\Theta = 73.34^\circ$, $R = 5000$ mm, $\sigma_y = 350$ MPa, $E_c = 32,800$ MPa, $D = 300$ mm and $t_t = 10$ mm.

for fixed ended arches. The anti-symmetric buckling load is determined by solving Eq. (53) when adopting the critical axial force defined by Eq. (51) and Eq. (52) for simply-supported and fixed-ended arches respectively. Alternatively, the critical buckling load can be obtained by solving employing System (31)–(36) and increasing the load q until the resulting axial force equals the critical value as given by Eqs.(51) or (52).

If strain Eq. (12) and equilibrium Eqs.(16) and (17) are perturbed instead, the buckling analysis yields a critical axial force for fixed arches as;

$$N_p = \frac{\widehat{EI}_c + \widehat{EI}_s}{S/2^2} [(\eta\pi)^2 - \Theta^2] \tag{56}$$

where η is a function of included angle Θ and varies from 1.4303 at $2\Theta = 0^\circ$ to 1.5 at $2\Theta = 180^\circ$, see [3]. The corresponding buckling load q can be iteratively obtained by solving Eqs. (31)–(36) for given values of q until N_p is obtained. The critical axial force for pinned arches derived in this case remains the same as given in Eq. (51). This buckling analysis adopts the axial in-extensibility condition and assumes a constant axial force N through the arch length. The axial in-extensibility condition is expressed as $w'_b - v_b = 0$. The reader is referred to [3] for further details.

The effect of uniform temperature fields on the anti-symmetric elastic buckling loads is shown in Fig. 8. It can be seen that the buckling strength of CFST arches deteriorate with increasing thermal load. Thus, thermal loading may trigger anti-symmetric bifurcation buckling in CFST arches. Furthermore, the critical buckling loads when neglecting TTS are depicted. The stability boundaries still reduce with an increase in temperature albeit at a lesser rate than the case when TTS is not considered. For slender deep arches, anti-symmetric buckling may occur whilst in the elastic range. Stocky shallow arches are likely to begin yielding prior to elastic buckling due to the development of large bending moments and axial forces with rise in temperature. Fig. 9 depicts the anti-symmetric buckling loads for the same arch when subjected to standard ISO-834 fire loading at various time intervals throughout a three hour heating period. The temperature distribution through the cross-section was obtained by conducting a transient thermal analysis using the Finite Element (FE) method with commercial software package ANSYS [46]. The details of the FE model are given in Section 6. Fire loading initially causes a drastic reduction in the anti-symmetric buckling strength of CFST arches due to the rapid heating of the steel tube. This is followed by a continual deterioration of buckling loads though at a slower rate, caused by delayed heating of the concrete core.

4.2. Symmetric snap-through buckling

Arches also feature the possibility of buckling in a symmetric shape. At the symmetric buckling load combination, the arch snaps away from its previous position on the equilibrium path to an adjacent buckled configuration. As symmetric snap-through buckling is equivalent to limit instability in arches [5], System Eqs. (31)–(36) for given values of q until N_p is obtained. The critical axial force for pinned arches derived in this case remains the same as given in Eq. (51). This buckling analysis adopts the axial in-extensibility condition and assumes a constant axial force N through the arch length. The axial in-extensibility condition is expressed as $w'_b - v_b = 0$. The reader is referred to [3] for further details.

The effect of uniform temperature fields on the anti-symmetric elastic buckling loads is shown in Fig. 8. It can be seen that the buckling strength of CFST arches deteriorate with increasing thermal load. Thus, thermal loading may trigger anti-symmetric bifurcation buckling in CFST arches. Furthermore, the critical buckling loads when neglecting TTS are depicted. The stability boundaries still reduce with an increase in temperature albeit at a lesser rate than the case when TTS is not considered. For slender deep arches, anti-symmetric buckling may occur whilst in the elastic range. Stocky shallow arches are likely to begin yielding prior to elastic buckling due to the development of large bending moments and axial forces with rise in temperature. Fig. 9 depicts the anti-symmetric buckling loads for the same arch when subjected to standard ISO-834 fire loading at various time intervals throughout a three hour heating period. The temperature distribution through the cross-section was obtained by conducting a transient thermal analysis using the Finite Element (FE) method with commercial software package ANSYS [46]. The details of the FE model are given in Section 6. Fire loading initially causes a drastic reduction in the anti-symmetric buckling strength of CFST arches due to the rapid heating of the steel tube. This is followed by a continual deterioration of buckling loads though at a slower rate, caused by delayed heating of the concrete core.

4.2. Symmetric snap-through buckling

Arches also feature the possibility of buckling in a symmetric shape. At the symmetric buckling load combination, the arch snaps away from its previous position on the equilibrium path to an adjacent buckled configuration. As symmetric snap-through buckling is equivalent to limit instability in arches [5], System (31)–(36) can be employed to analyse symmetric stability loss for all support conditions. Critical buck-

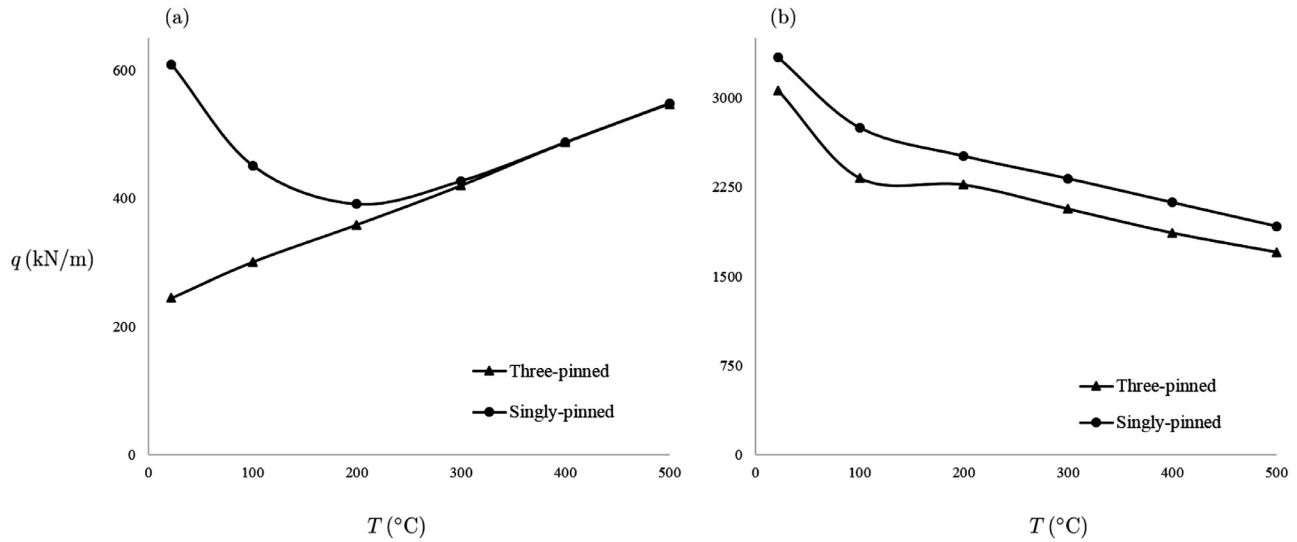


Fig. 10. Elastic symmetric buckling loads for crown-pinned CFST arches subjected to uniform temperature field. $2\theta = 19.06^\circ$ and $R = 18125$ mm (left) and $2\theta = 73.34^\circ$ and $R = 5000$ mm (right). $\sigma_y = 350$ MPa, $E_c = 32,800$ MPa, $D = 300$ mm and $t_r = 10$ mm.

ling loads q and/or temperature profiles $T(y)$ can be increased until a real solution no longer exists for System (31)–(36). A symmetric buckling analysis can also be conducted by following the procedure in Section 4.1 whilst assuming a symmetric buckled displacement v_b . Symmetric buckling is the governing buckling mode for crown-pinned arches and very shallow (approximately $2\theta < 20^\circ$) pinned or fixed arches. Though due to high load magnitudes required to trigger instability, it is likely that only slender arches will buckle symmetrically prior to development of plastic strain.

The effect of thermal loading on the elastic symmetric snap-through loads is dependant on the included angle, see Fig. 10. For arch with very low included angles, thermal loading may increase increased the elastic symmetric buckling loads. This may occur after an initial reduction in instability load as seen in singly-pinned case shown in Fig. 10 (a). Conversely for most other cases, a reduction of symmetric buckling strength with increase with temperature is observed.

5. Non-linear inelastic analysis

The numerical model proposed in Section 3.1 is now generalised to consider inelastic material behaviour in both the steel tube and concrete core. The following model is restricted to uniform temperature loading in order to avoid the derivation of cumbersome equations. Though the same methodology can be applied for the case of non-uniform temperature fields. Combining Eqs. (11), (12), (14) and (15) with inelastic material models (2) for steel and (7) for concrete yields the equations for axial force N and bending moment M . The axial force is obtained as

$$N = \frac{f'_c}{\epsilon_{max}} \left(\frac{(v'')^2 I_c}{R^2 \epsilon_{max}} + \frac{\epsilon_{c,th}^2 A_c}{\epsilon_{max}} + 2A_c \epsilon_{c,th} + \frac{A_c \epsilon_m^2}{\epsilon_{max}} \right) - \epsilon_m \left[Z_1 + \frac{2A_c f'_c}{\epsilon_{max}} \left(1 + \frac{\epsilon_{c,th}}{\epsilon_{max}} \right) \right] + Z_2, \tag{57}$$

where

$$N_p = -c_1 \sigma_y \epsilon_{s,th} + c_2 \sigma_y - c_3 \sigma_y^2 / E_s, \quad Z_1 = E_s A_{s,e} + c_1 \sigma_y A_{s,p} \quad \text{and} \\ Z_2 = E_s A_{s,e} \epsilon_{s,th} - A_{s,p} N_p + \frac{(v'' + w')}{R} (E_s Q_e + c_1 \sigma_y \widehat{Q}_p), \tag{58}$$

and the thermal section properties

$$\widehat{Q}_e = \int_{A_{s,e}} y dA_{s,e}, \quad \text{and} \quad \widehat{Q}_p = \int_{A_{s,p}} y dA_{s,p}, \tag{59}$$

are the first moment of area for elastic steel area $A_{s,e}$ and the plastic steel area $A_{s,p}$ respectively. The bending moment is derived as

$$M = -\frac{(v'' + w')}{R} \left[\frac{2 I_c f'_c}{\epsilon_{max}^2} (\epsilon_{max} - \epsilon_m + \epsilon_{c,th}) + E_s \widehat{I}_s + c_1 \sigma_y \widehat{I}_{s,p} \right] + (E_s \widehat{Q}_e + c_1 \sigma_y \widehat{Q}_p) (\epsilon_m) - E_s \widehat{Q}_e \epsilon_{s,th} + \widehat{Q}_p N_p \tag{60}$$

where the thermal section properties

$$\widehat{I}_s = \int_{A_{s,e}} y^2 dA_{s,e}, \quad \text{and} \quad \widehat{I}_{s,p} = \int_{A_{s,p}} y^2 dA_{s,p}, \tag{61}$$

are the second moment of areas for elastic plastic steel areas.

A system of differential equations is again obtained defined by equilibrium Eqs. (16) and (17) and constitutive Eqs. (57) and (60). Adopting the dependent variables defined in Eq. (30) and converting Eqs. (57) and (60) to first order form, the following system is derived;

$$x'_1 = x_2, \tag{62}$$

$$x'_2 = \frac{R \epsilon_{max}^2 [\epsilon_m (E_s \widehat{Q}_e + c_1 \sigma_y \widehat{Q}_p) + \widehat{Q}_p N_p - E_s \widehat{Q}_e \epsilon_{s,th} - x_3]}{2 I_c f'_c (\epsilon_{max} - \epsilon_m + \epsilon_{c,th}) + \epsilon_{max}^2 (E_s \widehat{I}_s + c_1 \sigma_y \widehat{I}_{s,p})} - x'_6, \tag{63}$$

$$x'_3 = x_4, \tag{64}$$

$$x'_4 = x_5 R (1 + x'_2 + x'_6) + x'_5 R (x_2 + x_6) - qR^2, \tag{65}$$

$$x'_5 = x_5 (x_6 + x_2) - \frac{x_3}{R}, \tag{66}$$

$$x'_6 = \epsilon_{max} + \epsilon_{th,c} + \frac{Z_1 \epsilon_{max}^2}{2 f'_c A_c} + x_1 - 0.5 (x_2 + x_6)^2$$

$$- \sqrt{\frac{\epsilon_{max}^2}{2 f'_c A_c} [2 f'_c A_c + 2 x_5 + Z_1^2 + Z_1 (\epsilon_{c,th} + \epsilon_{max}) - 2 Z_2] + \frac{I_c (v'')^2}{A_c R^2}}. \tag{67}$$

Eqs. (31)–(36) can be numerically solved with prescribed boundary conditions. Note that when solving quadratic Eq. (57) for the membrane strain x_6 , the lower solution was adopted which would otherwise always lead to a membrane strain ϵ_m exceeding the maximum strain ϵ_{max} for any

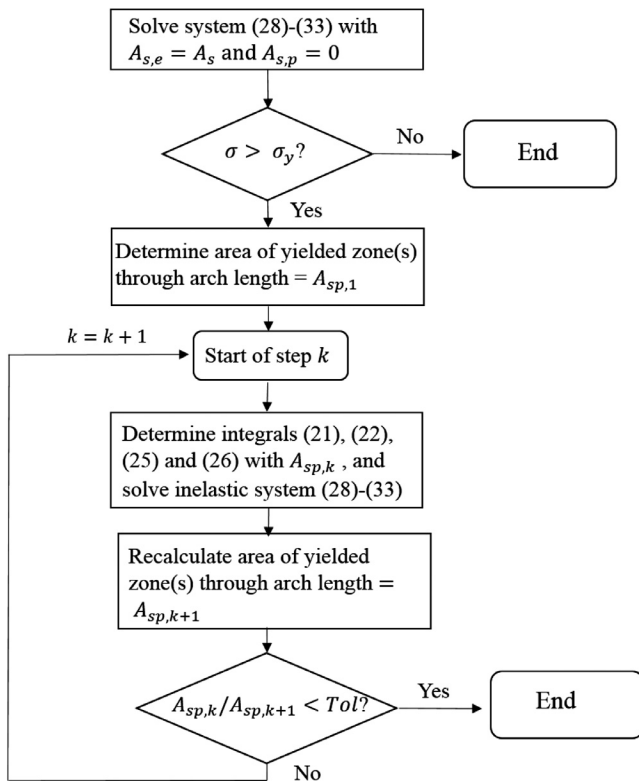


Fig. 11. Flowchart of numerical procedure to solve system (28)–(33).

real solution. Additionally, two higher order terms were neglected in solving for Eq. (67) which are negligible and would otherwise convolute the analysis. The term $I_c(v'')^2/A_cR^2$ in Eq. (67) may also be neglected as its influence on results is minute.

As the plastic area $A_{s,p}$ is initially unknown, the elastic solution is first obtained for a given load and temperature profile, either by solving Eqs. (77) and (75) or system (31)–(36) with $A_{s,p} = \hat{Q}_e = \hat{Q}_p = 0$. The stress in the steel σ_s is obtained from Eq. (2) and is subsequently compared to the yield stress σ_y . If $\sigma_s < \sigma_y$, the steel remains in the elastic range and the solution is complete. However, if $\sigma_s > \sigma_y$, inelastic behaviour occurs and system (31)–(36) must be solved using an approximate plastic area of steel obtained by the yield strength to stress com-

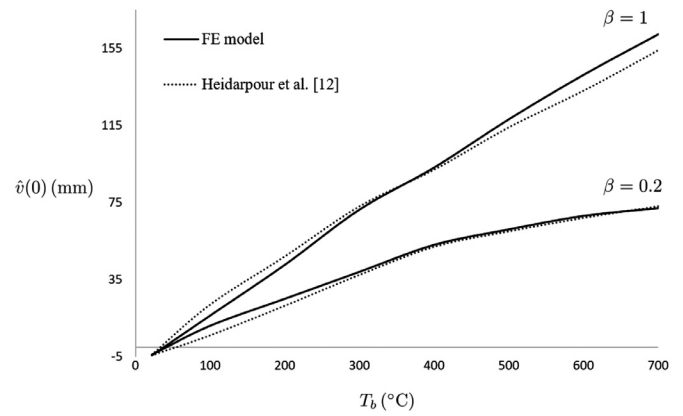


Fig. 13. Central radial deflections of steel I-section arch supported by elastic end restraints and subjected to vertically distributed loading and linear thermal gradients. $E_s = 200$ GPa, $\sigma_y = 300$ MPa, $A_s = 16000$ mm², $I_s = 986 \times 10^6$ mm⁴, $q = 30$ kN/m, $2\Theta = 60^\circ$ and $R = 15000$ mm.

parison. Once system (31)–(36) is solved, the steel strength is compared again to the stress allowing a more accurate estimation of the plastic area. This process is repeated until a desired accuracy (Tol) is achieved. This numerical procedure is graphically depicted in Fig. 11.

As uniform thermal loading causes a reduction in stress in the concrete core, the inelastic response of CFST arches is similar to the elastic behaviour prior to yielding of the steel tube. This can be seen upon comparison of Figs. 2(a), 3(a) and 12. The displacements, axial forces and bending moments are generally greater in the inelastic case due to the non-linear concrete material model. Upon yielding off the steel tube, the responses to elevated temperature fields as discussed in Section 3.2 begin to reverse; CFST arches displace downwards, the axial forces and bending moments reduce in magnitude and the stresses in the concrete increase. It is also noted that the favourable moment distribution associated with pin-ended and crown-pined arches delay initial yielding of the steel tube. Full yielding of the steel tube may induce bifurcation buckling in CFST arches due to the great reduction in buckling strength. This is probable in pinned arches. The higher stiffness associated with fixed arches increases the possibility that a stable configuration will be maintained despite full yielding of the steel, though the compressive stress levels in the core may become extremely large causing complete material failure.

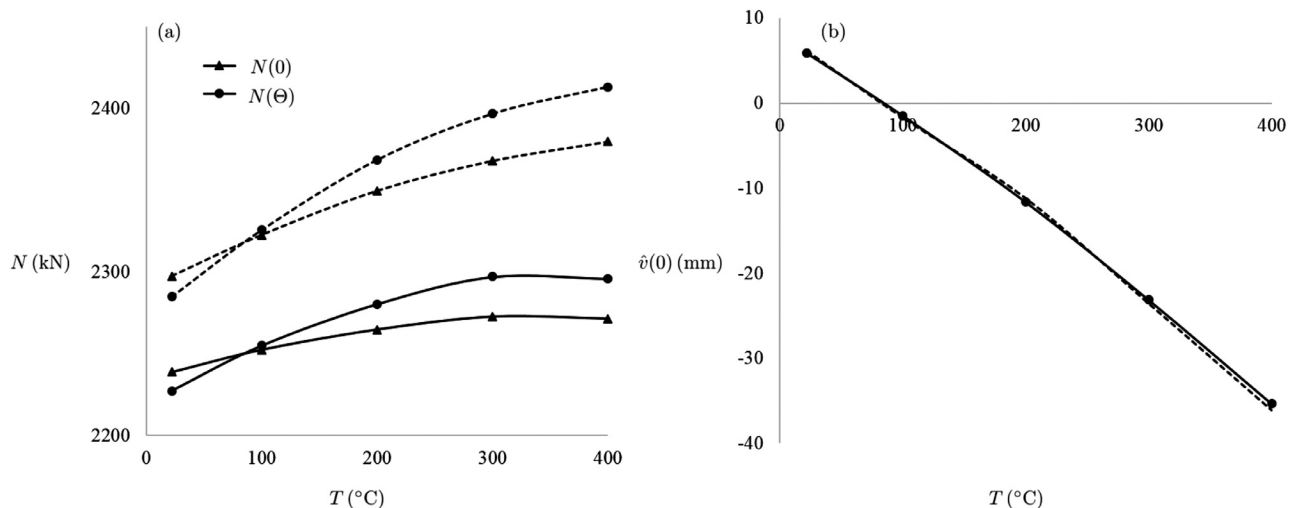


Fig. 12. Effect of uniform temperature field on axial force (a) and central radial deflection (b) for fixed arches (inelastic analysis). $2\Theta = 120$ and $q = 450$ kN/m. Dashed line depicts FE results.

6. Inelastic buckling analysis

6.1. Finite element model

The proposed system (63)–(64) is incapable of modelling anti-symmetric bifurcation buckling. Hence, a FE model is developed, using the commercially available software package ANSYS, in order to examine the inelastic in-plane buckling strength. This section details the development of the FE model.

The mechanical and thermal properties of steel and concrete at elevated temperatures have been adopted from the EC3 for carbon steels and the EC2 for siliceous concrete. These include thermal strain, thermal conductivity, density, stress-strain data and specific heat. All properties were defined at 22°C and from 100°C to 1200°C at intervals of 100°C. ANSYS employs linear interpolation to determine properties at intermediate temperatures. Poisson’s ratio was assumed independent of temperature and was defined as 0.18 for concrete and 0.30 for steel.

The available bi-linear isotropic hardening plasticity model and Von-Mises yield criterion were adopted to input the stress-strain relation of the steel. The yield stress and tangent modulus were input using Eq. (2). For comparison to the elastic analysis, the concrete core was modelled as a linear elastic material with elastic modulus defined by Eq. (6). For the inelastic analysis, the ASCE (7) concrete and EC2 (9) stress-strain relations were adopted and modelled using the Drucker-prager (DP) concrete and multi-linear isotropic hardening (IH) plasticity models. The DP model features two yield surfaces: for compressive loading and for tensile/tensile-compressive stress. A yield stress of $0.4f'_{c,T}$ was selected for compression with the elastic modulus input as the tangent at the yield stress in the DP model. Behaviour in tension was modelled as elastic perfectly plastic with the yield stress defined by Eq. (10). The MISO model makes no distinction between compressive or tensile stress states. Differences between the inelastic buckling loads predicted when adopting the two concrete material models and two plasticity models is analysed in Section 6.3.

A transient thermal analysis is required to obtain the time-varying temperature distribution through the CFST cross-section when subjected to heating. Solid70 elements were employed to mesh the CFST arch for the transient thermal analysis. Solid70 elements feature 8 nodes per element, with each node possessing a single degree of freedom; temperature. An element size of 50 mm was adopted. The outer face of the steel tube was subjected to radiation, with the surface emissivity of

steel taken as 0.7, and convection, with the convection coefficient taken as 25 W/m² K. The time-temperature relationship for standard ISO-834 fires is

$$T_g = T_0 + 345 \log(8t + 1), \tag{68}$$

and where t is time in seconds and T_0 denotes initial temperature taken as 22°C. An analysis period of 3 hours was adopted. For the case of uniform thermal loading, a transient thermal analysis is not required and the thermal load can be input in the non-linear structural analysis stage.

Solid186 elements were adopted to mesh the CFST arch which are a higher-order 3D element compatible with geometrical non-linearity, stress stiffening and plasticity. An element size of 50 mm was adopted. This element size was found to provide an efficient balance between computation time and accuracy. Smaller mesh sizes were not found to noticeably influence results. Geometric non-linearity is incorporated by activating the large deflection option. The arch ends were fully fixed from displacement and rotation in all three directions. A fully bonded contact model between the steel tube and concrete core was employed to comply with the assumption made in the derivations of the proposed numerical model. The influence of contact model on behaviour and in-plane strength is studied in Section 6.3. Loading was applied in two steps, ensuring the arches were mechanically pre-loaded prior to heating. Geometric imperfections are required to trigger anti-symmetric bifurcation buckling upon reaching a critical state. An imperfection size of arch length $S/1000$ is adopted herein. The formation of a new geometry with an anti-symmetric geometric imperfection is conducted using the UPGEOM command following an eigenvalue buckling analysis.

The radial deflections, axial forces, bending moments and stresses in the concrete core as predicted by system (31)–(36) and ANSYS are compared in Figs. 2, 3, 4, 5, 7 and 12 for the case of fixed end supports. It can be seen that the two models agree well. Comparisons between the anti-symmetric buckling modes are also made. The anti-symmetric elastic loads determined by both methods are depicted in Fig. 8. As with the pre-buckling behaviour, a high level of agreement exists between both models. The elastic buckling loads determined by both models vary between 5–10%. The FE results are slightly lower due to the initial anti-symmetric imperfection included in the FE model required to trigger bifurcation buckling under combined thermal and mechanical loading. The initial imperfections cause a deviation away from the theoretical buckling load. Moreover, the assumption of two-dimensional modelling adopted in the analytically derived models is validated as

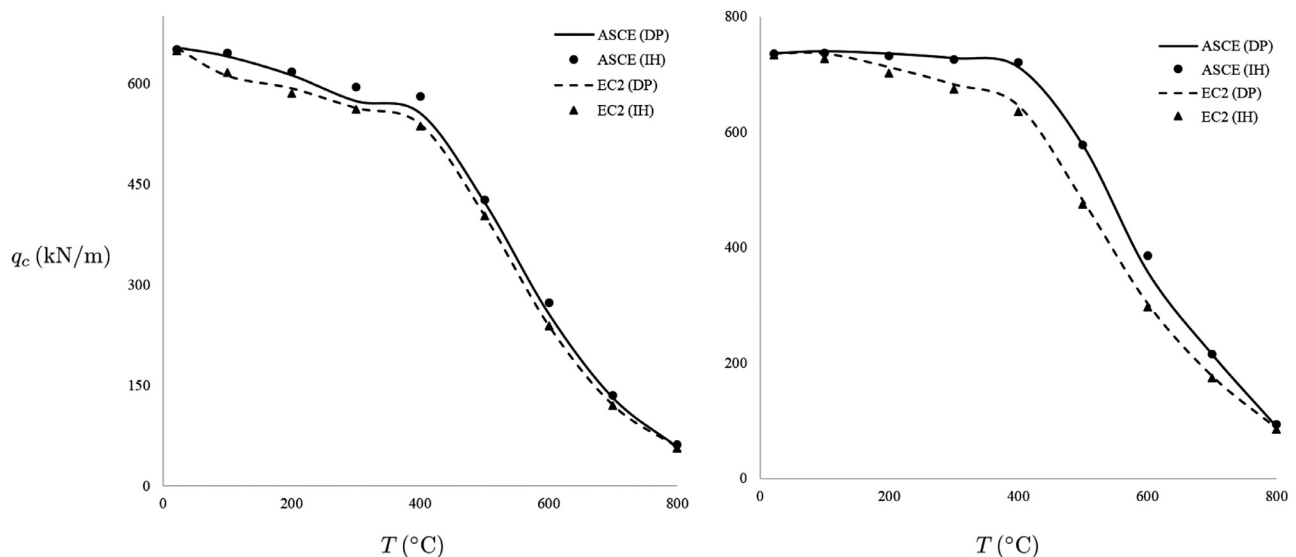


Fig. 14. Inelastic buckling strength of fixed CFST arches subjected to uniform temperature field. $E_c = 200$ GPa, $\sigma_y = 350$ MPa, $f'_c = 32$ MPa, $D = 300$ mm and $t_t = 10$ mm. Arch A (left) features $2\theta = 120^\circ$ and $R = 4450$ mm, and Arch B (right) features $2\theta = 73.74^\circ$ and $R = 5000$ mm.

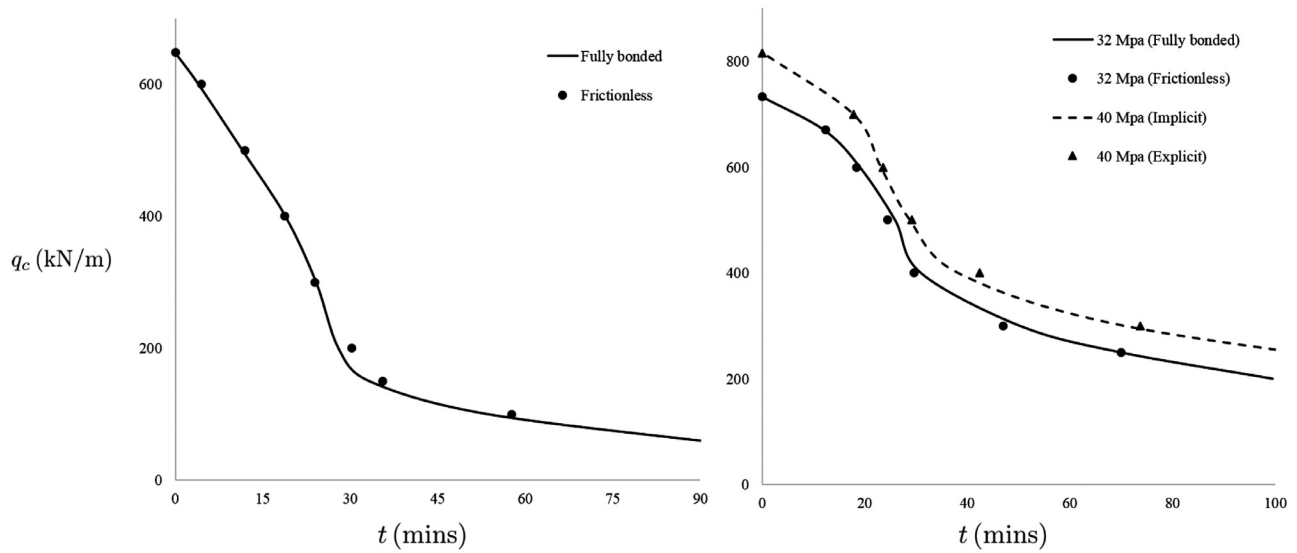


Fig. 15. Inelastic buckling strength of fixed CFST arches subjected to ISO fire loading. $E_s = 200$ GPa, $\sigma_y = 350$ MPa, $f'_c = 32$ MPa, $D = 300$ mm and $t_f = 10$ mm. Arch A (left) features $2\Theta = 120^\circ$ and $R = 4450$ mm, and Arch B (right) features $2\Theta = 73.74^\circ$ and $R = 5000$ mm.

the FE model considers thermal expansions and mechanical strains of the cross-section. The FE model is further validated by comparison the non-discretisation mechanical-based formulation proposed by Heidar-pour et al. [12] for the non-linear inelastic analysis of steel I-section arches under linear thermal gradients. The circular steel arches were supported by elastic end restraints and subjected to vertically distributed loading. The central radial deflections as determined by both models are depicted in Fig. 13 for two levels of thermal gradient. The temperature at the bottom of the cross-section is denoted by T_b and the ratio of the bottom temperature to top temperature is expressed as β . A small difference is observed in the results predicted by both models.

6.2. Inelastic in-plane buckling strength

The FE model was employed to investigate the in-plane buckling strength of CFST arches subjected to uniform temperature fields and ISO-834 fire loading. Two geometrical configurations were analysed herein labelled as Arches A and B. Uniform thermal loading reduces

the buckling strength of CFST arches, see Fig. 14. The deterioration of buckling load is gradual up until 400°C , after which a rapid decline in strength occurs. The considerable drop in strength above this temperature level is due to the reduction of steel yield strength and concrete compressive strength (in the case of the ASCE model). This result is common across both shallow and deep arches. In the case of fire loading, a great reduction of buckling load is observed during initial heating, which followed by a slower rate of deterioration. The buckling strength versus time for both Arches when subjected to fire loading are depicted in Fig. 15.

6.3. Sensitivity analysis

The sensitivity of results when adopting different material and plasticity models for the concrete core have been assessed, see Fig. 14. The critical buckling loads for arches under uniform thermal loading were determined when using the DP and IH plasticity models, and the ASCE and EC2 material models. It can be seen that the plasticity model makes

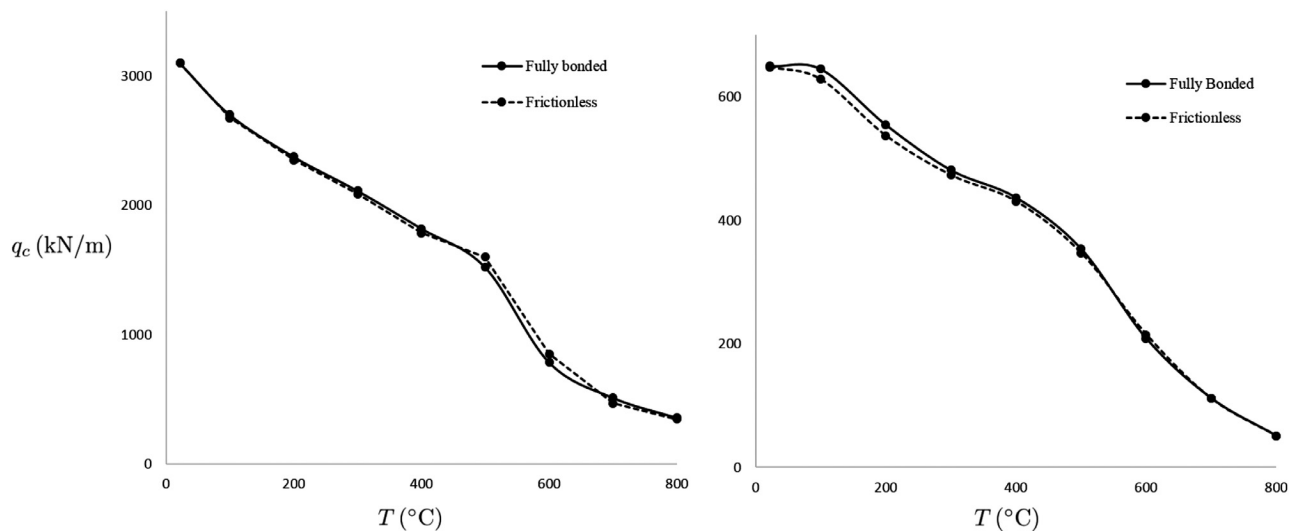


Fig. 16. Elastic (left) and inelastic (right) buckling strength of fixed CFST arches subjected to uniform thermal loading with fully bonded and frictionless contact models. $E_s = 200$ GPa, $\sigma_y = 350$ MPa, $f'_c = 32$ MPa, $D = 300$ mm, $t_f = 10$ mm, $2\Theta = 120^\circ$ and $R = 4450$ mm.

little difference to the predicted buckling loads. Upon comparison of the results for the two material models, it is observed that the ASCE model predicts a higher buckling load than the EC2 model across all temperature levels. This is to be expected as the ASCE model considers the effects of confinement and does not feature a degradation of concrete compressive strength below 400°C. This effect is greater in Arch B due to its larger cross-sectional size and stockiness.

By defining the elastic modulus as the tangent to the stress-strain curves at $\sigma = 0.4f'_{c,T}$, TTS is captured in the elastic modulus and is thus modelled implicitly. Consequently, development of TTS is independent of the order of heating and mechanical loading, and is reversible. The former is overcome by mechanically loading prior to heating. The significance of the latter is now analysed by comparing the results to the case when TTS is modelled as a plastic strain and hence irrecoverable. TTS was defined as a plastic strain using Eq. (5). Fig. 15 depicts the in-plane strength of Arch B with $f'_c = 40\text{MPa}$ when modelling the TTS as elastic (labelled as implicit) and plastic (labelled as explicit). It can be seen that modelling the TTS as an elastic or plastic strain caused little influence on results.

In order to validate the assumption of a perfect bond used in the preceding analyses, the influence of steel-concrete contact model on buckling loads has been analysed. The buckling strength when assuming a fully bonded or frictionless contact model is shown in Figs. 15 and 16 for the cases of fire loading and uniform thermal loading respectively. The results show that the contact model between the steel and concrete does not noticeably influence the in-plane elastic or inelastic buckling strength of CFST arches.

7. Conclusions

The non-linear behaviour and in-plane buckling modes of CFST arches under thermal and mechanical loading are investigated in this paper through analytical and numerical means. An energy method is invoked to derive the non-linear equations of equilibrium which, together with elastic or inelastic material models, results in a system of first-order differential equations which can be numerically solved using the boundary conditions of fixed arches, pinned arches or crown-pinned arches. Obtaining this solution is an iterative process due to the presence of elastic and plastic properties in the system, which are first estimated and subsequently refined by comparing the stress in the steel tube to the yield strength. Results show that upon initial heating, a CFST arch deflects upwards causing great increases to bending moment and, if shallow, axial force. Closed-form solutions are obtained for the elastic bifurcation buckling loads. The inelastic in-plane buckling strength is investigated by the development of a FE model. A reduction in elastic and inelastic anti-symmetric and symmetric buckling strength with thermal load is observed. Consequently, thermal loading may induce stability loss in CFST arches. The results of the derived models are compared to those predicted by the FE model developed and good agreement exists. Furthermore, a sensitivity analysis was conducted with the FE model which showed that the contact model for the steel-concrete interface, and concrete material and plasticity models did not noticeably influence in-plane buckling strength. The present analysis was limited to uniformly distributed radial loading, in-plane buckling behaviour and did not consider thermal separation of the tube and core, and interaction of local and global buckling behaviour. Varied mechanical loading conditions such as vertical distributed loading and concentrated loads require research attention. As CFST arches typically feature large free-standing portions, the influence of thermal loading on the out-of-plane stability is important. When heated, the steel tube may separate from the concrete core and buckle locally. Local buckling of the steel tube may reduce the global in-plane buckling strength of CFST arches. Additionally, an air-gap may be formed upon this separation influencing the transfer of heat from the tube to the core. These areas will form the subjects of future research works.

Acknowledgements

Victoria University is acknowledged for the financial support provided to the first author through the Vice Chancellor's Graduate Research Scholarship award.

Appendix

Closed-form solution for pre-buckling analysis of shallow arches

In the case of shallow arches, the effect of the membrane strain on the radial deformation may be neglected. Hence, strain Eqs. (12) can be reduced to;

$$\epsilon_m = w' - v + \frac{1}{2}(v')^2, \quad \epsilon_b = -\frac{y v''}{R}. \quad (69)$$

Applying the principle of virtual work whilst adopting strain Eq. (69), gives the simplified yet accurate non-linear equilibrium equations;

$$N' = 0, \quad (70)$$

$$-M'' + NR(1 + v'') - qR^2 = 0. \quad (71)$$

Substitution of the constitutive relation (28) into radial equilibrium Eq. (71) yields the following differential equilibrium equation

$$\frac{v''''}{\mu^2} + v'' = P, \quad (72)$$

where μ is termed the axial force parameter defined as

$$\mu^2 = \frac{NR^2}{\widehat{EI}_c + \widehat{EI}_s}, \quad (73)$$

and the dimensionless load parameter P is expressed as

$$P = \frac{qR - N}{N}. \quad (74)$$

The dimensionless radial displacement is obtained by solving Eq. (72) using the boundary conditions (18) and (19) or (20), as

$$v = \frac{P}{\mu^2} \left[\frac{\Phi[\cos(\mu\theta) - \cos(\mu\Theta)]}{\cos(\mu\Theta)} + \frac{1}{2}(\mu^2\theta^2 - \mu^2\Theta^2) \right]. \quad (75)$$

The parameter Φ is defined as

$$\begin{aligned} \Phi &= 1 && \text{for pin-ended arches,} \\ \Phi &= \mu\Theta / \tan(\mu\Theta) && \text{for fixed arches.} \end{aligned} \quad (76)$$

An equation relating μ and P is obtained by substituting Eqs. (69) and (75) into (25), which yields

$$B_1 P^2 + B_2 P + B_3 = 0, \quad (77)$$

with

$$B_1 = \frac{\Phi^2}{4\mu^2\Theta^2} \left[1 - \frac{\tan(\mu\Theta)}{\mu\Theta} + \tan^2(\mu\Theta) \right] + \frac{\Phi}{\mu^2\Theta^2} \left[1 - \frac{\tan(\mu\Theta)}{\mu\Theta} \right] + \frac{1}{6}, \quad (78)$$

$$B_2 = \frac{\Phi}{\mu^2\Theta^2} \left[1 - \frac{\tan(\mu\Theta)}{\mu\Theta} \right] + \frac{1}{3}, \quad (79)$$

$$B_3 = \frac{\mu^2\Theta^2}{\lambda^2} - \frac{\widehat{EA}_c \epsilon_{c,th} + \widehat{EA}_s \epsilon_{s,th}}{\theta^2 (\widehat{EA}_c + \widehat{EA}_s)}. \quad (80)$$

In Eq. (80), the geometric parameter λ is defined as

$$\lambda = R\Theta^2 / r_x = S\Theta / 2r_x. \quad (81)$$

The axial force N can be found by solving quadratic Eq. (77) for a given temperature distribution $T(y)$ and mechanical load q . The radial deflection v and bending moment M are subsequently obtained by solving Eqs. (75) and (15) respectively.

References

- [1] Bradford MA. In-plane nonlinear behaviour of circular pinned arches with elastic restraints under thermal loading. *Int J Struct Stab. & Dyn.* 2006;6(2):163–77.
- [2] Pi YL, Bradford MA. Thermoelastic behaviour of elastically restrained tubular steel arches. Taylor & Francis; 2008. p. 659–67. ISBN 978-0-415-46853-4.
- [3] Pi Y-L, Bradford MA. In-plane thermoelastic behaviour and buckling of pin-ended and fixed circular arches. *Eng Struct* 2010;32(1):250–60.
- [4] Bradford MA. Long-span shallow steel arches subjected to fire loading. *Adv Struct Eng* 2010;13(3):501–11.
- [5] Pi Y-L, Bradford MA. Nonlinear in-plane elastic buckling of shallow circular arches under uniform radial and thermal loading. *Int J Mech Sci* 2010;52(1):75–88.
- [6] Cai J, Xu Y, Feng J, Zhang J. Effects of temperature variations on the in-plane stability of steel arch bridges. *J Bridge Eng* 2010;17(2):232–40.
- [7] Moghaddasie B, Stanciulescu I. Equilibria and stability boundaries of shallow arches under static loading in a thermal environment. *Int J Non-Linear Mech* 2013;51:132–44.
- [8] Pi Y-L, Bradford MA. Effects of nonlinearity and temperature field on in-plane behaviour and buckling of crown-pinned steel arches. *Eng Struct* 2014;74:1–12.
- [9] Pi Y-L, Bradford MA. Nonlinear thermoelastic buckling of pin-ended shallow arches under temperature gradient. *J Eng Mech* 2010;136(8):960–8.
- [10] Cai J, Xu Y, Feng J, Zhang J. In-plane elastic buckling of shallow parabolic arches under an external load and temperature changes. *J Struct Eng* 2012;138(11):1300–9.
- [11] Heidarpour A, Abdullah AA, Bradford MA. Non-linear thermoelastic analysis of steel arch members subjected to fire. *Fire Safety J* 2010;45(3):183–92.
- [12] Heidarpour A, Abdullah AA, Bradford MA. Non-linear inelastic analysis of steel arches at elevated temperatures. *J Construct Steel Res* 2010;66(4):512–19.
- [13] Heidarpour A, Bradford MA, Othman KA. Thermoelastic flexural-torsional buckling of steel arches. *J Constr Steel Res* 2011;67(12):1806–20.
- [14] Asgari H, Bateni M, Kiani Y, Eslami M. Non-linear thermo-elastic and buckling analysis of fgm shallow arches. *Compos Struct* 2014;109:75–85.
- [15] Asgari H, Eslami M. Nonlinear thermal buckling analysis of fgm shallow arches under linear temperature gradient. In: ASME 2014 12th Biennial Conference on Engineering Systems Design and Analysis. American Society of Mechanical Engineers; 2014. V001T04A003–V001T04A003.
- [16] Bateni M, Eslami M. Effect of temperature gradient on the mechanical buckling resistance of fgm shallow arches. In: ASME 2014 12th Biennial Conference on Engineering Systems Design and Analysis. American Society of Mechanical Engineers; 2014. V001T01A006–V001T01A006.
- [17] Song X, Li SR. Nonlinear stability of fixed-fixed fgm arches subjected to mechanical and thermal loads. In: *Advanced Materials Research*, 33. Trans Tech Publ; 2008. p. 699–706.
- [18] Babaei H, Kiani Y, Eslami M. Geometrically nonlinear analysis of shear deformable fgm shallow pinned arches on nonlinear elastic foundation under mechanical and thermal loads. *Acta Mechanica* 2018:1–19.
- [19] Babaei H, Kiani Y, Eslami M. Thermomechanical nonlinear in-plane analysis of fix-ended fgm shallow arches on nonlinear elastic foundation using two-step perturbation technique. *Int J Mech Mater Design* 2019:1–20.
- [20] Li Z, Zheng J, Sun Q, He H. Nonlinear structural stability performance of pressurized thin-walled fgm arches under temperature variation field. *Int J Non-Linear Mech* 2019;113:86–102.
- [21] Li Z, Tang F, Chen Y, Zheng J. Material distribution optimization of functionally graded arch subjected to external pressure under temperature rise field. *Thin-Walled Struct* 2019;138:64–78.
- [22] Li Z, Zheng J, Chen Y. Nonlinear buckling of thin-walled fgm arch encased in rigid confinement subjected to external pressure. *Eng Struct* 2019;186:86–95.
- [23] Yang Z, Huang Y, Liu A, Fu J, Wu D. Nonlinear in-plane buckling of fixed shallow functionally graded graphene reinforced composite arches subjected to mechanical and thermal loading. *Appl Math Model* 2019;70:315–27.
- [24] Hong S, Varma AH. Analytical modeling of the standard fire behavior of loaded cft columns. *J Construct Steel Res* 2009;65(1):54–69.
- [25] Lie T. Fire resistance of circular steel columns filled with bar-reinforced concrete. *J Struct Eng* 1994;120(5):1489–509.
- [26] Lie T, Irwin R. Fire resistance of rectangular steel columns filled with bar-reinforced concrete. *J Struct Eng* 1995;121(5):797–805.
- [27] Espinos A, Romero ML, Hospitaler A. Advanced model for predicting the fire response of concrete filled tubular columns. *J Construct Steel Res* 2010;66(8):1030–46.
- [28] Huang S-S, Burgess I, Huang Z, Plank R. The buckling of slender concrete and concrete-filled columns in fire'. *Fib Workshop: Fire Design of Concrete Structures—from Materials Modelling to Structural Performance*, Coimbra, Portugal; 2007.
- [29] Yin J, Zha X-x, Li L-y. Fire resistance of axially loaded concrete filled steel tube columns. *J Constr Steel Res* 2006;62(7):723–9.
- [30] Yu M, Zha X, Ye J, Wang B. A unified method for calculating fire resistance of solid and hollow concrete-filled steel tube columns based on average temperature. *Eng Struct* 2014;71:12–22.
- [31] Moliner V, Espinos A, Romero M, Hospitaler A. Fire behavior of eccentrically loaded slender high strength concrete-filled tubular columns. *J Constr Steel Res* 2013;83:137–46.
- [32] Romero ML, Moliner V, Espinos A, Ibaez C, Hospitaler A. Fire behavior of axially loaded slender high strength concrete-filled tubular columns. *J Constr Steel Res* 2011;67(12):1953–65.
- [33] Pires TA, Rodrigues JPC, Silva JJR. Fire resistance of concrete filled circular hollow columns with restrained thermal elongation. *J Constr Steel Res* 2012;77:82–94.
- [34] Bouras Y, Vrcelj Z. Non-linear in-plane buckling of shallow concrete arches subjected to combined mechanical and thermal loading. *Eng Struct* 2017;152:413–23.
- [35] Heidarpour A, Pham TH, Bradford MA. Nonlinear thermoelastic analysis of composite steel concrete arches including partial interaction and elevated temperature loading. *Eng Struct* 2010;32(10):3248–57.
- [36] Luo K, Pi Y, Gao W, Bradford MA. Long-term analysis of crown-pinned concrete-filled steel tubular arches. In: *ICCM: Proceedings of the 5th International Conference on Computational Methods*, Cambridge, England, 28–30 July 2014; 2015.
- [37] Wang YF, Ma YS, Han B, Deng SY. Temperature effect on creep behavior of cfst arch bridges. *J Bridge Eng* 2013;18(12):1397–405.
- [38] Bažant ZP, Høgaard AB, Baweja S, Ulm F-J. Microprestressing-solidification theory for concrete creep. i: Aging and drying effects. *J Eng Mech* 1997;123(11):1188–94.
- [39] Bouras Y, Torres-Don E, Vrcelj Z. Thermal in-plane buckling of shallow concrete-filled steel tubular arches. *16th International Symposium on Tubular Structures*; 2017.
- [40] Lie T.T. *Structural fire protection*. American Society of Civil Engineers (ASCE); 1992.
- [41] EN 1993 1–2. Eurocode 3: Design of steel structures, Part 1–2, Structural fire design. European Committee for Standardization; 2005.
- [42] Gernay T, Franssen J-M. A comparison between explicit and implicit modelling of transient creep strain in concrete uniaxial constitutive relationships. In: *Proceedings of the fire and materials 2011 conference*. Interscience Communications Ltd; 2011. p. 405–16.
- [43] EN 1992 1–2. Eurocode 2: Design of concrete structures, Part 1–2, Structural fire design. European Committee for Standardization; 2004.
- [44] Pi Y-L, Trahair N. Non-linear buckling and postbuckling of elastic arches. *Eng Struct* 1998;20(7):571–9.
- [45] Pi Y-L, Bradford MA, Uy B. In-plane stability of arches. *Int J Solids Struct.* 2002;39(1):105–25.
- [46] ANSYS Workbench. Release 17.2. Ansys Inc, Canonsburg, PA; 2016.

6.5 Concluding Remarks

This chapter presented a comprehensive study into the in-plane response and buckling strength of CFST arches subjected to mechanical loading and elevated temperature fields. Analytical models for the elastic prebuckling and in-plane elastic anti-symmetric buckling loads were derived. Additionally, numerical models were formulated for elastic and inelastic prebuckling analyses. The in-plane inelastic buckling strength was subsequently investigated using FE analysis. The findings made in this chapter can be summarised as follows;

1. Elevated temperature fields significantly increase axial force in shallow fixed CFST arches and less so in deep or pinned arches;
2. Great increases to the magnitude of bending moments are observed with temperature rise in both shallow and deep arches;
3. Thermal and fire loading may induce in-plane stability loss in CFST arches due to simultaneous degrading material properties and increasing longitudinal stresses;
4. Elastic anti-symmetric buckling strength generally deteriorates with temperature level. The effect of temperature on buckling loads is significantly increased when considering TTS;
5. Symmetric snap-through buckling loads did not always degrade with increasing thermal load as shallow crown-pinned arches displayed an increase in elastic buckling strength;
6. Material failure is the governing in-plane failure mode in shallow fixed CFST when subjected to combined mechanical and thermal or fire loading. Limit instability only occurs in very shallow arches;

7. The effect of temperature on the in-plane inelastic buckling strength slightly increases with arch included angle and slenderness; and
8. The assumed contact model at the steel-concrete interface had a negligible effect on behaviour and buckling loads.

Chapter 7

Thermal out-of-plane stability of concrete filled steel tubular arches

7.1 Introduction

In this chapter, the elastic and inelastic out-of-plane buckling strength of CFST arches subjected to combined mechanical and thermal loading is numerically investigated. A flexural-torsional buckling analysis is conducted using energy methods resulting in a numerical model which is applicable to arches subjected to uniformly distributed or central concentrated loads, and for arches featuring pinned or fixed end supports. The critical loads are dependant on the pre-buckled state which must first be solved.

The BVP formulated in Chapter 6 is utilised for the required prebuckling analysis and generalised to consider central concentrated loads and basic creep strain: modelled using the fractional derivative-based creep law developed in Chapter 3. The inelastic out-of-plane buckling strength of CFST arches at elevated temperatures is then studied using FE analysis. The elastic flexural-torsional buckling loads determined by the derived numerical model, in addition to the results predicted by the prebuckling analysis, are employed to validate the developed FE model. Subsequently, parametric studies and sensitivity analyses are presented.

The following paper is included in this chapter;

1. Y. Bouras, and Z. Vrcelj. 2020. Out-of-plane stability of concrete-filled steel tubular arches at elevated temperatures. Submitted to *International Journal of Mechanical Sciences*, Under Review.



THE NEW WAY TO DO UNI

OFFICE FOR RESEARCH TRAINING, QUALITY AND INTEGRITY

DECLARATION OF CO-AUTHORSHIP AND CO-CONTRIBUTION: PAPERS INCORPORATED IN THESIS

This declaration is to be completed for each conjointly authored publication and placed at the beginning of the thesis chapter in which the publication appears.

1. PUBLICATION DETAILS (to be completed by the candidate)

Title of Paper/Journal/Book:	Out-of-plane stability of concrete-filled steel tubular arches at elevated temperatures		
Surname:	Bouras	First name:	Yanni
Institute:	Institute for Sustainable Industries and Liveat	Candidate's Contribution (%):	95
Status:			
Accepted and in press:	<input type="checkbox"/>	Date:	<input type="text"/>
Published:	<input type="checkbox"/>	Date:	<input type="text"/>

2. CANDIDATE DECLARATION

I declare that the publication above meets the requirements to be included in the thesis as outlined in the HDR Policy and related Procedures – policy.vu.edu.au.

Yanni Bouras	Digitally signed by Yanni Bouras Date: 2020.02.10 15:29:21 +11'00'	10/02/2020
Signature		Date

3. CO-AUTHOR(S) DECLARATION

In the case of the above publication, the following authors contributed to the work as follows:

The undersigned certify that:

1. They meet criteria for authorship in that they have participated in the conception, execution or interpretation of at least that part of the publication in their field of expertise;
2. They take public responsibility for their part of the publication, except for the responsible author who accepts overall responsibility for the publication;

PO Box 14428, Melbourne,
Vic 8001, Australia
+61 3 9919 6100

Victoria University ABN 83776954731
CRICOS Provider No. 00124K (Melbourne),
02475D (Sydney), RTO 3113



**VICTORIA
UNIVERSITY**

THE NEW WAY TO DO UNI

3. There are no other authors of the publication according to these criteria;
4. Potential conflicts of interest have been disclosed to a) granting bodies, b) the editor or publisher of journals or other publications, and c) the head of the responsible academic unit; and
5. The original data will be held for at least five years from the date indicated below and is stored at the following location(s):

Victoria University, Footscray Park, Ballarat Road, Melbourne, VIC 3011, Australia

Name(s) of Co-Author(s)	Contribution (%)	Nature of Contribution	Signature	Date
Yanni Bouras	95	Conceived concept. Literature review. Analytical/numerical modelling. Writing manuscript	[REDACTED SIGNATURE]	11/02/2020
Zora Vrcelj	5	Critical review of manuscript. Final approval of manuscript.		11/02/2020

Updated: September 2019

PO Box 14428, Melbourne,
Vic 8001, Australia
+61 3 9919 6100

Victoria University ABN 83776954731
CRICOS Provider No. 00124K (Melbourne),
02475D (Sydney), RTO 3113

Out-of-plane stability of concrete-filled steel tubular arches at elevated temperatures

Yanni Bouras, Zora Vrcelj¹

College of Engineering and Science, Victoria University, Melbourne, VIC, Australia

Abstract

This paper investigates the flexural-torsional buckling behaviour of concrete-filled steel tubular circular arches under mechanical and thermal loading. A thermo-elastic pre-buckling analysis is first conducted by employing the principle of virtual work to derive the non-linear equations of equilibrium. The governing geometrical, equilibrium and constitutive material relations are numerically solved as a system of first-order differential equations with boundary conditions of pinned or fixed ends. The prebuckling analysis is then generalised to consider basic creep strain which is found to have a negligible impact on the prebuckling response under short-term heating. Subsequently, an elastic out-of-plane buckling analysis is performed using energy methods and the influence of thermal loading on buckling loads is examined. The results show that stability boundaries decrease with an increase in thermal loading, and that the rate of reduction is independent of the type of end-supports. Additionally, a Finite Element (FE) model is developed to analyse the inelastic lateral buckling strength of CFST arches under both uniform thermal and fire loading. The FE analysis is validated by comparison to the numerical method derived herein for the elastic buckling analysis.

Keywords: Buckling, CFST, Creep, Finite Element, Fractional derivatives, Lateral stability, Thermal loading

1. Introduction

The use of concrete-filled steel tubular (CFST) members in conventional structures provides many benefits relating to both mechanical behaviour and constructibility. Advantages of the former include increased compressive strength, reduced shrinkage in the concrete core, concrete confinement and improved local buckling strength of the steel tube. Consequently, CFST sections have recently surged in popularity for use in arch bridges, with over 400 constructed worldwide [1]. As arches experience primarily compression, they are prone to stability loss. In-plane buckling of arches may be in an anti-symmetric or symmetric form. Additionally, an arch may suddenly displace laterally and twist out of plane when subject to in-plane bending and/or compression in a flexural-torsional type buckling mode [2]. The problem of stability is paramount in CFST arches as the increased compressive strength gained with CFST sections may result in the use of slender structures. Geometrical non-linearities in shallow arches [3, 4] convolute the stability analysis and reduce load carrying capacity.

Classic studies investigating elastic flexural-torsional buckling of arches include the work of Timoshenko and Gere [5], who developed closed form solutions for simply supported arches of rectangular cross-section under uniform

compression and bending, and Vlasov [6] who extended Timoshenko and Gere's study to mono-symmetric cross sections. Since these works, many researchers have investigated elastic flexural-torsional buckling of arches [7, 8, 9, 10, 11, 12, 13]. As with in-plane stability analysis, out-of-plane buckling problems have been investigated using two methods which include the static equilibrium and energy methods, adopted in [5, 6] and [5, 7, 8, 9, 10, 11, 12, 13] respectively. Critical reviews of these early studies were conducted by Papangelis and Trahair [9] and Kang and Yoo [12]. In these studies, classical buckling method was used to obtain the critical load, thus the effects of in-plane pre-buckling deformations were ignored. In-plane pre-buckling deformations alter the curvature of an arch, which significantly influences the out-of-plane buckling resistance [14].

The effect of pre-buckling deformations on the elastic lateral-torsional buckling of simply supported arches subjected to uniform bending was studied in [8, 7, 14]. In these works, the in-plane pre-buckling deformations were found to increase the moments causing lateral instability. Furthermore, Pi et al [14] discovered that incorporating pre-buckling deformations in stability analyses allows torsional buckling to occur, in the case when lateral displacements are fully restrained. As the lateral buckling behaviour of fixed arches differs from that of simply-supported arches, the pre-buckling effects on buckling of fixed arches cannot be assumed the same as for pinned arches [15]. Under uniform positive bending, the pre-buckling deformations reduce the moments causing lateral instability in fixed arches, contrasting the increase observed in pinned arches [15]. These effects are magnified with an increasing included angle and out-of plane slenderness ratio. The influence of pre-buckling deformations on the flexural-torsional buckling behaviour of arches under uniformly distributed radial loads has been researched [16, 17, 18]. Pi and Bradford [16] generated a three-dimensional curved beam finite element (FE) model for the numerical determination of flexural-torsional buckling loads and post-buckling analysis of circular thin-walled simply-supported shallow arches. Analytical solutions for arches subjected to the same conditions were produced by Pi et al. [19]. In these studies, it was found that the flexural-torsional buckling loads may be underestimated if in-plane pre-buckling behaviour is ignored [16, 19]. Generalisations to in-plane fixed supports and variable load height was made by Bradford and Pi [18]. The use of in-plane fixed connections greatly increased the lateral buckling load of the arch. Arches under a central concentrated load experience combined axial compression and bending moment, which are dependent on arch slenderness and included angle and vary throughout the length of the arch [20]. The buckling analysis of such arches is complicated and highly dependent on pre-buckling stresses. Pi et al [20] developed the first analytical solutions to the elastic lateral-torsional buckling problem of a circular arch subjected to a central concentrated load by using the principle of virtual work and the Rayleigh-Ritz method. The in-plane fixed and out-of-plane pinned cases were analysed, in addition to investigating the effects of load position. As with the uniformly distributed case, both in-plane boundary conditions and load application position greatly influenced critical loads. Building on this study, Pi and Bradford [21] investigated the generalised case of rotational end restraints, where the sensitive relationship between buckling load and rotational restraint stiffness was analytically derived. The results for both studies [20, 21] were verified by FE analysis and a curved beam element code developed by the authors in [22].

The failure modes of arches consist of buckling of slender arches, and the plastic collapse of stocky arches. Gen-

erally, failure will involve an interaction between stability loss and material yielding, which is dependent on the arch's loading and geometrical configuration, residual stresses and geometric imperfections [23]. Pi and Trahair [24] investigated the out-of-plane inelastic buckling strength of circular I-section steel arches in uniform compression and bending through the development of a non-linear three dimensional FE model. In-plane curvature, included angle, initial geometric imperfections, large deformations residual stresses and material inelasticity were all incorporated into the model. The effects of in-plane curvature and included angle were found to substantially influence the buckling and strength of the arches. An increase in arch angle and curvature results in a decreased flexural-torsional buckling strength. This model was extended to account for general loading scenarios including concentrated loads and uniformly distributed transverse loads by the authors in [25]. It was found that the buckling moments under central concentrated loads were generally less than for arches under a quarter point concentrated load. Similarly, buckling loads of arches subjected to uniformly distributed loading over their entire length were less than when loaded with a uniformly distributed load over half the arch. Pi and Bradford [26] conducted a study for fixed I-section arches subject to uniform compression, uniform bending and combined compression and bending. Design equations for pin-ended arches were deemed insufficient for use on fixed arches and novel design equations were proposed for fixed arches. The out-of-plane strength of high strength steel arches was analysed in [27] where design recommendation were proposed for the cases of uniform compression, uniform bending and combined compression and bending. The inelastic flexural-torsional buckling and strength of circular steel arches with central elastic-torsional restrains was studied in [28]. Central torsional restraint were found to increase the strength of steel arches. However, this improvement in strength reduces with decreasing arch slenderness. The stiffness of the central rotational restraint was determined to reach a threshold value at which further increases in stiffness did not strengthen the arch. Slenderness and included angle were found to be the key factors influencing the threshold stiffness. Furthermore, the threshold stiffness is less for arches that fail inelastically, then that for arches buckling elastically. Pi and Bradford [29] proposed a three-dimensional curved beam element model for the non-linear elastic-plastic flexural-torsional buckling and post-buckling analysis of circular steel arches under a central concentrated which accounts for large twist rotations. The included angle, arch slenderness, torsional parameter and material yielding were found to greatly influence buckling behaviour. Stocky arches featuring low included angles fail in an elastic-plastic mode. For the case when stocky arches feature large included angles, the elastic-plastic and elastic buckling loads for pin-ended arches are identical, whilst for fixed arches, the elastic-plastic critical load is smaller than the elastic buckling load. The elastic-plastic and elastic buckling loads for slender arches are equal as the arch loses stability prematurely. Wu et al. [30] investigated the elastic and elastic-plastic buckling of fixed parabolic CFST arches and developed a novel method for predicting the in-plane strength, and Pi et al. [31] proposed design equations considering non-linear bending actions.

Upon reaching a critical temperature, an arch may buckle laterally in a flexural-torsional mode due to the increased axial compression and bending moments induced by restrained thermal expansion and rotations. Heidarpour et al [32] investigated the thermo-elastic flexural-torsional buckling of steel I-section arches at elevated temperatures. Adopting the non-discretisation mechanical based method developed in [33] for the non-linear pre-buckling analysis, the critical

temperatures causing lateral instability were determined using classical buckling theory. A parametric study was then performed to investigate the effect of multiple parameters on critical buckling temperatures which included the included angle, slenderness ratio and imposed load for pinned, fixed and spring supported arches. Similarly to in-plane stability, an increase in included angle and stockiness of the member resulted in a higher magnitude of buckling temperature. In addition, the influence of the ratio of the temperature in the top fibre of the cross section to the temperature in the bottom fibre on the critical temperatures was analysed and deemed significant. Conversely, the size of external load was found to have a smaller impact on critical temperatures. However, thermal induced lateral instability in arches requires a greater research focus as studies on the subject are limited. Thermoelastic buckling of steel beams [34, 35, 36] and in-plane thermoelastic stability of steel arches [37, 38, 39, 32, 40, 41] have received more research attention. Temperature fields may trigger lateral-torsional buckling or in-plane flexural buckling in slender steel beams, and in-plane anti-symmetric bifurcation buckling or symmetric snap-through buckling in steel arches. Similar to temperature effects, studies on the out-of-plane stability loss caused by viscoelasticity in arches are also rare. Jiang and Lu [42] studied the reliability and sensitivity of the out-of-plane buckling loads of CFST arches while considering creep effects using a time-integrated approach and the finite element reliability method. Geng et al. [43] investigated the out-of-plane creep buckling behaviour of CFST arches caused by instantaneous overload. The significance of prebuckling time effects on the ultimate capacity of fixed-ended parabolic arches under uniformly distributed radial loading were analysed using FE analysis, and it was found that time effects may reduce buckling loads up to 18%.

Elevated temperature fields have been shown to significantly impact the in-plane elastic and inelastic buckling strength of CFST arches [44]. In addition to the effect caused by the increase in axial forces and bending moments, critical buckling loads in CFST arches further deteriorate due to the great reductions in concrete stiffness which is magnified when considering transient thermal strain (TTS). TTS is a thermo-mechanical strain only occurring in pre-loaded concrete upon virgin heating and is independent of time [45]. Despite this, studies investigating the thermal out-of-plane stability of CFST arches do not appear in the open literature. This is an important problem as exposure to extreme temperatures may induce flexural-torsional buckling in CFST arches if sufficient lateral restraints are not provided. Due to the lack of research on this subject, this paper investigates the effects of thermal and fire loading on the out-of-plane stability of CFST arches under uniformly distributed radial loading. A non-linear elastic prebuckling analysis is first presented for shallow CFST arches subjected to uniformly distributed radial loads and uniform thermal loading with pin or fixed end supports. Subsequently, an elastic out-of-plane buckling analysis is conducted which considers non-linear prebuckling deformations. These following assumptions are made for the elastic prebuckling and flexural-torsional buckling analyses:

- The Euler-Bernoulli hypothesis is valid, that is plain sections remain plane post deformation;
- The temperature field is constant through the length of the arch and cross-section;
- Cross-sectional thermal expansions are negligible;

- Fully bonded contact exists at the steel-concrete, and thus the longitudinal strains of both materials are equal along this face;
- The prebuckled arch does not deform laterally or twist;
- The mechanical load, elevated temperature level and in-plane prebuckling stresses and deformations are all constant during flexural-torsional buckling; and
- The direction of the radial load q remains acting at the centroidal axis of the arch and does not change during bifurcation.

The inelastic out-of-plane buckling strength is then analysed with FE analysis. Results predicted by the FE model and the derived numerical models are compared. Agreeable results would confirm validity of assumptions regarding Euler-Bernoulli theory and cross-sectional thermal expansions. Additionally, a sensitivity analysis is conducted to assess the influence of the contact model at the steel-concrete interface, and concrete material models on the out-of-plane buckling strength.

2. Material models

2.1. Steel

The total longitudinal strain ϵ in the confining steel tube is expressed as;

$$\epsilon = \epsilon_{ch} + \epsilon_{s,th}, \quad (1)$$

where ϵ_{ch} is the total instantaneous mechanical strain, consisting of the sum of the elastic and plastic strains, and $\epsilon_{s,th}$ is the thermal expansive strain. The temperature dependent stress-strain equation developed in [46] is employed, defined as

$$\sigma_s = \begin{cases} E_{s,T} \epsilon_{ch} & \text{for } \epsilon_{ch} \leq \epsilon_p \\ (c_1 \epsilon_{ch} + c_2) \sigma_{y,T} - c_3 \sigma_{y,T}^2 / E_{s,T} & \text{for } \epsilon_{ch} > \epsilon_p, \end{cases} \quad (2)$$

where the yield strain is

$$\epsilon_p = \frac{c_2 \sigma_{y,T} - c_3 \sigma_{y,T}^2 / E_{s,T}}{E_{s,T} - c_1 \sigma_{y,T}}, \quad (3)$$

with coefficients $c_1 = 12.5$, $c_2 = 0.975$ and $c_3 = 12.5$. The elastic modulus $E_{s,T}$, yield strength $\sigma_{y,T}$ and thermal strain $\epsilon_{s,th}$ are adopted from the Eurocode 3 (EC3) [47].

2.2. Concrete

The following linear elastic concrete model is utilised for the elastic analyses, defined as;

$$\epsilon = \frac{\sigma_c}{E_{c,T}} + \epsilon_{tr} + \epsilon_{c,th}. \quad (4)$$

The explicit Eurocode 2 (EC2) model [48] is adopted for the TTS, known as:

$$\epsilon_{tr} = \frac{\sigma_c}{f'_c} \phi(T) = \frac{2\sigma_c}{3f'_c} \left(\frac{\epsilon_{max} - \epsilon_{min}}{f'_{c,T}/f'_c} \right), \quad (5)$$

where $E_{c,T}$ is the temperature sensitive elastic modulus, $\epsilon_{c,th}$ is the thermal expansive strain in the concrete, f'_c is the compressive strength of concrete at ambient temperature, $f'_{c,T}$ is the compressive strength at an elevated temperature, ϵ_{max} is the peak stress strain (PSS) considering TTS and ϵ_{min} is the minimum PSS when ignoring TTS. These variables are available in the EC2 [49] (siliceous concrete). Substituting Eq. (5) into (4) gives;

$$\epsilon = \frac{\sigma_c}{\hat{E}_{c,T}} + \epsilon_{c,th} = \sigma_c \left(\frac{1}{E_{c,T}} + \frac{\phi(T)}{f'_c} \right) + \epsilon_{c,th}. \quad (6)$$

When considering basic creep strain, Eq.(4) is generalised as;

$$\epsilon = \frac{\sigma_c}{E_{c,T}} + \epsilon_{tr} + \epsilon_{c,th} + \epsilon_{cr}. \quad (7)$$

The linear component of the fractional viscoelastic rheological law formulated in [50] is adopted to model the high temperature creep in concrete. Basic creep strain is expressed as variable-order fractional derivative equation;

$$D_t^{\alpha(T)} \epsilon_{cr} = \frac{\sigma}{\eta(T)}. \quad (8)$$

$D_t^{\alpha(T)}$ is the operator of the variable-order fractional derivative of order $\alpha(T)$ with respect to time t with $0 < \alpha < 1$ and $t > 0$. The temperature dependent dynamic viscosity is denoted as $\eta(T)$. These parameters are available in [50]. The Caputo definition of the fractional derivative of a function $f(t)$ is adopted, defined as;

$$D_t^{\alpha(t)} f(t) = \frac{1}{\Gamma[1 - \alpha(t)]} \int_0^t \frac{D^1 f(\tau)}{(t - \tau)^{\alpha(t)}} d\tau, \quad (9)$$

with the Gamma function known as;

$$\Gamma(\alpha) = \int_0^{\infty} e^{-t} t^{\alpha-1} dt. \quad (10)$$

The ASCE [51, 46] constitutive law is one of two inelastic concrete models considered. The ASCE model incorporates confinement and implicitly considers TTS. It is defined as;

$$\sigma = f'_c \left[1 - \left(\frac{\epsilon - \epsilon_{max}}{\epsilon_{max}} \right)^2 \right], \quad (11)$$

where ϵ_{max} is the PSS. In the ASCE model, the relationship between compressive strength and temperature is;

$$f'_{c,T} = \begin{cases} f'_c & \text{for } 22^\circ\text{C} \leq T \leq 450^\circ\text{C}, \\ f'_c [2.011 - 2.353(T - 20) \times 10^{-3}] & \text{for } 450^\circ\text{C} \leq T \leq 874^\circ\text{C}, \\ 0 & \text{for } 874^\circ\text{C} < T. \end{cases} \quad (12)$$

The EC2 model is the second inelastic concrete model considered in this study;

$$\frac{\sigma}{f'_{c,T}} = \frac{3\epsilon}{\epsilon_{max}[2 + (\epsilon/\epsilon_{max})^3]}. \quad (13)$$

The reduction factors for the compressive strength are available in the EC2 [49]. The EC2 model for tensile strength at elevated temperatures is defined as:

$$f_{ck,t}(T) = \begin{cases} f_{ck,t} & \text{for } 20^\circ\text{C} \leq T \leq 100^\circ\text{C}, \\ f_{ck,t}[1.0 - (T - 100)/500] & \text{for } 100^\circ\text{C} \leq T \leq 600^\circ\text{C}, \end{cases} \quad (14)$$

where $f_{ck,t}$ is the concrete tensile strength under ambient conditions.

3. Non-linear elastic pre-buckling analysis

3.1. Uniformly distributed radial load

Consider a circular shallow CFST arch with pinned or fixed ends and subjected to a uniformly distributed radial load q and constant elevated temperature level T . The origin o is stationed at the arch's geometrical center with the axis os aligning with centroidal axis of the arch and the axis oy changing direction along the arch length being always directed to the center of the arch. The geometrical and loading configuration is depicted in Figure 1. The non-linear longitudinal normal strain equation accurate for shallow arches is adopted [3, 4];

$$\epsilon = \epsilon_m + \epsilon_b \quad (15)$$

where ϵ is the total strain in the CFST cross section at an arbitrary point \mathcal{P} , and

$$\epsilon_m = w' - v + \frac{1}{2}v'^2, \quad \epsilon_b = -\frac{yv''}{R}, \quad (16)$$

where ϵ_m and ϵ_b are the membrane and bending strains respectively, \hat{w} is the axial displacement, \hat{v} is the radial displacement, $w = \hat{w}/R$, $v = \hat{v}/R$, y is the vertical coordinate of \mathcal{P} , $(\)' = d(\)/d\theta$, $(\)'' = d^2(\)/d\theta^2$ and θ denotes the angular coordinate.

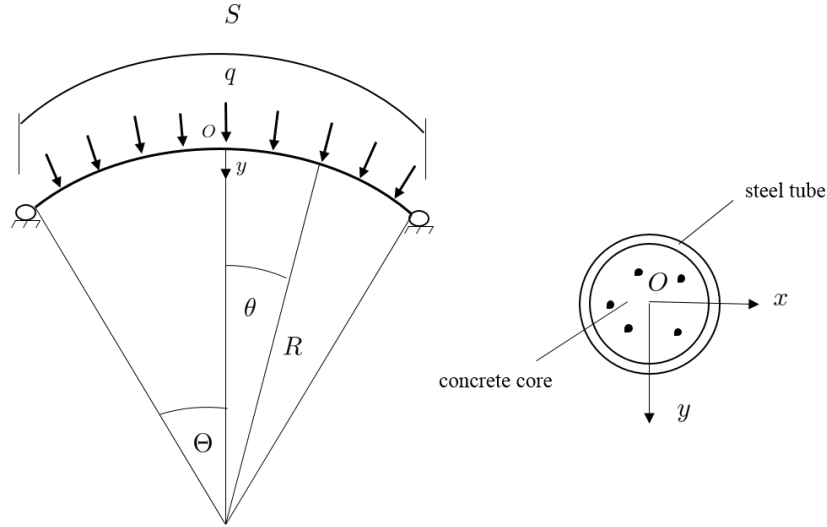


Figure 1: Geometrical and loading configuration of shallow CFST arch

The virtual work principle is utilised to obtain the non-linear equilibrium equations, which requires that;

$$\int_{V_s} \sigma_s \delta \epsilon dV_s + \int_{V_c} \sigma_c \delta \epsilon dV_c - \int_{-\Theta}^{\Theta} qR^2 \delta v d\theta = 0, \quad \forall \delta v, \delta v', \delta v'', \delta w, \delta w' \quad (17)$$

where Θ represents half the arch included angle, V_s is the volume of the steel tube, V_c is the volume of the concrete core and $\delta v, \delta v', \delta v'', \delta w$ and $\delta w'$ are kinematically possible variations of displacement. The definition for axial force N is;

$$N = - \int_{A_c} \sigma_c dA_c - \int_{A_s} \sigma_s dA_s, \quad (18)$$

and the bending moment M defined by

$$M = \int_{A_c} \sigma_c y dA_c + \int_{A_s} \sigma_s y dA_s. \quad (19)$$

In Eqs. (18) and (19), A_s and A_c are the areas of the outer steel tube and inner concrete core respectively. Substituting Eqs. (15), (18) and (19) into (17), and upon integration, gives the non-linear equilibrium equations;

$$N' = 0, \quad (20)$$

in the axial direction, and

$$-M'' + NR(1 + v'') - qR^2 = 0, \quad (21)$$

in the radial direction. Additionally, the static boundary condition for a pin-ended arch is obtained;

$$v''(\Theta) = v''(-\Theta) = 0. \quad (22)$$

This adjoins the geometric boundary conditions;

$$v(\Theta) = v(-\Theta) = w(\Theta) = w(-\Theta) = 0, \quad (23)$$

for an arch with pinned-ends, and

$$v(\Theta) = v(-\Theta) = v'(\Theta) = v'(-\Theta) = w(\Theta) = w(-\Theta) = 0, \quad (24)$$

for fixed-ended arch. The axial force equation is obtained by substituting Eqs. (1) and (6) into (18):

$$N = E_s A_s \epsilon_{s,th} + E_c A_c \epsilon_{c,th} - \epsilon_m (E_s A_s + E_c A_c). \quad (25)$$

The moment-curvature relationship is similarly derived by combining Eqs. (1), (6), (16) and (19):

$$M = - \frac{(E_s I_s + E_c I_c)}{R} v'', \quad (26)$$

Thus, a boundary value problem is formulated comprised of the system of ordinary differential equations (equilibrium Eqs. (20) and (21) and constitutive Eqs. (25) and (26)) and boundary conditions (23) or (24). Introducing a set of dependent variables:

$$x_1 = v, \quad x_2 = v', \quad x_3 = M, \quad x_4 = M', \quad x_5 = N, \quad x_6 = w, \quad (27)$$

which upon differentiation give,

$$x'_1 = x_2, \quad (28)$$

$$x'_2 = \frac{-x_3 R}{E_s I_s + E_c I_c}, \quad (29)$$

$$x'_3 = x_4, \quad (30)$$

$$x'_4 = x_5 R (1 + x'_2) - q R^2, \quad (31)$$

$$x'_5 = 0, \quad (32)$$

$$x'_6 = \frac{E_s A_s \epsilon_{s,th} + E_c A_c \epsilon_{c,th} - x_5}{E_s A_s + E_c A_c} + x_1 - 0.5 x_2^2. \quad (33)$$

Given load q and temperature T , system (28)-(33) can be numerically solved with the boundary conditions

$$x_1(\Theta) = x_1(-\Theta) = x_3(\Theta) = x_3(-\Theta) = x_6(\Theta) = x_6(-\Theta) = 0, \quad (34)$$

for an arch with pinned ends, or

$$x_1(\Theta) = x_1(-\Theta) = x_2(\Theta) = x_2(-\Theta) = x_6(\Theta) = x_6(-\Theta) = 0, \quad (35)$$

for a arch fixed at its ends. Solving system (28)-(33) has been found to be insensitive to initial guess values. An example of the results obtained by solving system (28)-(33) is shown in Figure 2 where the effect of uniform thermal loading on axial force N and central displacement at the arch centre $\hat{v}(0)$ of a shallow fixed CFST arch is demonstrated.

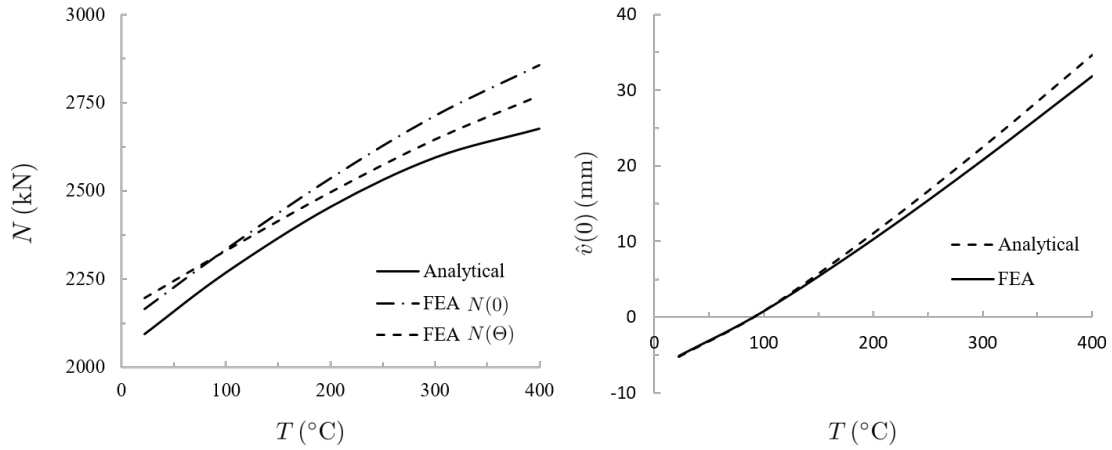


Figure 2: Influence of uniform thermal load on axial force (left) and central radial displacement (right) of fixed-ended CFST arch. $q = 450$ kN/m, $2\Theta = 73.34^\circ$, $R = 5000$ mm, $E_s = 200$ GPa, $E_c = 32,800$ MPa, Cross-section diameter = 300 mm and steel tube thickness = 10 mm.

3.2. Central concentrated load

The loading case of a central concentrated load Q is now considered. The equations of equilibrium and BC's are again derived by employing the virtual work principle;

$$\int_{V_s} \sigma_s \delta \epsilon dV_s + \int_{V_c} \sigma_c \delta \epsilon dV_c - \frac{Q}{2} \delta v(0) = 0, \quad \forall \delta v, \delta v', \delta v'', \delta w, \delta w'. \quad (36)$$

which upon integration over half the larch length gives the following non-linear equilibrium equations;

$$N' = 0, \quad (37)$$

in the axial direction, and

$$-M'' + NR(1 + v'') = 0. \quad (38)$$

If the arch is integrated over the left-side $[-\Theta, 0]$, the BC representing zero shear force at the arch centre is obtained;

$$-\frac{M'}{R} + \frac{Q}{2} + N v' = 0, \quad \text{at } \theta = 0. \quad (39)$$

Eq.(39) takes the form

$$-\frac{M'}{R} - \frac{Q}{2} + N v' = 0, \quad \text{at } \theta = 0. \quad (40)$$

when the arch is integrated over the right side $[0, \Theta]$. This adjoins the known static and geometric BC of pinned or fixed arches. Using the definition of dependent variables introduced earlier, considering symmetry and only the right side of the arch, the BC's may be expressed as,

$$x_1(\Theta) = x_2(0) = x_3(\Theta) = -\frac{x_4(0)}{R} - \frac{Q}{2} = x_6(\Theta) = x_6(0) = 0, \quad (41)$$

for an arch with pinned ends, or

$$x_1(\Theta) = x_2(\Theta) = x_2(0) = -\frac{x_4(0)}{R} - \frac{Q}{2} = x_6(\Theta) = x_6(0) = 0, \quad (42)$$

for a arch fixed at its ends.

System (28)-(33) can be utilised to analyse the prebuckling state of a CFST arch given central concentrated load Q and temperature level T by setting $q = 0$ and adopting BC's (41) or (42). An example is shown in Figure 3 where the effect of uniform thermal loading on the bending moment and axial force of a shallow fixed CFST arch under central concentrated loading is depicted. As with the case of uniformly distributed radial loading, elevated temperature fields cause the arch to displace upwards and greatly increase the magnitudes of axial force and bending moments.

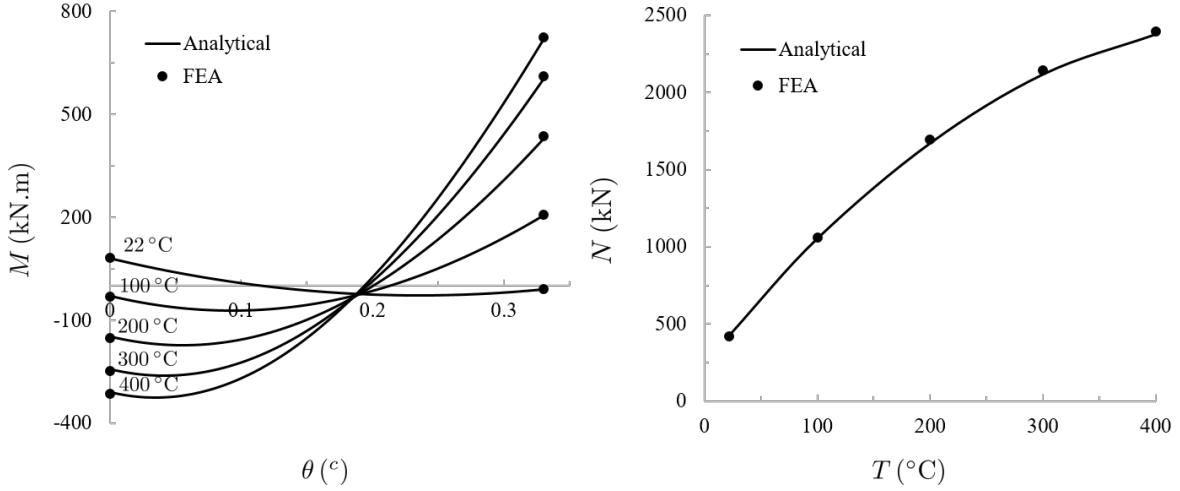


Figure 3: Influence of uniform thermal load on bending moment (left) and axial force (right) of fixed-ended CFST arch under central concentrated load. $Q = 200$ kN, $2\Theta = 37.85^\circ$, $R = 9250$ mm, $E_s = 200$ GPa, $E_c = 32,800$ MPa, cross-section diameter = 300 mm and steel tube thickness = 10 mm.

3.3. Effects of basic creep

The significance of basic creep strain on the prebuckling behaviour of CFST arches is now examined through generalising the preceding analysis by adopting of Eq. (7) to define the total strain in the concrete core. Discretisation of Eq. (8) is first conducted in order to numerically approximate the basic creep strain (see [50] for the derivation);

$$\epsilon_{cr,n} = \epsilon_{cr,n-1} - \sum_{j=0}^{n-2} (\epsilon_{cr,j+1} - \epsilon_{cr,j}) [(n-j)^{1-\alpha_n} - (n-j-1)^{1-\alpha_n}] + \frac{\sigma_n}{\eta_n} \Gamma(2-\alpha_n) \Delta t^{\alpha_n}, \quad (43)$$

where time $t = n \Delta t$ and Δt and n denote the time step size and current time step respectively. As the numerical procedure begins at $n = 2$, the creep strains at $t = 0$ and $t = 1$ are required to be predetermined. These are known as;

$$\epsilon_{cr}(1) = \frac{\sigma_1}{\eta_1} \Gamma(2-\alpha_1) (\Delta t)^{\alpha_1} + \epsilon_{cr}(0), \quad (44)$$

and $\epsilon_{cr}(0) = 0$.

The procedure outlined earlier to obtain the constitute equations for axial force and bending moment are followed. In this case, Eqs. (1), (8), (18) and (44) are combined to give the axial force at time step n ;

$$N_n = E_{s,n} A_s (\epsilon_{s,th,n} - \epsilon_{m,n}) + \frac{E_{c,n} A_c (\epsilon_{c,th,n} - \epsilon_{m,n}) - E_{c,n} \epsilon_{cr,N}}{1 + E_c \Gamma(2-\alpha_n) \Delta t^{\alpha_n} / \eta_n}, \quad (45)$$

where

$$\epsilon_{cr,N} = \epsilon_{cr,n-1}(N) - \sum_{j=0}^{n-2} (\epsilon_{cr,j+1}(N) - \epsilon_{cr,j}(N)) [(n-j)^{1-\alpha_n} - (n-j-1)^{1-\alpha_n}]. \quad (46)$$

Likewise, the bending moment is obtained at time step n upon combination of Eqs.(1), (8), (19) and (44);

$$M_n = \frac{E_{s,n} I_s v_n''}{R} - \frac{E_{c,n} I_c v_n'' / R + E_{c,n} \epsilon_{cr,M}}{1 + E_c \Gamma(2-\alpha_n) \Delta t^{\alpha_n} / \eta_n}, \quad (47)$$

with

$$\epsilon_{cr,M} = \epsilon_{cr,n-1}(M) - \sum_{j=0}^{n-2} \left(\epsilon_{cr,j+1}(M) - \epsilon_{cr,j}(M) \right) \left[(n-j)^{1-\alpha_n} - (n-j-1)^{1-\alpha_n} \right]. \quad (48)$$

Creep equations $\epsilon_{cr}(N)$ and $\epsilon_{cr}(M)$ are functions of axial force and bending moment respectively in place of longitudinal stress as seen in Eqs. (43) and (44). Substitution of dependant variables (27) into Eqs. (45) and (47), and after rearranging, yields;

$$x'_{2,n} = - \frac{x_{3,n} R (1 + E_{c,n} \Gamma(2 - \alpha_n) \Delta t^{\alpha_n} / \eta_n) + E_{c,n} R \epsilon_{cr,M}}{E_{s,n} I_s (1 + E_{c,n} \Gamma(2 - \alpha_n) \Delta t^{\alpha_n} / \eta_n) + E_{c,n} I_c}, \quad (49)$$

and

$$x'_{6,n} = \frac{E_{c,n} A_c \epsilon_{c,th,n} - E_{c,n} \epsilon_{cr,N} + (E_{s,n} A_s \epsilon_{s,th,n} - x_{5,n})(1 + E_{c,n} \Gamma(2 - \alpha_n) \Delta t^{\alpha_n} / \eta_n)}{E_{s,n} A_s (1 + E_{c,n} \Gamma(2 - \alpha_n) \Delta t^{\alpha_n} / \eta_n) + E_{c,n} A_c} + x_{1,n} - 0.5 x_{2,n}^2. \quad (50)$$

Although behaviour is now time-dependant and dynamic in nature, adoption of the static equilibrium equations remains valid for creep and creep buckling problems. Thus, the prebuckled state when considering viscoelastic effects can be solved numerically by replacing Eqs. (29) an (33) with (49) an (50) in the system (28)-(33) subjected to BC's (34), (35), (41) or (42). The BVP must be solved at every time step from $n = 2$ until the desired final time, and due to the history dependence of the creep law, $\epsilon_{cr}(N)$ and $\epsilon_{cr}(M)$ must be determined and recorded after every time step for use in the proceeding time steps. As stated earlier, solutions for the first two time steps must be initially known. These can be obtained by solving the corresponding elastic problem ($\epsilon_{cr}=0$) for when $n = 0$ and by setting $\epsilon_{cr,N} = 0$ and $\epsilon_{cr,M} = 0$ for when $n = 1$.

Two scenarios have been considered to analyse the significance of basic creep strain on the thermal response of CFST arches; constant elevated temperature levels and time-varying temperature fields. Of interest is short-term or transient heating which would be experienced during fire exposure. Hence, the total analysis time is limited to 300 mins. The effect of non-varying elevated temperatures on the axial force and bending moments are depicted in Figures 4 and 5 respectively for both pinned and fixed CFST arches. It can be seen that creep strain causes a slight reduction in axial force. The time-evolution of bending moment is more noticeable. CFST arches deflect downwards with progression of time due to creep resulting in the development of positive bending. This is shown in Figure 5 as a reduction on the magnitudes of the negative moments. Though it is noted that time-induced changes to bending moment are still small when compared to those caused by the thermal expansive strains. For the case of time-varying temperature, the CFST arch is subjected to a heating rate of 1.5°C/min with the time-evolutions of axial force and bending moment depicted in Figures 6 and 7 respectively. Practically identical results are obtained when creep strain is and is not considered. Therefore, due to the negligible effect basic creep strain has on the prebuckling behaviour under transient heating scenarios, in addition to the small changes to axial force observed under constant elevated temperatures, time effects will not be considered in the following flexural-torsional buckling analyses.

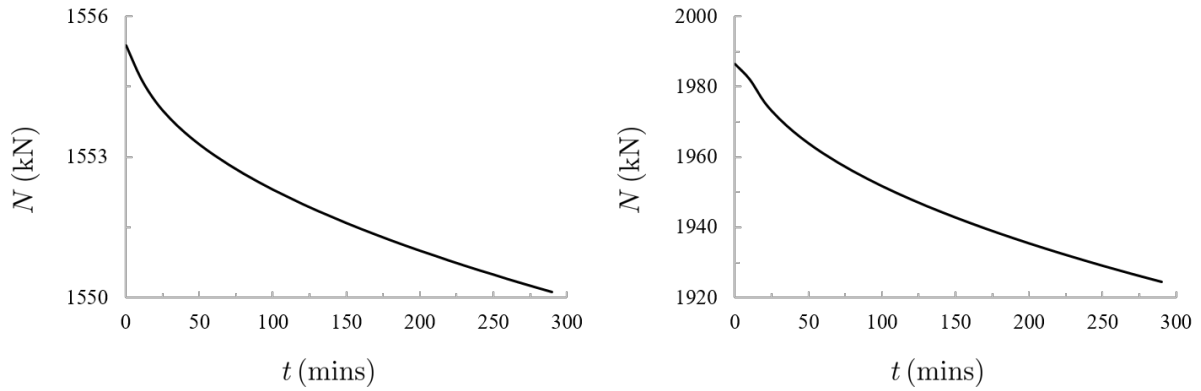


Figure 4: Effect of basic creep strain on axial force in pinned (left) and fixed (right) CFST arches at constant elevated temperature levels. $T = 400^{\circ}\text{C}$, $q = 300 \text{ kN/m}$, $2\Theta = 73.74^{\circ}$, $R = 5000 \text{ mm}$, cross-section diameter = 300, steel tube thickness = 10 mm and $\Delta t=10$.

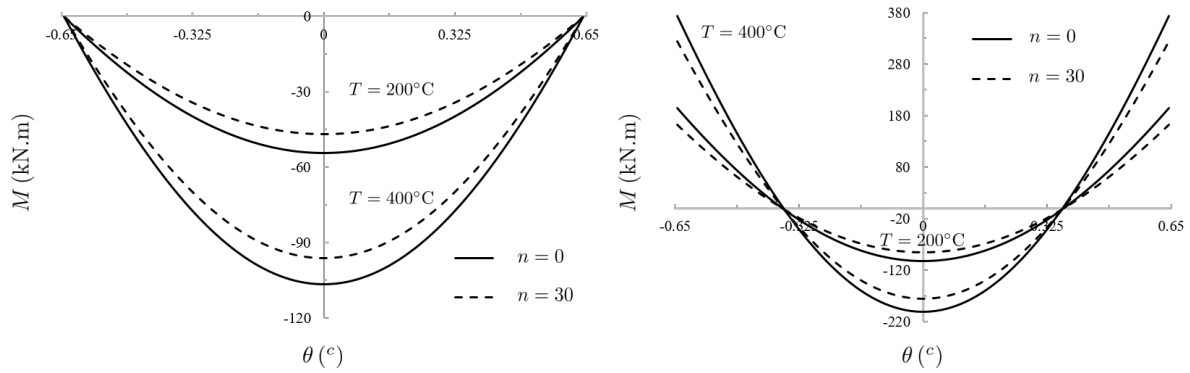


Figure 5: Effect of basic creep strain on bending moment in pinned (left) and fixed (right) CFST arches at constant elevated temperature levels temperature. $q = 300 \text{ kN/m}$, $2\Theta = 73.74^{\circ}$, $R = 5000 \text{ mm}$, cross-section diameter = 300, steel tube thickness = 10 mm and $\Delta t=10$.

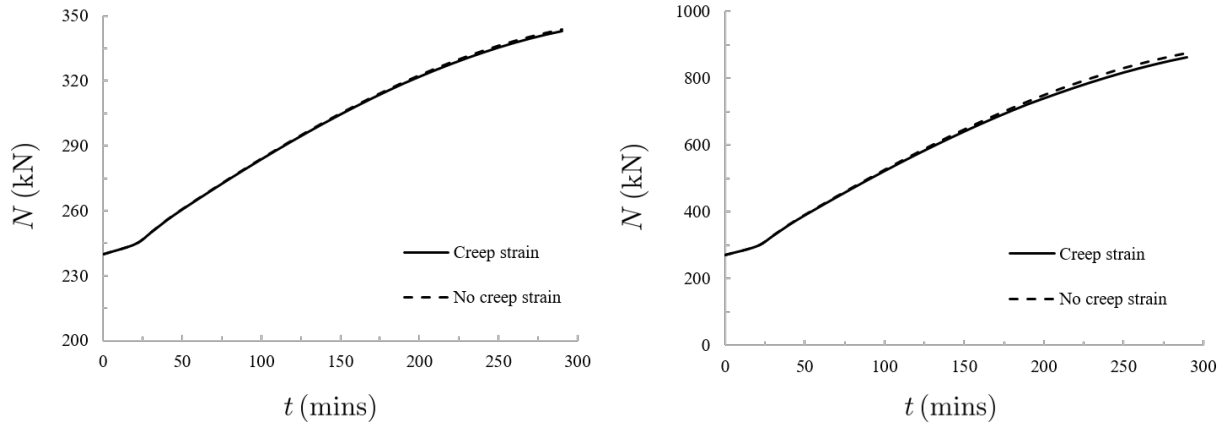


Figure 6: Effect of basic creep strain on axial force in pinned (left) and fixed (right) CFST arches subjected to time-varying uniform temperature fields. Heating rate is $1.5^{\circ}\text{C}/\text{min}$. $T = 400^{\circ}\text{C}$, $Q = 200\text{ kN}$, $2\Theta = 73.74^{\circ}$, $R = 5000\text{ mm}$, cross-section diameter = 300, steel tube thickness = 10 mm and $\Delta t=10$.

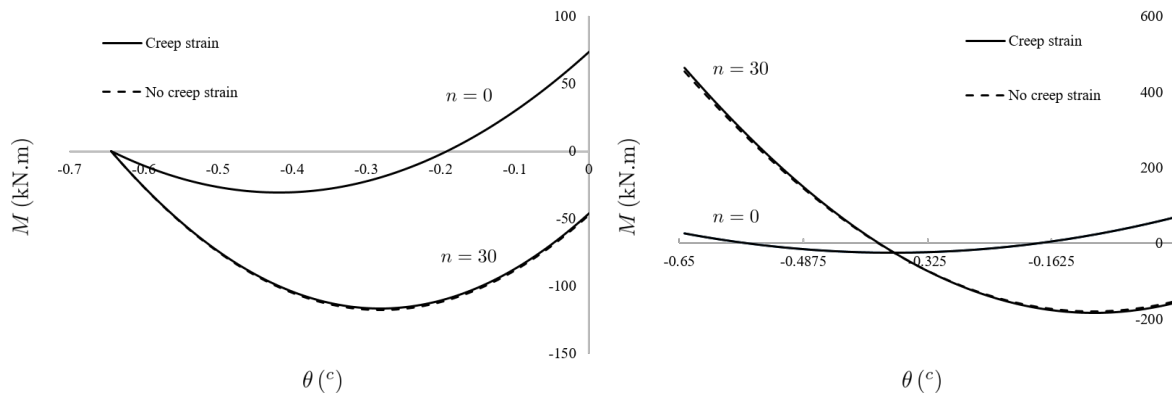


Figure 7: Effect of basic creep strain on bending moment in pinned (left) and fixed (right) CFST arches subjected to time-varying uniform temperature fields. Heating rate is $1.5^{\circ}\text{C}/\text{min}$. $q = 200\text{ kN}$, $2\Theta = 73.74^{\circ}$, $R = 5000\text{ mm}$, cross-section diameter = 300, steel tube thickness = 10 mm and $\Delta t=10$.

4. Elastic out-of-plane buckling analysis

The simultaneous stiffness reduction and longitudinal stress increase induced by elevated temperatures may cause a CFST arch to rapidly displace out-of-plane and buckle in a flexural-torsional mode, see Figure 8.

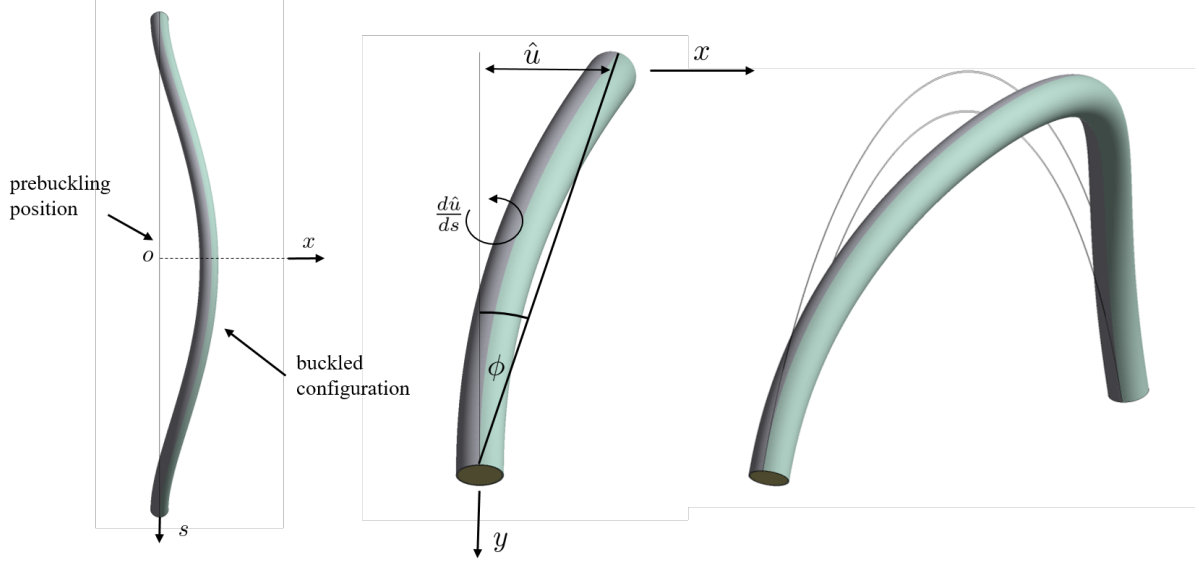


Figure 8: Flexural-torsional buckled configuration

The potential energy of the system in an infinitesimal flexural-torsional buckled state can be written as;

$$\Pi = \int_{V_s} \frac{1}{2} (E_s \epsilon_{ss}^2 + G_s \gamma_{sx}^2 + G_s \gamma_{sy}^2) + \sigma_{ss} \epsilon_{ss} dV_s + \int_{V_c} \frac{1}{2} (E_c \epsilon_{ss}^2 + G_c \gamma_{sx}^2 + G_c \gamma_{sy}^2) + \sigma_{sc} \epsilon_{ss} dV_c, \quad (51)$$

where σ_{ss} and σ_{sc} are the constant prebuckling longitudinal stresses in the steel tube and concrete core respectively. The steel G_s and concrete G_c shear moduli are;

$$G_s = \frac{E_s}{2(1 + \nu_s)}, \quad G_c = \frac{E_c}{2(1 + \nu_c)}. \quad (52)$$

Poisson's ratio is assumed to be independent of temperature and is adopted as $\nu_s = 0.3$ for steel and $\nu_c = 0.18$ for concrete. The out-of-plane buckling longitudinal ϵ_{ss} and shear strains γ_{sx} and γ_{sy} are expressed as [17];

$$\epsilon_{ss} = -\frac{x}{R} (u'' - \phi) - \frac{\omega}{R} (\phi' - u'') + \frac{1}{2} u'^2 + \frac{y}{R} (u'' \phi + \frac{1}{2} \phi^2) + \frac{1}{2R^2} (x^2 + y^2) (\phi - u')^2, \quad (53)$$

$$\gamma_{sx} = -\frac{1}{R} \left(y + \frac{\partial \omega(x, y)}{\partial x} \right) (\phi - u'), \quad \text{and} \quad \gamma_{sy} = \frac{1}{R} \left(x + \frac{\partial \omega(x, y)}{\partial y} \right) (\phi - u'), \quad (54)$$

with ϕ denoting the twist rotation of the cross-section about axis os , $u = \hat{u}/R$ where \hat{u} is the lateral displacement in direction of axis ox and $\omega(x, y)$ is the cross-sectional warping function. Upon substitution of Eqs. (53) and (54) into Eq.(51), and ignoring higher-order terms, Eq.(51) can be expressed as;

$$\Pi = \int_{-\Theta}^{\Theta} \frac{1}{2} \left[\frac{\widetilde{EI}_y}{R^2} (u'' + \phi)^2 + \frac{\widetilde{GJ}}{R^2} (\phi' - u'')^2 + \frac{\widetilde{EI}_w}{R^4} (\phi'' - u'')^2 \right] R d\theta + \int_{-\Theta}^{\Theta} \left[\frac{M}{R} \left(u'' \phi + \frac{1}{2} \phi^2 \right) - N \left(\frac{u'^2}{2} + \frac{\tilde{r}^2}{2R^2} (\phi' - u')^2 \right) \right] R d\theta. \quad (55)$$

The terms \widetilde{EI}_y , \widetilde{GJ} , \widetilde{EI}_w and \tilde{r} are the temperature dependant composite cross-sectional properties, defined as;

$$\widetilde{EI}_y = E_s I_{y,s} + E_c I_{y,c}, \quad \widetilde{GJ} = G_s J_s + G_c J_c, \quad \widetilde{EI}_w = E_s I_{w,s} + E_c I_{w,c} \quad \text{and} \quad \tilde{r} = \left(\frac{I_{x,s} + I_{y,s}}{A_s} + \frac{I_{x,c} + I_{y,c}}{A_c} \right)^{1/2} \quad (56)$$

J_s and J_c represent the torsional constants for the steel tube and concrete core respectively, and $I_{w,s}$ and $I_{w,c}$ denote the warping constants for the tube and core. As circular CFST cross-sections are doubly-symmetric, the in-plane ($I_{x,s}$ and $I_{x,c}$) and out-of-plane ($I_{y,s}$ and $I_{y,c}$) second moment of areas are equal.

The Rayleigh-Ritz method is employed to obtain the critical load. The first mode buckled shapes are assumed to behave according to;

$$\frac{u}{u_c} = \frac{\phi}{\phi_c} = \cos\left(\frac{\pi\theta}{2\Theta}\right), \text{ for pinned arches, and } \frac{u}{u_c} = \frac{\phi}{\phi_c} = \cos\left(\frac{\pi\theta}{\Theta}\right) + 1, \text{ for fixed arches.} \quad (57)$$

where u_c and ϕ_c are the dimensionless maximum (central) buckling lateral displacements and twist rotations respectively. Eq.(57) satisfies the boundary conditions for pinned ends $u = \phi = 0$ at $\pm\Theta$ and fixed ends $u = \phi = \phi' = 0$ at $\pm\Theta$. Substituting Eq.(57) into Eq.(55) and integrating by parts yields;

$$\Pi(u_c, \phi_c) = k_{11} u_c^2 + k_{12}^2 u_c \phi_c + k_{22} \phi_c^2. \quad (58)$$

The parameters k_{11} , k_{12} and k_{22} are derived as;

$$k_{11} = \frac{\widetilde{EI}_y}{2R} \alpha^4 \Theta + \frac{\widetilde{EI}_w}{2R^3} \alpha^4 \Theta + \frac{\widetilde{GJ}}{2R} \alpha^2 \Theta - NR \alpha^2 \Theta \left(\frac{1}{2} + \frac{\tilde{r}^2}{2R^2} \right), \quad (59)$$

$$k_{12} = -\frac{\widetilde{EI}_y}{2R} \alpha^2 \Theta - \frac{\widetilde{EI}_w}{2R^3} \alpha^4 \Theta - \frac{\widetilde{GJ}}{2R} \alpha^2 \Theta + N \alpha^2 \Theta \frac{\tilde{r}^2}{2R} - \frac{\alpha^2}{2} \left[M(\Theta) \frac{\Theta}{2} - M'(\Theta) \frac{\Theta^2}{4} + M''(\Theta) \frac{\Theta^3}{12} \right], \quad (60)$$

$$k_{22} = \frac{\widetilde{EI}_y}{2R} A \Theta + \frac{\widetilde{EI}_w}{2R^3} \alpha^4 \Theta + \frac{\widetilde{GJ}}{2R} \alpha^2 \Theta - N \alpha^2 \Theta \frac{\tilde{r}^2}{2R} + M(\Theta) \frac{\Theta}{4} - M'(\Theta) \frac{\Theta^2}{8} + M''(\Theta) \frac{\Theta^3}{24} \quad (61)$$

with

$$\alpha = \frac{\pi}{2\Theta} \text{ for pinned ends, } \alpha = \frac{\pi}{\Theta} \text{ for fixed ends, and} \quad (62)$$

given $A = 1$ for pin-ended arches and $A = 3$ for fixed-ended arches.

The equations governing the out-of-plane buckling state are obtained using the principle of stationary potential energy, which requires that;

$$\frac{\partial \Pi(u_c, \phi_c)}{\partial u_c} = 0 \text{ and } \frac{\partial \Pi(u_c, \phi_c)}{\partial \phi_c} = 0. \quad (63)$$

Performing partial differentiation with respect to lateral deformation and twist on potential energy function (58) yields the following algebraic relations;

$$\begin{bmatrix} k_{11} & k_{12} \\ k_{12} & k_{22} \end{bmatrix} \begin{Bmatrix} u_c \\ \phi_c \end{Bmatrix} = \begin{Bmatrix} 0 \\ 0 \end{Bmatrix}. \quad (64)$$

The determinant of the coefficient matrix (64) must vanish for non-trivial solutions for u_c and ϕ_c , giving;

$$k_{11} k_{22} - k_{12}^2 = 0. \quad (65)$$

The elastic out-of-plane buckling load for a pinned or fixed-ended arch under a uniform temperature field can be obtained from solving Eq.(65) for both uniformly distributed radial loading and central concentrated loading cases.

As k_{11} , k_{12} and k_{22} are functions of the in-plane pre-buckling moment M and axial force N , system (28)-(33) must first be solved for a given loading configuration (T and q or Q). The resulting values for bending moment, and its first and second derivative at the arch ends are substituted into Eqs.(60) and (61). Subsequently, Eq.(65) is solved for axial force N_{cr} . If the pre-buckling axial force N obtained from system (28)-(33) is equal to N_{cr} , the critical load combination has been reached (T_{cr} , q_{cr} and/or Q_{cr}). This method can be employed for either pin-ended or fixed-ended arches, with the differences lying in the BC's adopted when solving system (28)-(33) and the definitions of constants α and A .

To examine the effect of thermal loading on the elastic out-of-plane buckling loads of shallow CFST arches for the case of uniformly distributed radial loading, Eq.(65) was solved for three arch geometrical configurations. The results are shown in Figures 9, 10 and 11. It can be seen that critical buckling loads are sensitive to temperature, with buckling strength substantially decreasing with rise in thermal loading. This result contrasts the behaviour observed in steel arches where elastic out-of-plane buckling loads are dependant primarily by the thermal load and vary minimally with mechanical load level [32]. The magnitude of buckling strength deterioration with temperature level is compared for fixed and pinned ended arches, see Figure 10. The critical loads have been normalised by dividing them by the critical loads at ambient temperature. The results show that the out-of-plane buckling loads of pinned and fixed arches degrade at the same rate with temperature rise. Thus, the effect of thermal loading on the out-of-plane buckling loads of CFST arches is independent on the type of end supports. Moreover, the rate of strength degradation is identical across the three geometrical configurations when the cross-sectional parameters are the same. The steel-concrete ratio is the predominant parameter influencing buckling strength deterioration. Increasing the steel tube thickness for a fixed cross-section diameter relaxes the rate of buckling load reduction with temperature rise. This can be seen in Figure 11 where the critical out-of-plane buckling loads for a fixed arch are shown for three steel tube thicknesses. A noticeable delay in critical load deterioration is observed when increasing the confining tube thickness from 10 or 15 mm to 20 mm. Consequently, reduction factors may be easily obtained from these results for convenient prediction of out-of-plane buckling loads of shallow CFST arches at elevated temperatures for based only on the cross-section diameter and steel tube thickness.

Elevated temperature fields influence stability boundaries for fixed or pinned-ended shallow CFST arches under central concentrated loads in the same manner as the loading condition of uniformly distributed radial loading. The flexural-torsional buckling loads for a shallow fixed CFST arch subjected to a central concentrated load are depicted in Figure 12. It can be seen that the dimensionless buckling loads are practically identical to those shown in Figure 10 at all temperature levels for the same cross-section. The negligible effect of in-plane supporting conditions and arch geometry discussed previously also hold for central concentrated buckling loads with cross-sectional dimensions governing the influence of temperature on critical buckling loads. The influence of cross-section diameter with constant steel tube thickness on normalised buckling loads is represented in Figure 12. Increasing the cross-section diameter leads to a greater rate of strength reduction with temperature rise caused by the lower steel-concrete ratio. The results for the 100 and 200 mm diameters are terminated at 500°C and 600°C respectively due to the occurrence of in-plane

limit instability failure. At the lower temperature levels, and in all other geometrical configurations, flexural-torsional buckling preceded snap-through buckling. The limit instability, or symmetric snap-through buckling loads, can be obtained from system (28)-(33) by increasing the mechanical load or temperature level until numerical convergence cannot be achieved. As limit instability is approached, a drastic jump in forces and displacements is typically observed. These surprising results indicate that the governing failure mode may change with rise in temperature; an event likely to occur in very shallow and slender arches as in the present case. It is therefore important to consider both in-plane and out-of-plane stability of CFST arches in elevated temperature fields.

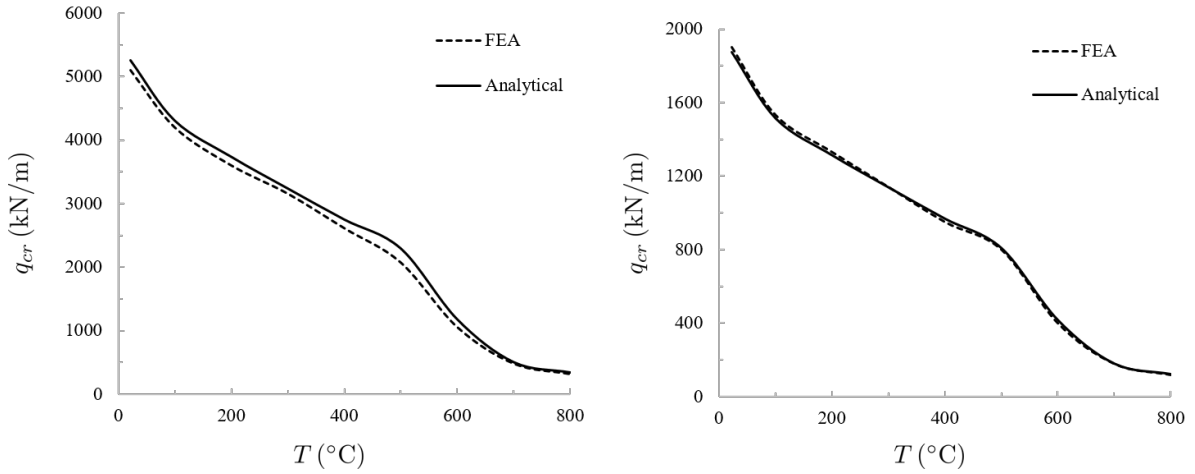


Figure 9: Elastic out-of-plane buckling loads of fixed CFST arches under uniformly distributed radial loading and uniform temperature field. $2\Theta = 73.34^\circ$ and $R = 5000$ mm (left) and $2\Theta = 56.15^\circ$ and $R = 8500$ mm (right). $E_s = 200$ GPa, $E_c = 32,800$ MPa, cross-section diameter = 300 mm and steel tube thickness = 10 mm.

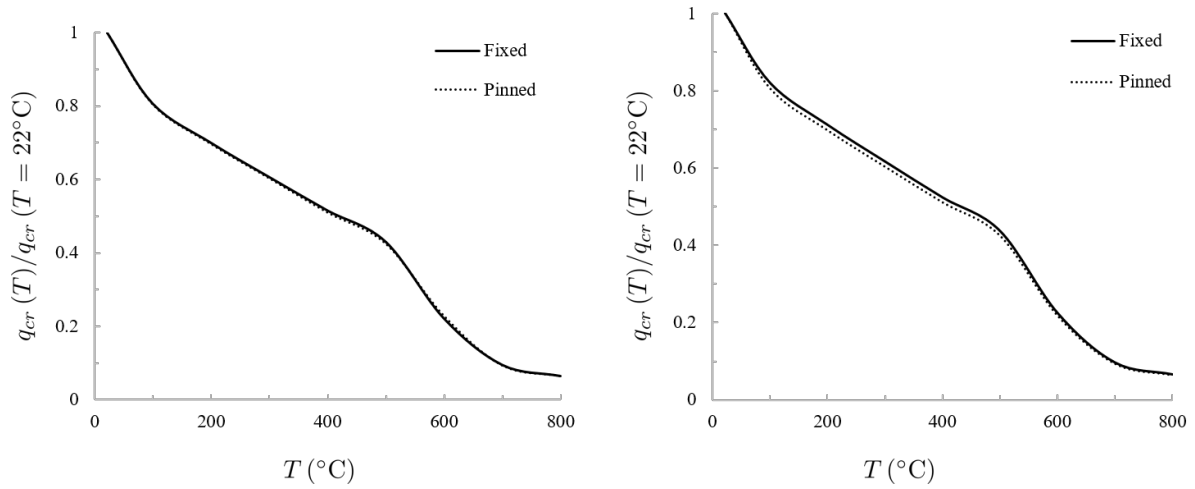


Figure 10: Dimensionless out-of-plane critical elastic buckling loads for CFST arches subjected to uniformly distributed radial loading and uniform temperature level with pinned or fixed ends. $2\Theta = 73.34^\circ$, $R = 5000$ mm, $q_{cr}(T = 22^\circ\text{C}) = 5100$ kN/m for fixed ends and $q_{cr}(T = 22^\circ\text{C}) = 1358$ kN/m for pinned ends (left). $2\Theta = 56.15^\circ$, $R = 8500$ mm, $q_{cr}(T = 22^\circ\text{C}) = 1900$ kN/m for fixed ends and $q_{cr}(T = 22^\circ\text{C}) = 482$ kN/m for pinned ends (right). $E_s = 200$ GPa, $E_c = 32,800$ MPa, cross-section diameter = 300 mm and steel tube thickness = 10 mm.

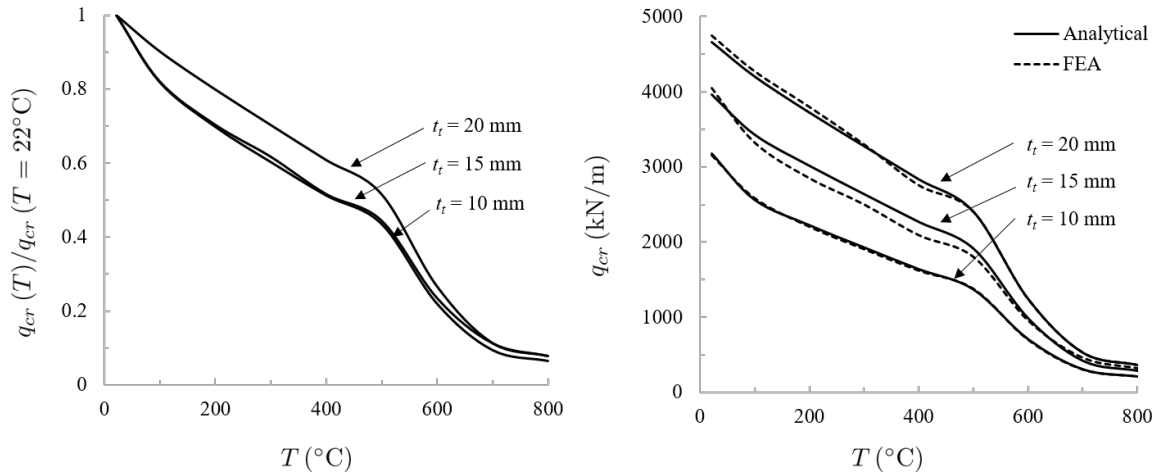


Figure 11: Effect of steel tube thickness on elastic out-of-plane buckling loads of fixed CFST arches under uniformly distributed radial loading and uniform temperature field. $2\Theta = 37.85^\circ$, $R = 9250$ mm, $E_s = 200$ GPa, $E_c = 32,800$ MPa and cross-section diameter = 300 mm.

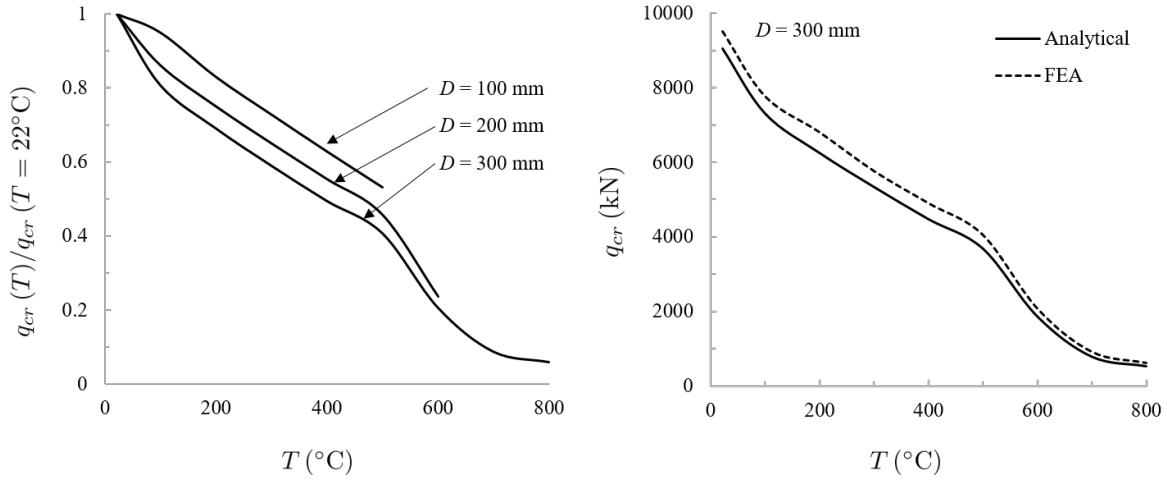


Figure 12: Elastic out-of-plane central concentrated buckling loads of fixed CFST arches under uniform temperature field. $2\Theta = 37.85^\circ$, $R = 9250$ mm, $E_s = 200$ GPa, $E_c = 32,800$ MPa and steel tube thickness $t_t = 300$ mm.

5. Inelastic out-of-plane buckling strength

5.1. Finite element model

A FE model is constructed using software package ANSYS [52] to investigate the inelastic lateral buckling strength of CFST arches. The following considerations have been made when developing the FE model:

1. The arch is meshed using Solid186 elements of 50 mm size. A finer mesh did not noticeably alter numerical results;
2. All thermal and mechanical properties are defined at ambient temperature, and from 100°C in intervals of 100°C to 1200°C. Parameter values at intermediate temperatures are obtained via linear interpolation.
3. A geometric non-linear analysis is conducted by assuming large deflections;
4. Lateral geometric imperfections are incorporated based on the buckled shape. Hence, an eigenvalue buckling analysis is first conducted for imperfect geometry formation. A size of arch length $S/1000$ is assumed for the initial imperfections;
5. The bi-linear isotropic hardening plasticity model is utilised to model the deformation characteristics of steel (Eq.(2)). This model adopts Von-Mises yield criterion and considers strain flow and hardening;
6. The mechanical behaviour of concrete is considered with the Drucker-prager (DP) concrete plasticity model. A yield stress of $0.4f'_{c,T}$ is assumed with elastic modulus taken as the tangent at this point. Tensile behaviour is assumed as elastic-perfectly plastic with the elastic modulus the same as in compression and the yield stress given by Eq.(14);
7. A perfect bond is assumed between the steel and concrete. The influence of contact model on numerical results is investigated in Section 5.3;

8. Mechanical loading is applied first, followed by the thermal load in a subsequent load step;
9. Displacements and rotations are fully fixed at the arch ends; and
10. Solid70 elements are adopted to mesh structure for the transient thermal analysis, with an element size of 50 mm, as required for the case of fire loading. The steel tube is exposed to radiation and convection. The steel surface emissivity and convection coefficient are assumed as 0.7 and 25 W/m²K respectively.

Verification of the FE model is made by comparing the results to the out-of-plane elastic buckling loads obtained using Eq.(65) and the elastic prebuckling behaviour determined using system (28)-(33) for fixed-ended arches. The results of these comparisons are depicted in Figures 2, 3, 9, 11 and 12. It is shown that a small variation exists across the models at all examined temperature levels. Further validation of the FE model has been made by the authors in [44] for the inelastic prebuckling behaviour, and the elastic in-plane buckling loads of CFST arches at elevated temperatures.

5.2. Inelastic buckling strength

The inelastic out-of-plane buckling loads of fixed-ended CFST arches under thermal loading has been analysed using the described FE model. Figure 13 depicts the effect of uniform thermal loading on the critical loads of CFST arches subjected to uniformly distributed radial loading and central concentrated loads. For both cases, the out-of-plane buckling strength mostly deteriorated with temperature rise. When considering the uniformly distributed radial loading scenario, the effect of temperature on buckling loads is sensitive to included angle and arch slenderness parameter $\lambda = R\Theta/r_x$, where r_x is the radius of gyration of the cross-section about either axis. It is shown that the rate of critical load degradation is greatest in the most slender arch. As the slenderness (and included angle) decreases the rate of buckling strength reduction reduces and approaches the normalised squash load, defined as the temperature dependant compressive strength of the cross-section ($A_c f'_{c,T} + A_s \sigma_{y,T}$) divided by the cold compressive strength of the cross-section ($A_c f'_c + A_s \sigma_y$). The higher slenderness ratio associated with deeper arches causes instability to govern failure. Whereas the buckling strength of stocky shallow arches are governed by material failure. Considering the case of central concentrated loads, it is shown in Figure 13 that slenderness and arch included angle do not impact the rate of strength deterioration with temperature rise. Instead, the normalised buckling load degrades with temperature at a rate very close to that of the squash load. Thus, it can be stated that material strength or section capacity governs failure on CFST arches at elevated temperatures under central concentrated loads. This result also holds when varying the cross-section parameters as shown in Figure 14. Though the magnitude of strength increases with cross-section diameter or steel tube thickness, the normalised buckling loads are not noticeably influenced. This contrasts the effects of cross-section parameters and steel-concrete ratio on elastic buckling loads as illustrated in Figure 12.

The effect of standard ISO-834 fire loading on the behaviour and critical buckling loads has been analysed. The out-of-plane strength versus heating time is depicted in Figure 15 for uniformly distributed radial loading and Figure 16 for central concentrated loading. For the case of uniformly distributed radial loading, the results show that there is an initial significant reduction in buckling strength during fire exposure, which is proceeded by a slow rate of

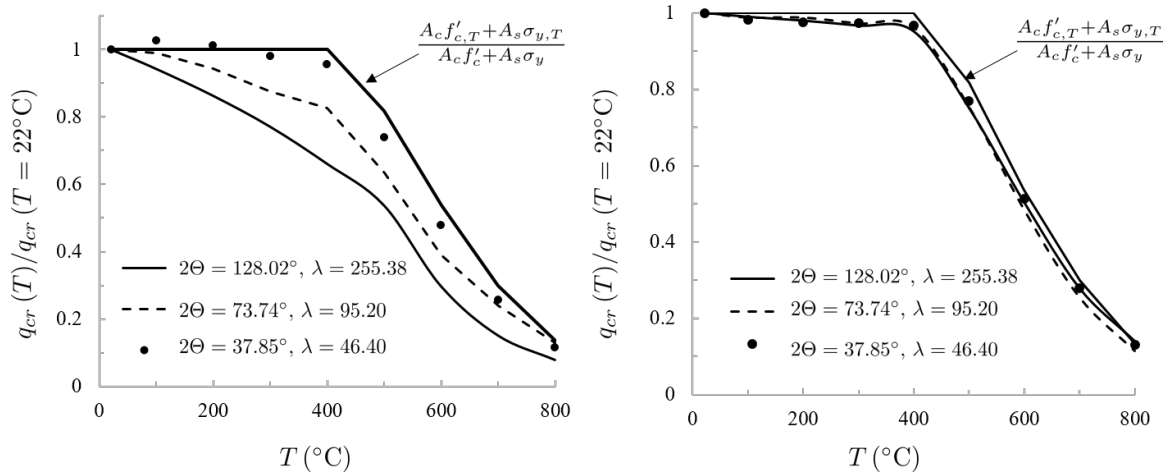


Figure 13: Inelastic out-of-plane buckling strength of fixed CFST arches at elevated temperatures subjected to uniformly distributed radial load (left) and central concentrated load (right). $\sigma_y = 300$ MPa, $f'_c = 32$ MPa, cross-section diameter 300 mm and steel tube thickness = 10 mm.

degradation. As with the case of uniform thermal loading, the effect of fire loading on buckling strength increases with slenderness. The results are depicted for two concrete strengths; 32 MPa and 40 MPa. Concrete compressive strength does not influence the rate of strength reduction. Additionally, the magnitudes of the out-of-plane critical loads at the two strength levels converge quickly indicating that out-of-plane buckling strength during fire loading is largely governed by stability. Behaviour varies when considering the central concentrated loading case. Buckling strength slightly deteriorates during the first approximately 20 mins of heating, see Figure 16. This is followed by the rapid drop in strength with decaying rate of change as observed in the uniformly distributed radial loading case. Slenderness is again shown to impact the effect of fire loading on the out-of-plane strength though to a lesser extent when compared to uniformly distributed radial loads.

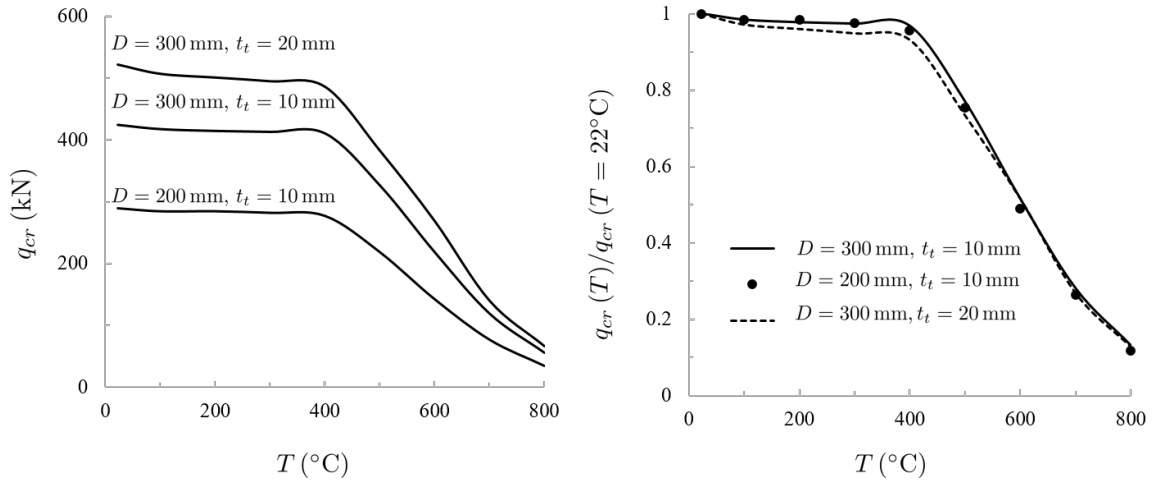


Figure 14: Inelastic out-of-plane buckling strength of fixed CFST arches under central concentrated loads and uniform temperature field. $2\Theta = 37.85^\circ$, $R = 9250$ mm, $\sigma_y = 300$ MPa and $f'_c = 32$ MPa.

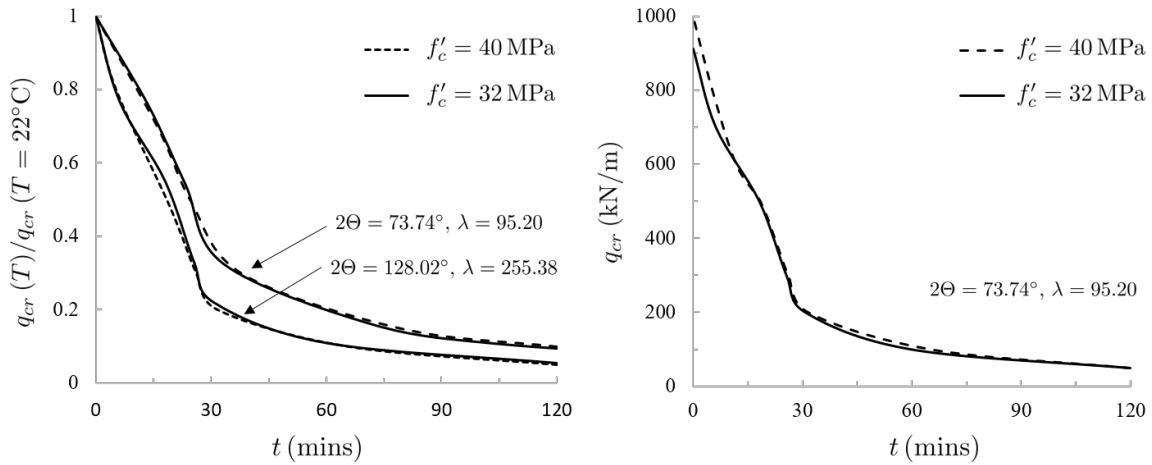


Figure 15: Inelastic out-of-plane buckling strength for fixed CFST arches under uniformly distributed radial load and standard ISO-834 fire. $\sigma_y = 300$ MPa, cross-section diameter 300 mm and steel tube thickness = 10 mm.

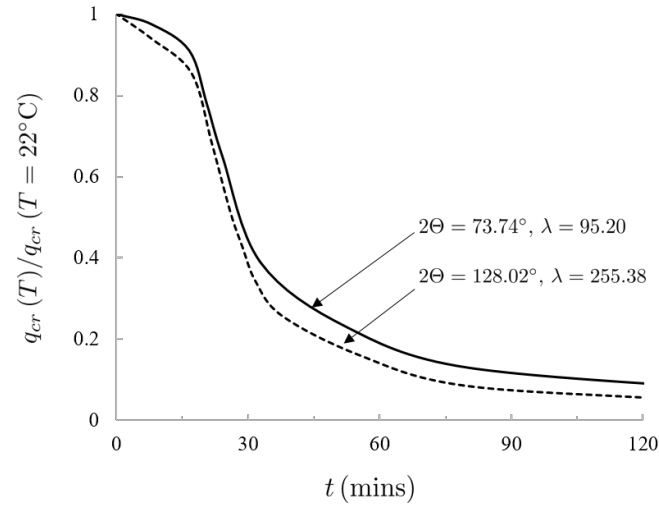


Figure 16: Inelastic out-of-plane buckling strength for fixed CFST arches under central concentrated loads and standard ISO-834 fire. $\sigma_y = 300$ MPa, cross-section diameter 300 mm and steel tube thickness = 10 mm.

5.3. Sensitivity analysis

The difference in buckling loads when adopting the ASCE concrete model, with and without TTS, and the EC2 model with TTS have been examined for the case of uniform temperature fields, see Figure 17. It can be seen that the ASCE and EC2 models lead to similar numerical results. When analysing the effect of TTS (ASCE model), it can be seen that TTS reduces buckling strength up significantly to approximately 500°C. Thus neglecting TTS may cause an over prediction of critical loads. Though the results converge at higher temperatures. Moreover, an increase in buckling load is observed at 100°C when neglecting TTS. This is due to the thermal strain exceeding the magnitude of mechanical strain in the steel tube caused by constant (or slightly reduced) elastic modulus and yield strength of steel within this range which leads to an increased buckling strength.

Hitherto, a perfect bond has been assumed between the steel tube and concrete core. The significance of the contact model is now investigated by comparing the inelastic out-of-plane buckling loads when adopting a frictionless or fully bonded contact. It is shown in Figure 18 that the contact model does not noticeably influence numerical results for the cases of uniform temperature fields and fire loading.

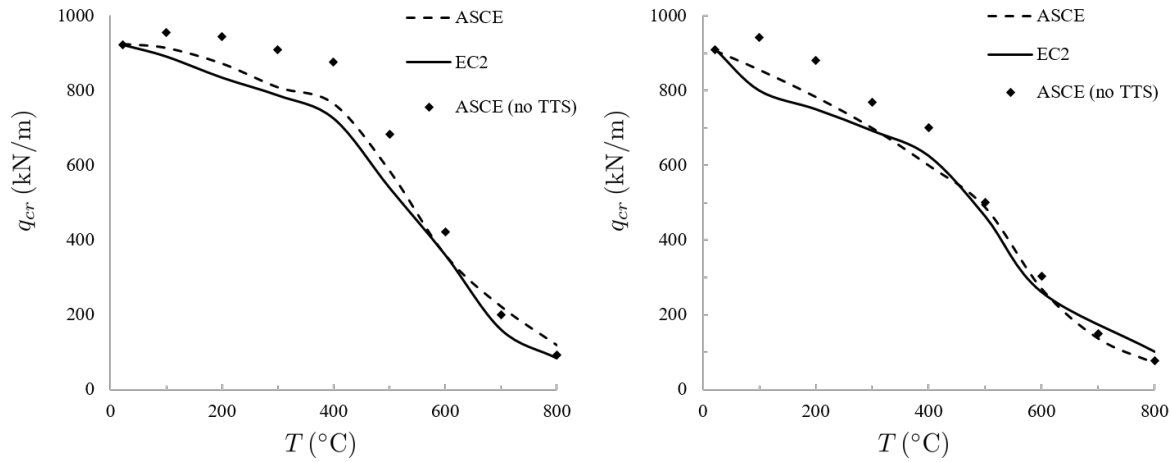


Figure 17: Inelastic out-of-plane buckling strength for fixed CFST arches under uniformly distributed radial load and constant temperature field. $2\Theta = 73.34^\circ$ and $R = 5000$ mm (left) and $2\Theta = 128.02^\circ$ and $R = 4450$ mm (right). $\sigma_y = 300$ GPa, $f'_c = 32$ MPa, cross-section diameter 300 mm and steel tube thickness = 10 mm.

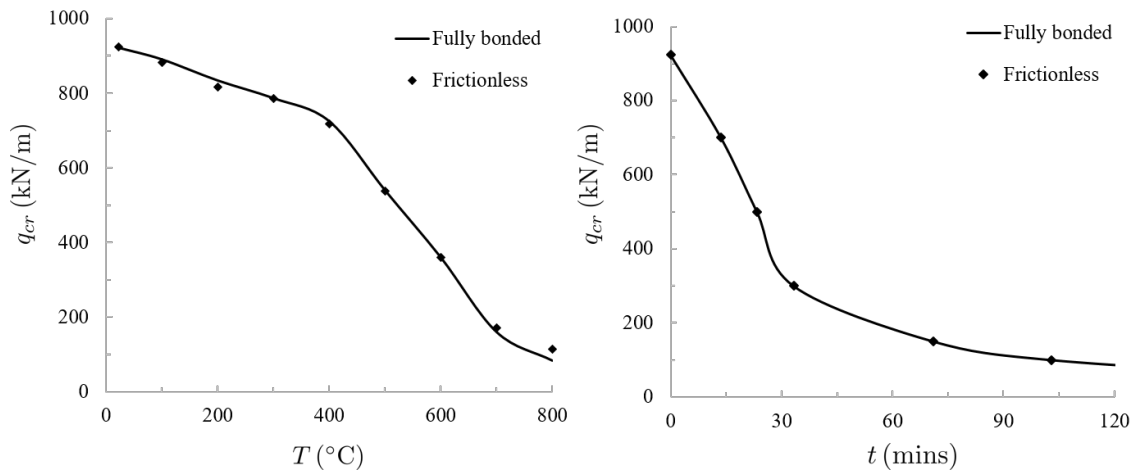


Figure 18: Effect of contact model at steel-concrete interface on out-of-plane inelastic buckling loads of fixed CFST arch under uniform thermal loading (left) and ISO-834 fire loading (right). $2\Theta = 73.34^\circ$, $R = 5000$ mm, $\sigma_y = 300$ GPa, $f'_c = 32$ MPa, cross-section diameter 300 mm and steel tube thickness = 10 mm.

6. Conclusions

The out-of-plane elastic and inelastic stability of concrete-filled steel tubular circular arches subjected to uniformly distributed radial loading or central concentrated loads and elevated temperature fields has been analysed in this paper. Energy methods are employed to conduct an elastic prebuckling and out-of-plane buckling analysis, resulting in numerical systems which may be solved for pinned or fixed-ended shallow arches. It was found that the elastic

buckling loads of CFST arches are sensitive to temperature, unlike in steel arches, and that the rate of buckling load degradation with temperature is independent of the supporting conditions. Basic creep strain was incorporated into the prebuckling analysis through discretisation of a fractional-viscoelastic rheological law. Time effects in transient heating scenarios were found to be negligible. The effect of elevated temperature and fire loading on the inelastic out-of-plane buckling loads of CFST arches was then studied with FE analysis. Validation of the FE model is made by comparison to the numerical system derived herein for the determination of elastic buckling loads. As with the elastic case, a decrease in lateral buckling loads with temperature rise is found when considering inelastic material behaviour. Effects of thermal and fire loading increased with arch slenderness for the uniformly distributed radial loading case. This can be elucidated by the failure mode; instability is triggered early in slender arches whereas stocky shallow arches are governed by material strength. For the case of central concentrated loads, arch slenderness did not influence the effects of thermal load on the buckling strength. Additionally, the significance of concrete material models and the assumption of the bond between the steel-concrete interface on numerical results was assessed. It was found that consideration of TTS has a substantial impact on buckling strength, however the difference between results when adopting the EC2 or ASCE concrete models is marginal. Adopting a perfect or frictionless bond at the steel-concrete interface did not noticeably influence behaviour. Future research works may consider varied loading and support conditions including elastic end supports and intermediate restraints through the arch length.

Acknowledgements

Victoria University is acknowledged for the financial support provided to the first author through the Vice Chancellor's Graduate Research Scholarship award.

References

- [1] M. A. Bradford, Y.-L. Pi, W. Qu, Time-dependent in-plane behaviour and buckling of concrete-filled steel tubular arches, *Engineering Structures* 33 (5) (2011) 1781 – 1795.
- [2] Y.-L. Pi, M. A. Bradford, N. Trahair, Y. Chen, A further study of flexural-torsional buckling of elastic arches, *International Journal of Structural Stability and Dynamics* 5 (02) (2005) 163–183.
- [3] Y.-L. Pi, N. Trahair, Non-linear buckling and postbuckling of elastic arches, *Engineering Structures* 20 (7) (1998) 571–579.
- [4] Y.-L. Pi, M. A. Bradford, B. Uy, In-plane stability of arches, *International Journal of Solids and Structures* 39 (1) (2002) 105–125.
- [5] S. Timoshenko, *Theory of elastic stability*, Engineering societies monographs, McGraw-Hill, 1961.
- [6] V. Z. Vlasov, *Thin-walled elastic beams*, National Technical Information Service, 1984.
- [7] C. H. Yoo, P. A. Pfeiffer, Buckling of curved beams with in-plane deformation, *Journal of Structural Engineering* 110 (2) (1984) 291–300.
- [8] P. Vacharajittiphan, N. S. Trahair, Flexural-torsional buckling of curved members, *Journal of the Structural Division* 101 (6) (1975) 1223–1238.
- [9] J. P. Papangelis, N. S. Trahair, Flexural-torsional buckling of arches, *Journal of Structural Engineering* 113 (4) (1987) 889–906.
- [10] S. Rajasekaran, S. Padmanabhan, Equations of curved beams, *Journal of engineering mechanics* 115 (5) (1989) 1094–1111.
- [11] N. S. Trahair, *Flexural-torsional buckling of structures*, Vol. 6, CRC Press, 1993.

- [12] Y. J. Kang, C. H. Yoo, Thin-walled curved beams. ii: analytical solutions for buckling of arches, *Journal of engineering mechanics* 120 (10) (1994) 2102–2125.
- [13] N.-H. Lim, Y.-J. Kang, Out of plane stability of circular arches, *International journal of mechanical sciences* 46 (8) (2004) 1115–1137.
- [14] Y.-L. Pi, J. Papangelis, N. S. Trahair, Prebuckling deformations and flexural-torsional buckling of arches, *Journal of Structural Engineering* 121 (9) (1995) 1313–1322.
- [15] Y.-L. Pi, M. A. Bradford, Effects of prebuckling deformations on the elastic flexural-torsional buckling of laterally fixed arches, *International journal of mechanical sciences* 46 (2) (2004) 321–342.
- [16] Y.-L. Pi, M. A. Bradford, F. Tin-Loi, Flexural-torsional buckling of shallow arches with open thin-walled section under uniform radial loads, *Thin-walled structures* 45 (3) (2007) 352–362.
- [17] Y.-L. Pi, M. A. Bradford, Effects of prebuckling analyses on determining buckling loads of pin-ended circular arches, *Mechanics Research Communications* 37 (6) (2010) 545 – 553.
- [18] M. A. Bradford, Y.-L. Pi, A new analytical solution for lateral-torsional buckling of arches under axial uniform compression, *Engineering Structures* 41 (2012) 14–23.
- [19] Y.-L. Pi, M. A. Bradford, Effects of prebuckling analyses on determining buckling loads of pin-ended circular arches, *Mechanics Research Communications* 37 (6) (2010) 545–553.
- [20] Y.-L. Pi, M. A. Bradford, G.-S. Tong, Elastic lateral–torsional buckling of circular arches subjected to a central concentrated load, *International Journal of Mechanical Sciences* 52 (6) (2010) 847–862.
- [21] Y.-L. Pi, M. A. Bradford, Lateral–torsional elastic buckling of rotationally restrained arches with a thin-walled section under a central concentrated load, *Thin-Walled Structures* 73 (2013) 18–26.
- [22] Y.-L. Pi, M. A. Bradford, B. Uy, A spatially curved-beam element with warping and wagner effects, *International journal for numerical methods in engineering* 63 (9) (2005) 1342–1369.
- [23] N. Trahair, Y. Pi, M. Clarke, J. Papangelis, Plastic design of steel arches, *Advances in Structural Engineering* 1 (1) (1997) 1–9.
- [24] Y.-L. Pi, N. S. Trahair, Out-of-plane inelastic buckling and strength of steel arches, *Journal of Structural Engineering* 124 (2) (1998) 174–183.
- [25] Y.-L. Pi, N. S. Trahair, Inelastic lateral buckling strength and design of steel arches, *Engineering structures* 22 (8) (2000) 993–1005.
- [26] Y.-L. Pi, M. A. Bradford, Out-of-plane strength design of fixed steel i-section arches, *Journal of structural engineering* 131 (4) (2005) 560–568.
- [27] M. A. Bradford, Y.-L. Pi, A. Liu, Out-plane elastic-plastic buckling strength of high-strength steel arches, *Journal of Structural Engineering* 144 (6) (2018) 04018053.
- [28] Y. Pi, M. Bradford, Inelastic buckling and strengths of steel i-section arches with central torsional restraints, *Thin-walled structures* 41 (7) (2003) 663–689.
- [29] Y.-L. Pi, M. A. Bradford, Elasto-plastic buckling and postbuckling of arches subjected to a central load, *Computers & structures* 81 (18) (2003) 1811–1825.
- [30] X. Wu, C. Liu, W. Wang, Y. Wang, In-plane strength and design of fixed concrete-filled steel tubular parabolic arches, *Journal of Bridge Engineering* 20 (12) (2015) 04015016.
- [31] Y.-L. Pi, C. Liu, M. A. Bradford, S. Zhang, In-plane strength of concrete-filled steel tubular circular arches, *Journal of Constructional Steel Research* 69 (1) (2012) 77–94.
- [32] A. Heidarpour, M. A. Bradford, K. A. Othman, Thermoelastic flexural-torsional buckling of steel arches, *Journal of Constructional Steel Research* 67 (12) (2011) 1806–1820.
- [33] A. Heidarpour, A. A. Abdullah, M. A. Bradford, Non-linear thermoelastic analysis of steel arch members subjected to fire, *Fire Safety Journal* 45 (3) (2010) 183–192.
- [34] Y.-L. Pi, M. A. Bradford, Thermoelastic lateral-torsional buckling of fixed slender beams under linear temperature gradient, *International Journal of Mechanical Sciences* 50 (7) (2008) 1183–1193.
- [35] Y. Pi, M. Bradford, W. Qu, Extremal thermoelastic buckling analysis of fixed slender beams, *Procedia Engineering* 14 (2011) 256–263.

- [36] Y.-L. Pi, M. A. Bradford, Out-of-plane buckling of beams having in-plane elastic restraints under gradient thermal action, *Journal of Engineering Mechanics* 142 (2) (2015) 04015080.
- [37] Y.-L. Pi, M. A. Bradford, In-plane thermoelastic behaviour and buckling of pin-ended and fixed circular arches, *Engineering Structures* 32 (1) (2010) 250–260.
- [38] Y.-L. Pi, M. A. Bradford, Nonlinear in-plane elastic buckling of shallow circular arches under uniform radial and thermal loading, *International Journal of Mechanical Sciences* 52 (1) (2010) 75–88.
- [39] J. Cai, Y. Xu, J. Feng, J. Zhang, Effects of temperature variations on the in-plane stability of steel arch bridges, *Journal of Bridge Engineering* 17 (2) (2010) 232–240.
- [40] J. Cai, Y. Xu, J. Feng, J. Zhang, In-plane elastic buckling of shallow parabolic arches under an external load and temperature changes, *Journal of Structural Engineering* 138 (11) (2012) 1300–1309.
- [41] B. Moghaddasie, I. Stanciulescu, Equilibria and stability boundaries of shallow arches under static loading in a thermal environment, *International Journal of Non-Linear Mechanics* 51 (2013) 132–144.
- [42] W. Jiang, D. Lu, Time-dependent reliability analysis of cfst arches for out-plane stability considering concrete creep, *Innovation, Communication and Engineering* 1 (2013) 465.
- [43] Y. Geng, G. Ranzi, Y.-T. Wang, Y.-Y. Wang, Out-of-plane creep buckling analysis on slender concrete-filled steel tubular arches, *Journal of Constructional Steel Research* 140 (2018) 174–190.
- [44] Y. Bouras, Z. Vrcelj, Thermal in-plane stability of concrete-filled steel tubular arches, *International Journal of Mechanical Sciences* 163 (2019) 105130.
- [45] V. Kodur, Properties of concrete at elevated temperatures, *ISRN Civil Engineering* 2014.
- [46] Lie, T.T, Structural fire protection, American Society of Civil Engineers (ASCE), 1992.
- [47] EN 1993 1-2, Eurocode 3: Design of steel structures, Part 1-2, Structural fire design, European Committee for Standardization, 2005.
- [48] T. Gernay, J.-M. Franssen, A comparison between explicit and implicit modelling of transient creep strain in concrete uniaxial constitutive relationships, in: *Proceedings of the fire and materials 2011 conference*, Interscience Communications Ltd, 2011, pp. 405–416.
- [49] EN 1992 1-2, Eurocode 2: Design of concrete structures, Part 1-2, Structural fire design, European Committee for Standardization, 2004.
- [50] Y. Bouras, D. Zorica, T. Atanacković, Z. Vrcelj, A non-linear thermo-viscoelastic rheological model based on fractional derivatives for high temperature creep in concrete, Unpublished.
- [51] T. Lie, Fire resistance of circular steel columns filled with bar-reinforced concrete, *Journal of Structural Engineering* 120 (5) (1994) 1489–1509.
- [52] ANSYS Workbench, Release 17.2, Ansys Inc, Canonsburg, PA, 2016.

7.4 Concluding Remarks

This chapter presented an investigation into the effects of elevated temperatures on the elastic and inelastic out-of-plane buckling strength of CFST arches. A novel numerical model was derived for the determination of flexural-torsional buckling loads of CFST arches subjected to uniformly distributed radial loads or central concentrated loads and with pinned or fixed ends. Additionally, the significance of basic creep strain on the thermo-elastic response was examined. FE analysis was employed to investigate the inelastic buckling strength of CFST arches under uniform thermal loading and fire loading and to conduct parametric studies. The following conclusions have been drawn from this chapter;

1. Elastic flexural-torsional buckling loads significantly decrease with rise in uniform thermal load;
2. The rate of elastic buckling load deterioration with temperature rise was found to be only dependant on the cross-section size and steel-concrete ratio, and is independent of other parameters including the type of end supports, arch slenderness/included angle and mechanical loading type;
3. Basic creep strain has a negligible effect on the elastic prebuckling behaviour of CFST arches under transient heating;
4. The dominant failure mode may transition from flexural-torsional buckling to in-plane limit instability as temperature increases in slender shallow arches;
5. For the case of uniformly distributed radial loading, the effect of temperature on the inelastic buckling strength increases noticeably with arch slenderness, indicating that instability governs buckling strength;

6. For the case of central concentrated loads, reduction of buckling strength with temperature was not influenced by arch slenderness and followed the squash load. Thus, section capacity governs the strength of CFST arches for this loading scenario; and
7. The contact model for the steel-concrete interface did not influence out-of-plane buckling strength.

Chapter 8

Conclusions

8.1 Summary

Presented in this research project is a comprehensive analytical and numerical investigation into the response and failure modes of circular concrete and CFST arches subjected to combined mechanical loading and elevated temperature fields. This research was necessitated by the increasing construction of CFST arch bridges and the pre-existing lack of knowledge on the subject.

In order to analyse the significance of time-temperature coupling on the thermal behaviour of concrete and CFST arches, a novel viscoelastic rheological model based on

fractional-derivatives was developed for basic creep in concrete at extreme elevated temperatures. Fractional viscoelastic models are able to accurately reflect material behaviour with few model parameters and can efficiently model time-varying stress and temperature conditions. The model parameters were calibrated using existing experimental data in the literature resulting in creep strain being governed a temperature dependant variable-order fractional differential equation. Discretisation of the variable-order fractional differential equations was conducted using finite-differences in order to solve for creep strain in the following analytical and numerical analyses.

Subsequently, the thermo-elastic prebuckling response and in-plane buckling behaviour of shallow concrete arches was examined. Energy methods and variational principles were employed to derive the non-linear equilibrium equations and buckling equilibrium equations respectively. TTS and basic creep strain were considered, the latter by adopting the elastic-viscoelastic analogy. It was found that the axial force and bending moment greatly increased with temperature level, and that the arch displaced downwards during heating. Moreover, thermal loading was found to significantly reduce the elastic in-plane anti-symmetric buckling and limit instability loads. These effects were greatly enhanced when TTS was considered, whilst incorporation basic creep strain resulted in a smaller influence on thermal response. Criteria delineating between buckling loads were analytically defined, and found to be temperature dependant. Consequently, a change in the governing buckling mode may occur during heating. This study was then extended by investigating the inelastic response and in-plane failure modes of shallow concrete arches subjected to mechanical and fire loading. A FE model was developed which considered material and geometric non-linearity. Verification of the FE model was made by comparison to a novel non-discretisation based numeral model derived for the inelastic analysis of concrete arches subjected to mechanical loads uniform temperature level. Further validation was achieved by analysing the inelastic buckling loads predicted by the FE analysis and the tangent modulus theory - employed through the

use of the derived numerical model and the closed-form solutions for the elastic buckling loads obtained previously. Extensive parametric studies were performed which assessed the influence of parameters on fire resistance time and failure modes. Overall it was observed that fire loading can trigger anti-symmetric bifurcation buckling in shallow concrete arches and that anti-symmetric buckling is the governing in-plane failure mode.

Stability of CFST arches were the focus of proceeding works. Their non-linear elastic and inelastic thermal behaviour and in-plane stability were analytically and numerically investigated. Closed-form expressions were obtained for the prebuckling and in-plane buckling loads of pinned or fixed-ended shallow CFST arches under uniformly distributed radial loading and elevated temperature fields. An original numerical model in the form of a BVP was also derived for the elastic or inelastic prebuckling analysis of shallow and deep CFST arches. The numerical model can be applied to boundary conditions including pinned, fixed or crown-pinned arches. As with concrete arches, thermal loading greatly influenced the prebuckling stresses and displacements and reduced the in-plane elastic buckling loads - substantially when TTS was considered. FE analysis was utilised to verify the derived models and to subsequently analyse the inelastic in-plane buckling strength of CFST arches under uniform temperature fields and fire loading. Extensive parametric studies were conducted to highlight the primary factors governing fire resistance times. Additionally, sensitivity analyses explored the influence of material and contact models on arch behaviour. Out-of-plane stability of CFST arches subjected to mechanical and thermal loading was then studied. Energy methods were employed to formulate a numerical model to determine the elastic flexural-torsional buckling loads. The model is dependant on the prebuckling state which can be numerically solved using the aforementioned BVP. By changing the boundary conditions and two constants, the model can be applied to uniformly distributed radial loading or central concentrated loading cases. The rate of elastic buckling strength deterioration was

shown to be independent on the end support conditions and arch geometry, only varying with cross-section parameters. Furthermore, the elastic prebuckling analysis was generalised to include the previously derived fractional derivative-based creep law. The significance of basic creep strain on the thermal response for transient thermal loading was found to be small. Assessment of inelastic flexural-torsional buckling strength was conducted through the development of a FE model. Comparison between the derived numerical model and the FE analysis showed a high level of agreement. Parametric studies revealed that the effect of temperature on buckling strength increased with arch slenderness for the loading case of uniformly distributed radial loading. Whereas inelastic strength of CFST arches subjected to central loads and elevated temperature fields were governed primarily by material strength. The impact of fire loading on the out-of-plane buckling strength was also examined for both mechanical loading cases.

8.2 Novel Contributions

Significant contributions have been made by this research thesis in the to subject area of thermal stability of structural arches and concrete creep modelling. Research outcomes are stated as follows:

1. Novel fractional viscoelastic rheological model developed for high temperature basic creep in concrete;
2. Derived non-linear equilibrium and in-plane buckling equilibrium equations of shallow concrete arches subjected to uniformly distributed radial loads and uniform temperature fields in addition to defining parameters delineating between buckling modes;

3. Illustrated the influence of thermal loads on the response and in-plane stability boundaries of shallow concrete arches whilst analysing the contributions of TTS and basic creep strain;
4. Formulated an original non-discretization mechanical based numerical model for the inelastic analysis of shallow concrete arches under mechanical loading and uniform temperature fields;
5. Discovered that fire loading may trigger anti-symmetric buckling in shallow concrete arches, and that for concrete arches it is the governing in-plane failure mode;
6. Developed analytical expressions for the non-linear elastic prebuckling state and anti-symmetric and symmetric buckling loads of CFST arches under uniformly distributed radial loading and non-uniform thermal loading
7. Proposed an original non-discretization mechanical based numerical model for the non-linear elastic and inelastic analysis of shallow and deep CFST arches with pinned, fixed or crown-pinned supports under mechanical loading and non-uniform temperature fields;
8. Derived numerical model to determine the elastic flexural-torsional buckling loads of shallow CFST arches at elevated temperatures with pinned or fixed ends and subjected to uniformly distributed radial loads or central concentrated loads;
9. Demonstrated the impact of basic creep strain in the concrete core on the thermal response of CFST arches subjected to short-term heating; and
10. Determined the primary factors governing the effect of elevated temperatures on the in-plane and out-of-plane buckling strength of CFST arches under uniform thermal or fire loading.

8.3 Further Research

In Chapter 2, gaps in the knowledge area of arch stability were identified one of which formed the research objectives of this thesis. The remaining knowledge gaps may be considered in future research projects. The following is a set of recommendations to further the work outlined herein:

1. Effects of extreme elevated temperatures on non-circular concrete and CFST arches can be investigated for example parabolic profiles;
2. Generalisations of the derived analytical and numerical models may be made to study varied loading and boundary conditions including vertically distributed loading, quarter-point concentrated loads, dynamic loading and elastic end supports;
3. Concrete spalling was not considered in the inelastic analysis of concrete arches subjected to fire loading. In-plane buckling strength may be reduced in slender concrete arches due to the possible occurrence of spalling;
4. All analyses were limited to uniform thermal and fire loading through the arch length. Non-uniform thermal loading and localised temperature fields may induce great magnitudes and asymmetric distributions of bending moment consequently leading to premature anti-symmetric buckling; and
5. Interaction effects between local buckling of the steel tube and global buckling of the CFST arch were not considered in this study and may be addressed in future works.

References

- [1] R. Ziemian, *Guide to Stability Design Criteria for Metal Structures*, John Wiley Sons, 2010.
- [2] N. S. Trahair, *Flexural-torsional buckling of structures*, Vol. 6, CRC Press, 1993.
- [3] G. J. Simitzes, D. H. Hodges, *Fundamentals of structural stability*, Butterworth-Heinemann, 2006.
- [4] Y.-L. Pi, M. A. Bradford, Nonlinear in-plane elastic buckling of shallow circular arches under uniform radial and thermal loading, *International Journal of Mechanical Sciences* 52 (1) (2010) 75–88.
- [5] M. A. Bradford, Y.-L. Pi, W. Qu, Time-dependent in-plane behaviour and buckling of concrete-filled steel tubular arches, *Engineering Structures* 33 (5) (2011) 1781 – 1795.
- [6] W. Jiang, D. Lu, In-plane creep buckling of concrete-filled steel tubular arches, *Transactions of Tianjin University* 20 (3) (2014) 168–173.
- [7] J. Kimeu, *Fractional calculus: Definitions and applications*, Master’s thesis, Western Kentucky University (2009).
- [8] A. Loverro, *Fractional calculus: history, definitions and applications for the engineer*, Report, Department of Aerospace and Mechanical Engineering, Notre Dame, IN 46556.
- [9] T. Pritz, Analysis of four-parameter fractional derivative model of real solid materials, *Journal of Sound and Vibration* 195 (1) (1996) 103 – 115.
- [10] Z. Bažant, L. Cedolin, *Stability of Structures: Elastic, Inelastic, Fracture and Damage Theories*, World Scientific, 2010.

- [11] R. Bagley, P. Torvik, On the fractional calculus model of viscoelastic behavior, *Journal of Rheology* 30 (1) (1986) 133–155.
- [12] M. Garlock, I. Paya-Zaforteza, V. Kodur, L. Gu, Fire hazard in bridges: Review, assessment and repair strategies, *Engineering Structures* 35 (2012) 89–98.
- [13] J.-C. Dotreppe, S. Majkut, J.-M. Franssen, Failure of a tied-arch bridge submitted to a severe localized fire, in: *IABSE Symposium Report, Vol. 90, International Association for Bridge and Structural Engineering*, 2005, pp. 15–22.
- [14] New York State Department of Transportation, *Bridge fire incidents in New York State* (2008).
- [15] N. Casey, Fire incident data for australian road tunnels, *Fire safety journal* 111 (2020) 102909.
- [16] T. Atanacković, *Stability theory of elastic rods, Vol. 1*, World scientific, 1997.
- [17] S. Timoshenko, *Theory of elastic stability*, Engineering societies monographs, McGraw-Hill, 1961.
- [18] V. Z. Vlasov, *Thin-walled elastic beams*, National Technical Information Service, 1984.
- [19] A. Gjelsvik, S. Bodner, The energy criterion and snap buckling of arches, *Journal of the Engineering Mechanics* 88 (1962) 87–134.
- [20] W. J. Austin, In-plane bending and buckling of arches, *Journal of the Structural Division* 97 (5) (1971) 1575–1592.
- [21] G. J. Simitses, J. Hutchinson, An introduction to the elastic stability of structures, *Journal of Applied Mechanics* 43 (1976) 383.
- [22] H. L. Schreyer, E. F. Masur, Buckling of shallow arches, *Journal of the Engineering Mechanics Division* 92 (4) (1966) 1–20.

- [23] J. F. Dickie, P. Broughton, Stability criteria for shallow arches, *Journal of the Engineering Mechanics Division* 97 (3) (1971) 951–965.
- [24] T. V. Galambos, *Guide to stability design criteria for metal structures*, John Wiley & Sons, 1998.
- [25] B. G. Johnston, *Guide to stability design criteria for metal structures*, John Wiley & Sons, 1976.
- [26] C. Japan, *Handbook of structural stability*, CORONA, Tokyo.
- [27] D. DaDeppo, R. Schmidt, Stability of an arch under combined loads; bibliography on stability of arches, *Industrial Mathematics, Journal of the IMS* 20 (Part 2) (1970) 71–89.
- [28] Y. Fukumoto, *Structural Stability Design, Steel and Composite Structures*, Pergamon, 1996.
- [29] Y.-L. Pi, N. Trahair, Non-linear buckling and postbuckling of elastic arches, *Engineering Structures* 20 (7) (1998) 571–579.
- [30] Y.-L. Pi, M. A. Bradford, B. Uy, In-plane stability of arches, *International Journal of Solids and Structures* 39 (1) (2002) 105–125.
- [31] A. K. Noor, J. M. Peters, Mixed models and reduced/selective integration displacement models for nonlinear analysis of curved beams, *International Journal for Numerical Methods in Engineering* 17 (4) (1981) 615–631.
- [32] H. Stolarski, T. Belytschko, Membrane locking and reduced integration for curved elements, *Journal of Applied Mechanics* 49 (1) (1982) 172–176.
- [33] P. R. Calhoun, D. A. DaDeppo, Nonlinear finite element analysis of clamped arches, *Journal of Structural Engineering* 109 (3) (1983) 599–612.

- [34] Z. Elias, K.-L. Chen, Nonlinear shallow curved-beam finite element, *Journal of engineering mechanics* 114 (6) (1988) 1076–1087.
- [35] R. K. Wen, B. Suhendro, Nonlinear curved-beam element for arch structures, *Journal of structural Engineering* 117 (11) (1991) 3496–3515.
- [36] R. K. Wen, J. Lange, Curved beam element for arch buckling analysis, *Journal of the Structural Division* 107 (11) (1981) 2053–2069.
- [37] Y. J. Kang, C. H. Yoo, Thin-walled curved beams. ii: analytical solutions for buckling of arches, *Journal of engineering mechanics* 120 (10) (1994) 2102–2125.
- [38] Y.-L. Pi, N. S. Trahair, Three-dimensional nonlinear analysis of elastic arches, *Engineering structures* 18 (1) (1996) 49–63.
- [39] Y.-L. Pi, M. A. Bradford, Effects of prebuckling analyses on determining buckling loads of pin-ended circular arches, *Mechanics Research Communications* 37 (6) (2010) 545 – 553.
- [40] M. A. Bradford, Y.-L. Pi, B. Uy, In-plane Stability of Arches Under a Central Concentrated Load, University of New South Wales, School of Civil Engineering, 2002.
- [41] M. Rubin, Buckling of elastic shallow arches using the theory of a cosserat point, *Journal of engineering mechanics* 130 (2) (2004) 216–224.
- [42] D. H. Hodges, Non-linear inplane deformation and buckling of rings and high arches, *International Journal of Non-Linear Mechanics* 34 (4) (1999) 723–737.
- [43] T. Gengshu, Y.-L. Pi, M. A. Bradford, F. Tin-Loi, In-plane nonlinear buckling analysis of deep circular arches incorporating transverse stresses, *Journal of engineering mechanics* 134 (5) (2008) 362–373.
- [44] J. P. Papangelis, N. S. Trahair, Flexural-torsional buckling of arches, *Journal of Structural Engineering* 113 (4) (1987) 889–906.

- [45] S. Rajasekaran, S. Padmanabhan, Equations of curved beams, *Journal of engineering mechanics* 115 (5) (1989) 1094–1111.
- [46] M. M. Attard, J. Zhu, D. Kellermann, In-plane buckling of circular arches and rings with shear deformations, *Archive of Applied Mechanics* 83 (8) (2013) 1145–1169.
- [47] J. Zhu, M. M. Attard, D. C. Kellermann, In-plane nonlinear buckling of circular arches including shear deformations, *Archive of Applied Mechanics* 84 (12) (2014) 1841–1860.
- [48] J. Zhu, M. M. Attard, D. C. Kellermann, In-plane nonlinear buckling of funicular arches, *International Journal of Structural Stability and Dynamics* (2014) 1450073.
- [49] J. Moon, K.-Y. Yoon, T.-H. Lee, H.-E. Lee, In-plane elastic buckling of pin-ended shallow parabolic arches, *Engineering Structures* 29 (10) (2007) 2611–2617.
- [50] J. Cai, J. Feng, Y. Chen, L. Huang, In-plane elastic stability of fixed parabolic shallow arches, *Science in China Series E: Technological Sciences* 52 (3) (2009) 596–602.
- [51] M. A. Bradford, Y.-L. Pi, G. Yang, X.-C. Fan, Effects of approximations on nonlinear in-plane elastic buckling and postbuckling analyses of shallow parabolic arches, *Engineering Structures* 101 (2015) 58–67.
- [52] M. A. Bradford, T. Wang, Y. Pi, R. Gilbert, In-plane stability of parabolic arches with horizontal spring supports. i: Theory, *Journal of Structural Engineering* 133 (8) (2007) 1130–1137.
- [53] M. A. Bradford, Long-span shallow steel arches subjected to fire loading, *Advances in Structural Engineering* 13 (3) (2010) 501–511.

- [54] J. Cai, J. Feng, Buckling of parabolic shallow arches when support stiffens under compression, *Mechanics Research Communications* 37 (5) (2010) 467–471.
- [55] J. Cai, Y. Xu, J. Feng, J. Zhang, Effects of temperature variations on the in-plane stability of steel arch bridges, *Journal of Bridge Engineering* 17 (2) (2010) 232–240.
- [56] Y. L. Pi, M. A. Bradford, F. Tin-Loi, Nonlinear analysis and buckling of elastically supported circular shallow arches, *International Journal of Solids and Structures* 44 2401–2425, *international Journal of Solids and Structures* ISSN = 0020-7683, DOI = 10.1016/j.ijsolstr.2006.07.011, year = 2007, type = Journal Article.
- [57] T. Wang, M. A. Bradford, R. I. Gilbert, Y.-L. Pi, In-plane stability of parabolic arches with horizontal spring supports. ii: Experiments, *Journal of Structural Engineering* 133 (8) (2007) 1138–1145.
- [58] Y.-L. Pi, M. A. Bradford, F. Tin-Loi, Non-linear in-plane buckling of rotationally restrained shallow arches under a central concentrated load, *International Journal of Non-Linear Mechanics* 43 (1) (2008) 1–17.
- [59] Y.-L. Pi, M. A. Bradford, Non-linear in-plane postbuckling of arches with rotational end restraints under uniform radial loading, *International Journal of Non-Linear Mechanics* 44 (9) (2009) 975–989.
- [60] L. P. Kiss, In-plane buckling of rotationally restrained heterogeneous shallow arches subjected to a concentrated force at the crown point, *Journal of Computational and Applied Mechanics* 9 (2) (2014) 171–199.
- [61] Y.-L. Pi, M. A. Bradford, Non-linear in-plane analysis and buckling of pinned–fixed shallow arches subjected to a central concentrated load, *International Journal of Non-Linear Mechanics* 47 (4) (2012) 118–131.

- [62] Y.-L. Pi, M. A. Bradford, Non-linear buckling and postbuckling analysis of arches with unequal rotational end restraints under a central concentrated load, *International Journal of Solids and Structures* 49 (26) (2012) 3762–3773.
- [63] R. H. Plaut, Buckling of shallow arches with supports that stiffen when compressed, *Journal of Engineering Mechanics* 116 (4) (1990) 973–976.
- [64] J. Cai, J. Feng, Effect of support stiffness on stability of shallow arches, *International Journal of Structural Stability and Dynamics* 10 (05) (2010) 1099–1110.
- [65] Y.-L. Pi, M. A. Bradford, N. Trahair, Y. Chen, A further study of flexural-torsional buckling of elastic arches, *International Journal of Structural Stability and Dynamics* 5 (02) (2005) 163–183.
- [66] C. H. Yoo, P. A. Pfeiffer, Buckling of curved beams with in-plane deformation, *Journal of Structural Engineering* 110 (2) (1984) 291–300.
- [67] P. Vacharajittiphan, N. S. Trahair, Flexural-torsional buckling of curved members, *Journal of the Structural Division* 101 (6) (1975) 1223–1238.
- [68] N.-H. Lim, Y.-J. Kang, Out of plane stability of circular arches, *International journal of mechanical sciences* 46 (8) (2004) 1115–1137.
- [69] Y.-L. PI, M. A. Bradford, N. Trahair, Y. Chen, Closure for discussion of:” a further study of flexural-torsional buckling of elastic arches”, *International Journal of Structural Stability and Dynamics* 6 (01) (2006) 157–162.
- [70] M. A. Bradford, Y.-L. Pi, Elastic flexural-torsional instability of structural arches under hydrostatic pressure, *International Journal of Mechanical Sciences* 50 (2) (2008) 143–151.
- [71] Y.-L. Pi, M. A. Bradford, Elastic flexural–torsional buckling of fixed arches, *The Quarterly Journal of Mechanics and Applied Mathematics* 57 (4) (2004) 551–569.

- [72] M. A. Bradford, Y.-L. Pi, Flexural–torsional buckling of fixed steel arches under uniform bending, *Journal of constructional steel research* 62 (1) (2006) 20–26.
- [73] C. Dou, Y.-L. Guo, Y.-L. Pi, S.-Y. Zhao, M. A. Bradford, Effects of shape functions on flexural–torsional buckling of fixed circular arches, *Engineering Structures* 59 (2014) 238–247.
- [74] F. Tokarz, R. S. Sandhu, Lateral-torsion buckling of parabolic arches, *Journal of the Structural Division* 98 (5) (1972) 1161–1179.
- [75] E. Tufekci, O. Dogruer, Exact solution of out-of-plane problems of an arch with varying curvature and cross section, *Journal of engineering mechanics* 132 (6) (2006) 600–609.
- [76] J. Moon, K.-Y. Yoon, T.-H. Lee, H.-E. Lee, Out-of-plane buckling of arches with varying curvature, *KSCE Journal of Civil Engineering* 13 (6) (2009) 441–451.
- [77] M. A. Bradford, Y.-L. Pi, Elastic flexural-torsional buckling of discretely restrained arches, *Journal of Structural Engineering* 128 (6) (2002) 719–727.
- [78] Y.-L. Pi, M. A. Bradford, Elastic flexural-torsional buckling of continuously restrained arches, *International journal of solids and structures* 39 (8) (2002) 2299–2322.
- [79] Y.-L. Guo, S.-Y. Zhao, C. Dou, Y.-L. Pi, Out-of-plane elastic buckling of circular arches with elastic end restraints, *Journal of Structural Engineering* 140 (10) (2014) 04014071.
- [80] Y.-L. Guo, S.-Y. Zhao, M. A. Bradford, Y.-L. Pi, Threshold stiffness of discrete lateral bracing for out-of-plane buckling of steel arches, *Journal of Structural Engineering* (2015) 04015004.

- [81] Y.-L. Pi, J. Papangelis, N. S. Trahair, Prebuckling deformations and flexural-torsional buckling of arches, *Journal of Structural Engineering* 121 (9) (1995) 1313–1322.
- [82] Y.-L. Pi, M. A. Bradford, Effects of prebuckling deformations on the elastic flexural-torsional buckling of laterally fixed arches, *International journal of mechanical sciences* 46 (2) (2004) 321–342.
- [83] Y.-L. Pi, M. A. Bradford, F. Tin-Loi, Flexural-torsional buckling of shallow arches with open thin-walled section under uniform radial loads, *Thin-walled structures* 45 (3) (2007) 352–362.
- [84] Y.-L. Pi, M. A. Bradford, Effects of prebuckling analyses on determining buckling loads of pin-ended circular arches, *Mechanics Research Communications* 37 (6) (2010) 545–553.
- [85] M. A. Bradford, Y.-L. Pi, A new analytical solution for lateral-torsional buckling of arches under axial uniform compression, *Engineering Structures* 41 (2012) 14–23.
- [86] Y.-L. Pi, M. A. Bradford, G.-S. Tong, Elastic lateral-torsional buckling of circular arches subjected to a central concentrated load, *International Journal of Mechanical Sciences* 52 (6) (2010) 847–862.
- [87] Y.-L. Pi, M. A. Bradford, Lateral-torsional elastic buckling of rotationally restrained arches with a thin-walled section under a central concentrated load, *Thin-Walled Structures* 73 (2013) 18–26.
- [88] Y.-L. Pi, M. A. Bradford, B. Uy, A spatially curved-beam element with warping and wagner effects, *International journal for numerical methods in engineering* 63 (9) (2005) 1342–1369.
- [89] N. Trahair, Y. Pi, M. Clarke, J. Papangelis, Plastic design of steel arches, *Advances in Structural Engineering* 1 (1) (1997) 1–9.

- [90] A. Mirmiran, A. M. Amde, Inelastic buckling of prestressed sandwich or homogeneous arches, *Journal of Structural Engineering* 119 (9) (1993) 2733–2743.
- [91] Y.-L. Pi, N. Trahair, In-plane inelastic buckling and strengths of steel arches, *Journal of Structural Engineering* 122 (7) (1996) 734–747.
- [92] J. Moon, K.-Y. Yoon, T.-H. Lee, H.-E. Lee, In-plane strength and design of parabolic arches, *Engineering Structures* 31 (2) (2009) 444–454.
- [93] Y.-L. Pi, N. S. Trahair, In-plane buckling and design of steel arches, *Journal of Structural Engineering* 125 (11) (1999) 1291–1298.
- [94] Y.-L. Pi, M. A. Bradford, In-plane strength and design of fixed steel i-section arches, *Engineering structures* 26 (3) (2004) 291–301.
- [95] Y.-L. Pi, N. S. Trahair, Out-of-plane inelastic buckling and strength of steel arches, *Journal of Structural Engineering* 124 (2) (1998) 174–183.
- [96] Y.-L. Pi, N. S. Trahair, Inelastic lateral buckling strength and design of steel arches, *Engineering structures* 22 (8) (2000) 993–1005.
- [97] Y.-L. Pi, M. A. Bradford, Out-of-plane strength design of fixed steel i-section arches, *Journal of structural engineering* 131 (4) (2005) 560–568.
- [98] M. A. Bradford, Y.-L. Pi, A. Liu, Out-plane elastic-plastic buckling strength of high-strength steel arches, *Journal of Structural Engineering* 144 (6) (2018) 04018053.
- [99] Y. Pi, M. Bradford, Inelastic buckling and strengths of steel i-section arches with central torsional restraints, *Thin-walled structures* 41 (7) (2003) 663–689.
- [100] X. Wu, C. Liu, W. Wang, Y. Wang, In-plane strength and design of fixed concrete-filled steel tubular parabolic arches, *Journal of Bridge Engineering* 20 (12) (2015) 04015016.

- [101] Y.-L. Pi, C. Liu, M. A. Bradford, S. Zhang, In-plane strength of concrete-filled steel tubular circular arches, *Journal of Constructional Steel Research* 69 (1) (2012) 77–94.
- [102] Y.-L. Pi, M. A. Bradford, Elasto-plastic buckling and postbuckling of arches subjected to a central load, *Computers & structures* 81 (18) (2003) 1811–1825.
- [103] D. La Poutré, R. Spoorenberg, H. Snijder, J. Hoenderkamp, Out-of-plane stability of roller bent steel arches an experimental investigation, *Journal of Constructional Steel Research* 81 (2013) 20–34.
- [104] C. Dou, Y.-L. Guo, S.-Y. Zhao, Y.-L. Pi, Experimental investigation into flexural-torsional ultimate resistance of steel circular arches, *Journal of Structural Engineering* (2015) 04015006.
- [105] Y.-L. Guo, S.-Y. Zhao, Y.-L. Pi, M. A. Bradford, C. Dou, An experimental study on out-of-plane inelastic buckling strength of fixed steel arches, *Engineering Structures* 98 (2015) 118–127.
- [106] M. A. Bradford, In-plane nonlinear behaviour of circular pinned arches with elastic restraints under thermal loading, *International Journal of Structural Stability Dynamics* 6 (2) (2006) 163–177.
- [107] Y.-L. Pi, M. A. Bradford, In-plane thermoelastic behaviour and buckling of pin-ended and fixed circular arches, *Engineering Structures* 32 (1) (2010) 250–260.
- [108] Y. L. Pi, M. A. Bradford, *Thermoelastic behaviour of elastically restrained tubular steel arches*, Taylor Francis, 2008, pp. 659–667.
- [109] A. Heidarpour, A. A. Abdullah, M. A. Bradford, Non-linear inelastic analysis of steel arches at elevated temperatures, *Journal of Constructional Steel Research* 66 (4) (2010) 512–519.

- [110] B. Moghaddasie, I. Stanciulescu, Equilibria and stability boundaries of shallow arches under static loading in a thermal environment, *International Journal of Non-Linear Mechanics* 51 (2013) 132–144.
- [111] Y.-L. Pi, M. A. Bradford, Effects of nonlinearity and temperature field on in-plane behaviour and buckling of crown-pinned steel arches, *Engineering Structures* 74 (2014) 1–12.
- [112] Y.-L. Pi, M. A. Bradford, Nonlinear thermoelastic buckling of pin-ended shallow arches under temperature gradient, *Journal of engineering mechanics* 136 (8) (2010) 960–968.
- [113] J. Cai, Y. Xu, J. Feng, J. Zhang, In-plane elastic buckling of shallow parabolic arches under an external load and temperature changes, *Journal of Structural Engineering* 138 (11) (2012) 1300–1309.
- [114] A. Heidarpour, A. A. Abdullah, M. A. Bradford, Non-linear thermoelastic analysis of steel arch members subjected to fire, *Fire Safety Journal* 45 (3) (2010) 183–192.
- [115] A. Heidarpour, T. H. Pham, M. A. Bradford, Nonlinear thermoelastic analysis of composite steelconcrete arches including partial interaction and elevated temperature loading, *Engineering Structures* 32 (10) (2010) 3248–3257.
- [116] H. Asgari, M. Bateni, Y. Kiani, M. Eslami, Non-linear thermo-elastic and buckling analysis of fgm shallow arches, *Composite Structures* 109 (2014) 75–85.
- [117] H. Asgari, M. Eslami, Nonlinear thermal buckling analysis of fgm shallow arches under linear temperature gradient, in: *ASME 2014 12th Biennial Conference on Engineering Systems Design and Analysis*, American Society of Mechanical Engineers, 2014, pp. V001T04A003–V001T04A003.
- [118] M. Bateni, M. Eslami, Effect of temperature gradient on the mechanical buckling resistance of fgm shallow arches, in: *ASME 2014 12th Biennial Conference*

- on Engineering Systems Design and Analysis, American Society of Mechanical Engineers, 2014, pp. V001T01A006–V001T01A006.
- [119] X. Song, S. R. Li, Nonlinear stability of fixed-fixed fgm arches subjected to mechanical and thermal loads, in: *Advanced Materials Research*, Vol. 33, Trans Tech Publ, 2008, pp. 699–706.
- [120] H. Babaei, Y. Kiani, M. Eslami, Geometrically nonlinear analysis of shear deformable fgm shallow pinned arches on nonlinear elastic foundation under mechanical and thermal loads, *Acta Mechanica* (2018) 1–19.
- [121] H. Babaei, Y. Kiani, M. Eslami, Thermomechanical nonlinear in-plane analysis of fix-ended fgm shallow arches on nonlinear elastic foundation using two-step perturbation technique, *International Journal of Mechanics and Materials in Design* 1–20.
- [122] Z. Li, J. Zheng, Q. Sun, H. He, Nonlinear structural stability performance of pressurized thin-walled fgm arches under temperature variation field, *International Journal of Non-Linear Mechanics* 113 (2019) 86–102.
- [123] Z. Li, F. Tang, Y. Chen, J. Zheng, Material distribution optimization of functionally graded arch subjected to external pressure under temperature rise field, *Thin-Walled Structures* 138 (2019) 64–78.
- [124] Z. Li, J. Zheng, Y. Chen, Nonlinear buckling of thin-walled fgm arch encased in rigid confinement subjected to external pressure, *Engineering Structures* 186 (2019) 86–95.
- [125] Z. Yang, Y. Huang, A. Liu, J. Fu, D. Wu, Nonlinear in-plane buckling of fixed shallow functionally graded graphene reinforced composite arches subjected to mechanical and thermal loading, *Applied Mathematical Modelling*.

- [126] A. Heidarpour, M. A. Bradford, K. A. Othman, Thermoelastic flexural-torsional buckling of steel arches, *Journal of Constructional Steel Research* 67 (12) (2011) 1806–1820.
- [127] G. Yang, M. A. Bradford, Thermoelastic buckling and post-buckling of weakened columns, in: *Structures*, Elsevier.
- [128] T. Wang, M. A. Bradford, R. Ian Gilbert, Creep buckling of shallow parabolic concrete arches, *Journal of structural engineering* 132 (10) (2006) 1641–1649.
- [129] Z. P. Bažant, Prediction of concrete creep effects using age-adjusted effective modulus method, in: *ACI Journal Proceedings*, Vol. 69, ACI, 1972.
- [130] Y.-L. Pi, M. A. Bradford, W. Qu, Long-term non-linear behaviour and buckling of shallow concrete-filled steel tubular arches, *International Journal of Non-Linear Mechanics* 46 (9) (2011) 1155 – 1166.
- [131] K. Luo, Y. Pi, W. Gao, M. A. Bradford, Creep of concrete core and time-dependent non-linear behaviour and buckling of shallow concrete-filled steel tubular arches, *Comput Model Eng Sci* 95 (1) (2013) 32–58.
- [132] K. Luo, Y.-L. Pi, W. Gao, M. A. Bradford, D. Hui, Investigation into long-term behaviour and stability of concrete-filled steel tubular arches, *Journal of Constructional Steel Research* 104 (0) (2015) 127–136.
- [133] M. A. Bradford, Y.-L. Pi, Geometric nonlinearity and long-term behavior of crown-pinned cfst arches, *Journal of Structural Engineering* (2014) 04014190.
- [134] M. A. Bradford, Y. Pi, Time-dependent response of three-hinged cfst arches, in: *Tubular Structures XV: Proceedings of the 15th International Symposium on Tubular Structures*, Rio de Janeiro, Brazil, 27-29 May 2015, CRC Press, 2015, p. 139.

- [135] K. M. Shrestha, B.-C. Chen, Y.-F. Chen, State of the art of creep of concrete filled steel tubular arches, *KSCE Journal of Civil Engineering* 15 (1) (2011) 145–151.
- [136] Z. P. Bažant, M. F. Kaplan, *Concrete at high temperatures: material properties and mathematical models*, Longman Group Limited, 1996.
- [137] W. Jiang, D. Lu, Time-dependent reliability analysis of cfst arches for out-plane stability considering concrete creep, *Innovation, Communication and Engineering* 1 (2013) 465.
- [138] Y. Geng, G. Ranzi, Y.-T. Wang, Y.-Y. Wang, Out-of-plane creep buckling analysis on slender concrete-filled steel tubular arches, *Journal of Constructional Steel Research* 140 (2018) 174–190.
- [139] B.-c. CHEN, J.-g. WEI, J.-y. LIN, Experimental study on concrete filled steel tubular (single tube) arch with one rib under spatial loads, *Engineering mechanics* 5 (2006) 017.
- [140] K. Luo, Y. Pi, W. Gao, M. A. Bradford, Long-term analysis of crown-pinned concrete-filled steel tubular arches, in: *ICCM: Proceedings of the 5th International Conference on Computational Methods*, Cambridge, England, 28-30 July 2014, 2015.
- [141] Y. F. Wang, Y. S. Ma, B. Han, S. Y. Deng, Temperature effect on creep behavior of cfst arch bridges, *Journal of Bridge Engineering* 18 (12) (2013) 1397–1405.
- [142] Z. P. Bažant, A. B. Hauggaard, S. Baweja, F.-J. Ulm, Microprestress-solidification theory for concrete creep. i: Aging and drying effects, *Journal of Engineering Mechanics* 123 (11) (1997) 1188–1194.
- [143] M. Gillen, Short-term creep of concrete at elevated temperatures, *Fire and Materials* 5 (4) (1981) 142–148.

- [144] C. R. Cruz, Apparatus for measuring creep of concrete at high temperatures, Tech. rep. (1900).